Development of Cellulose-Titanium dioxide-Porphyrin Nanocomposite Films with High-barrier, UV-blocking, and Visible Light-Responsive Antimicrobial Features

Belladini Lovely

Dissertation submitted to the faculty of the Virginia Polytechnic Institute and State University in partial fulfillment of the requirements for the degree of

Doctor of Philosophy

In

Forest Products

Young Teck Kim
Audrey Zink-Sharp
Maren Roman
Haibo Huang

May 1st, 2024
Blacksburg, Virginia

Keywords: Cellulose nanofibrils (CNF); Titanium dioxide (TiO_2); Porphyrinic metal-organic framework (MOF); Photosensitive antibacterial agents; Homogenization cycles/passes

Development of Cellulose-Titanium dioxide-Porphyrin Nanocomposite Films with High-barrier, UV-blocking, and Visible Light-Responsive Antimicrobial Features

Belladini Lovely

ABSTRACT

The packaging does not serve as a mere containment but also can be designed to play a key role in preserving the product from quality-deteriorating factors, including oxygen, light irradiation, and foodborne pathogenic microorganisms (e.g., *Escherichia coli*). There has been a growing interest in employing ultra-porous metal-organic frameworks (MOF) with visible light-responsive antibacterial mechanisms to generate reactive oxygen species (ROS) that can eliminate bacteria via an oxidative burst. MOF is made of inorganic metal ions/nodes/clusters/secondary building units linked by organic bridge ligands, where titanium dioxide (TiO_2) and tetrakis(4-carboxyphenyl)porphyrin) (TCPP) were selected for these components, respectively. TiO_2 is an exceptional UV-A/B/C-blocker; meanwhile, TCPP dye performs a remarkable photocatalytic ability even under visible light, on top of its macro-heterocyclic structure that is ideal as a MOF linker. Both have good compatibility but suffer from the notorious tendency to self-quench/aggregate. The incorporation of MOF-based conjugates into a polymeric matrix, like cellulose, is among the proven-successful solutions. Cellulose is the Earth's most abundant and naturally biodegradable, and cellulose nanofibril (CNF) was particularly chosen for its high specific surface area and surface activity. However, a straightforward, cheap, and environmentally friendly approach of multicycle homogenization (0-25 passes) was conducted to solve neat cellulose's challenge of natural hydrophilicity, where low pressure (<10 MPa) was applied to prevent the common over-shearing effect. The antibacterial efficacy of CNF films functionalized with TiO_2-TCPP conjugate on inhibiting *E. coli* growth was analyzed with and without light of different intensities (3000 and 6000 lux). The positive impacts of CNFs' promoted fibrillation and subsequent inter/intra-molecular hydrogen bonding post-homogenization were evidenced in an array of functional properties, i.e., crystallinity, TiO_2-TCPP conjugate dispersion, surface smoothness, mechanical properties, thermal stability, hydrophobicity, oxygen barrier (comparable to ethylene-vinyl alcohol (EVOH), a commercial high-barrier polymer), and 100%-antibacterial rate (under 6000 lux after 72 hours). Varying optimum cycles of homogenization demonstrated the prospect of the proposed homogenization approach in preparing CNF with diverse processability and applicability. These findings also exhibited a promising potential for a myriad of high-barrier, UV-blocking, and/or visible light-responsive antibacterial film applications, including food packaging and biomedical.

Development of Cellulose-Titanium dioxide-Porphyrin Nanocomposite Films with High-barrier, UV-blocking, and Visible Light-Responsive Antimicrobial Features

Belladini Lovely

GENERAL AUDIENCE ABSTRACT

Packaging is useful not only as a container but can also be designed to help prevent products from being spoiled due to various reasons such as oxidation, light, and bacterial contamination. Researchers have discovered the promising antibacterial feature of the metal-organic framework (MOF). Packaging made with MOF technology can harness light and oxygen in the environment to produce a special form of oxygen called reactive oxygen species (ROS) that can kill unwanted bacteria. MOF is an extremely porous sponge-like material made of two ingredients: an inorganic metal cluster and an organic linker; in this study, titanium dioxide (TiO_2) and a porphyrin called TCPP were selected, respectively. TiO_2 is an excellent ultraviolet blocker, while TCPP has a unique, ring-like geometry that is ideal for use as a linker and an antimicrobial feature that works well under the visible light spectrum. The pair are compatible but still suffer from MOF's notorious challenge, where it tends to clump together because of its tiny size. To resolve this problem, TiO_2-TCPP MOF can be deposited evenly in a cast made of polymer. Cellulose has been proven to work effectively as a polymeric cast; moreover, it is natural, biodegradable, and in abundant supply. A type of nanosized cellulose—cellulose nanofibril (CNF)—was specifically chosen because its high surface area and activity are useful when blended with other materials. However, cellulose is naturally a poor water-repellant that is not ideal for packaging applications. As a solution, cellulose can be treated with a homogenization technique by passing the material through a very narrow hole under high pressure. Homogenization can be problematic as it possibly damages the cellulose's structure, and its high pressure can also be expensive and energy-consuming. Therefore, low pressure with multiple cycles was applied in this work. CNF-TiO_2-TCPP films were tested for their ability to slow down *E. coli* bacteria growth with and without light of varying brightness to compare its light-sensitive antimicrobial feature. Homogenization was found helpful in producing higher-quality CNF, which improved several of the film's final characteristics, including an even material dispersion, structural order, smoothness, strength, heat resistance, and water repellency. Most importantly, it produced films with oxygen barrier ability comparable to commercial high-barrier plastics and completely eliminated bacteria after 72 hours. The optimum number of homogenization cycles was found to be dependent on the desired characteristics and application. Overall, these findings carry a promising potential for a variety of applications, including food packaging and the biomedical field.

Dedication

To my (الله يرحمها) late, beloved Grandma (Uci): **Ranimah** (1930-2024).

The one who made me love schools. The one who believed in me the most.

You passed right the moment I passed my defense; I knew you were by my side regardless. As promised, I dedicate my last degree to you, Uci.

Acknowledgments

I would like to first and foremost thank my committee for their tutelage throughout my PhD study. Dr. Kim, for his thorough supervision, encouragement, and trust in me despite my many challenges. Dr. Zink-Sharp, for her discipline in training me yet the tenderness when sharing wisdom about life; thank you for believing in me. Dr. Roman, for her comprehensive guidance as well as passion and enthusiasm during discussions. Dr. H. Huang, for his model leadership throughout our projects and always being so kind.

I am also very thankful to other faculty, lab technicians, staff, and lab manager-students for their help at these different labs across VT. Dr. Frazier (Dept. Sustainable Biomaterials; and his students—Eky, Ryan, Mark C, Ata, JC, Emilie); Dr. Cheng (Dept. Food Science and Technology; and his students—Elle and Babak); Dr. Moore (Dept. of Chemistry; and his students—Michelle, Garrett, Mark M, Isabela); Patrick, Steve, Dr. Rit, Dr. Tao (Materials Characterization Facility; Institute for Critical Technology and Applied Science; Nanoscale Characterization and Fabrication Laboratory); and others in our department including Trish, Matt, Angie, Debbie, Shannon, David, and most importantly Head of Dept. Dr. C. Huang for her immense kindness, and Mimi for her exemplary hard work in managing our labs yet being such a ray of sunshine—a wonderful friend.

To my fellow lab-/classmates, I am grateful for all sorts of help and simply happy memories: Soohyung, Vivian, Chenxi, Dr. Wu, Tim, G, Abas, Esra, Mona, Reyyan, Bhawna, Mary, Isa, Daniel, Viv, Bryan, Taylor, Jisoo, Regina, Youngju, Arash, Laura, Zunhuang, and other SBIO/MACR friends; most especially, my PhD project partner, Zane, for his heartfelt spirit throughout our research together, making it a truly fun experience.

Out of lab/class, I will be forever filled with gratitude for the joy of having these friends by my side. VT Indonesians (Eky, Bela, Tian, Adhis-Nisa, Dini-Didi-Kal, Virell, Gian, Casey, Bu Endang, Taufiq, Syafiq, Fred), for their absolute warmth being family far from home. Indonesian Fulbrighters (Budi, Iin, Febri, Agus), for being a solid support system through ups and downs pursuing our dream degree journey here in the States. Blacksburg friends (Indu, Udi, Shank, Brandy, Geoffrey, Alex, Sue, Jarek, Eranga), for cheering me up every time. And—though separated so far away—my best friends at home (Damay, Astri, Vini, Lisa, Kiki, Miza, Riris, Anden, Janjani, Kalvin, Churchill), for their sincere belief in me.

I am in debt of the assistance of VT Cook's Counseling team and other parties on campus (especially Catherine, Dr. Kamran, Maureen), who have always made sure to take the best care of me both physically and mentally. I am also indebted to my former supervisors since my undergraduate years; those recommending me during PhD applications and/or guiding me through these 15 years in university: Prof. Iskandar, Dr. Sintho, Dr. Dase, Prof. Titi, Prof. Farah, Dr. Evi, Prof. Taufik, Prof. Nastiti, Prof. Suprihatin, Prof. Justinus, Dr. Wayah.

Last but not least, I am endlessly grateful for the non-stop prayers by my precious family (Papa, Mama, Zaky-Salsa, Yuyun-Hamdi, Umma, Junaya-Rami-Elias-Idrees, Iman, Raghad-Ibrahim-Nejma, Rayyan, Uda Vando's, Uni Boy's, and others from Bukittinggi and Gadut side). And, most importantly, my husband, my love, my better half—Ahmed Aiman Nakhal—for the utter and constant affection, faith, encouragement, support, patience, and reminder about my lifelong dreams, which became the sole reason at times during my lowest of the lows to not give up and keep going.—I cannot thank all these people enough.

Table of Contents

List of Figures

List of Tables

List of Abbreviations

CNF	cellulose nanofibril
TiO_2	titanium dioxide
TCPP	tetrakis(4-carboxyphenyl)porphyrin
MOF	metal-organic framework
N-film	neat, homogenized-cellulose film
F-film	functionalized-cellulose film
HPLC	high-performance liquid chromatography
T	temperature
RH	relative humidity
FTIR	Fourier transform infrared
ATR	attenuated total reflectance
XRD	x-ray diffraction
CI	crystallinity index
SEM	scanning electron microscope
Sa	arithmetical mean height
UV-vis	ultraviolet-visible
OTR	oxygen transmission rate
OP	oxygen permeability
ASTM	American Society for Testing and Materials
UTS	ultimate tensile strength
TS	tensile strength
E	tensile or Young's modulus
EAB	elongation-at-break
DMA	dynamic mechanical analyzer
E'	storage or elastic modulus
E"	loss or imaginary modulus
Tan(δ)	loss or damping factor
TGA	thermogravimetric analyzer
$T_{d,5\%}$	temperature at 5%-weight loss
W	weight
CFU	colony-forming units

CHAPTER 1

General Introduction

Product quality/freshness can worsen after many factors, primarily oxygen, light irradiation, and contamination; hence, packaging advancement to tackle this constraint is of profound significance. Lately, photodynamic inactivation has been an emerging topic of an antimicrobial modality, one of which is through metal-organic frameworks (MOFs). MOF combines photosensitizer materials with light of a specific wavelength and molecular oxygen in the environment to generate reactive oxygen species (ROS) with a remarkable ability to kill microorganisms via an oxidative burst with no high heat nor harmful substances required and/or released. Made of metal ions/nodes (as inorganic building blocks) and ligands (as organic linkers), MOF is an ultra-porous sponge-like system with versatile functionalities. Porphyrin-based MOF (where the organic porphyrin acts as the bridging ligand) is among the extensively studied MOF types with feasible structural tunability, stable crystalline structure, open channels, and high ROS yield, mainly due to its heterocyclic structure. Among many popular porphyrin derivatives, tetrakis (4-carboxyphenyl) porphyrin (TCPP) has been gaining interest after its exceptional visible light excitation-induced photodynamic feature and efficient coordination with metal ions (Castro et al. 2019; M. Chen et al. 2020; Min et al. 2021; J. Park et al. 2016; X. Zhao et al. 2023; K. Lu, He, and Lin 2014; Zheng et al. 2018; Ahmadi et al. 2015; Q. Wang et al. 2018; Tian et al. 2020; Jian Zhao et al. 2007).

Titanium (Ti) precursors like titanium dioxide (TiO_2) are among the most studied metal ions to be paired with porphyrin. TiO_2 is cheap, ubiquitous, and FDA-approved, with proven antibacterial activity against an array of microorganisms under UV. By pairing it with TCPP, photocatalytic activity and ROS production under UV and visible light spectrums can be achieved. Despite their biocompatibility together, the notorious challenge of MOFs on self-aggregation/quenching tendency remains, and incorporating them into a polymeric carrier has been considered to be one of the viable options (El-Wakil et al. 2015; An et al. 2016; Castro et al. 2019; Gao et al. 2019; Roberta Grazia Toro et al. 2020; Wan et al. 2016; M. Chen et al. 2020; Tu et al. 2017; Cherian and Wamser 2000). Cellulose has been evidenced to be one of the ideal carriers for MOF conjugates due to its plentiful hydroxyl groups that have the potential to be employed as a stable and robust anchoring site or matrix through ex-situ loading. Cellulose-based composite also provides large surface areas, mechanical strength, and barrier properties (Adel et al. 2021; Roberta Grazia Toro et al. 2020; M. Chen et al. 2020; G.-Q. Liu et al. 2021; Min et al. 2021; J. Park et al. 2016; X. Zhao et al. 2023; An et al. 2016). Many have discovered the photosensitivity and antimicrobial potentials of one or more combinations of cellulose, TCPP, and TiO_2 with other materials intended for varying applications from food/biomedical packaging, gas storage/separation, pollutant removal, to energy (G.-Q. Liu et al. 2021; Rathod et al. 2018; Roberta Grazia Toro et al. 2020; Gao et al. 2019; Min et al. 2021; J. Park et al. 2016; El-Wakil et al. 2015); yet, no report on the prospect of cellulose-based packaging incorporated with TiO_2-TCPP. This study's objective was to determine the optimum preparation of the cellulose-based matrix with desired functional properties before exploring the prospect of cellulose-TiO_2-TCPP nanocomposite packaging, especially with its high barrier, UV-blocking, and visible-light responsive antimicrobial features.

CHAPTER 2

Literature Review

2.1. Active packaging

The rapidly increasing world population in the past centuries (Ritchie et al. 2023) has led to hikes in global food supplies—an estimated 50-60% between 2010 and 2050 (Guillard et al. 2018; van Dijk et al. 2021). Likewise, the rising food packaging demands, followed by the constantly upgraded/updated and strict safety guidelines, became the pairing constraint to the food security aspect (Kusuma et al. 2023). The urbanization-derived global dietary change and rising reliance on processed foods (World Packaging Organisation 2008) also create urgency in the need for modernized packaging technology to be progressively applied in the industries. Though the vital functions of food packaging are to protect (contain and preserve), convey information, and transport (Ahmed et al. 2022), it plays a crucial role in the global burden of food contamination and foodborne pathogens that are recorded to be more than 600 million foodborne illnesses cases and 420,000 deaths could occur in a year (WHO 2022). Packaging plays an even greater role in keeping freshness/quality and preventing spoilage from microorganisms, water content, oxygen, humidity, temperature, and light (Magoulas 2016), thereby minimizing food waste (Almenar 2023; Verghese et al. 2015). In the United States alone, 30-40% of the food is wasted, which costs the nation roughly 1.3% of GDP (EPA 2016a; FAO 2013a, 2021a). Together, food and its packaging contribute almost half of the solid waste in American landfills (EPA 2015a). Many waste management hierarchies (European Commission 2023; EPA 2016a; FAO 2022b) stated their highest preference for "prevention" over any other options; hence, the exceptionally growing field of food packaging advancing in food waste prevention through shelf life extension—one of which is through active packaging.

Active packaging is defined as a modified packaging system that incorporates subsidiary constituents ("active agent") in or on either the packaging material or headspace that intentionally releases spoilage-preventive compounds and/or absorbs spoilage-causing compounds from the product or packaging headspace, aiming to preserve and/or improve shelf-life, quality/freshness, sensory, and food safety (Ahmed et al. 2022; Sand 2020; Janjarasskul and Suppakul 2018; Robertson 2012; Monção et al. 2022). Other possible properties of the added active agents include blocking and buffering (Kuswandi and Jumina 2020; Rehman et al. 2020). Having been developed as early as the 1980s, active packaging can be classified generally into two types based on how it functions in keeping the product quality or freshness (Contreras et al. 2017; Kusuma et al. 2023; Firouz, Mohi-Alden, and Omid 2021; Yildirim et al. 2018; Dainelli et al. 2008; Wyrwa and Barska 2017; Ahmed et al. 2022; F. Charles, Sanchez, and Gontard 2006; D. S. Lee 2016):

- Non-migratory (scavengers/absorbers): It absorbs or reacts with unwanted components (e.g., oxygen, carbon dioxide, ethylene, moisture, light, flavors, odor) that negatively impact the product and removes them from the packaging environment without intentional migration.

- Oxygen accelerates spoilage through fat/lipid and vitamin oxidation, which promotes molds, aerobic bacteria, and yeast growth and causes bad aroma, unpleasant taste/off-flavor, fats/oils rancidity, color changes, oxidative browning, and/or nutrient damage, especially in baked goods, fresh dark meats, and fruits/vegetables.
- Carbon dioxide is the main product of catabolic reactions in the biological systems of most non-pasteurized fermented or roasted foods, causing physiological injury (discoloration, off-flavor, and internal tissue breakdown). Two types of agents are used: physical (zeolite and active carbon powder) and chemical (calcium hydroxide, sodium carbonate, magnesium hydroxide).
- Moisture/humidity/water vapor affects texture, appearance, and microbial activity, especially in high-water-activity products like meat and produce.
- Light-absorbing agents (e.g., hydroxy benzophenone, benzophenone, benzotriazole, triazine, etc.) provide effective light-transmission reduction or stabilization, especially to light-sensitive foods that are particularly susceptible to oxidation and nutritional degradation, such as fruit juices, tea, sports drinks, and extra virgin oils.

- Migratory (emitters/releasers/diffusion): It allows controlled migration of desired substances (e.g., carbon dioxide, ethanol, sulfites, flavors, antioxidants, antimicrobials) that positively impact the product into the packaging environment.
  - Carbon dioxide benefits from its high solubility in food, ability to reduce physiological activities (respiration and ethylene production), and ability to balance pressure/volume between the packaging's inner headspace and external environment. It preserves freshness, reduces microorganisms' growth, and inhibits spoilage-associated odor formation, especially in fresh meat, fish, poultry, and non-climacteric fruits.
  - Ethanol vapor in the packaging headspace maintains the original textural quality and suppresses the growth of yeasts, anaerobic bacteria, and molds, especially in fruits and vegetables.
  - Sulfites (e.g., sulfur dioxide, sodium sulfite, sodium bisulfite, sodium metabisulfite, potassium metabisulfite, potassium sulfite), classified as major allergens, prevent (non)enzymatic browning or coloration during processing and storage by acting against oxidative decay, polyphenol oxidase, fungi and bacteria responsible for malo-lactic fermentation.
  - Flavor addition overcomes oxidation-derived flavor scalping.
  - Antioxidant agent limits oxidation of the fatty components.
  - Antimicrobials prevent microbe's growth by utilizing agents such as essential oils, metals (silver, silver zeolite, gold, copper, titanium dioxide, zinc oxide), triclosan, glucose oxidase, chlorine dioxide, natamycin, and allyl isothiocyanate.

Several mechanisms can be applied to incorporate the aforementioned active agents and obtain an active packaging system (Vidal et al. 2022; Patiño Vidal et al. 2022; Ahmed et al. 2022; Firouz, Mohi-Alden, and Omid 2021; Bahrami et al. 2020). Some of the examples are listed and illustrated below (**Fig. 2.1.**).

- Active agent-loaded external device (e.g., label, pad, sachet, tablet, film, wrap, tray) placed inside the packaging together with the product or attached/glued on the packaging's inner surface that contacts the headspace.
- The active agent is immobilized with a polymer through ion or covalent linkages by utilizing certain functional groups depending on the interactions/bondings.
- The active agent is added either in the form of filler (as the dispersed phase of a composite) or in the form of the matrix itself (as the continuous phase). In the case of multilayered films, the composite is positioned as the packaging's inner layer that contacts the headspace.
- The active agent is sprayed/coated in the packaging's inner surface that contacts the headspace, which would suffice for a compound that is non-compatible or immiscible with the desired polymer, either through immobilization or matrix-filler composite formation route.

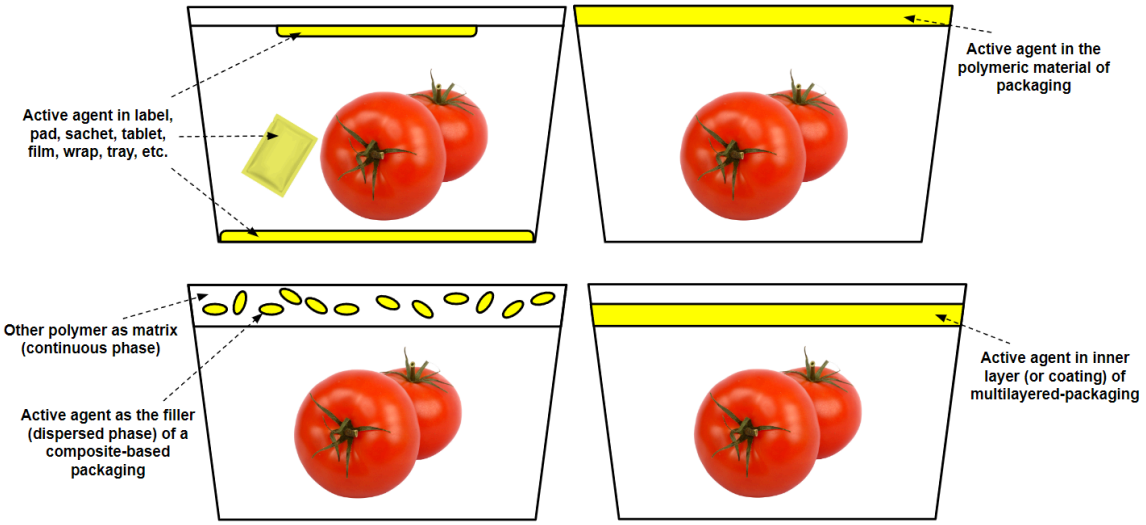

Fig. 2.1. Different mechanisms in the active packaging system

The growing interest in active food packaging research was evidenced by the fivefold increase in publications in the past decade, amounting to over ten thousand in 2021 (Ahmed et al. 2022). This prompts the regulatory agencies to set the legal basis for requirements and standards in active packaging production and use, especially in regard to the added substances and their potential impact on the packaged product. European Food Safety Authority acts as the European Union's regulator; meanwhile, the Food and Drug Administration (FDA) is responsible for American markets (Misko 2022).

2.2. Metal-organic framework (MOF)

Active agents contained in the highly stable metal-organic framework (MOF) have been one of the emerging topics among active packaging researchers. MOF is a synthetic polymeric hybrid material characterized by ultra-highly porous coordination, high surface area, crystalline structure, low density, tunable morphology, fully exposed active sites, abundant coordination-unsaturated metal sites, and substitutable components (Carrasco 2018; Furukawa et al. 2013; Omar M. Yaghi et al. 2003). The terminology defined by the International Union of Pure and Applied Chemistry (IUPAC) (Batten et al. 2013) is stated

as a further subset of coordination networks (a subset of coordination polymers) that contains potential voids. Similar terminologies exist besides MOF when describing hybrid inorganic and organic framework materials or the nonmolecular/extended solid-state structures containing metal ions and organic spacer ligands. “Coordination polymers” term was the popular term up until the year of 2000 when the trend of “MOF” term use took over ever since (Biradha, Ramanan, and Vittal 2009). As illustrated in **Fig. 2.2**, It is constructed by joining inorganic, metal ions/nodes/clusters (secondary building units (SBUs)) and organic linkers (bridge ligands) by strong bonds to create open crystalline frameworks with permanent porosity through what is termed reticular synthesis. Reticular synthesis is a process of assembling judiciously designed rigid molecular building blocks into predetermined ordered structures (networks), which are held together by strong bonding. Coordination polymerization and cross-linking occur between the inorganic and organic precursors (Furukawa et al. 2013; Omar M. Yaghi et al. 2003). Besides, MOF possesses high compatibility with both organic and aqueous solvents as the mixing media (Burtch, Jasuja, and Walton 2014). Aluminum, iron, zirconium, titanium, copper, and zinc are among the commonly used metal components in fabricating MOFs (Sultana, Kathuria, and Gaikwad 2022).

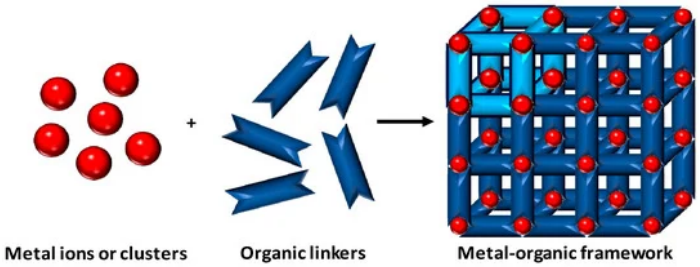

Fig. 2.2. The schematic metal-organic frameworks (MOFs) (Carrasco 2018)

There are numerous ways to categorize types of MOFs. For example, based on synthesis stages, first-generation MOFs have the basic structure of organic and inorganic moiety, while the second-generation undergoes surface modification. Lastly, the MOFs that include biomolecules in their structural design are called the third-generation. Based on stimuli, there are single-stimuli and multi-stimuli MOFs (Sultana, Kathuria, and Gaikwad 2022). Since both of the building components of MOF are easily tailorable, where specifically, the metal is easily doped, and the organic linker is easily replaced/modified, this increases the applicability. The abundant surface active groups also can facilitate modifications to enable synergistic or dual effects (Zacher et al. 2009). Since first introduced in 1995 (O. M. Yaghi, Li, and Li 1995), the number of MOF-themed publications has been facing popularity, reaching almost five thousand in 2019 (J. Meng et al. 2020). MOF is applicable in a broad range of fields depending on the properties, e.g., catalysis (Bavykina et al. 2020), gas storage-separation (Jia, Gu, and Li 2022), purification (Jun et al. 2020), drug delivery (He et al. 2021), sensors (Weiwei Cheng et al. 2021), energy (X. Li et al. 2020).

However, lately, MOF-based materials have also become a hotspot for antibacterial research that involves photocatalytic abilities, particularly by employing Reactive Oxygen Species (ROS) as the primary antibacterial mechanism. MOF can be designed to contain a photosensitive component that is able to combine visible light irradiation of a

specific wavelength and molecular/diatomic oxygen (O_2) in the air to generate ROS (Castro et al. 2019; I. Kim et al. 2022). More specifically, there is a gap in molecular orbitals of MOF called the Highest Occupied Molecular Orbital—Least Unoccupied Molecular Orbital (HOMO-LUMO) gap where electron transition occurs (from the HOMO to LUMO, leaving holes (h+) in the HOMO) and become conducive and responsible for the formation of varied photogenerated ROS that targets multiple sites in bacteria (R. Li, Chen, and Pan 2021; Vaishampayan and Grohmann 2021). Though bacteria deploy defense mechanisms against oxidative stress caused by ROS, excess accumulation of ROS eventually leads to an oxidative burst that allows ROS first to penetrate through and disrupt the outer cell envelope (cell wall and plasma membrane) and destroy the cell integrity/viability, then damage DNA, lower the coenzyme A (an essential cofactor of cellular metabolism) level, increase plasma membrane permeability, oxidize membrane fatty acids/lipids and proteins, depolarize the membrane, carbonylate protein, and eventually leak the intracellular content—effectively killing the bacteria (Vaishampayan and Grohmann 2021; Bogdan, Zarzyńska, and Pławińska-Czarnak 2015; Sultana, Kathuria, and Gaikwad 2022; Y. Hong et al. 2019). Chelation, or coordination bonds between organic molecules and metals (Sears 2013), also plays a role in MOF-mediated microbial inhibition. It reduces the polarity of the metal component and enhances lipophilicity, which is beneficial in facilitating penetration to bacterial cell membranes (Tweedy 1964). MOF antibacterial function by the ROS formation and valorization using different metal components (TiO_2 and ZnO) are illustrated in **Fig. 2.3(a)** and **Fig. 2.3(b)**, respectively.

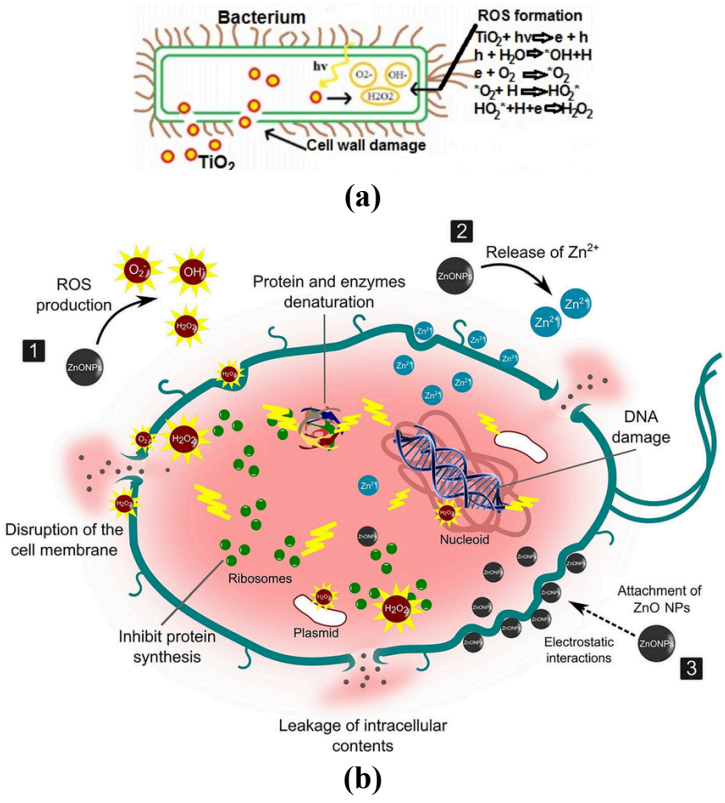

Fig. 2.3. The antibacterial mechanisms by reactive oxygen species (ROS) using different metal components: (a) TiO_2 (Maryani et al. 2020) and (b) ZnO: (Gomaa 2022)

Bacteria physiology shall be taken into consideration when assessing the bactericidal efficiency of ROS since the bacterial structure (complexity and thickness) and chemical composition govern susceptibilities to oxidative damage. For example, the Gram-positive bacteria cell wall is made of a thick and porous peptidoglycan layer with attached teichoic acids, while the Gram-negative bacteria have a thin peptidoglycan layer with surrounding, asymmetric, highly-impermeable bilayer, as well as inner and outlet leaflets of phospholipids and strongly-negatively charged lipopolysaccharides, respectively. Hence, the permeation limitation of neutral/negatively charged photosensitizers (in MOF) against Gram-negative bacterial cells, in contrast to the positively charged ones, which are capable of advancing a strong electrostatic interaction and achieving a considerable bactericidal inhibition performance (Castro et al. 2019; Delcour 2009; Bogdan, Zarzyńska, and Pławińska-Czarnak 2015). In addition, peptidoglycan content in the targeted bacteria cell wall is another factor affecting bacteria resistance to oxidative damage and ROS activity. Though peptidoglycan degradation does not necessarily occur during bacteria inactivation, neither with Gram-negative nor with Gram-positive bacteria, peptidoglycan provides an efficient physical barrier from ROS gaining entry into the bacteria cell (Bogdan, Zarzyńska, and Pławińska-Czarnak 2015; Dalrymple et al. 2010). ROS formation is initiated by electron transfer reactions from the added photosensitizer's triplet state, which are followed by two (2) possible oxidative mechanisms or pathways: Type 1, to surrounding substrates, generating radical ions or cytotoxic oxygen species (i.e., superoxide anion, hydroxyl, and lipid-derived radicals); and/or Type II, to ground state molecular oxygen ($^3O_2$), generating excited-state singlet oxygen ($^1O_2$) (Castro et al. 2019; Vaishampayan and Grohmann 2021)—to be employed in bacteria inactivation. Overall, the order of ROS ability in various infectious agent inactivation is reported as follows (from the most susceptible to ROS-derived oxidative damages to the least): viruses > prions > Gram-negative bacteria > Gram-positive bacteria > yeasts > molds (Bogdan, Zarzyńska, and Pławińska-Czarnak 2015).

2.3. Titanium dioxide (TiO_2) in MOF

Titanium (Ti)-clusters have been among the most appealing choices as a multifunctional metal component of metal-organic frameworks (MOFs) due to their excellent optical response (photoactivity), (photo)chemical stability, varying structure, redox activity (transition between Ti^{3+} and Ti^{4+}), and biocompatibility (D. Pinto et al. 2015; Schneider et al. 2014; J. Zhu et al. 2018). The first recorded success of exceptionally porous and crystalline Ti-based MOF fabrication was by a photochromic study in 2019 (Dan-Hardi et al. 2009). As the naturally occurring oxide of Ti that can be prepared in various degrees of purity, TiO_2 continuously gains attention for its many advantageous properties, such as spectral, structural, mechanical, optical, dielectric/electronic, catalytic, and anti-corrosion. In addition, nano-engineering modification of the pairing component in MOFs—organic ligands—allows researchers to accomplish tunable optical band gap of TiO_2 with added functional moieties (Fang et al. 2017; Fang, Zhang, and Zhang 2016; J.-X. Liu et al. 2016; Santiago Portillo et al. 2017; D. Pinto et al. 2015). Its photocatalytic applicabilities extend from being used in fields of UV protection (sunscreens, paints, ointments, toothpaste, pigments, plastics, photo-/electrochromics, thermal sprays), energy and electricity (dye-sensitized solar cells or photovoltaics, photo-conductor, lithium batteries, piezoelectric capacitors, fuel cell),

food/biomedical (antimicrobial, sensors, nanomembrane, gene therapy), and environmental (water splitting, pollutant degradation, gas storage/separation, including H_2 generation and CO_2 reduction) (D. Pinto et al. 2015; Assi et al. 2017; D. Sun and Li 2017; Schneider et al. 2014; J. Zhu et al. 2018). Specifically in food packaging applications, TiO_2 is proven to possess exceptional antimicrobial and UV rays-blocking performances (Varghese et al. 2023) due to its promising light absorbance (at wavelengths of 275-405 nm) and high refractive index; moreover, for nanosized TiO_2 (Ghamarpoor, Fallah, and Jamshidi 2023; Khorasaninejad et al. 2017). When selecting the right metal component, it is no less crucial to correlate between investigations of their bacteria photocatalytic inactivation with the reactive oxygen species (ROS) generation under both light and dark conditions. TiO_2 was found to perform better than its biggest metal ion contender—zinc oxide (ZnO)—in regards to ROS production and loss of cell viability assessed on representative bacteria to both Gram-positive (*S. aureus* and *B. subtilis*) and Gram-negative (*E. coli*). The same study also evidenced the more prevalent self-agglomeration issue in ZnO specimens (Barnes et al. 2013). An earlier, similar study confirmed the notion as well (Qamar and Muneer 2009). Despite their nearly identical band gap energy, ZnO suffers from worsened photosensitivity in aqueous media (e.g., water) due to photo-corrosion tendency under UV illumination (Hariharan 2006; van Dijken et al. 1998; Neppolian et al. 1999)**.**

2.4. Tetrakis(4-carboxyphenyl)porphyrin (TCPP) in MOF

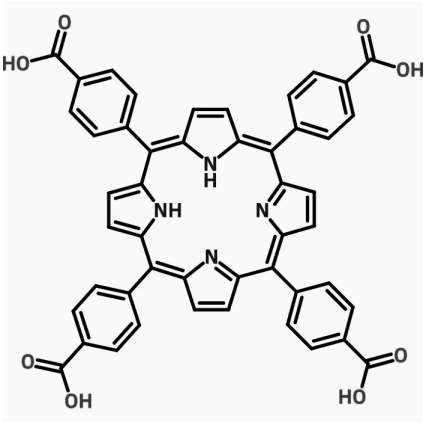

Fig. 2.4. Chemical structure of tetrakis(4-carboxyphenyl)porphyrin (TCPP)

Porphyrins are among the classes of organic chromophores and N-heterocycles, consisting of macromolecular compounds of porphin ($C_{20}H_{14}N_4$), whose meso/β-position can be substituted by varieties of functional groups (Gottfried 2015). In fact, porphyrin naturally exists in many vital functions of living organisms, such as hemoglobin (blood), chlorophylls, catalase, heme, cytochromes, and vitamin B12 (J. Chen, Zhu, and Kaskel 2021; H. Huang et al. 2015; Jasat and Dolphin 1997). The free-base porphyrin (center or periphery) can be bound with metal ions to produce metalloporphyrins (metal complexes) with various tunable substitution patterns, molecular cages, and framework solids due to its intricate binding modes. Other reasons behind the metalized porphyrin derivatives versatility are their large π-aromatic system, chemical-thermal stability, energy transfer, fluorescence characteristic, chemical catalytic activity, photophysical, and

electrochemical properties (Adler et al. 1970; Longevial et al. 2018; Durot, Taesch, and Heitz 2014). Porphyrins (derivatives) famously possess electromagnetic spectrum absorption in the visible light section, which is the strongest around 400–450 nm (Soret band) with gradually reduced intensity at 500-700 nm (Q-bands) (Gottfried 2015). Their applications include light harvesting, solar cells, molecular electronics, biomedical (photodynamic therapy, tumor treatment), and (photo-/electro-/or biomimetic) catalysts (Steer 2018; Rezaeifard and Jafarpour 2014). However, the drawbacks limit their further development, one of which is the self-quenching/aggregation tendencies. The growing solution nowadays is through proposing multifunctional carriers (including incorporation into metal-organic frameworks or MOFs) to encapsulate, physically adsorb, or covalently bind porphyrins (derivatives), such as micelles, liposomes, carbon nanotubes, inorganic nanoparticles, and polymer nanoparticles (J. Chen, Zhu, and Kaskel 2021). This advanced concept also leads to improved physicochemical behaviors, maximum highly active and functional building units, and minimum inactive constituents (Freund et al. 2018). Particularly in the past two decades (A. Li et al. 2020), porphyrin and derivatives as neutral organic linkers in MOFs have garnered popularity among researchers. Owing to their unique macro-heterocyclic geometry (**Fig. 2.4**), the advantages include exposed metal sites, long-lived excited states, and high triplet quantum yield, which subsequently leads to their pronounced entire-spectrum visible-light responsive photocatalytic and redox-active photosensitizer abilities (C. Liu et al. 2020; J. Liu et al. 2018; X. Zhang et al. 2021; C. Y. Lee et al. 2011). Another promising finding was also obtained on photo-oxidation involving ROS (singlet oxygen) formation by porphyrin-based MOFs (Xie et al. 2011; J. A. Johnson et al. 2014; Z. W. Jiang et al. 2020), which is described more in detail in **Fig. 2.3.** in regards to ROS generation and antibacterial mechanism in MOFs. The carboxyl group-substituted 5,10,15,20-tetrakis (4-carboxyphenyl) porphyrin (TCPP), or $C_{48}H_{30}N_4O_8$, is a derivative and a member of the porphyrin family with remarkable prospects, especially after their visible light excitation-induced photosensitization (Y. Wang et al. 2018; Ahmadi et al. 2015). TCPP is especially compatible with TiO_2 as it adsorbs strongly onto TiO_2 nanoparticles as photosensitizer (Cherian and Wamser 2000; Kalyanasundaram et al. 1987; Dabestani et al. 1988; Vlachopoulos et al. 1987). Other advantageous characteristics of TCPP over other porphyrin-based photosensitizers are its superior simplicity, efficient coordination with the metal ions, reduced self-quenching behavior, and preserved photosensitivity even under a high dose (Tian et al. 2020; Jian Zhao et al. 2007).

2.5. Cellulose-MOF composite

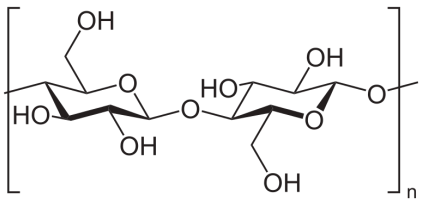

Fig. 2.5. Chemical structure of cellulose

Cellulose is named the Earth's most abundant and naturally biodegradable polymer (Klemm et al. 1998) and can be extracted from a myriad of sources (e.g., wood, plant,

algae, tunicate, bacteria) naturally or through controlled synthesis. Cellulose is made of D-glucose monomers linked via β(1→4) glycosidic bonds (**Fig. 2.5**), which creates the chemical formula of $(C_6H_{10}O_5)n$ (where n is the degree of polymerization ranging from 10,000-15,000 depending on the source). Cellulose is synthesized biologically in nature by the joining of glucose molecules with the loss of 1 H_2O molecule for each bond formed (Werpy and Petersen 2004; Manahan 2011). Its multifaceted applicability is mainly due to its ease of modification and high biocompatibility (Abdelhamid and Mathew 2022); moreover, it is able to be incorporated with organic and/or inorganic conjugates (Erlantz Lizundia et al. 2020). Nanocellulose is a 'top-down' nanoscaled product of cellulose that is commonly preferred for the further valorization of cellulose materials due to its increased surface area and extensive network structure (H. Lee, Sundaram, and Mani 2017). There are two types: 1) the rigid and rod-like cellulose nanocrystals or CNCs, which are prepared chemically, e.g., acid hydrolysis, oxidation, and cationization, by removing amorphous region and leaving purely-crystallines; and 2) the flexible cellulose nanofibrils or CNFs, which are prepared mechanically, e.g., micro-fluidization, homogenization, grinding process, sonication, by preserving both amorphous and crystalline structure (Dias et al. 2020; Ibrahim et al. 2019; Sofla et al. 2016). However, despite its nano-size, neat cellulose still suffers from various issues such as natural insolubility, non-dispersibility, moisture absorption, and hydrophilic/hygroscopicity, which all lead to weakened interfibrillar hydrogen bonding and many other functional properties (Nechyporchuk, Belgacem, and Bras 2016; Xia et al. 2018; B. Yang et al. 2019); therefore, modification is often necessary. Mechanical modification—especially through homogenization employing pressure, velocity, cavitation, shear, and impact forces for solution passed through a very small vessel/orifice—is among the favored solutions. It is owing to its simplicity and environmental-friendliness for having no requirement of high temperatures and mostly requiring sole water as mixing media (L. Wang et al. 2021; Deepa et al. 2019; W. Huang 2018). Homogenization for years has proven its success in promoting fibrillation, surface area, hydrogen bonding, 3D network strength, and structural stability (Nagarajan et al. 2021; H. Lee, Sundaram, and Mani 2017; Chun et al. 2011; Wenjian Cheng et al. 2010; Flores et al. 2021; Usenko et al. 2013). However, the recurring issues with the traditional homogenizer approach are the use of high conditioning pressure, meaning high energy consumption, cost, and risk of over-shearing/over-heating/over-pressure (which leads to material destruction and/or agglomeration), on top of clogging (H. Lee, Sundaram, and Mani 2017; Nagarajan et al. 2021; Boulemkahel et al. 2021). The use of lower pressure and/or multiple passes/cycles of homogenization has been explored as an effort to resolve these limitations (Boulemkahel et al. 2021; Fu et al. 2011; Yu et al. 2021). Moreover, several reports highlighted the potential of a homogenizer equipped with novel "Emulsifying Cell" technology (BEE International 2015) at multiple passes in preparation of a variety of materials, including cellulose. As illustrated in **Fig. 2.6**, such cell design allows the multiple passes effect, thus optimizing the number of cycles and operating time the solution has to pass through the cell. Varieties of nozzle diameter are available as well to customize the overall impacts.

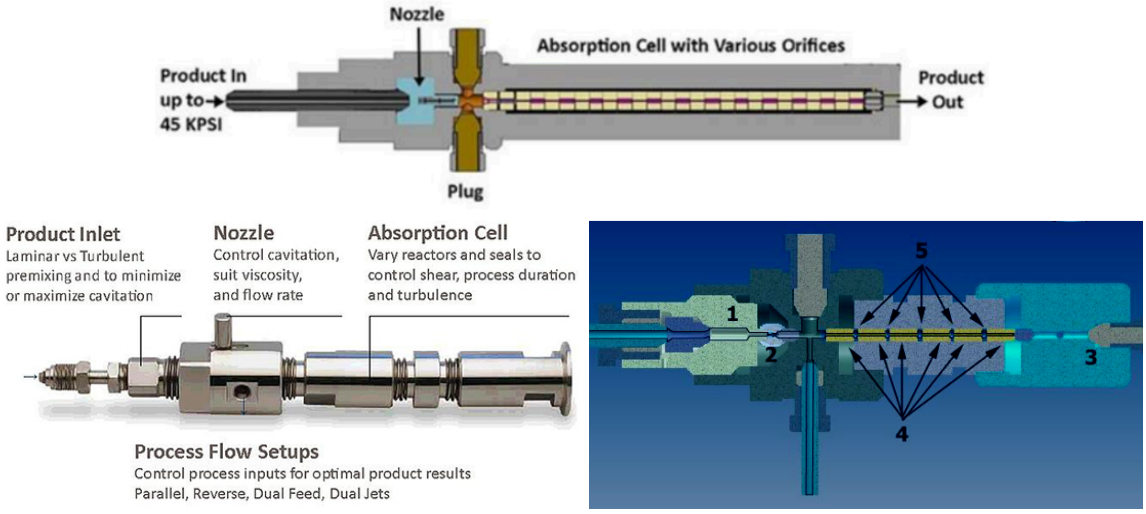

Fig. 2.6. Schematic general principle of homogenizer equipped with emulsifying cell technology (BEE International 2015)

Cellulose, just like many other polymers, has been proven to be a noteworthy pairing material (either carrier, support, modulator, binder, or filler) of metal-organic frameworks (MOF) to solve its notorious constraint of low stability (X.-F. Zhang et al. 2021; Xiongli Liu et al. 2021; X.-M. Liu, Xie, and Wu 2020; S. Wang et al. 2020). Cellulose contains advantageous functional (carboxyl/hydroxyl) groups that can interact with the positive charge of MOF's metal nodes. It is also reported that the fruitful use of photosensitizer dye in maximizing the final product's adsorption capacity (C. Zhu, Monti, and Mathew 2020). Non-cytotoxicity yet possessing excellent antibacterial efficacy (with or without stimuli such as light) is another appealing factor of cellulose being commonly used in antibacterial product developments. Many developed cellulose-MOFs offered remarkable porosity (pore volume), mechanical properties (e.g., compression strength, flexibility, shapeability), thermal stability, and low density (Y. Wu et al. 2020; L. Zhu et al. 2018; Lei et al. 2019). Moreover, it is also possible to combine characteristics of both cellulose and MOFs in order to acquire the final product with multifaceted functions, e.g., UV-blocking, hydrophobicity, photoluminescence, and biodegradability, including lowered cytotoxicity derived from the neat-MOF (L. Lu et al. 2018; Ozer and Hinestroza 2015; D. Huang et al. 2020). The advantageous functional groups of cellulose also play a crucial role in preventing the leaching of metal nodes of the MOF conjugate out of the system. In addition, MOF is beneficial as well in maintaining nano-cellulosic structure and preventing aggregation by inhibiting the interaction between cellulose surface and the abundant hydroxyl groups, especially at high-content cellulose (D. Huang et al. 2020). There are two (2) distinct mechanisms to prepare cellulose-MOF:

- In-situ synthesis: MOF precursors (either inorganic metals and/or organic linkers) are added to the cellulose to allow MOF to 'in-situ' grow into the cellulose fibers. Fiber modification (e.g., esterification (Abdelhameed, Rehan, and Emam 2018)) is often necessary to ensure high metal-fiber interaction. The conformational structure of cellulose is possibly altered post-MOF incorporation (Valencia et al. 2020).

- Ex-situ synthesis: Multi-step procedures of loading/doping the separately and initially synthesized MOFs into cellulose (which plays a role as carrier/support). It allows the more precise loading control of MOF conjugate. The most notorious challenge is MOFs' severe aggregation and uneven dispersion within the cellulose network (Tan et al. 2020).

Table 2 below lists the examples of developed cellulose-MOF in the past decade specifically intended for high-performance antibacterial application use against one of the main pathogens *Eschericia coli* or *E. coli* (da Silva Pinto, Sierra-Avila, and Hinestroza 2012; Abdelhamid and Mathew 2022). Detailed description on antimicrobial test and *E. coli* are at the next sections.

Table 2. Application of cellulose-MOF as antibacterial films against *E. coli*

Reference	Building components	Efficiency	Contact duration
(Y. Yang et al. 2020)	cellulosic cotton fabric; zeolitic imidazolate framework (ZIF-8) as MOF	100%	18 h
(Qian et al. 2018)	cellulose paper; cellulose nanofiber; zeolitic imidazolate framework-67 (ZIF-67) as MOF	100%	24 h
(Rodríguez et al. 2014)	cellulosic woven cotton fabrics; Cu-BTC or copper benzene-1,3,5-tricarboxylate (MOF-199 or HKUST-1)	100%	24 h
(Rubin, Neufeld, and Reynolds 2018)	carboxymethylated cellulosic cotton fiber; $Cu_3(NH_2BTC)_2$ as MOF	99%	24 h
(Nie et al. 2020)	cellulosic woven cotton fabrics; porphyrinic MOF (PCN-224)	99%	24 h
(L. Lu et al. 2018)	cellulosic cotton fabric; ZnBDC as MOF (zinc(II)acetate+1,4-benzenedicarboxylic acid)	99%	24 h
(Duan et al. 2019)	oxidized cellulose-rich corncob; copper/zinc-based MOF	90%	24 h
(Noorian, Hemmatinejad, and Navarro 2019)	cellulosic cotton fabric; zinc glutamate BioMOF; nitric oxide; 5-fluorouracil (5FU)	90%	24 h

2.6. Characterization

2.6.1. Fourier transform infrared (FTIR) analysis

Fourier transform infrared (FTIR) spectroscopy, as illustrated in **Fig. 2.7(a)**, is a form of vibrational spectroscopy that employs infrared radiation and is often used as a physicochemical quantitative analytical method to 'fingerprint' substances and determine their identity, quality, impurities, and changes based on the molecular composition and bonding mechanisms. A specific wavelength of infrared is produced by the instrument to be absorbed/transmitted through the sample to the detector that scans the 'fingerprints.' The functional groups existing in the specimen's composition are identified by detecting their vibrations (either through stretching or bending in various ways) and their intensity (either in %transmission or absorbance unit), which are plotted against the light

frequency (cm^{-1}) to produce an FTIR spectrum. Molecular vibration types can be related directly to molecules' symmetry, which is helpful in precisely identifying how a molecule is bonding on surfaces or as a component in a solid phase from its infrared spectrum. The bands' position and intensity are related to changes in surface groups (Hamad et al., 2018; Wade, 2003). The resulting spectra are characteristic of the bonds in molecular species (or extended bonded structures such as in solid lattices) and are further identified by referring to the spectral library. The advantages include the wide spectral and wavelength ranges (400–4000 cm^{-1}), no required derivatization, and the fact that it is non-destructive yet still considerably a rapid and low-cost technique. FTIR is among the vital characterizations when analyzing materials as it addresses one's chemical composition (Peak 2005; Daéid 2005; Tranter 2017; Bhunia 2008; Ercolini 2014; Dwivedi et al. 2017; Pednekar et al. 2017).

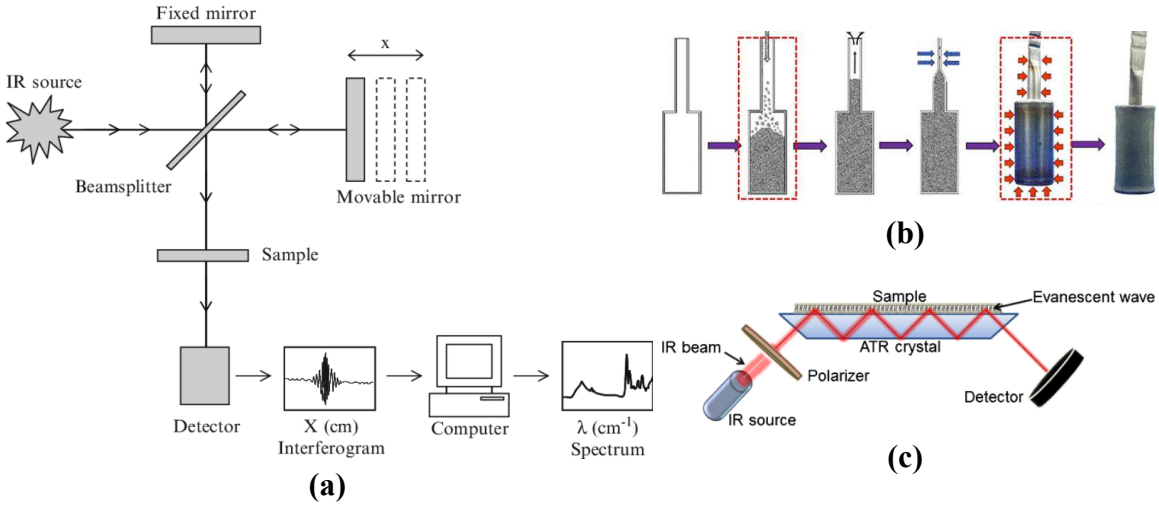

Fig. 2.7. Schematic general principles: **(a)** basic FTIR (Ojeda and Dittrich 2012); **(b)** sample pellet preparation (Kintek 2024); **(c)** ATR-FTIR (Ausili, Sánchez, and Gómez-Fernández 2015)

The two most common FTIR approaches are 1) the pellet (**Fig. 2.7(b)**), which is placed in the path of the infrared beam, and 2) Attenuated Total Reflectance (ATR) (**Fig. 2.7(c)**). Potassium bromide (KBr) is among the most universal salts/crystals to be used as specimen carriers when preparing FTIR pellets due to being simple and optically transparent or having a 100%-transmittance or no absorption bands in the range of FTIR tested wavenumber (4000-400 cm^{-1}) as well as good reproducibility (Goriletsky et al. 2001; Gendreau and Burton 1979). On the other hand, in the ATR approach, the sample is placed on top of the ATR crystal lens (fully covered), where the infrared beam passes through, and the resulting evanescent wave penetrates and gets absorbed into the specimen. The polarizer generates the parallel-perpendicular polarized incident beams (Ausili, Sánchez, and Gómez-Fernández 2015). Optical contact between the specimen and the ATR crystal lens shall be maintained using stable and constant pressure in order to generate data with decent reproducibility. The ATR-FTIR approach is sometimes preferable as it does not require the traditional KBr pellet preparation, enhancing its simplicity (especially beneficial for sample types unable to be incorporated evenly in

pellets) and the ability for real-time decision-making (Keshavarzi et al. 2020; Sauer et al. 2019; Tiernan, Byrne, and Kazarian 2020).

2.6.2. Crystallinity

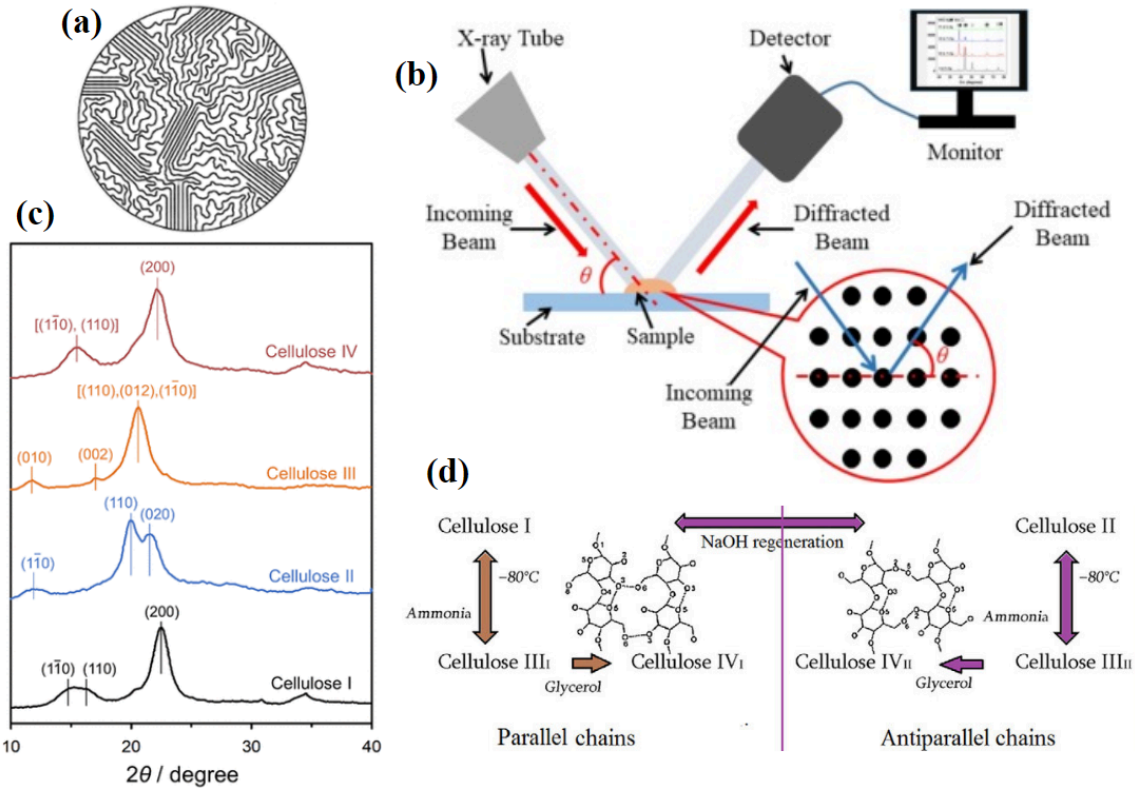

Fig. 2.8. Schematic: **(a)** illustration of polymers' crystalline-amorphous regions (Uzun 2023)**; (b)** general principle of XRD (C. Zhao et al. 2023); **(c)** and **(d)** cellulose's crystalline allomorphs (Y. Liu et al. 2022; Nasir et al. 2017)

Polymers structurally comprise crystalline (ordered/aligned) and amorphous (less ordered/aligned) regions (Nisizawa 1973), as illustrated in **Fig. 2.8(a)**. Crystallinity represents the mass fraction of the crystalline regions and has an important effect on many physical and chemical properties of polymers, especially in governing one's hardness and density, by defining the material's crystal structure and microstructure. The degree of crystallinity, often called the Crystallinity Index (CI), can be determined by X-ray diffraction (XRD) (**Fig. 2.8(b)**). X-rays are high-energy electromagnetic waves at a wavelength ranging from 10^{-3}-10^{1} nm (Spiess et al. 2009). The crystalline region in the tested specimen scatters the incoming X-ray beam and produces sharp reflections, leading to beam diffraction at an angle (2θ) that obeys Bragg's Law (Bragg 1913). Bragg's Law accounts for the relationship between the electromagnetic radiation wavelength and the specimen-diffraction angle's lattice spacing. On the other hand, the amorphous region generates a diffuse background in the resulting XRD pattern. XRD spectra plot the diffraction signal intensity against either the produced diffraction angle (2θ) or spacing between the atomic planes or *d* (nm). The most common wavelength used

is 1.54 Å (Cu Kα) (Uzun 2023; C. Zhao et al. 2023; Sharma et al. 2012; H. Khan et al. 2020; Evans and Radosavljevic Evans 2004; Epp 2016). XRD is often considered among the most relevant characterizations when analyzing materials as the determined crystallinity implies mass fraction or microstructure of one's crystalline regions, which governs the ability to form a uniform network and subsequent physical-mechanical properties (Siti Syazwani et al. 2022; I. S. Goldstein 2004). Crystallinity signifies an active and stabilized surface charge of a suspension and a more homogenized mixture, which correlates with the ability to form a uniform network (Hafid et al. 2023). It is also an inherent property that governs the mechanical property, affinity for water, and accessibility to chemical reagents. The amorphous region, with its higher porosity than crystallines, allows water to penetrate through and increases reactivity to either chemical (acids and alkalines) or enzymatic hydrolysis (Nunes 2017; Pérez and Samain 2010).

Several methods, instruments, and equations can be employed in characterizing crystallinity; however, the Segal et al. method (Segal et al. 1959) is named the most popular due to its superior ease of use and time efficiency (S. Park et al. 2010). Also known as the "XRD peak height" method, it utilizes the produced XRD patterns to calculate CI using Segal's empirical equation, or the intensity ratio between the specimen's crystalline and amorphous peaks. The crystalline peak (major peak, or I_{total}) is located around 2θ = 23°, which measures the maximum intensity of the crystalline peak. Meanwhile, the amorphous peak is also known as the minima between the major (indices (200) at 2θ = 22.5°) and secondary peaks (indices (10$\bar{1}$) at 2θ = 14.7°–16.1°), or I_{am}, located around 2θ = 18°, which is the minimum intensity of the amorphous peak or the maximum point where the entirely amorphous cellulose would be (Segal et al. 1959; Nurhadi et al. 2022). In these equations, n is an integer (1, 2, 3, 4,…); d_{hlk} is interplanar spacing generating diffraction between atomic planes; θ is X-ray incident angle; CI is crystallinity index; I_{total} is the crystalline (major) peak, at 2θ = 23°; and I_{am} is the amorphous (minor) peak, at 2θ = 18°.

$$n\,\lambda = 2\,d\,\sin\theta \;\; ; \quad CI \;=\; \left(1 - \frac{I_{am}}{I_{total}}\right) x\; 100\%$$

Furthermore, another crystallinity profile of cellulosic specimens identifiable through XRD spectra is crystalline allomoprhs. Among the four (4) crystalline allomorphs introduced, Cellulose I is the naturally obtained or parent/native form, thus being the most abundant. Cellulose I is cellulose chains assembly with interchain hydrogen-bonding networks to form van der Waals-bonded, densely-stack sheets. Cellulose I can be converted to Cellulose II through either mercerization (alkali treatment) or regeneration (solubilization-recrystallization). By treating Cellulose I and II with liquid ammonia, Celluloses III (either III_I or III_{II}, depending on the cellulose source) and IV can be further obtained, respectively. Cellulose III can also be transformed to cellulose IV (either IVI or IV_{II}) using thermal treatment (Hayashi et al. 1975; Nishiyama et al. 2003; Nishiyama, Langan, and Chanzy 2002; Isogai et al. 1989; Z. Wu et al. 2018; Kulshreshtha 1979). **Fig. 2.8(c)** and **Fig. 2.8(d)** demonstrated the comparison between four different crystalline allomorphs of cellulose as well as how to identify each type by analyzing their characteristic peaks and patterns in the resulting XRD spectra.

2.6.3. Morphology, surface roughness, and transparency

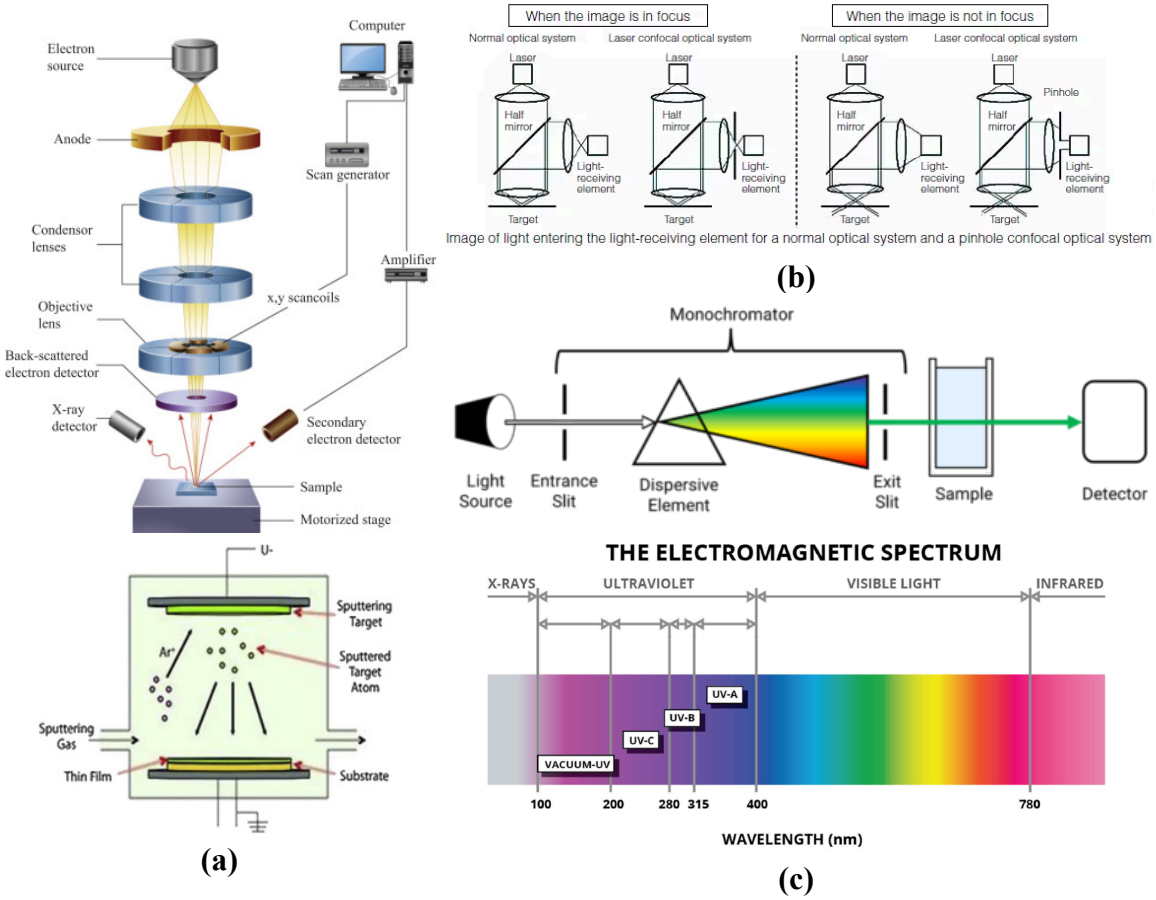

Fig. 2.9. Schematic general principles: **(a)** SEM and ion sputter coater (Inkson 2016; Kafle 2020); **(b)** roughness (Keyence 2021), and **(c)** UV-vis spectroscopy and ranges of different electromagnetic spectrums (Houck and Siegel 2015; Forte 2014)

Morphology, topography (surface roughness), and optical behavior (including optical transparency) are among the crucial characterizations whose impacts often correlate when analyzing a material's functional properties and applicability. Morphology describes the structural conformation and molecular arrangement, extending from the nanoscale (nanoparticles and crystalline lamella) to the microscale (homogeneity and domains) to the macroscale (surface and mechanical properties). The defining factors include molecular weight, crystallinity, branching, and crosslinking. Morphological findings are of great importance to the product's final properties, such as mechanical, chemical, electrical, thermal, adhesiveness, and wettability (Khalifeh 2020; Popelka, Zavahir, and Habib 2020; Araki, Shibayama, and Tran-Cong 1998; Gnanasekaran et al. 2016) Morphological analysis can be conducted either directly or indirectly. The material's surface and internal structures can be directly observed by employing a variety of microscopic techniques depending on measurable sizes, attainable resolutions, and magnifications, which can be combined when necessary (Maxfield 1994). Electron microscopes are among the most popular advanced imaging tools, even compared to the most common choice—light microscopes. Despite its low cost and non-destructiveness,

the light microscope has limited imaging resolution at visible light radiation wavelength (400–700 nm), where radiation with shorter wavelengths would be more susceptible to interact with nanomaterials, producing higher resolution (J. C. H. Spence 2013). Factors that can affect wavelengths include voltage and electrons' momentum and acceleration (Vinet and Zhedanov 2011; L. Reimer 2000). The use of electrons is also beneficial after their negative charge, hence the extremely strong interaction with atoms and subsequently produced emission signals (even for specimens sized under 15 nm). Another advantage offered by electron microscopy is the ultra-high magnification ranges. Scanning Electron Microscopy (SEM) is one of two generic types of electron microscopes, which is primarily designed for material surface testing, unlike Transmission Electron Microscopy (TEM), which is preferable when observing the internal structure (Inkson 2016; Popelka, Zavahir, and Habib 2020). As demonstrated in **Fig. 2.9(a)**, SEM scans a few micrometers of the surface where the produced images are based on the reflected electron beams that are ejected out of a probe. Since the electron beam charging leads to high-voltage burning, specimens must be non-conductive; therefore, low accelerating voltage (1–4 kV) is required at times (Egerton 2005; J. I. Goldstein et al. 2003). In addition, during specimen preparation, ion sputter coating with an electrically conductive material (e.g., gold, platinum, carbon, palladium, or combination) is also among the common solutions, usually by utilizing argon as the sputtering gas of choice due to its high atomic weight (meaning higher kinetic energy), inert chemistry, and non-destructiveness, unlike oxygen/air that possess risks of surface oxidation (Kleiner, Matthes, and Rößler 2021; Hatano et al. 2022; West and Kelly 2011). The specimen is kept in a vacuum chamber, with the probe on the top that emits electrons (accelerated based on voltage difference ranging from 0.1–50 keV) focused on a small spot to be scanned sequentially across the surface. Operating vacuum pressure may range from 0.1–10^{-4} Pa, to be maintained low to eliminate electrons-air interaction (J. I. Goldstein et al. 2017; B. Reimer 2006; Popelka, Zavahir, and Habib 2020). Imaging can be conducted on either the surface or (fractured or microtomed) cross-section of the sample (Mohan et al. 2016).

Sometimes referred to as surface morphology in 3D (topography), surface texture and roughness quantify surface irregularities (Mirabal et al. 2023). Roughness property is of a great importance as it affects structural integrity & interaction with environment e.g., wettability, wear behavior, stresses (G. Song, Wang, and Tan 2022; Antonov, Islamova, and Strizhak 2023). Surface roughness can be analyzed by observing 3D microscopic and Z-stack or focus-stack images. The latter is produced by combining multiple images taken at different focal distances to generate a composite image with a greater field depth (e.g., the plane of focus' thickness) than the individual source images (Ray 2002; D. Johnson 2008). In-focus images are accomplished through filtering by referring the reference plane to the films' real surface to reduce height variability. This step would solve the notorious issue of lowered depth-of-field for numerical and high-magnifying apertures (Larson and Banks 2022). As illustrated in **Fig. 2.9(b)**, digital microscopes can be employed to observe topography/roughness, which is sometimes classified as surface morphology in 3D. The instrument is equipped with a camera and wide-range zoom lens connected to the free-angle observation stand where the Z-axis lens can be moved around (followed by the changing focus level), and then the surface irregularities height can be measured. Topographically, the highest points of an object come into focus first, while

the lowest points come into focus last. The height positions of the individual focal planes are simultaneously recorded to generate the final 3D images that can be used to analyze the specimen's surface roughness/waviness. This surface micro-geometry and irregularity characteristic is expressed by the arithmetic mean deviation of the height of a line, also expressed as Ra (Woch et al. 2022). Furthermore, the extension of Ra to a surface, Sa, is the difference in height compared to the surface's arithmetical mean. Simply put, Ra is the average of the surface heights along a measurement trace, while the Sa is the average roughness over a measurement area (Adamčík et al. 2023; Keyence 2021; Mike 2022).

Lastly, transparency or optical polarization functionality is among the optical properties heavily associated with morphology findings when analyzing a material. A matter's color is governed by its light-emitting ability (Owen 1996). A spectrophotometer (**Fig. 2.9(c)**) can be used for this testing by employing an artificial UV light source to determine the percentage transmission/absorbance of UV regions/spectrums (Gadgil 1981), whose wavelength ranges from 100-400 nm and is divided into three (3) bands: UV-A (320–400 nm), UV-B (280–320 nm), and UV-C (200–280 nm) (Parit et al. 2018; WHO 2016; Forte 2014). Furthermore, the instrument can also measure the transmission/absorbance of visible light whose wavelength goes up to 800 nm. Light at a certain wavelength passes through the specimen, then reflects off both opaque and transparent surfaces and is refracted by crystals (Rocha et al. 2018). The instrument is equipped with a mirror as a light source selector and the desired light wavelength to analyze is set by a monochromator through a diffraction grating. Two coupled detectors are used to subtract the resulting light absorption from the tested specimen (Houck and Siegel 2015; Reusch 1999). Speaking of the significant impacts by UV, its radiation exposure under sunlight brings a myriad of risks, such as biological damage, organic compound degradation, discoloration, weathering, and mechanical loss (cracking); thus, UV-protection stability influences material's shelf and service life (Sadeghifar et al. 2017; Parit et al. 2018), solidifying the significance of UV-vis spectrophotometry characterization on many relevant applications, other than solely determining transparency or opacity.

2.6.4. Barrier property

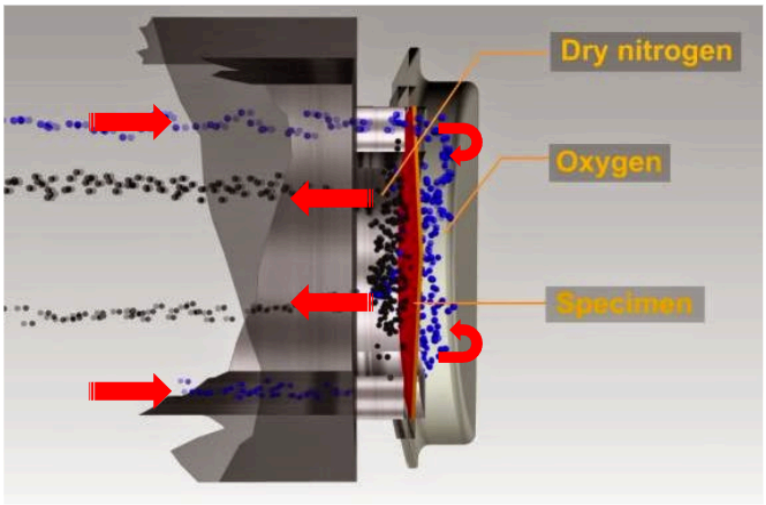

Fig. 2.10. Schematic general principle of oxygen barrier testing (Labthink 2018)

Barrier properties are vital when fabricating materials with sensitiveness of water vapor or humidity, gases (e.g., oxygen), and/or temperature so that degradation can be delayed and shelf life extended. In particular, oxygen permeability dictates how easily oxygen passes through (Ehrmann 2024) and is among the most studied main permeants, one of which is due to its ability to move from/to the internal/external environment (Siracusa 2012; Germain 1997). The molecular diameter of oxygen is 2.98×10^{-8} cm; thus, specimens with pore size larger than that would possess higher permeation. Oxygen has a major role in a myriad of degradation processes, such as lipid oxidation, microorganism growth, enzymatic browning, ethylene production acceleration, and losses in organoleptic qualities such as flavor, color, and nutrients (Brown 1992; S.-I. Hong and Krochta 2006; Ayranci and Tunc 2003; Oms-Oliu, Soliva-Fortuny, and Martín-Belloso 2008; Rojas-Graü et al. 2007; Russo, Simon, and Incarnato 2006). Testing relative humidity and temperature can be set as desired when measuring oxygen permeability. Other influencing factors include cohesive energy density, polarity, crystallinity, and chemical structure, which dictate the material's free volume (Abdul Khalil et al. 2019; Miller and Krochta 1997; Koontz 2016). **Fig. 2.10.** demonstrated the schematic principle of one of the oxygen permeability testing instruments (Labthink 2018). The machine employs a dual-chamber system where one flows oxygen or air (as desired) while purged nitrogen is in the other chamber, which creates a concentration difference that allows the gases to flow between chambers. In it, a pre-conditioned sample film is mounted at ambient atmospheric pressure. A coulometric sensor scans the generated electrical signals after oxygen permeates through the sample film before flowing into the inner chamber full of dry nitrogen, which plays the role of the gas carrier for the permeated oxygen.

2.6.5. Mechanical properties

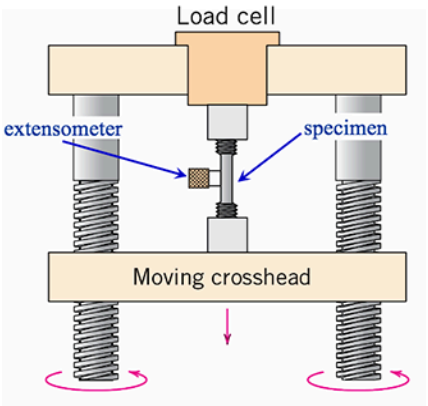

Fig. 2.11. Schematic general principle of stress-strain test (Callister and Rethwisch 2019)

Mechanical properties depict how a material behaves with the principal phenomena under the applied force of a load, making them of great significance. Deformation, disintegration, fractures, shape/dimension change, or any other subsequent macroscopic responses are heavily influenced by the material's structure. The resistance depends on both the material's interatomic forces and the subjected external forces. The most important terms in regard to material characterizations are "stress" (the acting force per unit area) and "strain" (the displacement per unit distance) (Pelleg 2012). The

stress-strain relationship is determined by applying tension or compression in the form of a steadily increasing axial force to the sample. As illustrated in **Fig. 2.11**, as the load is increased, the deflection occurs, which is dependent on the material's elastic modulus and geometry (area and length), where, at last, the load-deflection curve is plotted. The effect of geometry can be removed by converting the values, i.e., from load to stress and/or from deflection to strain (Budynas and Nisbett 2006; Dowling 2007; Gere 2003; Hibbeler 2016; Lindeburg 2013).

Many principal mechanical behaviors can be explained by stress-strain findings such as tensile strength (or ultimate strength), elastic modulus (or modulus of elasticity; or Young's modulus; or tensile modulus), and elongation-at-break (or fracture strain or ductility). The tensile test is standardized based on the American Society for Testing and Materials (ASTM), specifically ASTM D638 (ASTM 2022), which corresponds to the material's strength and stiffness. Sample films' prior conditioning at a controlled temperature and humidity for 40 hours aims to decrease inconsistency. A tensile load is applied to the sample mounted between two crossheads and stopped once it breaks (Jain, Pandey, and Rao 2009; Koo et al. 2017). From the generated stress-strain curve, the tensile strength value can be obtained, which points to the maximum stress value. Post-ultimate stress, 'necking'—significant decrement of the cross-sectional area in a localized region—occurs in the case of ductile/stretchy samples. Tensile strength is important for its ability to determine the maximum stresses one can withstand before falling. Furthermore, the elastic modulus is the next behavior that can be determined from the stress-strain graph. Below the curve's proportionality limit portion, there is a linear stress-strain relationship whose slope locates the elastic modulus value (hence, the "constant of proportionality" term), which is overall expressed by Hooke's law. Elastic modulus depicts the material's relative stiffness or rigidity, whose formula is the ratio of stress to strain. The stiffer one material, the higher its elastic modulus, and vice versa for flexible materials (Vaidya and Pathak 2019; V. C. Pinto et al. 2015). Elastic modulus' importance is after its definition of how much material would deflect, hence displacement of structure, under an applied load (Pavlík, Pavlíková, and Záleská 2019; Jurowski and Grzeszczyk 2015). In the case of composite-based specimens, composition, matrix-filler interface, and characteristics of the incorporated filler (e.g., shape, concentration, diameter, content, dispersion) play a vital role (Wazzan, Al-Turaif, and Abdelkader 2006). The other point of interest is elongation at break, which is calculated by the ratio between length difference (post-breakage) and original length. This percentage is an important characteristic as it expresses the material's resistance to shape changes without crack formation (Djafari Petroudy 2017). A material can be classified as ductile when it possesses the capability to withstand large strains even after it has begun to yield (Budynas and Nisbett 2006; Dowling 2007; Gere 2003; Hibbeler 2016; Lindeburg 2013). The relationships between these mechanical behaviors are described through these equations below:

$$\sigma = \frac{P}{A_0} \quad ; \quad \varepsilon = \frac{L - L_0}{L_0} = \frac{\delta}{L_0} \quad ; \quad \sigma = E\,\varepsilon$$

where σ is stress; ε is strain; P is load; A_0 is the sample's initial cross-sectional area; L is the sample's current length; L_0 is the sample's initial length; E is elastic modulus.

2.6.6. Thermal properties

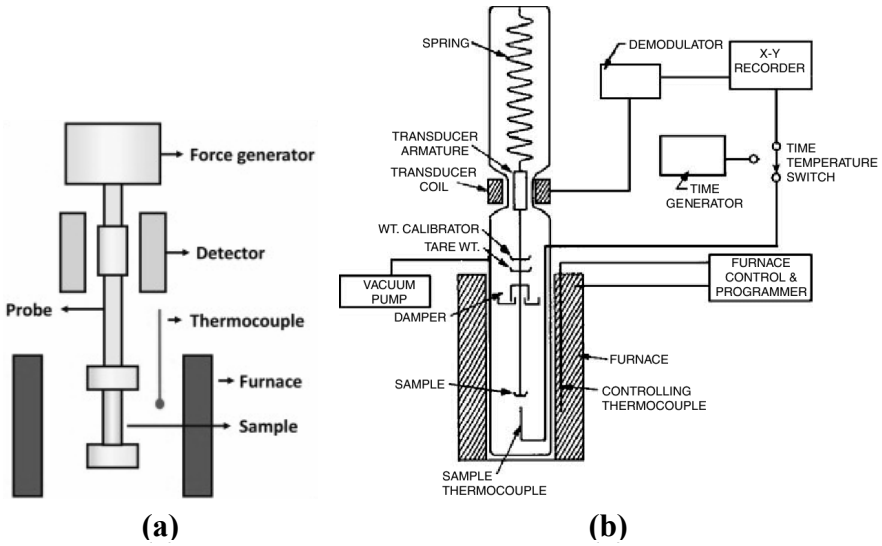

Fig. 2.12. Schematic general principles: **(a)** DMA (Tripathy, Padhiari, and Hota 2023) and **(b)** TGA (Rowell and LeVan-Green 2005)

Thermal analysis investigates a material's physical property as a function of an externally applied and programmed temperature at a predetermined rate (Ewing 1997). Phenomena that can be observed include endothermic (i.e., melting, boiling, sublimation, vaporization, desolvation, solid-solid phase transitions, and chemical degradation) and exothermic processes (i.e., crystallization and oxidative decomposition) (Brittain 2011). Mechanical behavioral responses (stress/strain) of a material over changing temperature can be determined by dynamic mechanical analysis (DMA). As seen in its schematic (**Fig. 2.12(a)**), the instrumental probe subjects a sinusoidal force to the sample clamped in the measuring head so the force-deformation relationship can be studied afterward. Viscoelastic variables (e.g., storage modulus or elastic modulus; loss modulus or imaginary modulus; and loss tangent or loss factor or damping factor) can be obtained (Roodbar Shojaei et al. 2019; Tripathy, Padhiari, and Hota 2023). In analyzing these properties, two common reference temperatures to highlight the transition of interest are: 1) room temperature (~25°C) to 32°C; and 2) boiling points at ≥ 100°C (Kwan 1998). Associated with strength, stiffness, and rigidity, the storage/elastic modulus typically decreases as temperature increases, back rises at some point before reaching a maximum value due to the altered network structure post-curing, and decreases again post-glass transition temperature, indicating thermal degradation and devitrification (Candan, Gardner, and Shaler 2016; Sanyang et al. 2016). Meanwhile, the loss/imaginary modulus property represents the material's viscous response and is usually related to internal friction. The value is obtained as the energy loss under stress/deformation (Jawaid et al. 2015; Saba et al. 2017). Lastly, the loss tangent or loss/damping factor, being the E" to E' ratio, depicts molecular movement. When exposed to varying temperatures and the sample distortion occurs, the measured recoverable strain energy indicates internal energy dissipation. The higher the temperature, the higher the damping; it is maximized in the transition region and decreases in the rubbery region. The higher the peak intensity, the higher the molecular

mobility degree and the faster the energy dissipation process, suggesting better dispersion and the eventual polymer movement/rotation inhibition. In contrast, aggregation/agglomeration allows more vacant space for the polymer chain movement/rotation, hence the visco-elastic damping factor increment (W. Chen et al. 2018; Saba et al. 2017; Sanyang et al. 2016).

Another simple and popular thermoanalytical technique is thermogravimetric analysis (TGA), as seen in **Fig. 2.12(b)**. A small amount of sample on a metal pan is positioned inside a furnace which is heated at a desired rate, with nitrogen and oxygen as the employed gases. Afterward, the thermally induced weight loss as a function of temperature is plotted (Rowell and LeVan-Green 2005; Duval 1963; Keattch and Dollimore 1975). TGA is useful for studying the material's total volatile content, desolvation, decomposition (or other composition change), and, ultimately, thermal stability—crucial as kinetic parameters when designing the product's processability and applicability (Brittain 2011; Tripathy, Padhiari, and Hota 2023). It is likewise important when analyzing degradability (Brunšek et al. 2023).

2.6.7. Contact angle or wettability

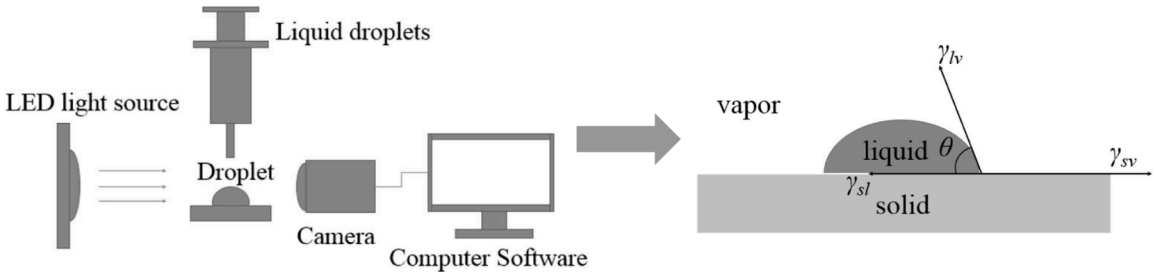

Fig. 2.13. Schematic general principle of optical tensiometer (J. Zhang et al. 2023)

Surface wettability/hydrophilicity (or hydrophobicity), also known as contact angle property, corresponds to a material solid surface behavior and intermolecular interactions, heavily linked to surface/adhesion energy, wetting/non-wetting, and absorption abilities, making it an essential criterion. Wetting is simply described as the possibility of a liquid to flow or, in contrast, form droplets when subjected to a solid's surface (L. Feng et al. 2014; Good 1992; Deville and Cojocaru 2006). As illustrated in **Fig. 2.13**, an optical topography instrument in the form of a drop-shape analyzer, also called a tensiometer, is employed. A dropper containing the testing liquid suspension is set; meanwhile, a camera and LED light source are adjusted to illuminate and record the droplet's contact with the solid surface of the tested specimen. At a point on the solid-liquid-vapor three-phase contact line and phase interface, a tangent (γ) vapor-liquid contact line is created whose the formed angles of γ_{lv}, $\gamma_{sl,}$ and γ_{sv} represent the surface tension/energy between liquid-vapor, solid-liquid and solid-vapor, respectively. Interfacial tensions between these phases govern the aforesaid three (3) angles and can be calculated by the Young–Laplace equation (de Laplace 1805; Young 1805) to determine the sample's contact angle. Hydrophilic material is categorized for contact angle lower than 90^{o}; and hydrophobic for one higher than 90^{o} (M. Q. Khan et al. 2019; Tripathy, Padhiari, and Hota 2023; J. Zhang et al. 2023; Río and Neumann 1997). This technique is named among the easiest and cheapest for regular evaluation on material surfaces (Selva, Selva, and Prata 2023; Cobb,

Ayres, and Macpherson 2018; Macpherson 2015; B. Yang et al. 2019; Deville and Cojocaru 2006).

2.6.8. Antibacterial activity

Food safety becomes an issue once pathogenic microorganisms contaminate. Named among the main foodborne pathogens that cause recurrent annual outbreaks (Koutsoumanis et al. 2020; FDA 2022, 2019a), *Escherichia coli* (*E. coli*) is a common aerobic Gram-negative bacilli in a normal intestinal tract and regarded as a fecal pollution indicator. Despite being an important member of mammals' normal intestinal microflora, the species contains pathotypes/toxins that may cause an array of health issues, both intestinal and extraintestinal, e.g., diarrhea/dysentery, vomiting, (intra)abdominal infections, septicemia, hemolytic uremic syndrome, urinary tract infections, meningitis, necrosis, end-stage renal disease, hemorrhagic colitis, atherosclerosis, and immunological diseases (reactive and rheumatoid arthritis). This may also include one of the most notorious of all, Shiga intoxication symptoms, which can range from mere discomfort to death. There are a variety of strains depending on virulence factors, from commensal to lethal (Majowicz et al. 2014; S.-C. Yang et al. 2017; Obrig 2010; J. B. Kaper 2005; Munekata et al. 2020; Murray, Rosenthal, and Pfaller 2009; Yen et al. 2011; Olsvik et al. 1991; James B. Kaper, Nataro, and Mobley 2004).

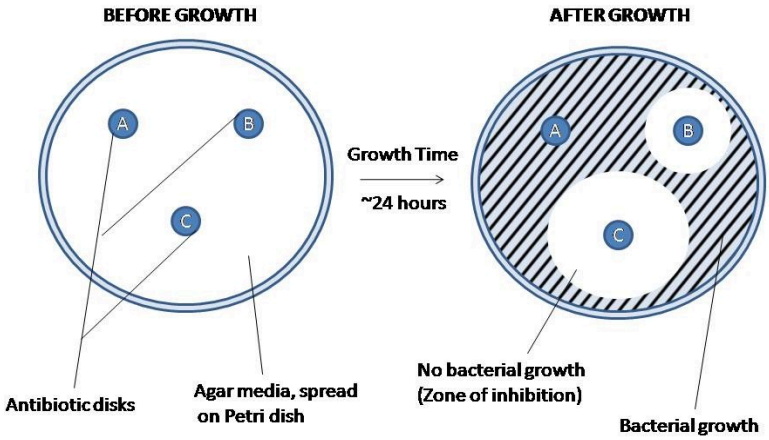

Fig. 2.14. Schematic antimicrobial susceptibility testing: disc diffusion (EUCAST 2021)

Among the several antimicrobial susceptibility tests in line with the Clinical and Laboratory Standards Institute guidelines (CLSI 2024), the agar disc-diffusion approach is very popular. Developed in the 1940s (Heatley 1944), it permits the testing of a myriad of critical bacterial pathogens. It is excellent because of its straightforwardness and cost-effectiveness (Fourati-Ben Fguira et al. 2005; Das, Tiwari, and Shrivastava 2010; Konaté et al. 2012). As seen in **Fig. 2.14**, standardized inoculum of the microorganism of choice is prepared to innoculate on an agar plate before placing on it a disc at a certain diameter made of the antimicrobial agent-incorporated specimen. The contained petri dishes are then incubated under the proper conditions to allow the said microorganism to grow. The growth inhibition zone surrounding the disc can be observed afterward, which indicates the inhibition efficacy of the antimicrobial agent (Hossain et al. 2022).

CHAPTER 3

Impacts of cycles of a novel homogenization process on nanocellulose and its film properties

ABSTRACT

The abundant and naturally biodegradable cellulose nanofibrils (CNF) have been among the most researched materials for their myriad advantages, yet are still facing challenges toward advanced developments due to their natural hydrophilicity affecting a broad range of properties. A simple, cheap, and plasticizer-free novel homogenization approach ('emulsifying cells'–equipped, low pressure at <10 MPa, for 0-25 cycles) was proposed, and its effects on the Northern bleached softwood based-CNF films' properties were investigated. XRD results showed a maintained high crystallinity (CI=64%). Promoted fibrillation and hydrogen bonding were also observed morphologically through surface SEM images, aligned with the 44% smoother surface of homogenized CNF films (Sa=2.637µm) compared to the untreated CNF films. The resulting 48% decrease in oxygen permeability (0.250 cc.µm/m^2.day.kPa at 50%RH) is comparable to ethylene-vinyl alcohol (EVOH) and other oxygen barrier plastics. Significant improvements in mechanical (tensile strength, tensile/Young's modulus, and elongation-at-break) and thermal (storage/elastic modulus, loss/imaginary modulus, loss/damping factor, and degradation temperature) properties were confirmed. Hydrophobicity improvement (0-60 seconds) was also obtained. With varying optimum cycles of homogenization, this work demonstrates the prospect of a straightforward, cheap, and environmentally friendly homogenization approach in preparing CNF with enhanced processability and applicability.

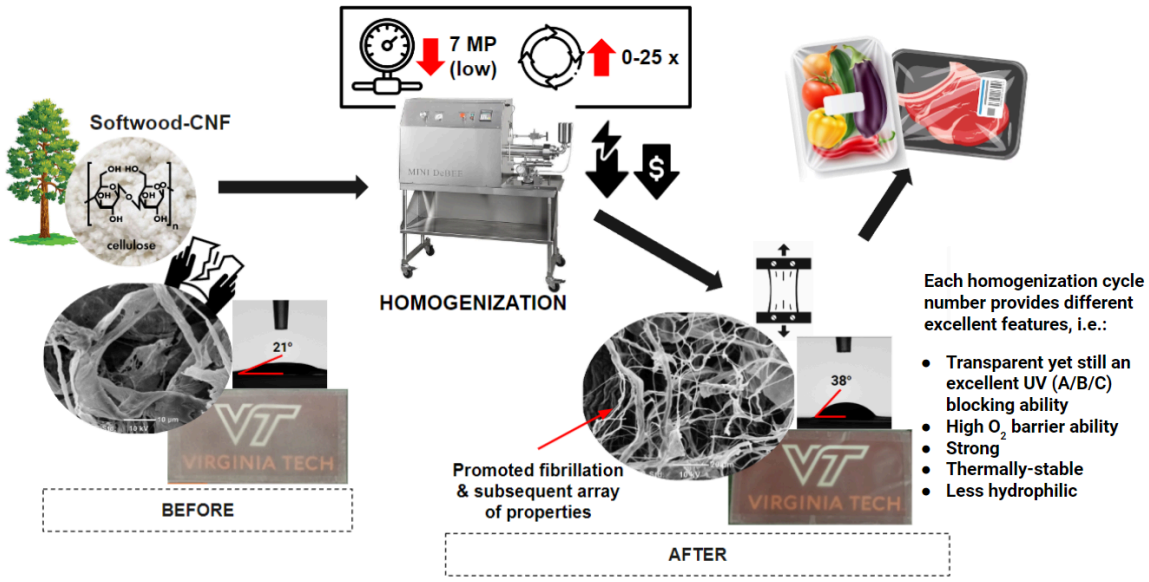

Graphical abstract

3.1. Introduction

Americans waste 40% of their food, costing 1.3% of GDP (FAO 2021b, 2013b; EPA 2016b). Food spoilage is mainly triggered by microorganisms, water content, oxygen, humidity, temperature, and light (Magoulas 2016), creating waste. Together, food and its packaging comprise roughly 45% of the solid wastes landfilled in the USA (EPA 2015b). To produce such food waste, one-third of the global agricultural land is used annually, releasing large amounts of greenhouse gas. Around 98% of single-use plastic products (including food packaging) are made of non-sustainable and/or non-biodegradable fossil fuel or "virgin" feedstock (D. Charles and Kimman 2023); thus, 80% have entered landfills and nature (Geyer, Jambeck, and Law 2017). Composting merely covers 6% due to limitations in infrastructure, upfront/expensive labor, material supply assurance, and contamination (ReFED 2018; NRDC 2020). Only 12% and 9% are incinerated and recycled, respectively, as they suffer from losses, degradation, reduced mechanical performance, high cost, complexity, released toxic chemicals, micro-/nano-plastics, volatile organic compounds, and carbon oxides. The remaining in landfills and oceans results in uncontrolled degradation and methane contaminating soil/water, especially when left indefinitely under anaerobic conditions (UNEP 2022; Geyer, Jambeck, and Law 2017; Birkett et al. 2017; Byun et al. 2015). Due to the urbanization-derived global dietary change and rising reliance on processed foods (World Packaging Organisation 2008), food packaging remains in high demand.

In response to these lingering constraints of food and food packaging waste, “prevention” (e.g., spoilage-prevention packaging) is largely encouraged over “recovery” and “recycling” actions (FAO 2022a; EPA 2016b; European Commission 2023); thus, studies of food primary packaging are continually advancing in shelf life extension through moisture and oxygen-barrier properties improvement, aiming for lower food spoilage rates (Verghese et al. 2015; Almenar 2023). Likewise, research on packaging materials with biodegradation characteristics in various environmental conditions has also been prioritized to help tackle the lingering issue of accumulating packaging waste. The Earth’s most abundant naturally biodegradable polymer is cellulose (Klemm et al. 1998). It comprises several linear β-(1,4)-d-glucose chains, forming (micro)fibril structures whose individual chains are joined by a network of inter-/intramolecular hydrogen bonding and van der Waals forces (Xiaowen Liu et al. 2023). Cellulose can be converted into two (2) ‘top-down’ nanosized products that excel in ability to form more extensive network structures due to their nanoscale dimensions (H. Lee, Sundaram, and Mani 2017): the rigid rod-like cellulose nanocrystals/CNC (chemically, e.g., acid hydrolysis, oxidation, and cationization; removing amorphous region, leaving purely-crystallines) and the flexible cellulose nanofibrils/CNF (mechanically, e.g., micro-fluidization, homogenization, grinding process, sonication; preserving both amorphous and crystalline structure) (Dias et al. 2020; Ibrahim et al. 2019; Sofla et al. 2016). Sometimes referred to as cellulose nanofibers or nanofibrillated cellulose, CNF is among the most researched materials due to its high specific surface area, crystallinity, surface activity, oxygen barrier ability, and an even better aspect ratio than CNC, while having low porosity and density (B. Yang et al. 2019). In the past decades, many have researched the growing potential of CNF in improving barrier properties in packaging applications (Roilo et al. 2018; Fukuzumi et al. 2013, 2009; Aulin, Gällstedt, and

Lindström 2010) as well as its biodegradability in diverse environments (Arun et al. 2022; Niu et al. 2021; Jinchuan Xu et al. 2021; Babaee et al. 2015). However, neat CNF film still possesses some challenges that hinder its further processability and applicability, including in the packaging field, especially if compared to conventional polymers. CNF is insoluble and non-redispersible in water and most organic solvents due to strong hydrogen bonding between the nanofibrils (Nechyporchuk, Belgacem, and Bras 2016). CNF is also hydrophilic/hygroscopic by nature, and moisture absorption weakens its interfibrillar hydrogen bonding and causes swelling, resulting in loss of strength, durability, oxygen barrier ability, and thermal stability (Xia et al. 2018; B. Yang et al. 2019).

Homogenization is among the most popular treatments for cellulose-based materials as it does not require high temperatures and organic solvents or chemicals other than simply water, highlighting its simplicity and environmental friendliness (L. Wang et al. 2021). Cellulose-based aqueous suspension is pumped through a spring-loaded valve assembly that opens and closes repetitively, allowing the suspension to be subjected to certain pressure drops, inducing high shear, cavitation, and impact forces in the narrow slit of the valve. It promotes fibrillation that eventually improves hydrogen bonding and 3-dimension network strength (Nagarajan et al. 2021; H. Lee, Sundaram, and Mani 2017; Chun et al. 2011). The structural stability would be improved since the optimized homogenization affects rheology, particle size, surface area contact, and distribution/dispersity, both before and after the film drying stage, especially for polysaccharides like CNF (Flores et al. 2021; Usenko et al. 2013; Wenjian Cheng et al. 2010). Homogenization is categorized based on the conditioning pressure range, i.e., ultra-high (>250 MPa), high (50-250 MPa), and low (<50 MPa) (Aguayo et al. 2017). However, the most notorious drawback of conventional homogenization is the high pressure that leads to high energy consumption and cost (Nagarajan et al. 2021; H. Lee, Sundaram, and Mani 2017). High-pressure homogenization also has a negative linear effect on CNF crystallinity due to surface crystallites peeling off under high shear and impact forces (Davoudpour et al. 2015). Therefore, homogenization under lower pressures (<50 MPa) is prospective for a significantly less costly homogenization (Boulemkahel et al. 2021), including for CNF processing, which has yet to be studied to date. In the case of a solely homogenization strategy in cellulose-based material treatment, multiple passes or cycles are usually required to obtain a well-controlled manner (Nakagaito and Yano 2004). The number of cycles determines the final homogenates' degree of fibrillation and subsequent properties (Davoudpour et al. 2015; Kalia et al. 2014). Some studies even emphasized the importance of the number of passes over other homogenization operating conditions, like pressure (Fu et al. 2011; Yu et al. 2021). Another common challenge in the homogenization technique is the clogging issue (Nagarajan et al. 2021; H. Lee, Sundaram, and Mani 2017) therefore, this work also explored the utilization of a homogenizer equipped with the novel, patented modular 'emulsifying cells' that allows easier control of pressure, impact, shear, cavitation force, flow mechanisms, and process duration to prevent clogging, agglomeration/aggregation, and destruction in the resultant CNF films due to overheating, over-shearing, and/or over-pressure (BEE International 2015). Such design has been evidenced to be fruitful in an array of materials, including CNF-based products where the effect of varying cycles/passes and/or pressures were investigated, e.g., TEMPO-based CNF/8 passes/151

MPa (V. C. F. Li et al. 2018), CNF aggregates/5 passes/69-207 MPa (Q. Cheng and Via 2017), CNF-polyamide/10-30 passes/70-310 MPa (J.-C. Lee et al. 2018), TEMPO-based CNF/3 passes/160 MPa (Du et al., 2016), and CNF-PLA/4-20 passes/110-290 MPa (T. Wang and Drzal 2012). However, to date, the utilization of the aforesaid 'emulsifying cell' based homogenization system at low pressure on neat-CNF preparation has yet to be found.

Softwood-based CNF, specifically one derived from northern bleached softwood kraft pulp, was selected for this study. Besides being the first raw material used in CNF manufacturing (Turbak, Snyder, and Sandberg 1983; Herrick et al. 1983) and today's most popular (H. Lee, Sundaram, and Mani 2017), softwood-based CNF was more flexible and responsive to be fibrillated than hardwood, whose spirally-layered outer secondary wall reduces flexibility and accessibility to the inner secondary wall (Stelte and Sanadi 2009). Softwood is also easier to modify chemically due to glucomannan being the dominant component of its hemicellulose, which contains C6 primary hydroxyls easily convertible into other functional groups. In contrast, the hemicellulose of hardwood is mainly xylan, which does not have C6 primary hydroxyl groups (Fukuzumi et al. 2009; Sjostrom 2013). In addition, films produced using softwood-based CNF also possessed a higher light transmittance (Fukuzumi et al. 2009).

Accordingly, plasticizer addition to a film-forming solution for biopolymers is usually essential to increase film flexibility, although it may also lead to poor mechanical properties and low thermal stability. Plasticizer was not used in this study because of numerous concerns, such as aging, leaching, migration, volatility, extraction, exudation, evaporation, segregation phenomenon (phase separation), and anti-plasticization effects (Eslami et al. 2023; Paixão et al. 2019; Sothornvit and Krochta 2005). Plasticizer addition may also negatively affect the film's permeability. Hydrophilic plasticizers affect water vapor permeability; hydrophobic plasticizers affect oxygen, aroma, and oil permeability (Daniels 1989). Even without any plasticizer, drying the colloidal aqueous CNF dispersions produces the typical CNF non-porous film, with random-in-plane orientation and slightly swirled conformation of nanofibrils (Henriksson et al. 2008). In this instance, capillary forces arise from the water, seeking to minimize the liquid/air interface. This force is the main adhesion mechanism through liquid bridges (Z. Zhou, Li, and Zhao 2006). Since the crystalline region of the cellulose surface is strongly hydrophilic, this capillary force can be strong enough to plastically deform the nanofibrils (Ogawa, Nishiyama, and Mazeau 2020). In addition, the plastic yielding (yield strength) in CNF films is related to interfibril shearing in the interphase region (C. Zhang et al. 2021; Sinko and Keten 2014), showing the significance of abundant H-bonding sites on the nanofibril surfaces. As the water between the fibers evaporates, the capillary pressure increases, pulling the fibers together, whereas when still wet, the delignified fiber wall is highly hydrated, and the water acts as a strong plasticizer (Wohlert et al. 2022).

Ultimately, the development of plasticizer-free softwood-based CNF film treated with a novel, milder-conditioned homogenization in varying cycles was conducted. This study aimed to determine the influence of homogenization in the aforesaid operating conditions on the functional properties of the resulting CNF. The effect of different numbers of homogenization passes was hypothesized to properly promote the fibrillation of CNF that governs the final product's properties, including, but not limited to, physical, mechanical, morphological, and thermal stability.

3.2. Materials and Method

3.2.1. Materials

CNF slurry with 3% solids derived from northern bleached softwood kraft pulp was obtained from the Process Development Center of the University of Maine (Orono, ME, USA). HPLC-grade water was purchased from EMD Millipore (Burlington, MA, USA).

3.2.2. Homogenization process

CNF slurry (3% solids) was diluted with water (1:3) by mixing under constant stirring (30 mins) to produce neat-CNF solution. The solution was further treated with a Mini DeBEE 30 homogenizer (BEE International, South Easton, MA, USA) with a 0.20 mm (0.008 inch) nozzle at 7 MPa, repeated for a different number of cycles (0, 5, 10, 15, 20, 25; labeled as N-0, N-5, N-10, N-15, N-20, N-25, respectively). Homogenization cycles were maintained under 30 passes according to the preliminary studies, as well as referring to optimized results of previous studies on homogenized cellulose prepared at a medium/low conditioning pressure range (Chun et al. 2011; V. C. F. Li et al. 2018; Q. Cheng and Via 2017; Du et al. 2016; J.-C. Lee et al. 2018; T. Wang and Drzal 2012). On top of the internal cooling system, the homogenizer was equipped with an Isotemp Refrigerated Circulating Bath 910 chiller (Fisher Scientific, Waltham, MA, USA).

3.2.3. Film production

The homogenized CNF solution (30 mL) was poured into a 9 cm x 1.5 cm petri dish using a solvent casting technique and left to dry in the Forma Environmental Chamber (Thermo Scientific, Waltham, MA, USA) (50 %RH, 23 °C, 48 hours). The same preconditioning parameters were completed prior to each test of the films. The schematic is presented in **Fig. S.1**.

3.2.4. Characterizations

3.2.4.1. Fourier transform infrared (FTIR) analysis

FTIR spectra indicating functional groups were determined by the the Nicolet 8700 spectroscopy equipped with Attenuated Total Reflectance (ATR) (Thermo Scientific, Waltham, MA, USA) at a wave number range of 400–4000 cm^{-1} and a total of 32 scans. The results were reported as an average of three (3) replicates.

3.2.4.2. Crystallinity

X-ray diffraction (XRD) pattern and relative crystallinity were investigated by the D8 (Bruker Corporation, Billerica, MA, USA) equipped with twin/twin optics and a cooler (15-20 ºC). Using the diffrac.commander software, the "Motorized Slit: Slitwidth" setting was applied for both primary (0.6 mm) and secondary (5 mm) twins. The sample was irradiated in the range of 2θ = 5–35° with total scans of 1181 steps and 0.025º increment for 0.5 s. The generator was set with 40 kV energy, 40 mA current, and Cu Kα irradiation (λ = 1.54056 Å = 0.154 nm). The resulting data in *.brml* format were processed using PowDLL (Kourkoumelis 2013) and Profex (Doebelin and Kleeberg 2015) software. The crystallinity index (CI) was evaluated using the "height XRD" method or Segal's empirical equation (Segal et al. 1959), which is deemed the easiest and most

time-efficient, thus being the most popular (S. Park et al. 2010). It measures the ratio of the intensity between the crystalline and amorphous peaks, which are located around 2θ = 23° and 2θ = 18°, respectively. The crystalline peak can also be called the major peak or I_{total}. Meanwhile, the amorphous peak is also known as the minima between the major (indices (200) at 2θ = 22.5°) and secondary peaks (indices (10$\bar{1}$) at 2θ = 14.7°–16.1°), or I_{am}. Ultimately, I_{total} measures the maximum intensity of the crystalline peak, while I_{am} is the minimum intensity of the amorphous peak or the maximum point where the entirely amorphous cellulose would be (Segal et al. 1959; Nurhadi et al. 2022). The results were reported as an average of three (3) replicates.

$$CI = (1 - \frac{I_{am}}{I_{total}}) \, x \, 100\%$$

3.2.4.3. Morphology, surface roughness, and transparency

Surface morphology was characterized by the NeoScope JCM 5000 Scanning Electron Microscope (SEM) (JEOL Ltd., Tokyo, Japan). For surface SEM observation, the sample (25 mL) was initially prepared by lyophilization or freeze-drying (Millrock Technology, Kingston, NY, USA) after being kept in a -80 °C Forma 88000 ultra-low freezer (Thermo Scientific, Waltham, MA, USA). It was then mounted onto a pin stub mount using copper tape before being coated with roughly 100 Å of gold in an ion sputter coater (Denton Vacuum, Moorestown, NJ USA) using argon gas (10-15 psi) at pressure and current of 50 mTorr and 45 milliamps, respectively, for 45 seconds. Specimens were subsequently imaged at different magnifications under a vacuum at an operating voltage of 10 kV. Furthermore, the surface roughness of films was investigated using the Keyence VK-X3000 3D surface profilometer (Keyence Corporation, Osaka, Japan) referring to ISO 25178. Three-dimensional images of the film surfaces were analyzed with the Keyence VK-X3000 MultiFileAnalyzer (Keyence Corporation, Osaka, Japan) software to perform filtering according to the reference plane to the films' real surface to smooth out height variability before the roughness parameters measurement. Afterward, arithmetical mean height (Sa) or the average absolute height value at each point in the definition area was reported as an average of three (3) replicates. Lastly, to determine transparency, light transmission spectra were analyzed using a Genesys 10S UV-vis spectrometer (Thermo Scientific, Waltham, MA, USA) in the wavelength range of 190–900 nm with 0.5 nm interval, in addition to the visual observation

3.2.4.4. Barrier property

According to ASTM D 3985-95, Oxygen Permeability (OP) was characterized using the C230 Oxygen Transmission Rate Testing System (Labthink International Inc., Medford, MA, USA). The 700-118-20 Quick Mini digital thickness gauge (Mitutoyo, Kawasaki, Japan) was used to measure ten random readings to the nearest 0.001 mm, which were then averaged. The plate was then inserted into the cell chamber. The "Film-ASTM" test type without compensation was selected. To maintain purity, cycle process mode with rezero purging for N_2 gas in the cells was performed for 30 seconds with one cycle interval. The system was preheated for 2 hours. The flow rate, test humidity, and test temperature were adjusted to 100 mL/min, 50%RH, and 23 °C receptively. Six (6) cycles under standard test mode were completed at 30-minute intervals in each cell. The results were reported as an average of six (6) replicates.

3.2.4.5. Mechanical properties

Mechanical properties were measured with Universal Testing Machines (UTM) Material Test Systems 10-GL 27-00112 (MTS Systems Corporation, Eden Prairie, MN, USA). The films' tensile strength (TS), tensile/Young's modulus (E), and elongation-at-break percentage (%EAB) were measured with 0.1 N preload at a test speed of 0.40 mm/s until the films (2 × 8 cm) were ruptured. TS was calculated from the ratio of maximum load to the cross-sectional area of the film. Meanwhile, %EAB was the ratio between the increased length pre-rupture and the film's initial length. Lastly, E was the ratio between stress and strain from the linear portion of the stress-strain curve. The results were reported as an average of twenty (20) replicates.

3.2.4.6. Thermal properties

Thermomechanical properties were measured using the Discovery Q850 Dynamic Mechanical Analyzer (DMA) (TA Instruments, New Castle, DE, USA). The film strip (13 × 7 mm) was loaded using the dual screw film clamp type. The multi-frequency strain was employed at a % oscillatory strain of 0.05%, and a static force of 0.01 N was applied in tension. Using temperature ramp mode (-60–150 °C), conditions were maintained at 5 °C/min. Force track and soak times were adjusted to 125 % and 5 minutes, respectively. The data was then recorded at 1 Hz. E' (elastic/storage modulus), E" (loss/imaginary modulus), and Tan(δ) (loss/damping factor; Tanδ = E"/E') plots were observed. Furthermore, thermal degradation analysis was performed using a Thermogravimetric Analyzer (TGA) 550 (TA Instruments, New Castle, DE, USA). Pan loading-taring was conducted using the auto sampling technique using a platinum (100 μL) pan. An amount of freeze-dried CNF (5-15 mg) was spread in the pan to maximize surface area. It was equilibrated at 50 °C, then ramped from 10 °C/minute to 800 °C. Temperature was recorded when the sample's weight loss reached 5% ($T_{d,5\%}$). Data analysis using the TRIOS or TA Universal Analysis (TA Instruments, New Castle, DE, USA) software was then performed. The results were reported as an average of six (6) replicates.

3.2.4.7. Contact angle or wettability

The water contact angle or wettability was tested by the OneAttension® Theta Flow optical tensiometer (Biolin Scientific, Stockholm, Sweden). Using the "sessile drop" experiment type equipped with a 200 μL pipette tip at 25 μL/min dispenser speed, a drop (5 μL) of HPLC-grade water was deposited onto the film surface to measure the contact angle in varying regions. "Light" and "heavy" phases were set as air and water (20 ^{o}C), approximately, which are selected to determine the density difference value for the surface tension measurement. The drop images and subsequent contact angles were obtained with a total duration of 60 seconds at ten-second intervals and reported as an average of three (3) replicates.

3.2.5. Statistical analysis

Data were analyzed by a one-way variance analysis (ANOVA) followed by Tukey's test and Student's t-test, using the Microsoft Excel 2019 (Microsoft Corporation, Redmond, WA, USA) and/or JMP 16 Pro (SAS Institute, Cary, NC, USA) software to establish significant differences (p-value $\leq$ 0.05). The use of different letters on graphs data denotes statistically significant differences.

3.3. Results and Discussion

3.3.1. Fourier transform infrared (FTIR) analysis

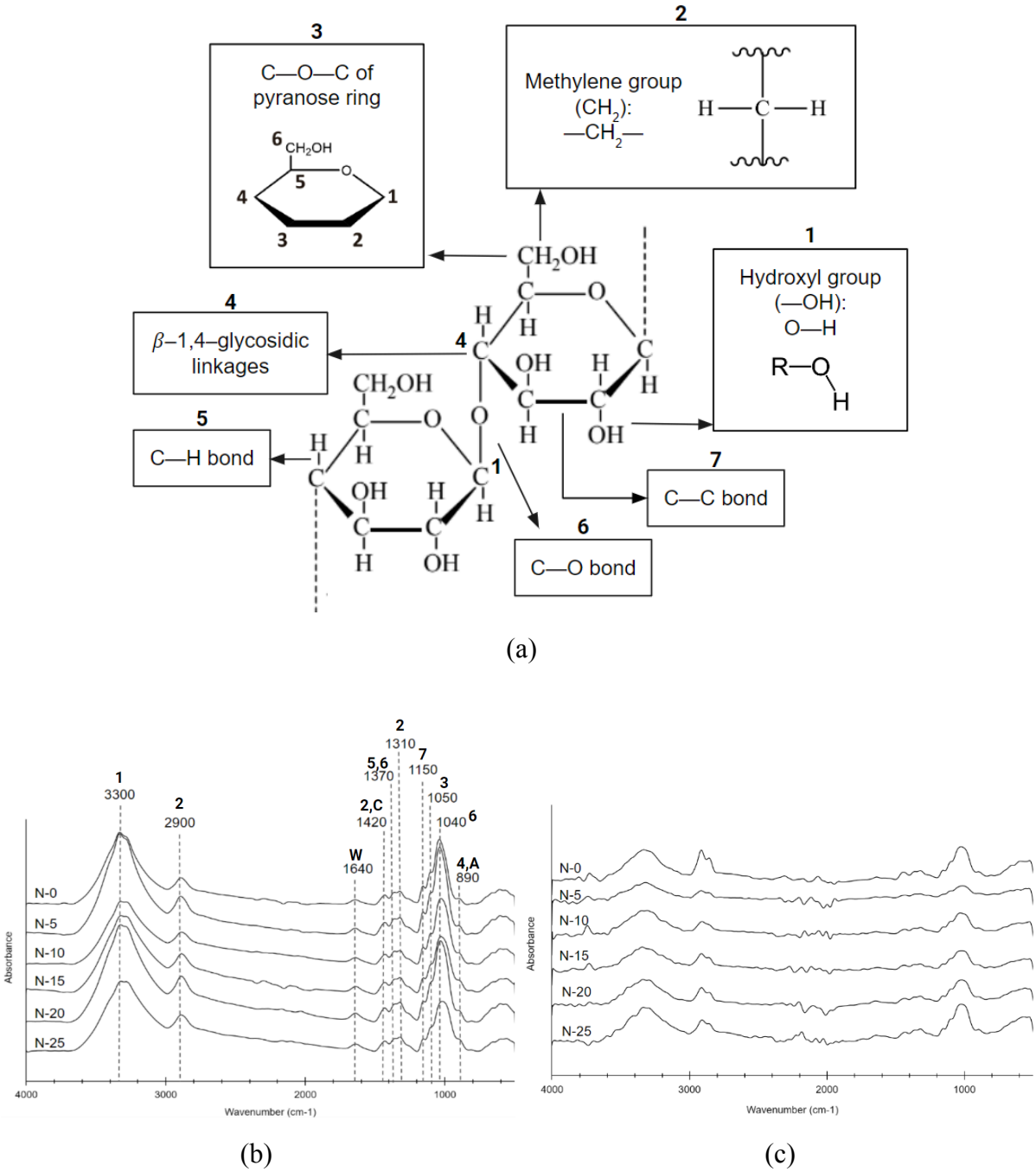

(a) (b) (c)

Fig. 3.1. (a) Chemical structure of cellulose and its major functional groups; (b) FTIR spectra of freeze-dried CNFs and (c) CNF films

Table 3.1. FTIR peaks assignment (functional group and molecular vibration type) of freeze-dried CNFs

Approximate wavenumber (cm^{-1})	Functional group and molecular vibration type
3300–3340	stretching of O—H hydroxyl groups
2900	(anti)symmetric stretching of C—H (of CH_2 or methylene group)
1640	bending of O—H and H–O–H (absorbed of H_2O or water)
1420	scissoring of C—H (of CH_2 or methylene group); cellulose's crystalline region
1370	bending of C—H and C–O bond
1310	wagging of C—H (of CH_2 or methylene group)
1150	stretching of C—C bond
1050	antisymmetric stretching of C—O—C (of pyranose ring)
1040	stretching of C—O bond
890	cellulosic β–1,4–glycosidic linkages; cellulose's amorphous region

Fig. 3.1(a) illustrates the chemical structure and major functional groups of cellulose, whose presence was confirmed and discussed in this section through FTIR analysis. **Fig. 3.1**(b) showcases the resultant FTIR spectra of the freeze-dried CNFs, and **Table 3.1** lists the approximate wavenumber (cm^{-1}) of dominant peaks or spectral bands observed in each spectrum and their assigned functional group (Soni, Hassan, and Mahmoud 2015; Morán et al. 2008). Firstly, the intramolecular and intermolecular hydrogen (—OH) bonds are characterized by the observed O–H stretching vibrations that belong to hydroxyl groups. These bonds were observed in all CNFs, likewise for the methylene (CH_2) groups, C—H, C—C, C—O, and C—O—C bonds. These bonds occurred not only as glycosidic linkages but also within each of the pyranose rings of glucose units. The spectral bands indicating the water ("W") O—H and H—O—H bending were present in all CNFs spectra. This finding indicates the presence of remaining moisture even after the drying process due to the cellulose-water interaction (Morán et al. 2008; Korhonen et al. 2011). FTIR analysis in this study used freeze-dried CNFs (**Fig. 3.1**(b)) instead of CNF films (**Fig. 3.1**(c)). The eliminated water content produced FTIR spectra with more obvious peaks, making it easier to observe the dominant spectral bands. Besides water, other volatile degradation products emitted during the freeze-drying could be hydrocarbons (3100–2600 cm^{-1}), carbon dioxide (2420–2240 cm^{-1}), carbon monoxide (2240–2040 cm^{-1}), carboxyl and carbonyl functional groups: C=O (1800–1600 cm^{-1}) and C–O functional groups (1130–1050 cm^{-1}) (Quiévy et al. 2010)—which are all indeed present in CNF films spectra, but unapparent in freeze-dried CNF's. All spectra discussed were similarly observed in several other studies on homogenization impact on cellulose-based materials (Quiévy et al. 2010; Rahbar Shamskar, Heidari, and Rashidi 2019; D. Huang et al. 2020). Conclusively, no new bonds were formed after homogenization, indicating no chemical composition change, as seen in similar studies (D. Huang et al. 2020; Ilyas et al. 2019). In addition, the resulting FTIR spectra also confirmed that, despite the mechanical treatments, the desired high crystallinity of CNF was successfully maintained, whose more in-depth analysis is discussed in the next section.

3.3.2. Crystallinity

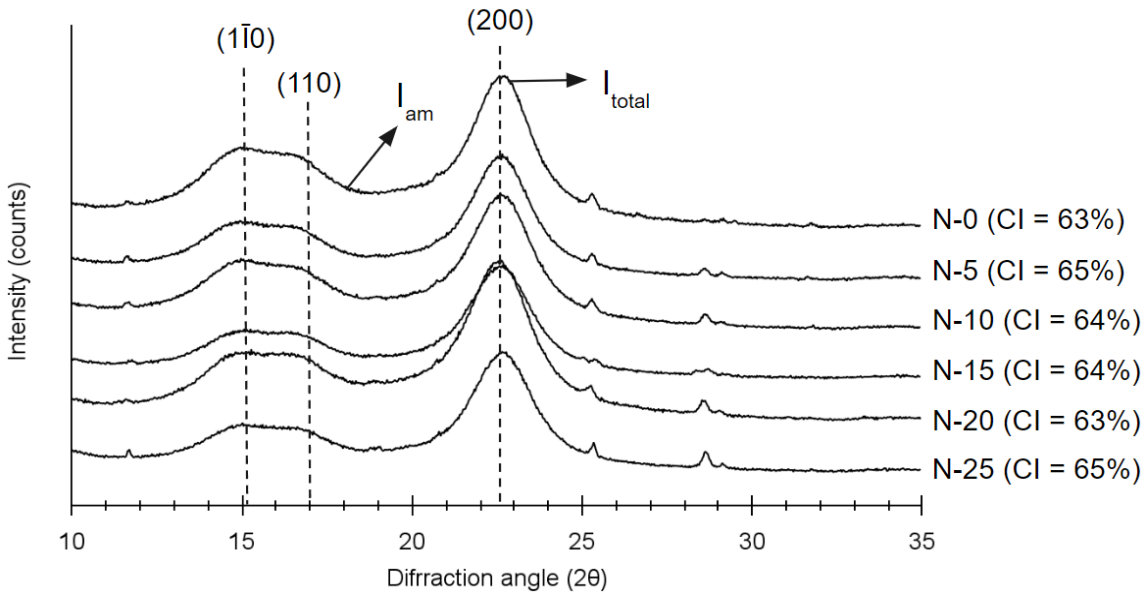

Fig. 3.2. XRD diffraction spectra and crystallinity index (CI) of CNF films

Fig. 3.2 presents diffraction peaks of each CNF films, which is described further by referring to several other reports (Manimaran et al. 2019; Siti Syazwani et al. 2022; SriBala et al. 2016; Hafez, Amini, and Tajvidi 2020; G. Zhao et al. 2019). Overall, referring to the characteristic peaks of each cellulose type (Y. Liu et al. 2022), all of the resulting diffraction patterns evidenced the Cellulose I type. The peaks typically found in Cellulose I are the Miller indices of (1$\bar{1}$0) at 2θ=15°, (110) at 2θ=17°, and (200) at 2θ=22.5°, and (004) at 2θ=35°—which are similarly displayed for each CNFs. It indicates that, despite the mechanical treatment, CNFs retained the crystallinity profile and structure of the native cellulose contained in the rawest form of softwood, as found in nature. Lastly, minuscule peaks arising at 2θ = 25°, 2θ = 28.5° and 2θ = 32° are likely attributed to the crystalline phase of impurities/trace elements or residual salts.

Fig. 3.2 also displays the crystallinity index (CI) that defines the mass ratio of the crystalline substance in the total dry sample based on the crystallographic two-phase model (Daicho et al. 2018). CI is measured by determining two peaks: the sharp, high, and obvious major/crystalline/monoclinic peak (I_{total}, around 2θ = 20-25°); and the broad secondary/amorphous peak (I_{am}, around 2θ = 12-20°). As seen in the XRD spectra comparison, the results showed no significant difference in CI values, averaging 64%. It signifies that the applied milder-conditioned homogenization (7 MPa for 0-25 cycles) did not significantly alter the molecular structure and crystalline rearrangement/reorganization of the homogenized CNFs. Similar findings of low-pressured homogenizations causing only slight crystalline structure loss were reported in previous studies, e.g., 30-50 MPa for 0-3 cycles (Boulemkahel et al. 2021), 30-60 MPa for one cycle (Kasemwong et al. 2011), and 60 MPa for one cycle (B. Wang et al. 2008). In comparison, some researchers investigated the considerable effects of homogenization on CNF's crystallinity profiles under higher pressure and/or cycles, e.g., 20-50 MPa for 20-40 cycles (Davoudpour et al. 2015), 40 MPa for four cycles (Xiaowen

Liu et al. 2023), 140 MPa for 4-20 cycles (Chun et al. 2011), and 150 MPa for 0-20 cycles (Ueda et al. 2022). Though mechanical treatment promotes water binding capacity and gel-like structure formation (Ulbrich and Flöter 2014), harsh conditions (e.g., excessive pressure and number of passes) during homogenization may possibly lead to the destruction of (sub)crystal zones and covalent bonds within and between molecules (Hoover and Ratnayake 2002). Particles passing through such a "high energy zone" results in aggravated particle structure and compact layer structure damage, decreased amorphous region stability, and even branched molecules in the crystal region to be cut into short straight-chain molecules (Guo et al. 2019; S. Meng et al. 2014). This highlighted the influence of the applied lower pressured homogenization, despite multiple passes, in maintaining the crystallinity profile. This technique would suit certain CNF processing where the preserved long cellulose chain is essential to the final product, e.g., reinforcement agent (Yano et al. 2018) and thermal-conductive filler (Lou et al. 2021).

3.3.3. Morphology, surface roughness, and transparency

The surface SEM images of the freeze-dried CNFs post-homogenization are presented in **Fig. 3.3**. Prior homogenization (N-0) images showed a compact but rough and uneven appearance of CNF, consisting of strongly entangled fibrils forming thick bundles with an average width of 8-10 μm. The degree of fibrillation was improved after homogenization due to the provided shear impact as the suspensions flew through extremely small gaps under intensive shear (L. Wang et al. 2021), even after only five (5) cycles (N-5). As shown in N-5 images, fibrils began to loosen and detach from each other, significantly reducing the bundles' dimensions and releasing separated, individual fibrils with nanosized diameter. The increasing specific surface areas eventually promoted hydrogen bonding with water (Kose et al. 2011). Images also showed less roughness due to the reduced number of big fibril bundles. Though much more undetached, some thick fibril bundles could still be seen in N-5 surface micrograph images. Furthermore, it was investigated that the more homogenization passes, the higher the degree of fibrillations, the more hydrogen bonds with water, and ultimately, a web-like network of thin and long fibrils was formed. Furthermore, more obvious and drastic fibrillation was observed after 20 homogenization cycles (N-20). A complex web was formed, made of numerous fine fibrils connected with each other, indicating the successfully promoted hydrogen bonds. However, the over-shearing occurrence was discovered in the higher number of homogenization cycles, indicated by the individual fibrils that began to agglomerate at N-15, N-20, and even worse at N-25. The apparent aggregation caused by such excessive mechanical treatment was observed in other reports (Malucelli et al., 2018; Pelissari et al., 2017). Overall, identical behavior was observed in previous studies that prepared nanocellulose using other homogenization approach (multiple passes with high-pressure/shear-speed) coupled with other physical/chemical treatments (Kose et al. 2011; Dilamian and Noroozi 2019), showing the effectiveness of the conducted method in this study despie the much milder conditions applied (ultra-low pressure).

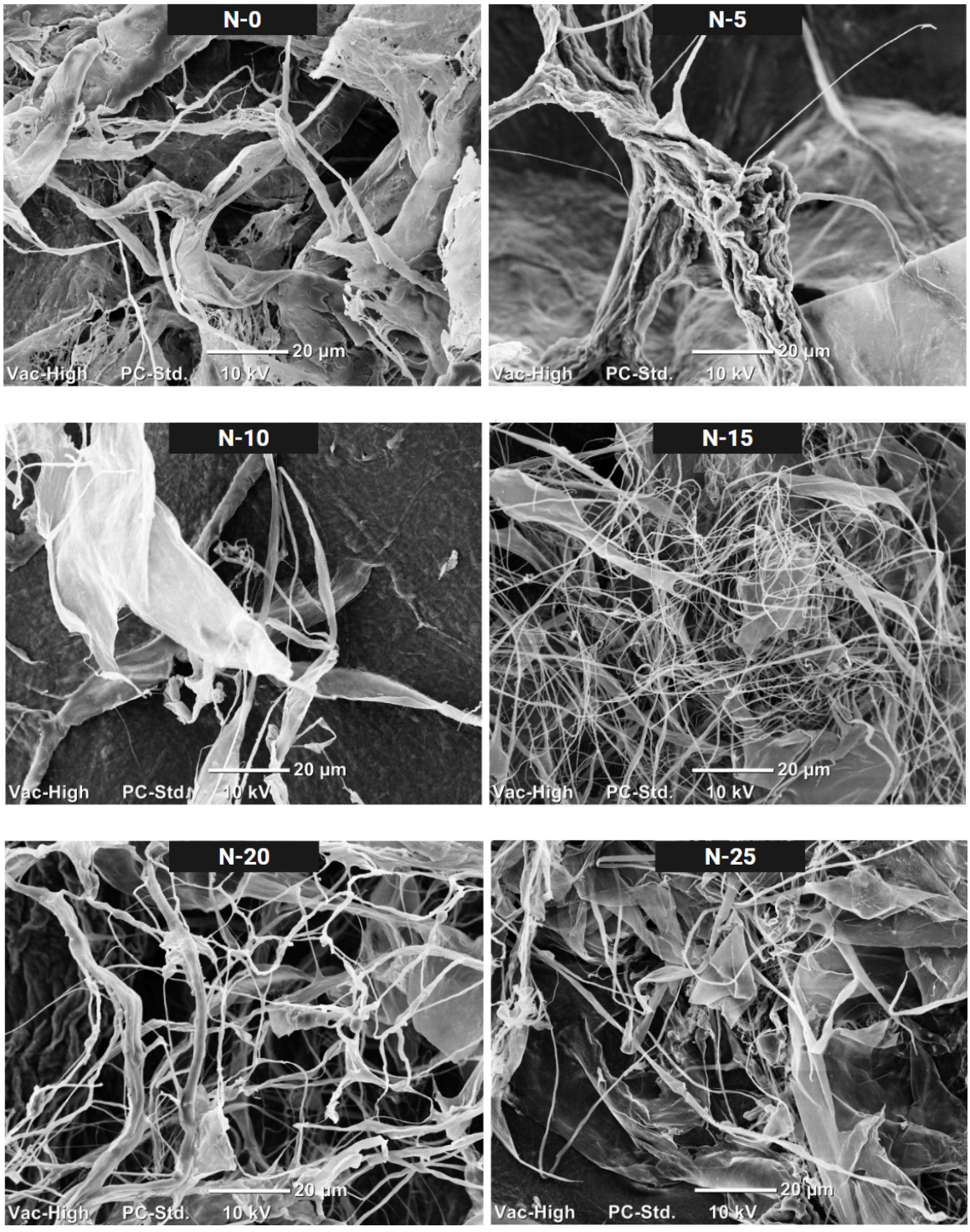

Fig. 3.3. Surface SEM images of freeze-dried CNFs at 1000x magnification

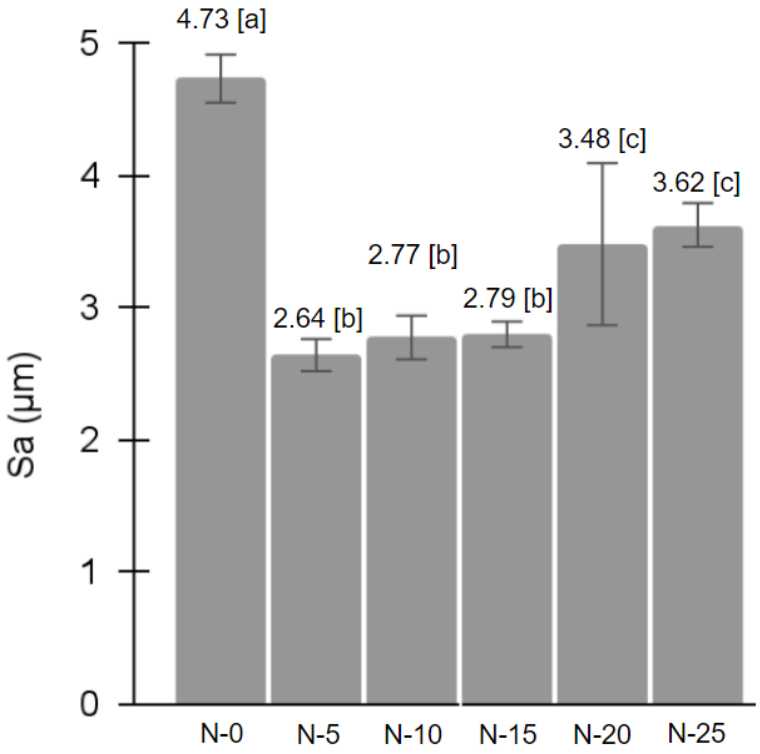

Fig. 3.4. Surface roughness of CNF films: arithmetical mean height or *Sa*

The roughness characteristics of the CNF films' top surface were presented in both microscopic images (**Fig. S1**) and *Sa* values (**Fig. 3.4**), which can be defined as the arithmetic mean deviation of the height of a line, where this basic parameter depicts the surface micro-geometry of the specimen (Woch et al. 2022). The obtained range of values was comparable to that of other CNF reports (Miettinen, Chinga-Carrasco, and Kataja 2014). It can be seen that solely five (5) cycles of homogenization managed to successfully decrease the roughness of the CNF control film, making it approximately 44% smoother, from 4.73 µm (N-0) to 2.64 µm (N-5). However, the effect of over-shearing was evidenced after 20 passes (N-20), where the surface became rougher. Although, N-20 is still significantly smoother, specifically 27% smoother, than the surface of the unhomogenized CNF film (N-0). A similar finding of the recovered roughness was investigated in other studies confirming protuberance prominences on the material's surface, which might occur whether aggregation ensued (Xue et al. 2021) or not (Żołek-Tryznowska et al. 2023). Evidently, the effect of such protuberance on the film's roughness was more obtrusive despite the promoted fibrillation and no aggregation (as observed in morphological results in **Fig. 3.3**). Additionally, other roughness profiles investigated were z-stack and three-dimensional microscopic images (**Fig. S1**). Z-stacking or focus-stacking combines multiple images taken at different focal distances to provide a composite image with a greater depth of field, including the thickness of the plane of focus, than any of the individual source images (Ray 2002; D. Johnson 2008). During analysis, filtering referred the reference plane to the CNF films' real surface to reduce height variability. Especially when conducting characterization with such high magnification and numerical apertures that suffer from decreasing depth-of-field, this

image processing can capture in-focus images (Larson and Banks 2022). The obtained images confirmed the findings on roughness value analysis, where the surface of N-5 showed a significantly smoother appearance compared to N-0 and was even better at N-20. These roughness results were supported by the morphological findings (**Fig. 3.3**) of surface examination, as the surface roughness is highly influenced by residual fibers and the morphology of fibrils (Chinga-Carrasco et al. 2014). Micro-pores likely existed in locations along the thicker parts of the CNF films, which are usually attributed to containing more residual fibers (Miettinen, Chinga-Carrasco, and Kataja 2014). Residual fibers are the non-fibrillated microscopic fibers and fiber fragments whose amount dictates the morphology of a CNF (Nechyporchuk, Belgacem, and Bras 2016; Chinga-Carrasco et al. 2014). CNF films with smooth features are commonly used as gloss finishes; meanwhile, the roughly-surfaced CNF films possess noteworthy implications on electrical behavior when used in organic field-effect transistors (Lehmann and Zahn 2009).

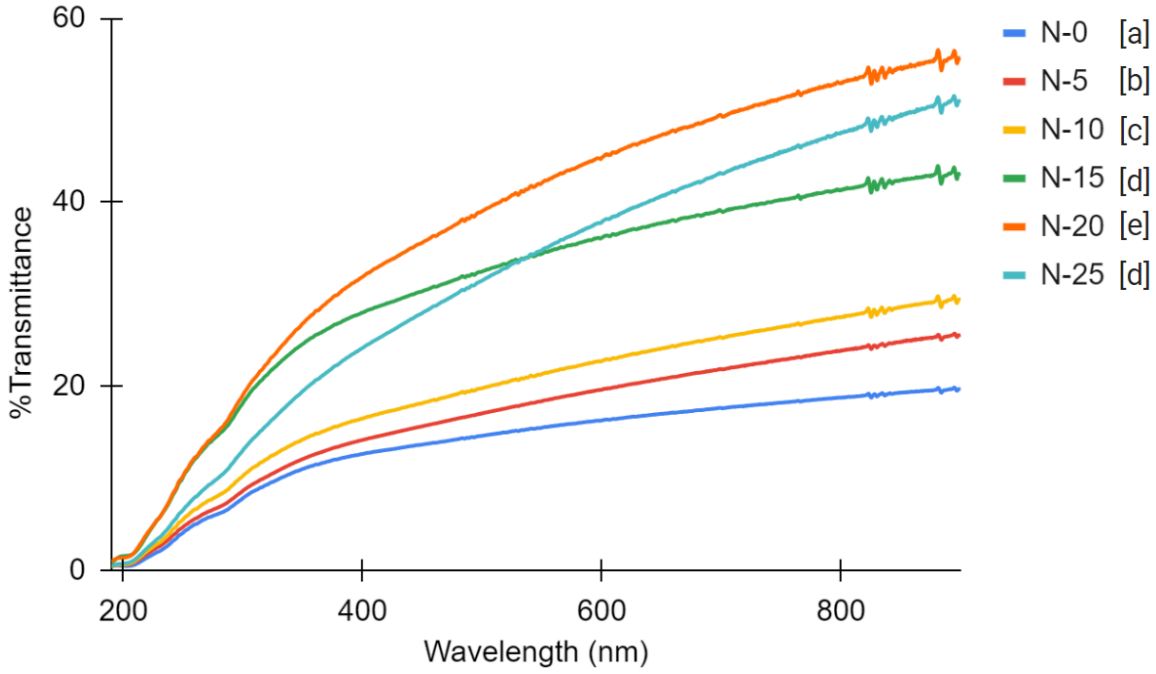

(**a**)

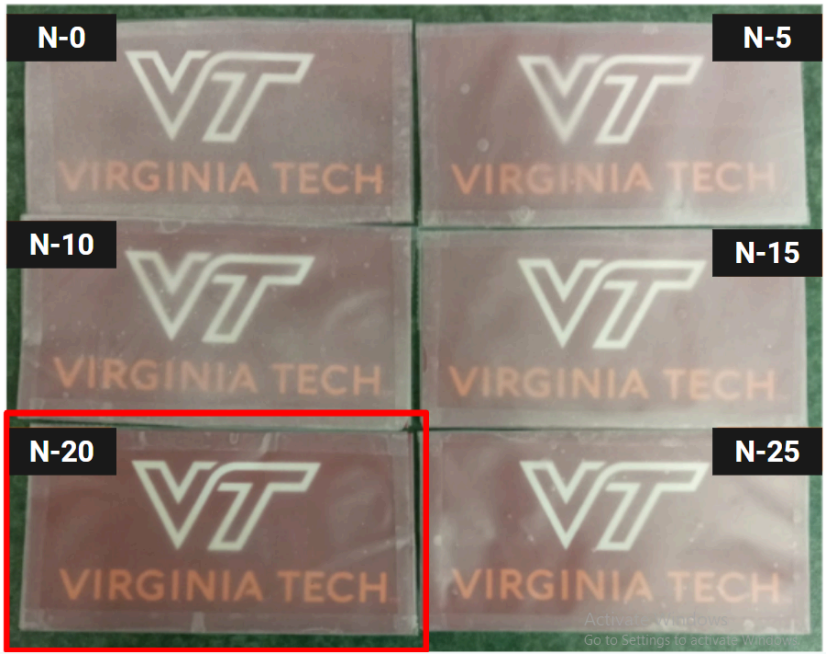

(**b**)

Fig. 3.5. Transparency of CNF films: (**a**) UV-vis spectra and (**b**) visual observation

The homogenization effect on the transparency of the CNF films was also analyzed, supporting the morphological and surface roughness results. Optical properties help determine major appearance quality that governs suitability for use in myriad applications. Transparency is directly related to the degree of homogeneity, internal microstructure, porosity, surface roughness, materials size, and distribution/dispersity (S. Cheng et al. 2015; Leppänen et al. 2022; Toivonen et al. 2018; H. Zhu et al. 2013). As seen in **Fig. 3.5**, either through UV-vis spectra (**Fig. 3.5**(a)) or simple visual observation (**Fig. 3.5**(b)), it is evident the homogenized films showcased better transparency due to the enhanced fibrillation (Dinesh and Kandasubramanian 2022). N-20 displayed the best transparency among all films, whose transmittance reached 56% at 900 nm. It is nearly thrice as transparent as the control film (N-0), where merely 20% of the transmittance of light is managed to pass through. This finding is superior to other nanocellulose reports (X. Sun et al. 2018; M. Herrera 2015; M. A. Herrera, Mathew, and Oksman 2012). Decreasing transparency was observed after 25 passes of homogenizations (N-25) due to the over-shearing effect. The fibrils agglomerated to the point where the bundles' diameter or width was significantly increased. It led to more scattered light and eventually decreased optical transmittance (E. Lizundia et al. 2016). Such a negative effect of agglomeration on nanocellulose films' transparency was also discussed in other reports (S. Cheng et al. 2015). The produced films exhibited high transmittance not only in the visible spectrum but also high absorption in the UV spectrum. UV-blocking ability is important because excessive exposure to UV sunlight radiation increases biological damage and degradation of organic compounds. This property is responsible for the discoloration, weathering, and loss of mechanical properties (cracking) (Sadeghifar et al. 2017). The UV region covers the wavelength range 100-400 nm and is divided into three (3) bands: UV-A (320–400 nm), UV-B (280–320 nm), and UV-C (200–280 nm) (Parit et

al. 2018; WHO 2016). The most transparent film (N-20) partially blocked UV-A, B., and C, where the resulting transmittances at the aforementioned ranges were 9-15%, 15-23%, and 23-32%, respectively. On the other hand, the resulting transmittances of the least transparent film (N-0) in the three (3) UV spectrums were 9-13%, 6-9%, and 0.5-6% for UV-A, B, and C, respectively. These findings are superior to previous cellulose studies (Sadeghifar et al. 2017; Guzman-Puyol et al. 2022; Bian et al. 2022), showing the excellence of homogenized films in UV-blocking features despite the accomplished transparency. Both transparent and opaque CNFs have potential in a variety of applications, e.g., transparent wound dressing (Baş et al. 2023) and opaque thermal insulation film (Grabowska and Kasperski 2018; Pan et al. 2023) or opaque mulching film (N. Yang et al. 2015).

3.3.4. Barrier property

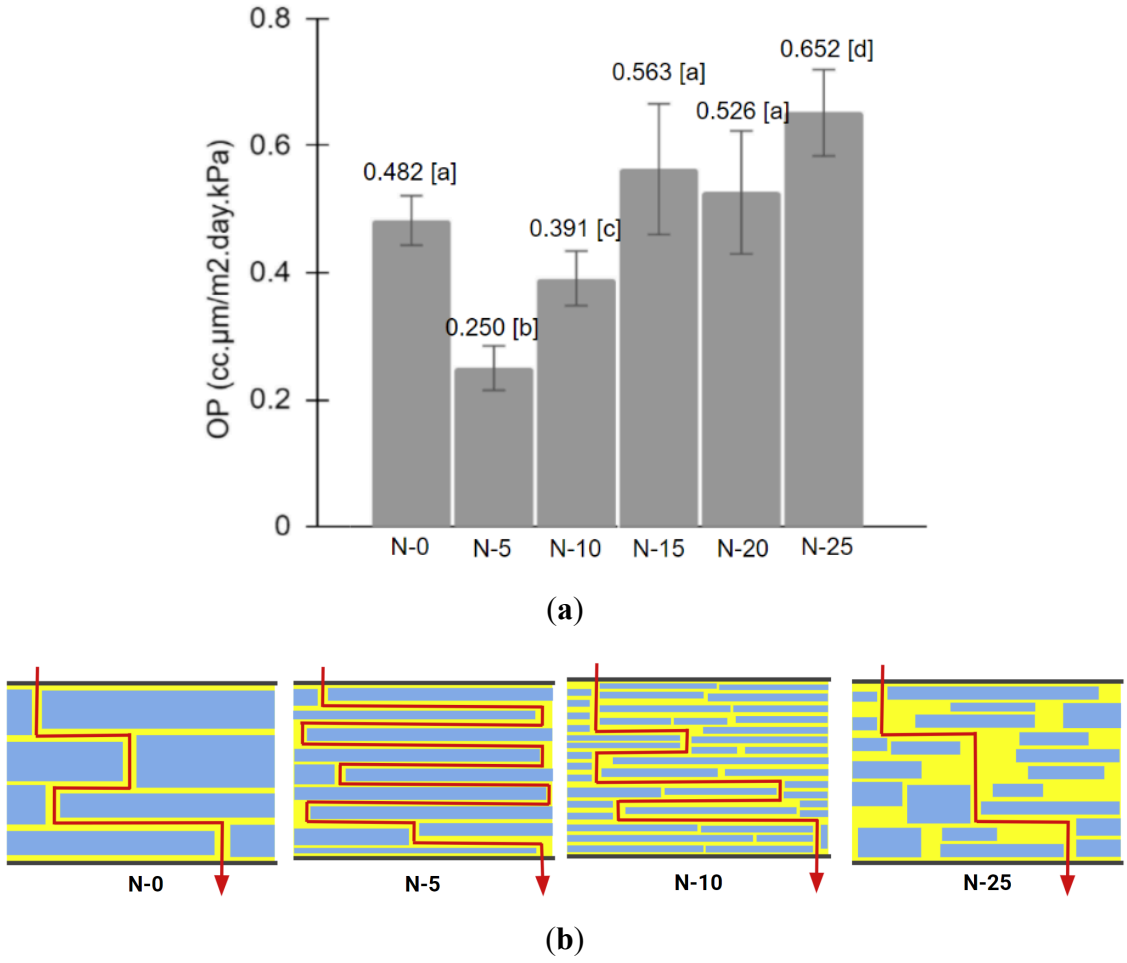

Fig. 3.6. (**a**) Oxygen permeability (OP) of CNF films at 50%RH; and (**b**) illustration of oxygen diffusion paths comparison (where blue blocks represents cellulose fibrils and red arrow represents oxygen flow)

Fig. 3.6(a) displays the oxygen permeability (OP) of the homogenized CNF films at 50%RH. The varying homogenization cycles and their influences on the oxygen diffusion path are illustrated in **Fig. 3.6**(b). OP significantly decreased by 48% after five (5) cycles of homogenization, from 0.482 (N-0) to 0.250 (N-5) cc.μm/m^2.day.kPa at 50%RH. This showed the impact of promoted fibrillation post-homogenization that provides a more hydrogen-bonding network between fibrils, creating a more densely packed structure (Peresin et al. 2017), as evidenced in morphological findings. The obtained OP values were compared with ethylene vinyl alcohol (EVOH), a commercial polymer with exceptional oxygen permeability. EVOH is usually applied in multilayer structures with other polymers through blow molding, thermoforming, and orientation techniques. Its composition dictates its performance, and 25–45 mol % ethylene content is required for high barrier resin standards (Artzi, Narkis, and Siegmann 2005). At 50%RH, it was revealed that the best oxygen barrier–CNF (N-5) possessed a noteworthy barrier performance compared to EVOH, falling between EVOH38 and EVOH44 (EVOH with 38 and 44 mol% ethylene, respectively), in particular H and E type of the EVAL™ brand (approximately 0.099–0.138 and 0.197–0.375 cc.μm/m^2.day.kPa), respectively (Kuraray, 1972). OP of N-5 is also notably superior against several common synthetic oxygen barriers–plastics, i.e., PVA, MXD6, PET, and PVC at 0.197-9.869, 0.493, 10-50, and 20-79 cc.μm/m^2.day.kPa, respectively, even some PVDC (0.099-2.961 cc.μm/m^2.day.kPa), at 50%RH (Michiels, Van Puyvelde, and Sels 2017). This result is comparable to the findings of the latest CNF report (Z. Cheng et al. 2024). Nonetheless, the OP increased when more cycles of homogenization were applied, which is presumably after fibril length reduction as the aftermath of "over-shearing." Similar phenomena were reported where the initially observed long fibrils at small numbers disappeared with continued mechanical treatment, alongside the appearance of newly-produced fibrils (Redlinger-Pohn, Petkovšek, et al. 2022; Y. Zhou et al. 2018). Instead of the long fibrils with a high aspect ratio turning and entangling into a web structure, the hydrogen-bonded shorter fibrils and subsequent more void volumes made a significantly less tortuous diffusion path for oxygen (L. Wang et al. 2020). Therefore, despite the promoted fibrillation, N-10 and beyond suffered from lower oxygen barrier ability.

The high oxygen barrier property is among cellulose's diverse advantages that have gained attention for centuries. Oxygen permeability (OP) is one of the most important functionalities in food/pharmaceutical packaging as it dictates the material's ability to reduce/prevent oxygen permeation, resulting in responsible for many degradation processes (e.g., lipid oxidation, microorganism growth, enzymatic browning, and losses in flavor, color, and nutrients)—it is even identified as the most common cause of packaged food's quality loss (Brown 1992; S.-I. Hong and Krochta 2006; Ayranci and Tunc 2003). Despite the necessary presence of oxygen for any living tissue's respiration, oxygen also accelerates ethylene production, leading to senescence (Oms-Oliu, Soliva-Fortuny, and Martín-Belloso 2008; Rojas-Graü et al. 2007). The oxygen barrier characteristics provide the degree of protection necessary to achieve the desired shelf life of a product whose oxygen sensitivity may vary (Koontz 2016). Moreover, under high humidity, the hydrophilic nature of cellulose leads to swelling and excessive moisture-absorbing tendencies of hydroxyl groups, allowing the water to replace hydrogen bonds between cellulose. This phenomenon eventually loosens the film's

structure and allows gas, such as oxygen, to penetrate and diffuse. Several techniques have been explored aiming to solve this issue, but each is faced with different limitations. Combinations with other polymers through the coating (Bayer et al. 2011; Stanssens et al. 2011) or composite formation (Benhamou et al. 2015; D. Liu et al. 2014) may reduce biodegradability (Xia et al. 2018) or matrix-filler compatibility issues that might require surface modification (Aziz et al. 2023). Whereas the introduction of a hydrophobic group chemically, especially those reacting with hydroxyl groups (Jonoobi, Harun, Mathew, Hussein, et al. 2010; Missoum et al. 2013), is potentially retarding the existing hydrogen bonding in cellulose, subsequently affecting an array of major properties (Xia et al. 2018). Such an approach involving solvent exchange can also be tedious, reagent-intensive, and time-consuming (Peresin et al. 2017). Thermal modification was also reported (Xia et al. 2018), though the required high temperatures are likely destructive to some extent (L. Wang et al. 2021; Neto et al. 2021). Therefore, the effectiveness of a milder-conditioned homogenization approach in retaining the low oxygen transmission rate of cellulose, especially under humid conditions, was explored. OP measurement involves two (2) different gas streams, oxygen, and nitrogen, each at one side of the film. Nitrogen acts as the carrier gas of the oxygen, and a dedicated analyzer monitors the transmitted oxygen. OP is highly dependent on relative humidity (%RH), which dictates the amount of water molecules interacting with the tested sample, and temperature, which affects gas transference. To favor mobility and extensive mass transfer across the sample, controlled %RH and temperature shall be conducted (Bonilla et al. 2012; S.-I. Hong and Krochta 2006). Temperature at 23°C and 50%RH were chosen, which considerably deviated from the realistic chilled storage conditions (Jakobsen et al. 2005).

3.3.5. Mechanical properties

The mechanical properties of CNF are directly dependent on individual fibrils' strength. Fibril-fibril hydrogen bonding interaction is also important since it facilitates stress transfer and is influenced by dimensions, orientation, surface functionalities, counterions, and porosity. Strong fibril-fibril interfacial adhesion eases the stress distribution during deformation, improving the final film's strength due to the repeated breakage/reformation of hydrogen bonds between neighboring fibrils and the energy dissipation under stress (Mokhena et al. 2021). Other factors include preparation method, source, degree of polymerization, porosity, moisture content, fibril alignment, surface functionality, and counterions presence, which are often interdependent, thus making it difficult to separate their individual effects (Fukuzumi et al. 2013). **Fig. 3.7** displays the mechanical properties of CNF films: tensile strength or TS (**Fig. 3.7**(a)); tensile/Young's modulus or E (**Fig. 3.7**(b)); and elongation-at-break or EAB (**Fig. 3.7**(c)). The highest TS and E were achieved by N-10 (157.4 MPa) and N-15 (3843.3 MPa), respectively, which produced a significant 67% and 46% increase from the performances of untreated CNF (N-0). These optimum results proved the enhanced nanofibrils association within the polymer network and the increased resistance from rupturing. Furthermore, EAB was found the lowest at N-25 (3.90%) or a 31% decrease from N-0 (5.69%). EAB is highly influenced by aspect ratio; thus, CNFs with a lower aspect ratio post-homogenization are rigid and easy to pull out from the aggregated fibers (Pelissari et al. 2017; Saïd Azizi Samir et al. 2004). These mechanical analysis results are comparable with values

obtained in other reports: softwood CNF (TS = 98 MPa, E = ~3000 MPa) (Fein, Bousfield, and Gramlich 2021), kenaf CNF (TS = 75 MPa and E = ~1190 MPa) (Atiqah et al. 2019), eucalyptus CNF after 25 grinding passages (E = ~3600 MPa and tensile strain = 6.3%) (Malucelli et al. 2018), and banana starch composite reinforced with banana peel-CNF (TS = 11.1 MPa, E = 1047.7 MPa) (Pelissari et al. 2017). The observed 'plateauing' of mechanical properties after ten passes of homogenization (N-10) was similar to the phenomenon found in the previous homogenized cellulose reports (Naderi, Lindström, and Sundström 2015; Josset et al. 2014; K. L. Spence et al. 2010; Iwamoto, Nakagaito, and Yano 2007). Overall, N-25 showcased the effect of 'over-shearing' whose effects were highlighted as well in other properties such as morphological, surface roughness, transparency, and thermal stability (**Fig. 3.3, Fig. 3.4, Fig. 3.5, Fig. 3.8**(a-b), respectively) and discussed in each section. The apparent agglomeration after an excessive mechanical treatment impaired contact among the fibrils, weakening mechanical properties and making it more prone to rupture. Similar behavior was evident in other studies investigating the extent or severity of mechanical treatment to the CNFs' properties (Malucelli et al. 2018; Pelissari et al. 2017).

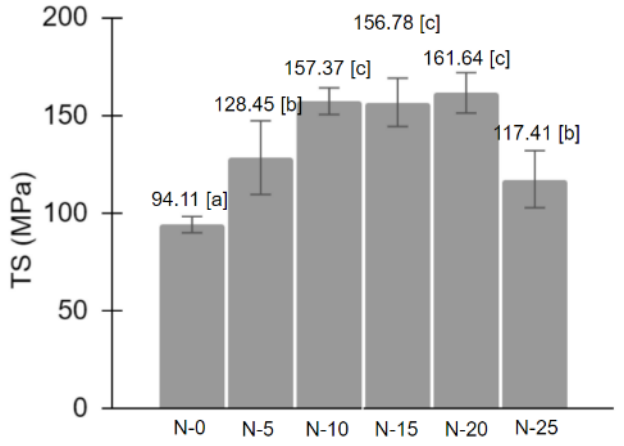

(**a**)

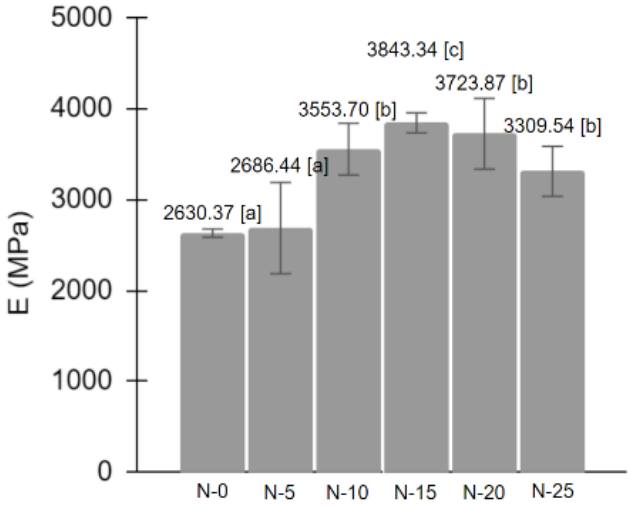

(**b**)

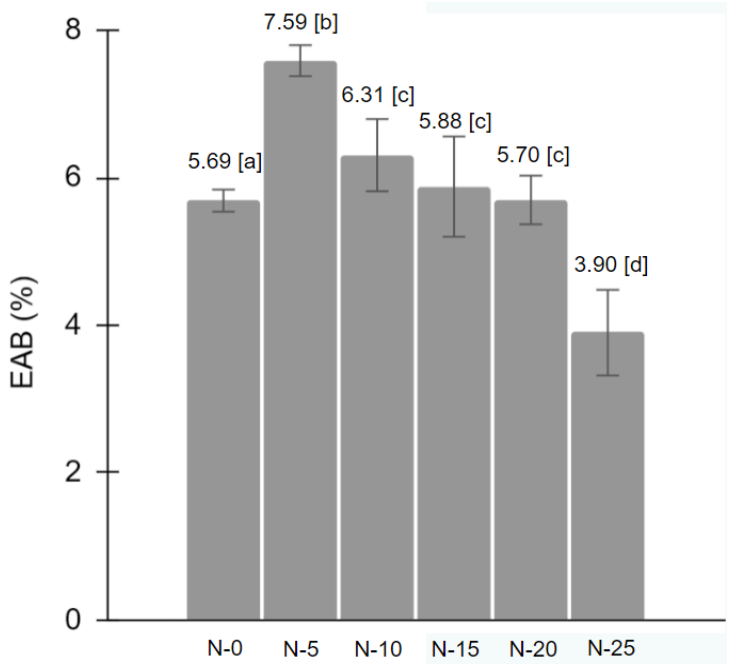

(**c**)

Fig. 3.7. Mechanical properties of CNF films: (**a**) tensile strength or TS, (**b**) tensile/Young's modulus or E, (**c**) elongation-at-break or EAB

3.3.6. Thermal properties

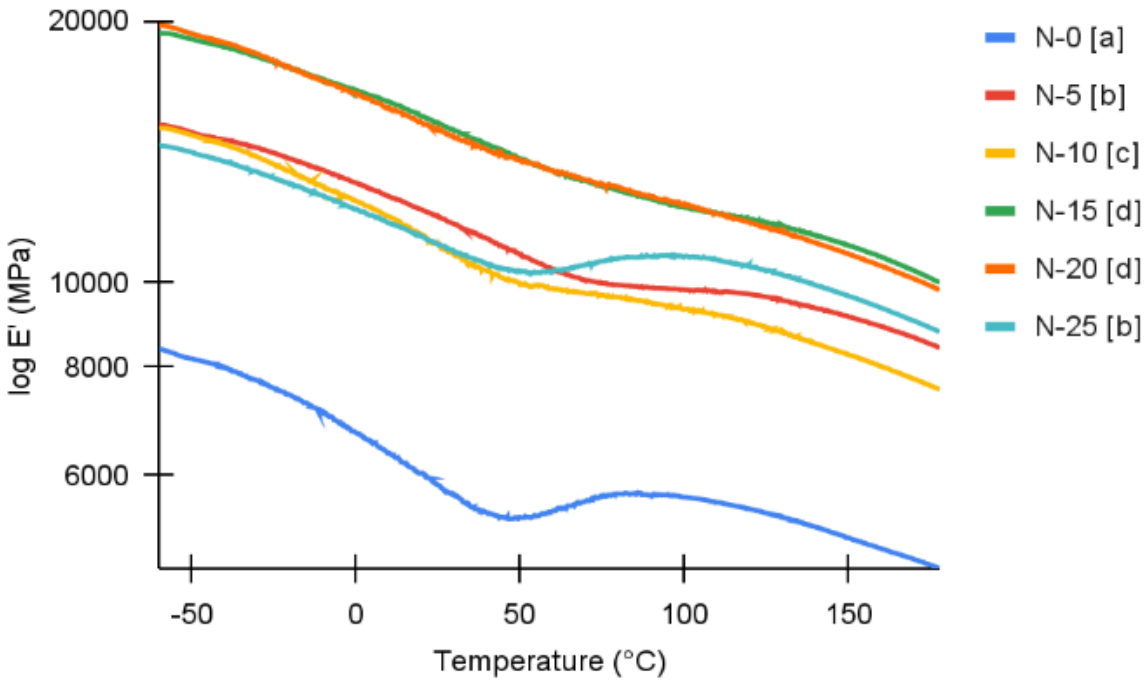

(**a**)

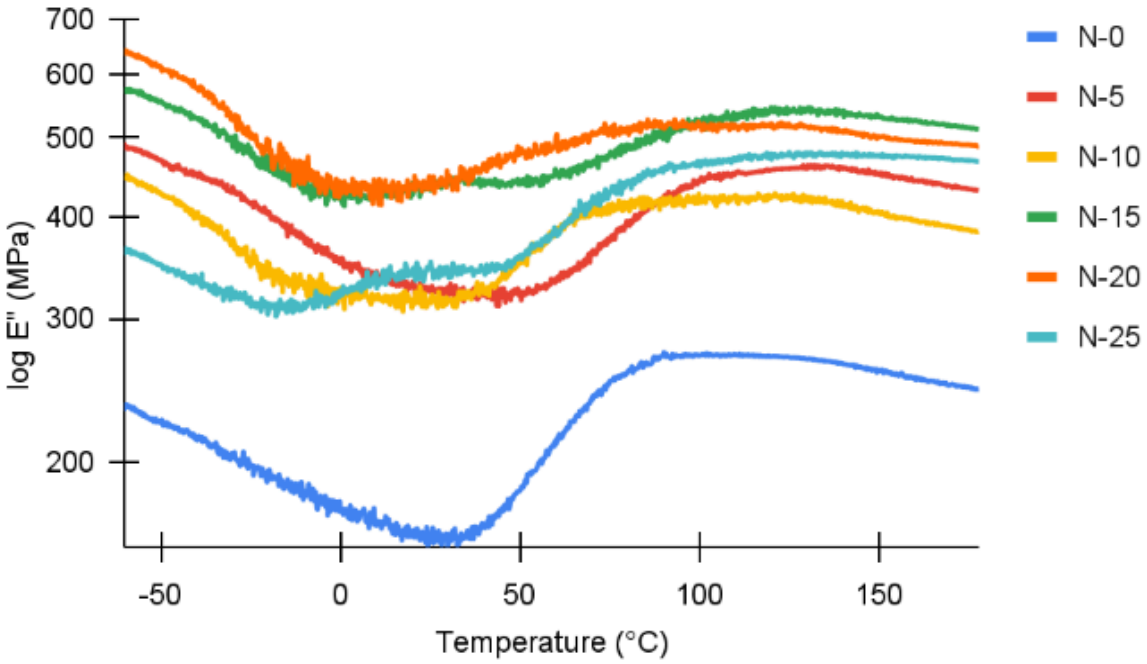

(**b**)

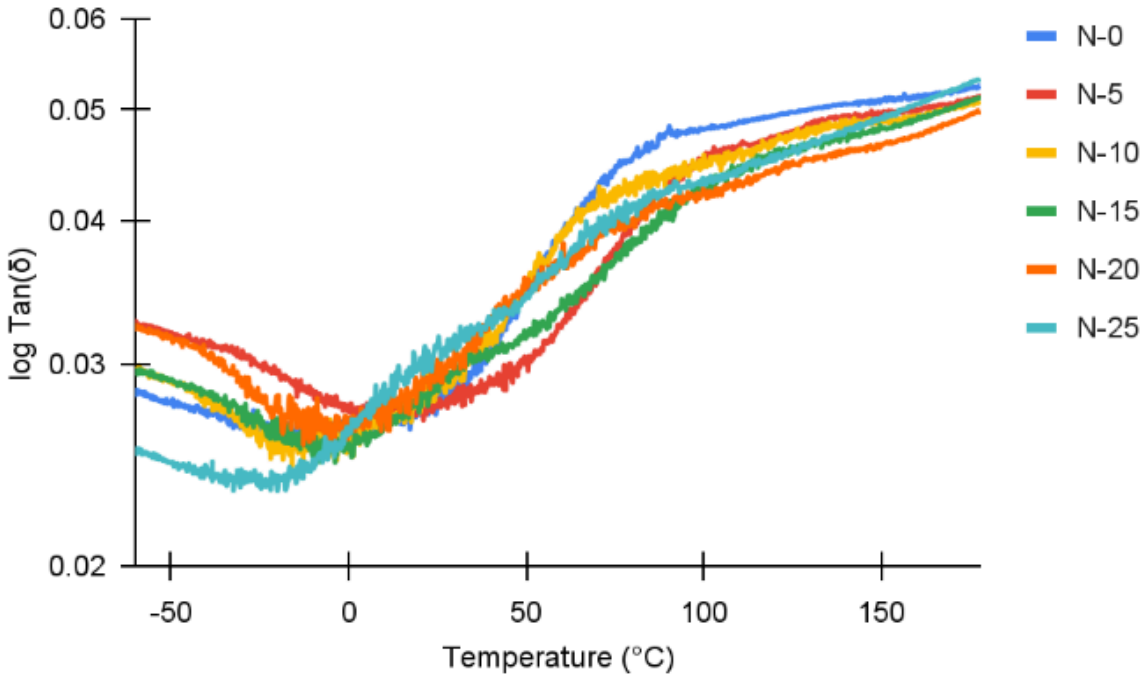

(**c**)

Fig. **3.8**. Thermomechanical properties of CNF films: (**a**) storage/elastic modulus [E'], (**b**) loss/imaginary modulus [E"], and (**c**) loss/damping factor [Tan(δ) = E"/E']

Table 3.2. Thermomechanical properties of CNF films at 25 and 100 ºC

CNF	T (ºC)	E' (MPa)		E" (MPa)		Tan(δ)	
N-0	25	5855	[a]	160	[a]	0.028	[a]
	100	5668		270		0.048	
N-5	25	11,916	[b]	324	[b]	0.028	[b]
	100	9811		444		0.046	
N-10	25	11,092	[c]	314	[c]	0.028	[b]
	100	9315		427		0.046	
N-15	25	15,265	[d]	434	[d]	0.029	[c]
	100	12,199		520		0.043	
N-20	25	14,953	[d]	449	[e]	0.030	[c]
	100	12,268		520		0.043	
N-25	25	11,073	[e]	347	[f]	0.031	[c]
	100	10,722		468		0.044	

Thermal stability, be it thermomechanical properties (**Fig. 3.8**) or thermogravimetric weight loss (**Fig. 3.9**), makes a considerable difference to not only the material's processability and applicability but also degradability. Dynamic mechanical analysis (DMA) plots the storage/elastic modulus or E' (**Fig. 3.8**(a)), loss/imaginary modulus or E" (**Fig. 3.8**(b)), and loss/damping factor or Tan(δ) (**Fig. 3.8**(c)), where the values obtained specifically at 25 and 100 ºC were highlighted in **Table 3.2**. E' defines the material's strength, stiffness, and rigidity. It typically decreases as temperature increases, and at some point increases again, reaching a maximum value because of a change in network structure, before decreasing back after reaching the final cure due to thermal degradation and devitrification after glass transition temperature (Sanyang et al. 2016; Candan, Gardner, and Shaler 2016). An in-depth thermal characterization study on CNF also reported that, at low temperatures, E' remains roughly constant (~2–3 GPa) with temperature before a sharp modulus drop corresponding to the glass–rubber transition at –3–27 ºC. This drop corresponds to an energy dissipation phenomenon during the concomitant relaxation (Saïd Azizi Samir et al. 2004). Such a pattern is often also found in the E" plots (Ilyas et al. 2018), to be discussed in the next paragraph. At the N-0 E' plot (**Fig. 3.8**(a)), a large improvement after the relaxation was observed, with a formed 'plateau' indicating entangled nanofibers (Jonoobi, Harun, Mathew, and Oksman 2010; Saïd Azizi Samir et al. 2004), as confirmed by morphological images (**Fig. 3.3**(a)). As the cycle of homogenization increased, the plateau began to fade due to the promoted fibrillation, hence the less and less tangling effect. However, at N-25, 'over-shearing' occurred, resulting in significantly shorter fibrils, in addition to some new fibrils broken apart from the initial structure. At this state, CNF became highly prone to be back entangled—hence, the reappearance of the 'plateau.' A similar phenomenon on barrier ability (**Fig. 3.6**) was discussed. Regardless, N-25 still produced a much higher thermal resistance than N-0, showing much higher E' values than N-0 at the same temperatures due to the enhanced hydrogen bonding. Additionally, it can be noted that all E' plots are significantly different, except the similarly-valued N-5–N-25 and N-15–N-20. After only five (5) cycles of

homogenization (N-5), E' was significantly increased by 104% (11,916 MPa) and 73% (9811 MPa) at 25 and 100 ºC, respectively, compared to the untreated CNF (N-0), valued at 5855 MPa and 5668 MPa at 25 and 100 ºC, respectively. Even better at N-15, the E' increase was by 161% (15,265 MPa) and 115% (12,199 MPa) at 25 and 100 ºC, respectively. These evidenced the enhanced heat stability and incorporated rigidity due to stronger interfacial interactions post-homogenization. These values are on par with previously-researched materials, e.g., PLA-CNF (4400 MPa and 2500 MPa at 25 and 70 ºC, respectively) (Jonoobi, Harun, Mathew, and Oksman 2010), PVAc-CNF (3485 MPa and 32 MPa at 30 and 70 ºC, respectively) (Gong et al. 2011), CNF-epoxy (~2000 MPa at 25 ºC) (Saba et al. 2017), and sugar palm-based CNC-starch composite (~1600 MPa and ~800 MPa at 25 and 100 ºC, respectively) (Ilyas et al. 2018).

The value of E" (loss/imaginary modulus) represents the material's viscous response by measuring energy loss under stress or deformation as heat/cycle, hence its association with 'internal friction' (Saba et al. 2017; Jawaid et al. 2015). As mentioned, an identical trend between E' and E" plots was apparent. **Fig. 3.8**(b) shows E" plots that are all significantly different. After only five (5) cycles of homogenization (N-5), E" rose by 102% (324 MPa) and 64% (444 MPa) at 25 and 100 ºC, respectively, compared to N-0, valued at 160 MPa and 270 MPa at 25 and 100 ºC, respectively. The highest improvement was achieved after 20 cycles (N-20), with a 180% (449 MPa) and 93% (520 MPa) increase at 25 and 100 ºC, respectively. These values are superior to the optimum results of other similarly-designed studies, such as sugar palm-based CNC-starch composite (~150 MPa and ~100 MPa at 25 and 100 ºC, respectively) (Ilyas et al. 2018) and CNF-epoxy (~170 MPa at 25 ºC) (Saba et al. 2017). Higher E" values emphasize a more homogenous dispersion/distribution and less visible agglomeration (Saba et al. 2017; S. Xu et al. 2013).

The loss/damping factor or Tan(δ) (**Fig. 3.8**(c)) measures the ratio of E" to E'. Regarding the material's molecular movement, it characterizes the recoverable strain energy in the distorted specimen, providing valuable information about internal energy dissipation when exposed to varying temperatures (Sanyang et al. 2016). As the temperature increases, damping increases to its maximum in the transition region and decreases in the rubbery region (Saba et al. 2017). The higher the peak intensity, the higher the degree of molecular mobility; the lower the peak intensity, the slower the energy dissipation process (G. Chen et al. 2008), which suggests better dispersion that effectively inhibits polymer movement. Agglomeration increases the vacant space for the polymer chain to move/rotate, thereby increasing the visco-elastic damping behavior (Saba et al. 2017). The increase in E', together with a positive shift in the Tan(δ) peak, can be attributed to the promoted interaction that restricts the segmental mobility of the polymer chains. Viscoelastic behavior agrees with the mechanical properties (**Fig. 3.7**), where the reinforcing effect restricts molecular chain mobility (Bondeson, Syre, and Niska 2007; Jonoobi, Harun, Mathew, and Oksman 2010). These theories supported the findings, including N-0 showing the highest Tan(δ) at high temperatures (~70-100 ºC), indicating the most molecular mobility in the chains of the untreated CNFs that consisted of entangled fibrils. As the fibrillation was enhanced after more homogenization cycles, there became less moving space for the polymer chains, as confirmed by morphological images (**Fig. 3.3**(a)). Compared to the N-0 Tan(δ) peak at 100 ºC (0.048), a significant decrease of 5% and 10% were observed at N-5 (0.046) and N-25 (0.044), respectively.

These results are comparable to other reports, e.g., PLA-CNF (~0.4 at 90 ºC) (Jonoobi, Harun, Mathew, and Oksman 2010), PVAc-CNF (~0.4 at 90 ºC) (Gong et al. 2011), CNF-epoxy (~0.5 at 100 ºC) (Saba et al. 2017), and sugar palm-based CNC-starch composite (~0.2 at 100 ºC) (Ilyas et al. 2018).

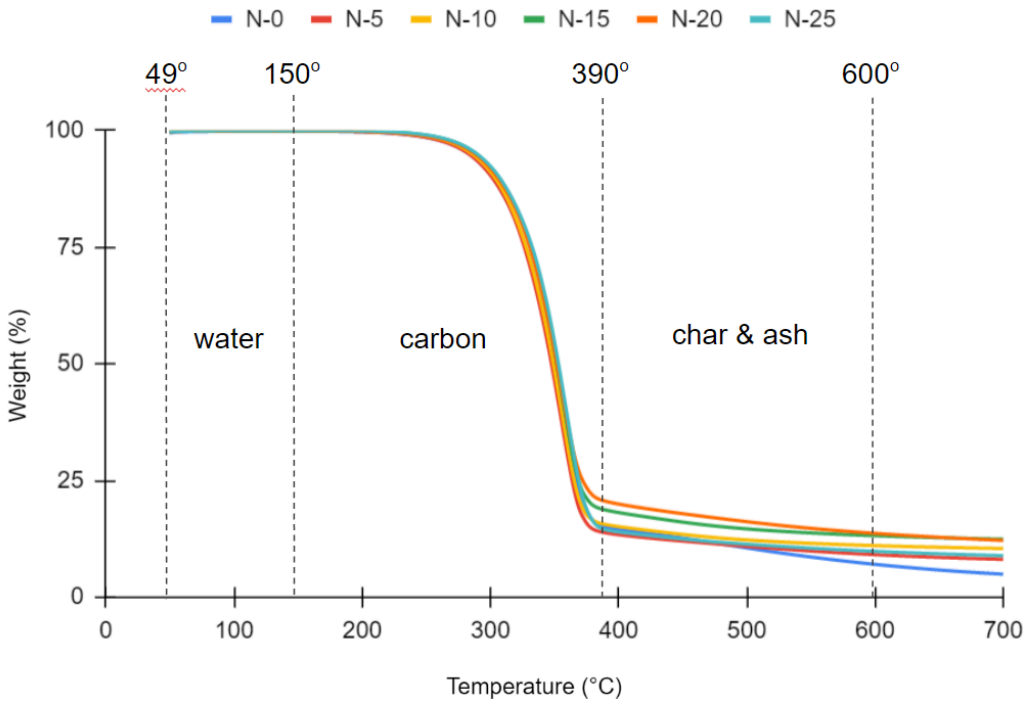

Fig. 3.9. Thermogravimetric weight loss profile of freeze-dried CNFs

Table 3.3. Degradation temperature and weight loss profile of freeze-dried CNFs

CNF	$T_{d5\%}$ (ºC)	%W at 700ºC
N-0	281	5
N-5	281	8
N-10	283	11
N-15	287	12
N-20	286	12
N-25	287	9

Thermogravimetric analysis (TGA) provides insights into thermal stability and decomposition behavior by measuring mass loss as a function of temperature or time. Thus, it can be crucial when determining a material's (bio)degradibility (Brunšek et al. 2023). Regarding the TGA results (**Fig. 3.9** and **Table 3.3**), it is worth noting that the first decomposition of CNFs generally takes place at temperatures as low as 40-47 ºC due to the absorbed moisture, typically through the evaporation or dehydration of loosely bound water contained in the CNF films. Since freeze-dried CNF was used for the measurement, the first decomposition was not obviously initiated until around the water boiling point at 100 ºC (B. Yang et al. 2019; Ilyas et al. 2018). However, N-0 still displayed the earliest decomposition, implying the water's highest evaporation effect due to its still-natural high hydrophilicity (Abral et al. 2020), confirmed in the hydrophobicity discussion in the next

section. The second significant weight loss was next investigated, which is typically caused by cellulose decomposition at 260-360 °C, marking the start of pyrolysis (Abral et al. 2019; Araújo et al. 2018), followed by the third after 360 °C that can be attributed to the final, thermal-oxidative decomposition of char/ash (Asrofi et al. 2018; Jiangqi Zhao et al. 2013). An improvement in thermal resistance was evident in the TGA results, where post-homogenization, CNFs did not fully degrade even after reaching 800 °C and maintained 8-12% of their initial weight. It is a substantial resistance compared to the untreated CNF that reached the same weight loss at a far lower temperature and only maintained a little over 5% of its initial weight at 800 °C. This is owing to the enhanced amount of interlinking hydrogen bonding between the polymer chains post-homogenization, forcing a higher energy requirement to be decomposed (A. Islam, Yasin, and Rehman 2014; U.-J. Kim, Eom, and Wada 2010). Temperatures, when the samples endured the 5%-weight loss (Td,5%), were enhanced by over 10% post-homogenization (281-287 °C). Such finding was a significant improvement from other similar studies, including other softwood-based CNF (227.8 °C) (B. Yang et al. 2019), softwood-based raw cellulose (275 °C) (Fukuzumi et al. 2010), softwood-based TEMPO-oxidized cellulose (222 and 211 °C) (Fukuzumi et al. 2010), and oil palm empty-fruit-bunch based CNF (201 °C) (Supian et al. 2020). For heat-resistant applications, it is known that the recommended ambient temperature should not exceed 250 °C to ensure fit-for-use strength retention. Therefore, the obtained CNFs would suffice for the aforementioned applications (B. Yang et al. 2019). In addition, such thermostable films exhibit high potential as conducting films in touch panels, displays, lighting devices, flexible printed circuit boards, solar cells, and medical devices (L. Sun et al. 2023).

3.3.7. Contact angle or wettability

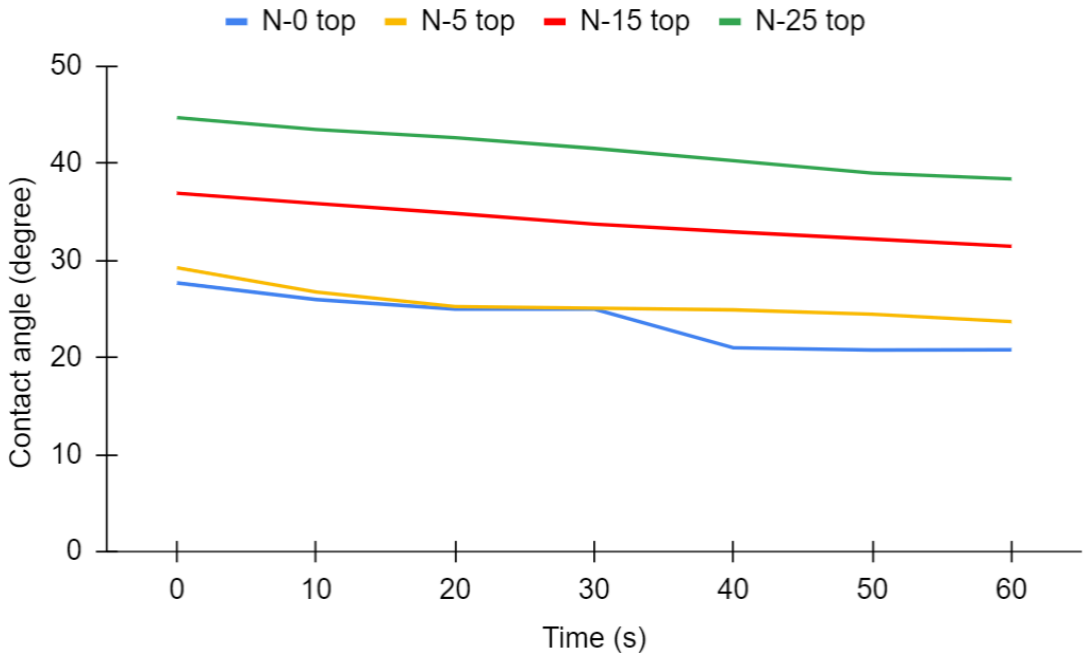

(a)

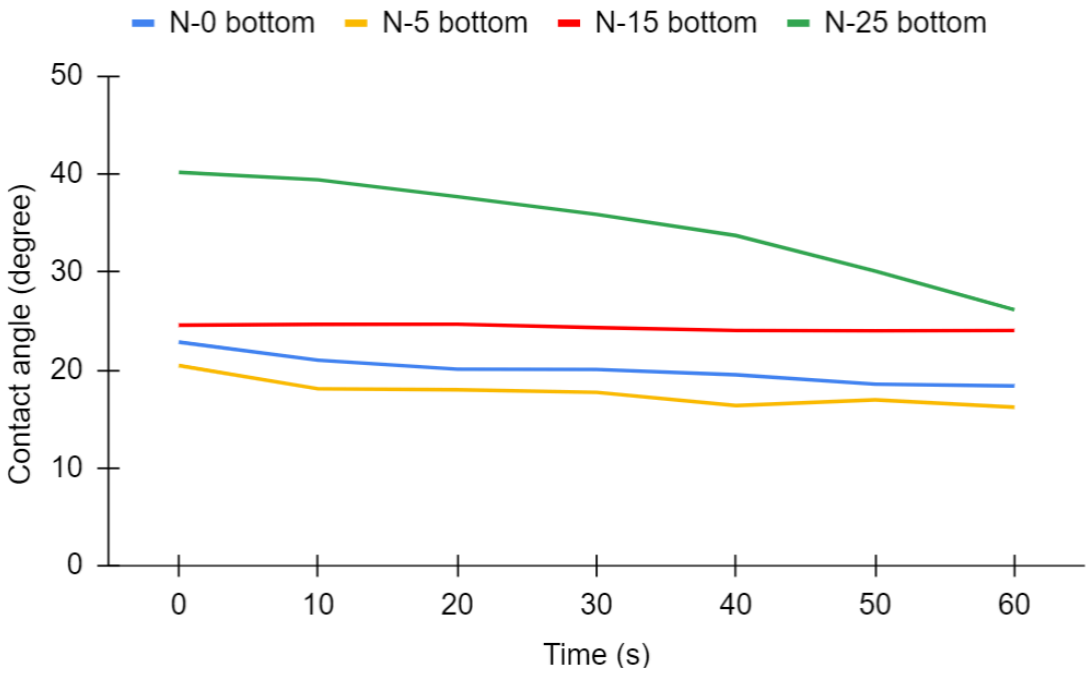

(**b**)

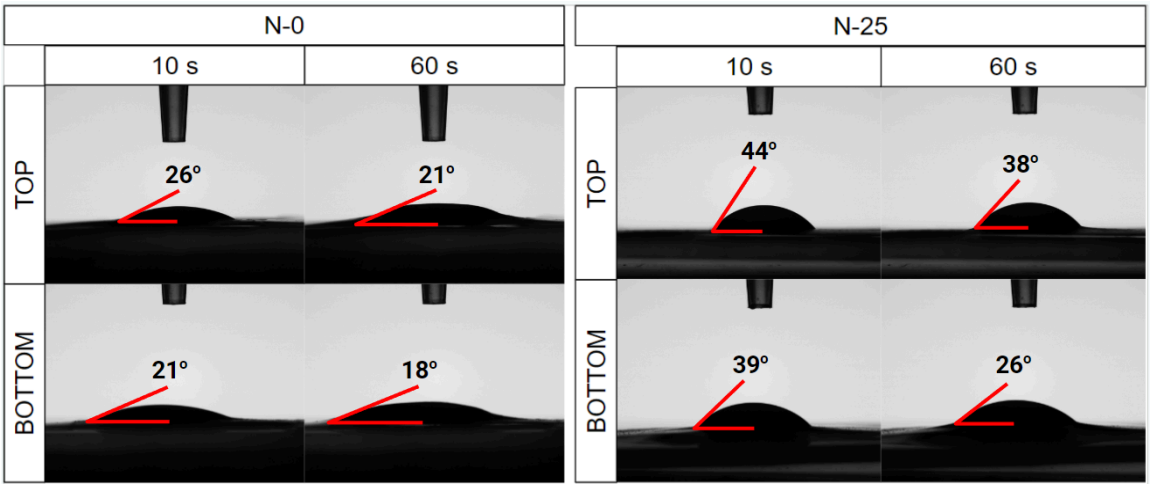

(**c**)

Fig. 3.10. Contact angle of the CNF film's surface : (**a**) top, (**b**) bottom, and (**c**) image comparison

Contact angle is the angle between the tangent to the droplet at the point of contact with the surface under test and that surface, as a measure of the hydrophobicity or wettability. The standard measuring liquid should be of low volatility so that its eventual evaporation does not affect the testing, not chemically reactive because that can cause the surface layer of the tested specimen to swell, and capable of producing droplets with sufficiently high wetting angle, identicality, and repeatability, for the sake of testing ease and precision. The droplet volume should be small enough to eliminate the impact of

gravitational forces yet large enough to prevent the surface micro-roughness from obscuring the measurement. The sitting droplet method was chosen in this study due to its simplicity and low cost. Other influencing factors include physical/chemical homogeneity, roughness, contamination, droplet size, liquid dispenser speed, humidity, and ambient temperature (Jagodzińska et al. 2021; Wawro and Kazimierczak 2008). Studies have also discovered a variance in microstructure, porosity, and pore size between the top and bottom surface of the cellulose-based film due to the casting method; therefore, the top surface tends to be significantly more hydrophobic (Jagodzińska et al. 2021; McGaughey et al. 2020). **Fig. 3.10** showcased the effect of homogenization cycles on the contact angle of CNFs, where it indeed found that the top surface (**Fig. 3.10**(a)) was more hydrophobic than the bottom (**Fig. 3.10**(b)) regardless of the cycle of homogenization. It was observed that the more passes of homogenization, the higher the wettability. The highest hydrophobicity was performed by the top surface of CNF after 25 cycles of homogenization (N-25), with contact angles of 45° (after 10 s) and 38° (after 60 s), which is 62% (after 10 s) and 85% (after 60 s) increase from hydrophobicity of N-0 top surface. This wettability is comparable to that of other CNFs, for example, softwood (44.2°) and kenaf (33° after 10 s, 0° after 60 s) (Jonoobi, Harun, Mathew, Hussein, et al. 2010). Though surface roughness plays a crucial role in creating better hydrophobicity (Jonoobi, Harun, Mathew, Hussein, et al. 2010), the high hydrophilicity nature of cellulose, owing to the plentiful polar groups, e.g., −OH and −COOH (Q. Wang et al. 2018), is also taken into account. Studies have proven a negative relationship between the number of polar functional groups and the contact angle values (G. Zhou et al. 2015; X. Sun et al. 2021). Hence, despite possessing the roughest surface (as confirmed in **Fig. 3.4**), N-0 did not display the highest contact angle. Furthermore, N-5, being the least hydrophobic, is also aligned with its surface roughness findings that indicate its utmost smoothness. Hydrophobic CNFs are applicable for coating (S. Huang et al. 2022), while hydrophilic ones would be suitable for hydrogel/aerogel as a drug-delivery system (De France, Hoare, and Cranston 2017).

3.4. Conclusions

In summary, this work comprehensively investigated the effect of varying cycles of mild-conditioned homogenization on the properties of Northern bleached softwood-based CNF. This technique shows significant advantages over CNF in fibrillation and the subsequent hydrogen bonding, promoting several functional properties, such as surface smoothness (44% increase by N-5), OP (48% decrease by N-5), mechanical properties (TS increase of 67% by N-10; E increase of 46% by N-15; EAB decrease of 31% by N-25), thermal properties (E' increase of 161% at 25 °C and 115% at 100 °C by N-15; E" increase 180% at 25 °C and 93% at 100 °C by N-20; Tan-δ increase of 10% at 100 °C by N-25; and $T_{d,5\%}$ increase over 10% post-homogenization), hydrophobicity (62% after 10 s and 85% after 60 s by N-25), on top of the successfully-maintained high crystallinity (averaged CI = 64%). Those impressive improvements confirmed the prospect of the developed novel approach in preparing CNF, which was homogenization equipped with an 'emulsifying cell,' low pressure, and no plasticizer. These operating conditions would overcome the recurring complications in myriad other techniques in preparing CNF, e.g.,

costly and clogging issues in conventional high-pressure homogenizers that also destructs crystallinity; hydrophilicity nature of CNF that suffers from declining oxygen barrier ability over time under humidity; polymer blending through coating or composites formation that may retard biodegradability while still having to address the matrix-filler compatibility; chemical modifications that may disrupt the existing hydrogen bonding; solvent methods that can be tedious, reagent-intensive, and time-consuming; and a thermal process that can cause partial degradation. With the offered characteristics, the resultant CNFs prepared using a simple, fast, and cheap approach would be comparable to conventional oxygen barrier polymers like EVOH. As the optimum homogenization cycle differs per property, further development can be designed according to the intended applications, e.g., high oxygen-barrier and UV-blocking food/pharmaceutical packaging, smooth/glossy finishes, rough-surfaced semiconductor, transparent wound dressing, opaque thermal insulation or mulching film, strong/elastic/stretchy film, thermostable display/electronic conducting film, hydrophobic coating, and hydrophilic drug-delivery hydrogel/aerogel.

3.5. Supplemental Data

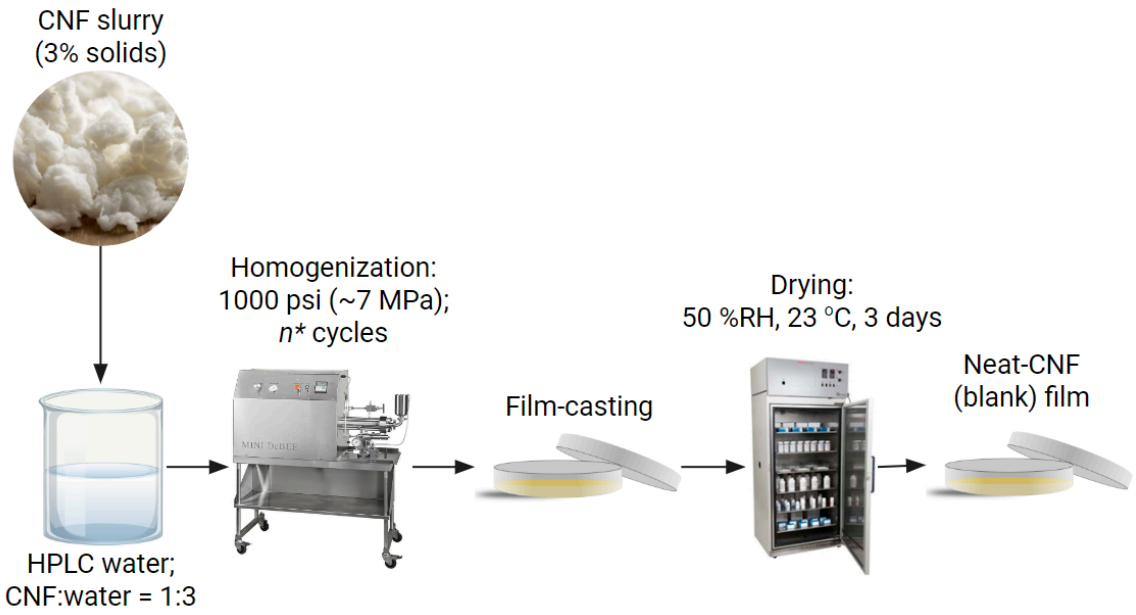

Fig. S.1. Schematic method of homogenized CNF films preparation

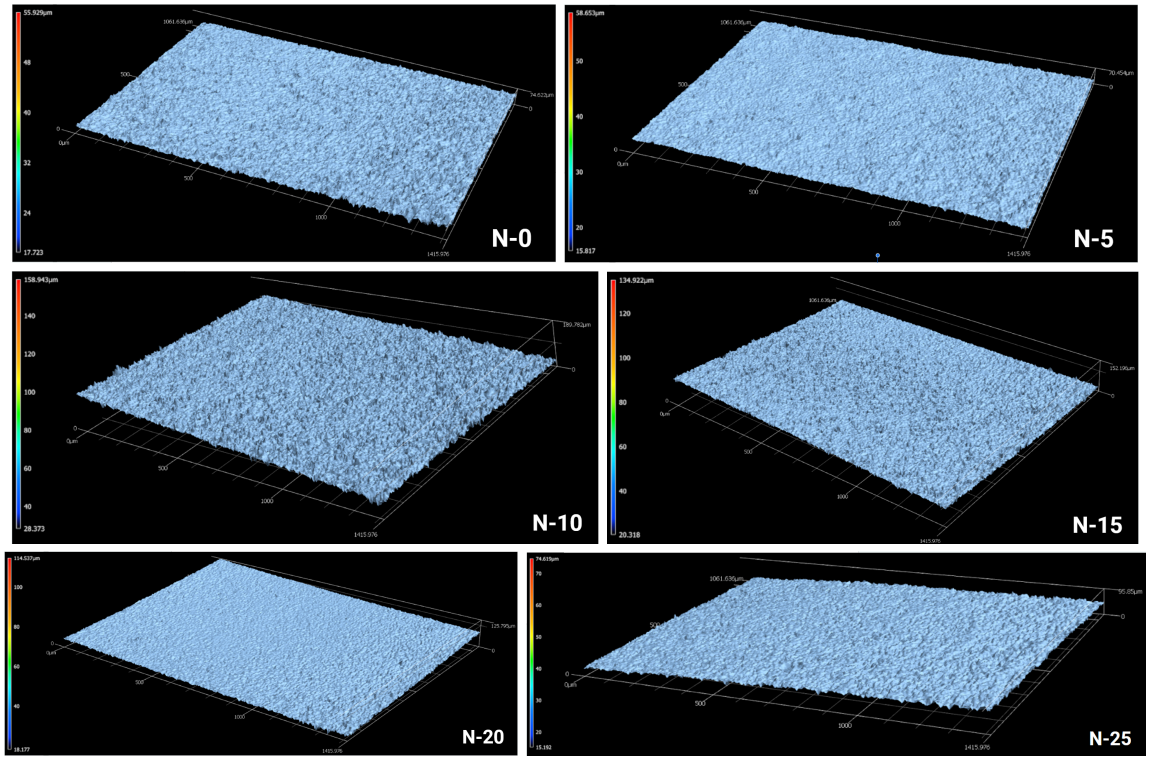

(**a**)

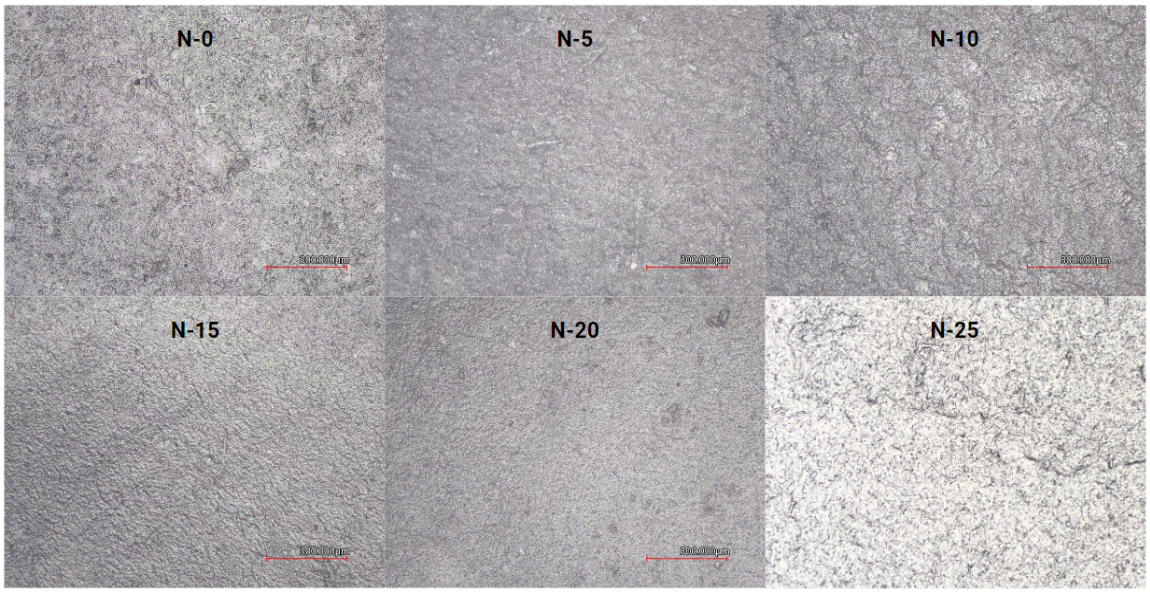

(**b**)

Fig. S.2. Surface roughness of CNF films: (a) 3D and (b) z-stack images

CHAPTER 4

Functionalization of nanocellulose film using TiO_2-TCPP as photosensitive antibacterial agents

ABSTRACT

Freshness and quality of food may deteriorate due to infectious contamination of bacteria, including Escherichia coli, a common foodborne pathogen. Metal-organic frameworks (MOF) have drawn growing interest through their ability to combine light, oxygen, and photosensitizer to generate reactive oxygen species that can kill microorganisms via an oxidative burst. Titanium dioxide (TiO_2) and tetrakis(4-carboxyphenyl)porphyrin) (TCPP) were selected as the developed MOF's inorganic secondary building blocks and organic ligands/linkers, respectively, which were incorporated into a homogenized (0-25 cycles) cellulose nanofibril (CNF) matrix. TCPP's performance as a photosensitizer dye was proven by the resulting complete inhibition of *E. coli* growth (100% antibacterial rate) under 6000 lux-light irradiation after 72 hours by functionalized films prepared using homogenized CNF. Likewise, TiO_2's UV-blocking ability was also evidenced by the complete UV-A/B/C absorption. In addition, surface smoothness, mechanical properties, thermal stability, and hydrophobicity of the functionalized films using homogenized CNF were improved, indicating the positive effect of enhanced fibrillation and the subsequent inter/intra-molecular hydrogen bonding post-homogenization. This work also certified cellulose's capability as a MOF carrier that solved its notoriously challenging self-aggregation/quenching tendency, as shown morphologically which confirmed the even dispersion of the TiO_2-TCPP conjugate. These findings overall exhibited a promising potential for a myriad of antibacterial film applications, including food packaging and biomedical.

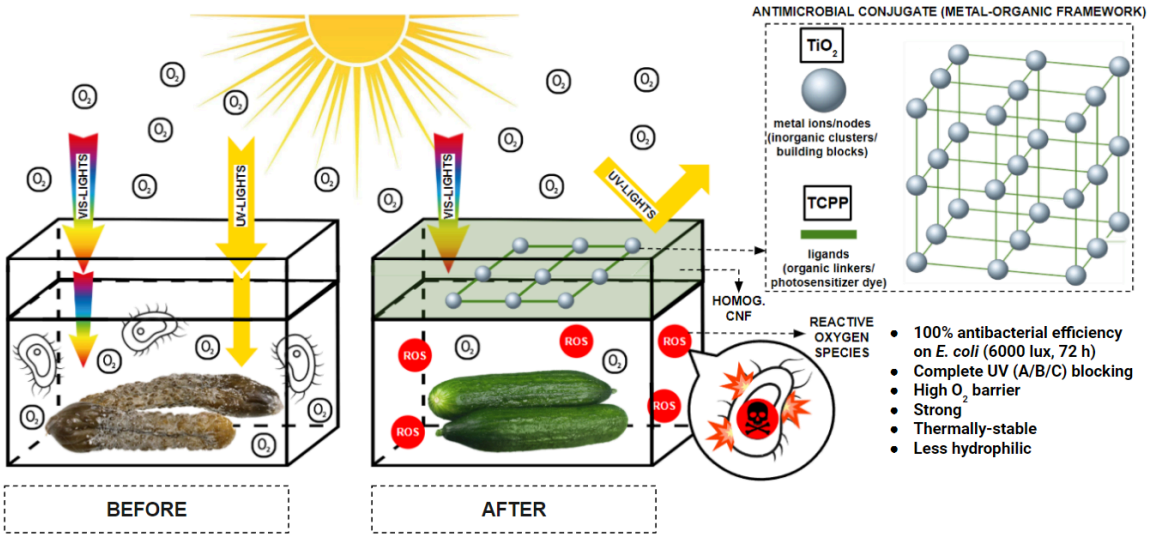

Graphical abstract

4.1. Introduction

The freshness and quality of food can deteriorate due to infectious bacterial contamination. As it has been on the rise in recent years, advancement in the packaging field to tackle such concerns is of profound significance. Especially as using chemical disinfectants is not ecologically convenient after the occupational and operational risks that come with it. Traditionally, packaging is mainly made of synthetic materials derived from fossil fuel, meaning they are non-renewable and non-biodegradable. In this context, it has been increasingly encouraged to employ natural alternatives that are available in abundance, one of which is cellulose. It is named among the most abundant biopolymers in nature, with remarkable biocompatibility, low cost, and nontoxicity. In spite of the significant strengthening of the mechanical and barrier properties of nanocellulose-based packaging materials, the threat from pathogens may still remain. Nowadays, photosensitization or photodynamic inactivation has been proposed as an alternative antimicrobial modality. One of the emerging schemes is through metal-organic frameworks (MOFs); it combines light of a specific wavelength, molecular oxygen, and photosensitizer to generate reactive oxygen species (ROS), especially singlet oxygen ($^1O_2$), that can kill microorganisms via an oxidative burst. The process involves electron-transfer reactions from the photosensitizer's triplet state to surrounding substrates, thereby facilitating cytotoxic species, such as superoxide anion, hydroxyl, and lipid-derived radicals (mechanism Type I) and/or energy transfer from the triplet state to ground state molecular oxygen ($^3O_2$) to produce excited-state singlet oxygen ($^1O_2$) (Type II) (Castro et al. 2019). No high heat nor harmful substances are required and/or released. MOF is a crystalline porous system consisting of ligands (as organic linkers) and metal ions/nodes (as inorganic clusters or building blocks) whose composition, structure, and porosity can be modulated to the desired functionality. It is also appealing for the ease of synthesis and surface modification, as well as the sustained releasing capacity. Porphyrin-based MOF is among the many photosensitive porous coordination networks with feasible structural tunability, stable crystalline structure, open channels, and biocompatibility. The highly-conjugated macromolecular and heterocyclic-structured porphyrin and its derivatives act as a photosensitizer to generate relatively high-yielding $^1O_2$ for antibacterial packaging applications under simply visible light irradiation, as UV light may harm normal cells and tissues (Min et al. 2021; M. Chen et al. 2020; J. Park et al. 2016; X. Zhao et al. 2023). It can also help to avoid photosensitizer's quenching under the excited states or energy, as well as to enable facile accessibility of ROS diffusion over the rigid and porous network (K. Lu, He, and Lin 2014; Zheng et al. 2018).

Titanium (Ti) is one of the most studied examples of the inorganic metal ions in the case of porphyrin-based MOFs, where its high oxidative state leads to a preference to coordinate with the carboxyl functional group rather than the porphyrinic core. Titanium dioxide (TiO_2) is among the common Ti precursors. As a photocatalyst, it has been utilized for its antimicrobial feature, including in food packaging, as it holds FDA approval as a "food contact substance." Its antibacterial activity is proven against a broad spectrum of microorganisms due to the high redox potential of the surface species formed by photoexcitation (under UV illumination), affording non-selective oxidative attack of microorganisms (El-Wakil et al. 2015). TiO_2 is also attractive for its high availability, low price, safety (non-toxicity), non-corrosiveness, ease of production, excellent optical

properties, high surface areas, and stability in physical, chemical, and photoactivity aspects (Gao et al. 2019; Castro et al. 2019; Roberta Grazia Toro et al. 2020; An et al. 2016). Three (3) crystal structures of TiO_2 comprise rutile, brookite, and anatase; the latter possesses better photocatalytic activity and is most widely used in practical applications due to its wider band gap. However, the unsatisfactory photocatalytic activity of TiO_2 under visible light limits its applicability. Dye sensitization using porphyrin-based MOF as the organic bridging ligand is among the solutions, one of which is tetrakis(4-carboxyphenyl)porphyrin) (TCPP). Some semiconductor studies highlighted the effect of incorporating such photosensitizer that enlarged the wavelength response range, enhanced the interfacial charge migration and separation, as well as inhibited the recombination of photo-generated electron-hole pairs in the photoreduction system—essentially improving the photocatalytic activity of TiO_2 under visible light region (Wan et al. 2016; Gao et al. 2019). Ti also boosts ROS generation, especially superoxide anion radicals, due to the improved photo-electron transfer from TCPP. The effectiveness was proven on Gram-positive/negative pathogens, besides the biocompatibility, minimal cytotoxicity, and minimal inflammatory effect (M. Chen et al. 2020; Tu et al. 2017). A study has determined the potential of TCPP dye-sensitized TiO_2 for solar-energy-converting electrodes. The strong adsorption of TCPP onto nano-TiO_2 was observed, as well as its efficiency as a photosensitizer. Effective coupling between the orbitals of the two materials was accomplished, allowing efficient electron transfer from the excited TCPP to the TiO_2 conduction band. Another advantage of porphyrins as one of the common photosensitizers is their strong absorption in both Soret (400–450 nm) and Q-bands (500–700 nm) (Cherian and Wamser 2000).

Cellulose has been explored as an ideal carrier for MOFs. Its repeat unit comprises a cyclic backbone of sugar rings with three hydroxyls on each ring alongside ether groups, where these high-density oxygenated functional groups provide the chemical functionalities of cellulose (Adel et al. 2021; Adel, El-Shafei, et al. 2019; Adel, Ibrahim, et al. 2019). The aforementioned hydroxyl groups present on the nanocellulose fibers' surface act as stable and robust anchoring sites as matrices for ex-situ loading and stabilization of pre-formed TiO_2 nanoparticles. Improved mechanical and barrier properties were also evidenced (Roberta Grazia Toro et al. 2020). In regards to MOFs (including TCPP) and TiO_2, the problem lies in self-aggregation and self-quenching tendency, besides the remaining metal toxicity and complexity during recycling/reusing and separation from the reaction medium due to its nanoscale size (An et al. 2016). In this regard, incorporating them into polymeric nanofibers/nanotubes (as carriers) has attracted considerable attention in improving their processability and biosafety (Min et al. 2021; M. Chen et al. 2020; J. Park et al. 2016; X. Zhao et al. 2023; G.-Q. Liu et al. 2021). It can also help to avoid photosensitizer's quenching under the excited states or energy, as well as to enable facile accessibility of ROS diffusion over the rigid and porous network (K. Lu, He, and Lin 2014; Zheng et al. 2018). Embedding/immobilizing TiO_2 onto dispersive supporting materials with large surface areas (e.g., cellulose (An et al. 2016), graphene (Bhirud et al. 2015), and carbon nanofibers (M. Kim et al. 2014)), has been proven successful by previous studies in addressing TiO_2 agglomeration issue and subsequently enhancing the photocatalytic activity. The development of composite between nanocellulose (as matrix) and TiO_2-TCPP (as photosensitive MOF) is expected

to promote a more efficacious dispersion of catalyst nanoparticles and enhance the functional properties of the as-synthesized composite (Roberta G. Toro et al. 2022).

Several reports found that Gram-positive and Gram-negative bacterial strains are susceptible to ROS produced by porphyrins; however, their efficacy highly depends on the used porphyrin structure and its charge. In particular, neutral, cationic, or anionic porphyrin derivatives can inactivate Gram-positive bacteria (Gomes et al. 2013), but an effective photo-inactivation of Gram-negative bacteria (without membrane disrupting agents) requires the presence of positive charges in the porphyrin structure. The relationship between the porphyrin surrounding charges and the capability to inactivate Gram-negative bacteria can be explained by considering the bacteria's physiology. While the Gram-positive bacteria cell wall is composed of a thick porous layer of peptidoglycan with attached teichoic acids, the Gram-negative bacteria cell wall includes a relatively thin layer of peptidoglycan surrounded by an asymmetric highly impermeable bilayer with an inner leaflet of phospholipids and outer leaflets of lipopolysaccharide. Each lipopolysaccharide imparts a strongly negative charge on the surface of Gram-negative bacterial cells, limiting the permeation of neutral and negatively charged photosensitizers (Delcour 2009). However, photosensitizers containing positive charges are able to promote a strong electrostatic interaction with the negatively charged sites at the outer surface of the bacterial cells, thus facilitating their accumulation in key subcellular compartments (Castro et al. 2019).

Many studies have explored the photosensitivity and antimicrobial potentials of CNF-TiO_2 (G.-Q. Liu et al. 2021; An et al. 2016), CNC-TiO_2 (Roberta G. Toro et al. 2022; Rathod et al. 2018), cellulose paper-TiO_2 (Roberta Grazia Toro et al. 2020), TiO_2-TCPP (Cherian and Wamser 2000; Gao et al. 2019), pullulan-PVA-TCPP-thymol (Min et al. 2021), PP-CNC-TiO_2 (Zielińska et al. 2022), gluten-CNC-TiO_2 (El-Wakil et al. 2015), polycaprolactone-TCPP (X. Zhao et al. 2023), CNF-porphyrin (Fularz, Almohammed, and Rice 2021), CNC-porphyrin (Carpenter et al. 2012; Fularz, Rice, and Ballone 2021) and Zr-TCPP (J. Park et al. 2016) intended for varying applications from food packaging (El-Wakil et al. 2015; X. Zhao et al. 2023; Larrea et al. 2024; Min et al. 2021), solar-energy converter (Cherian and Wamser 2000), CO_2 photoreductor/converter (Gao et al. 2019), photodynamic therapy (J. Park et al. 2016; Carpenter et al. 2012), spectroscopy (Fularz, Almohammed, and Rice 2021), hydrogen generator (An et al. 2016), nanodevices (Fularz, Rice, and Ballone 2021), until micropollutants removal or dye wastewater treatment through adsorption/photodegradation (Rathod et al. 2018; Roberta Grazia Toro et al. 2020; G.-Q. Liu et al. 2021). Yet, no report on the photocatalytic disinfection properties of CNF films functionalized by TiO_2-TCPP has been conducted. The objective of the present study is to be a step toward using active biobased packaging in food applications instead of petrochemical-based plastics by improving the functional properties, processability, and applicability of nanocellulose-based films. In this regard, the films' oxygen permeability, mechanical properties, thermal stability, morphology, roughness, opacity, wettability/contact angle measurements, and bactericidal inhibition rate against the pervasive pathogen *Escherichia coli* were investigated.

4.2. Materials and method

4.2.1. Materials

Cellulose nanofibrils (CNF) slurry with 3% solids derived from northern bleached softwood kraft pulp was obtained from the Process Development Center of the University of Maine (Orono, ME, USA). TCPP, labeled as meso-Tetra(4-carboxyphenyl)porphine, was purchased from Frontiers Scientific (Newark, DE, USA), while nano-titanium dioxide (TiO_2, AEROXIDE® P25) was acquired from Acros Organics (Geel, Antwerp, Belgium). HPLC-grade water and 96%-ethanol (190 proof) were from EMD Millipore (Burlington, MA, USA) and Decon Laboratory (King of Prussia, PA, USA), respectively. Tryptic soy agar and broth (TSA, TSB) were purchased from Becton Dickinson (Franklin Lakes, NJ, USA). Phosphate Buffered Saline (PBS) was from VWR International (Radnor, PA, USA). All chemicals were analytical grade.

4.2.2. Homogenization process

The CNF slurry (3% solids) was diluted with water (1:3) by mixing under constant stirring (30 mins) to produce neat-CNF solution. The solution was further treated with a Mini DeBEE 30 homogenizer (BEE International, South Easton, MA, USA) with a 0.20 mm (0.008 inch) nozzle at 7 MPa, repeated for a different number of cycles (0, 5, 15, 25; or labeled as N-0, N-5, N-15, N-25, respectively). Homogenization cycles were maintained to be under 30 passes according to the preliminary studies, as well as referring to optimized results of previous studies on homogenized cellulose prepared at a medium/low conditioning pressure range (Chun et al. 2011; V. C. F. Li et al. 2018; Q. Cheng and Via 2017; Du et al. 2016; J.-C. Lee et al. 2018; T. Wang and Drzal 2012). On top of the internal cooling system, the homogenizer was equipped with an Isotemp Refrigerated Circulating Bath 910 chiller (Fisher Scientific, Waltham, MA, USA).

4.2.3. Antibacterial TiO_2-TCPP conjugates preparation

TCPP (1 mmol) was mixed into 96%-ethanol before adding nano-TiO_2 (1% w/v of TCPP solution). The mixing was conducted while the solution was kept and covered in the dark overnight (75 ^oC). The antibacterial conjugate solution was prepared by mixing water and the TiO_2-TCPP conjugate powder (0.2% w/v of water).

4.2.4. Film production

The homogenized neat-CNF (30 mL) and antibacterial conjugate solution (14 mL) were mixed using Mini Vortexer (VWR International, Radnor, PA, USA) on high speed for a few minutes to produce 2.2 mg/cm^2 functionalized-CNF film solution or labeled as F-0, F-5, F-15, and F-25. The mixture was then poured into a 9 cm x 1.5 cm petri dish using solvent casting technique and left to dry in the Forma Environmental Chamber (Thermo Scientific, Waltham, MA, USA) (50 %RH, 23 °C, 48 hours). The same preconditioning parameters were set before each test of the films.

4.2.5. Characterizations

4.2.5.1. Fourier transform infrared (FTIR) analysis

FTIR spectra indicating functional groups were determined by the Nicolet 8700 spectroscopy equipped with Attenuated Total Reflectance (ATR) (Thermo Scientific, Waltham, MA, USA) at a wave-number range of 400–4000 cm^{-1} and a total of 32 scans. The results were reported as an average of three (3) replicates.

4.2.5.2. Morphology, surface roughness, and opacity

Surface and cross-sectional morphology were characterized by the NeoScope JCM 5000 Scanning Electron Microscope (SEM) (JEOL Ltd., Tokyo, Japan). For surface SEM observation, the sample (25 mL) was initially prepared by lyophilization or freeze-drying after being kept in a -80 °C ultra-low freezer (Millrock Technology, Kingston, NY, USA). It was then mounted onto a pin stub mount using copper tape before being coated with roughly 100 Å of gold in an ion sputter coater (Denton Vacuum, Moorestown, NJ USA) using argon gas (10-15 psi) at pressure and current of 50 mTorr and 45 milliamps, respectively, for 45 seconds. Specimens were subsequently imaged at different magnifications under a vacuum at an operating voltage of 10 kV. Furthermore, the surface roughness of films was investigated using the Keyence VK-X3000 3D surface profilometer (Keyence Corporation, Osaka, Japan) referring to ISO 25178. Three-dimensional images of the film surfaces were analyzed with the Keyence VK-X3000 MultiFileAnalyzer (Keyence Corporation, Osaka, Japan) software to perform filtering according to the reference plane to the films' real surface to smooth out height variability before the roughness parameters measurement. Afterward, arithmetical mean height (Sa) or the average absolute height value at each point in the definition area was reported as an average of three (3) replicates. Lastly, to determine opacity, transmission spectra of the films were carried out using a Genesys 10S UV-vis spectrometer (Thermo Scientific, Waltham, MA, USA) in the wavelength range of 190–900 nm with 0.5 nm interval, in addition to the visual observation

4.2.5.3. Barrier property

Oxygen Permeability (OP) was characterized using the C230 Oxygen Transmission Rate Testing System (Labthink International Inc., Medford, MA, USA). The 700-118-20 Quick Mini digital thickness gauge (Mitutoyo, Kawasaki, Japan) to the nearest 0.001 mm was used to measure ten (10) random readings, which were then averaged. The plate was then inserted into the cell chamber and closed tight. The "Film-ASTM" test type without compensation was selected. To maintain purity, cycle process mode with rezero purging for N_2 gas in the cells was performed for 30 seconds with one cycle interval. The system was preheated for 2 hours. The flow rate, test humidity, and test temperature were adjusted to 100 mL/min, 50%RH, and 23 °C receptively. Six (6) cycles under standard test mode were completed at 30-minute intervals in each cell. The results were reported as an average of six (6) replicates.

4.2.5.4. Mechanical properties

Mechanical properties were measured with Material Test Systems 27-00112 (MTS Systems Corporation, Eden Prairie, MN, USA). The films' tensile strength (TS), tensile/Young's modulus (E), and elongation-at-break percentage (%EAB) were

measured with 0.1 N preload at a test speed of 0.40 mm/s until the films (2 × 8 cm) were ruptured. TS was calculated from the ratio of maximum load to the cross-sectional area of the film. Meanwhile, %EAB was the ratio between the increased length pre-rupture and the film's initial length. Lastly, E was the ratio between stress and strain from the linear portion of the stress-strain curve. The results were reported as an average of ten (10) replicates.

4.2.5.5. Thermal properties

Thermal analysis was performed using a Thermogravimetric Analyzer (TGA) 550 (TA Instruments, New Castle, DE, USA). Pan loading-taring was conducted using the auto sampling technique using a platinum (100 µL) pan. A sample (5-15 mg) was spread in the pan to maximize surface area. It was equilibrated at 50 °C, then ramped from 20 °C/minute to 700 °C. Temperature when the sample's weight loss reached 5% ($T_{d,5\%}$) was recorded. Data analysis using the TRIOS or TA Universal Analysis (TA Instruments, New Castle, DE, USA) software was then performed. The results were reported as an average of five (5) replicates.

4.2.5.6. Contact angle or wettability

The water contact angle or wettability was tested by the OneAttension® Theta Flow optical tensiometer (Biolin Scientific, Stockholm, Sweden). Using the "sessile drop" experiment type equipped with a 200 µL pipette tip at 25 µL/min dispenser speed, a drop (5 µL) of HPLC-grade water was deposited onto the film surface to measure the contact angle in varying regions. "Light" and "heavy" phases were set as air and water (20 °C), approximately, which are selected to determine the density difference value for the surface tension measurement. The drop images and subsequent contact angles were obtained with a total duration of 60 seconds at ten-second intervals and reported as an average of three (3) replicates.

4.2.5.7. Antibacterial activity

Escherichia coli (ATCC 25922) was selected as the representative bacteria to test the bactericidal efficacy of TiO_2-TCPP conjugate-incorporated CNF films (F-films). The stock culture was inoculated in 10 mL of TSB in 15-mL centrifuge tubes and incubated at 37 °C for 16 hours until the Optical Density (OD) reached ~1.0. Bacteria were harvested by centrifugation at 5,524g for 5 minutes and re-suspended into 10 mL PBS solution (pH 7). After resuspension, 10-fold serial dilutions were performed to yield an *E. coli* concentration of ~10^5 CFUs (colony-forming units)/mL. To start the antibacterial efficacy assessment, the initially prepared F-films were cut into 5/8-inch circular discs. The films were then placed into a sterile 24-well plate (VWR, Allentown, PA, USA), with a volume of 3.7 mL (diameter:1.66 cm; height:1.72 cm), completely submerged in 900 µL of the prepared bacterial suspension on an orbital shaker (4 °C, 200 rpm) with an 800D LED 40W panel (GVM, Philadelphia, PA, USA) as the light source under different intensities (3000 and 6000 lux) and color temperature adjusted to 4100K, as confirmed using an SDL 4000 light meter (Extech Instruments, Nashua, NH, USA). Sampling was performed at a 24-hour interval for 72 to 96 hours. One duplicate dark control was also prepared by wrapping the 24-well plate with aluminum foil. After incubation, 100 mL of bacterial suspension was withdrawn from the well and plated onto TSA plates using an Autoplate 4000 spiral plater (Spiral Biotech Inc., Norwood, MA, USA). The TSA plates were

incubated at 37 °C for 24 hours, and plate counting was conducted to determine bacterial viability. The antibacterial rate was evaluated using the equation below (Mao et al. 2019; Tao et al. 2020; Min et al. 2021), where N is the average number of *E. coli* colonies calculated from control groups and experimental groups. The results were reported as an average of duplicates.

$$Antibacterial\ rate\ (\%) = \frac{N_{control} - N_{sample}}{N_{sample}}\ x\ 100\%$$

4.2.6. Statistical analysis

Data were analyzed by a one-way variance analysis (ANOVA) followed by Tukey's test and Student's t-test, using the Microsoft Excel 2019 (Microsoft Corporation, Redmond, WA, USA) and/or JMP 16 Pro (SAS Institute, Cary, NC, USA) software to establish significant differences (p-value < 0.05). The use of different letters on graphs data denotes statistically significant differences.

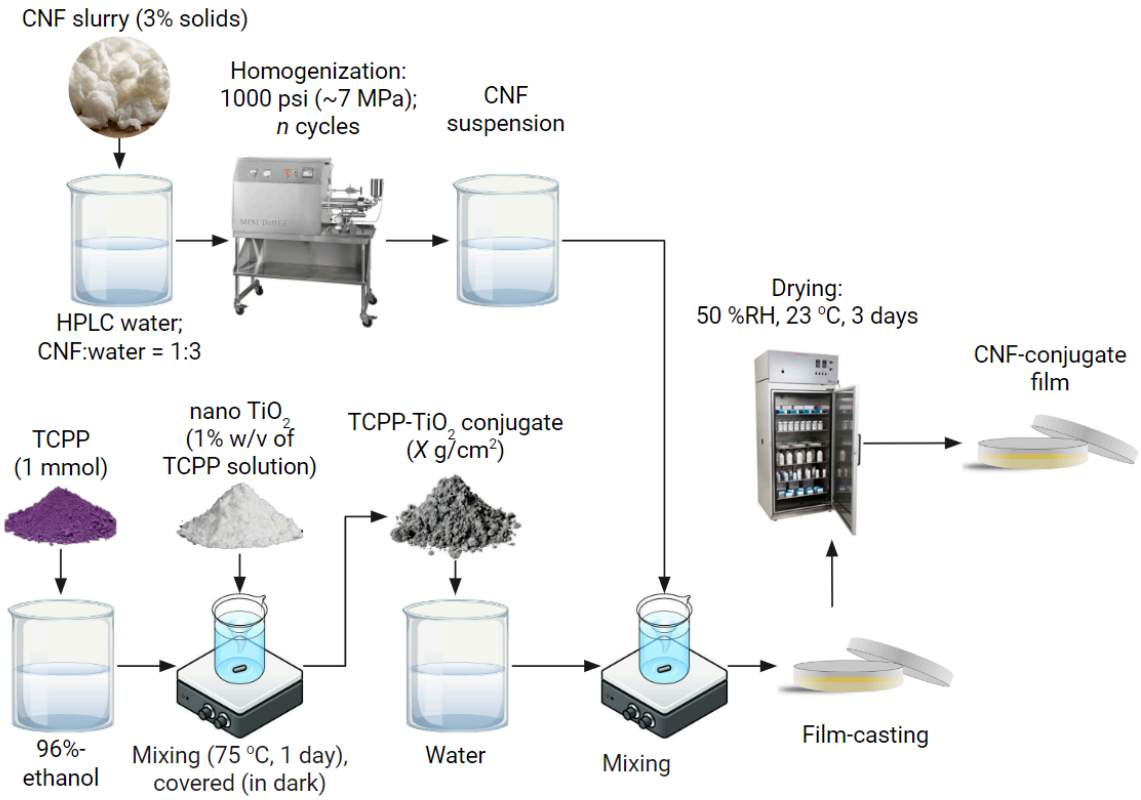

(a)

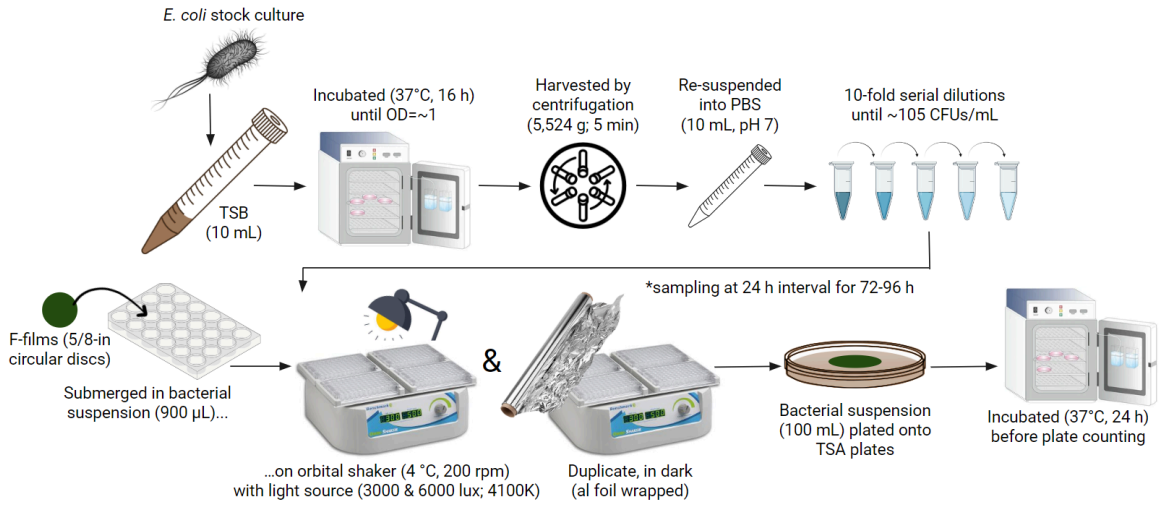

(b)

Fig. 4. Schematic methods: (**a**) CNF-conjugate preparation and (b) antibacterial activity

4.3. Results and discussion

4.3.1. Fourier transform infrared (FTIR) analysis

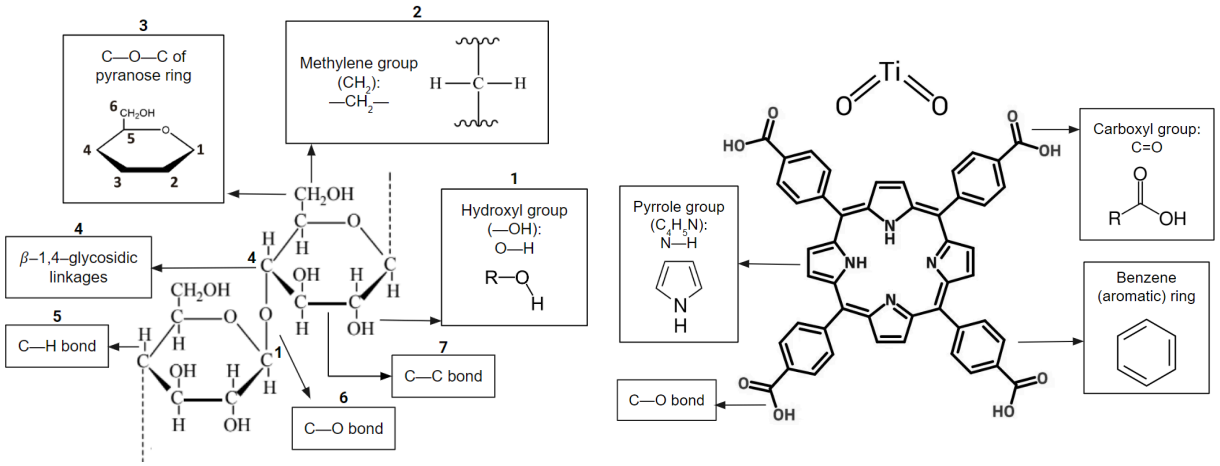

(a) **(b)**

Fig. 4.1. Chemical structure and major functional groups of (**a**) cellulose; (**b**) TiO_2 and TCPP

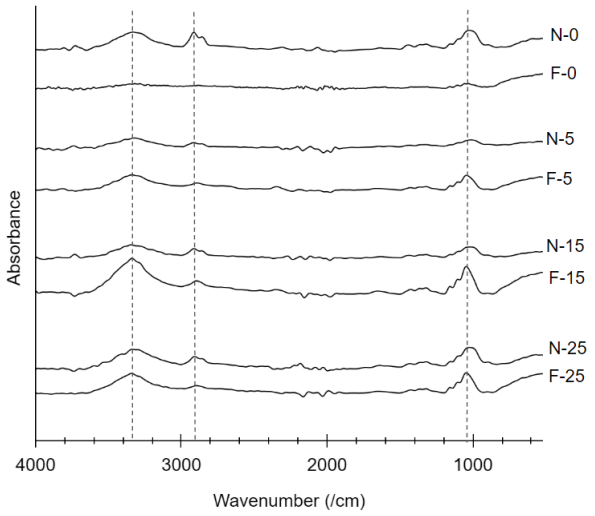

Fig. 4.2. FTIR spectra comparison between N-films and F-films

Table 4.1. FTIR peaks assignment (functional group and molecular vibration type)

Approximate wavenumber (cm^{-1})	Functional group and molecular vibration type
3350	stretching of O—H (of —OH or hydroxyl groups)
2910	stretching/bending of N—H (of C_4H_5N or pyrrole group)
2900	(anti)symmetric stretching of C—H (of CH_3/methyl or CH_2/methylene group)
1650	bending of O—H and H–O–H (of H_2O or absorbed water)
1600	benzene (aromatic) ring skeleton
1530	stretching of C=O or carboxyl group
1510	benzene (aromatic) ring skeleton
1450	benzene (aromatic) ring skeleton
1420	scissoring of C—H (of CH_2 or methylene group); cellulose's crystalline region
1395	benzene (aromatic) ring skeleton
1390	TiO_2 lattice
1370	bending of C—H and C–O
1310	wagging of C—H (of CH_2 or methylene group)
1160	stretching of C—O
1150	stretching of C—C
1130	Ti—OH
1050	antisymmetric stretching of C—O—C (of pyranose ring)
1045	Ti—O—C
1040	stretching of C—O
990	bending of C=C
970	in-plane bending of N—H (of C_4H_5N or pyrrole group)
890	cellulosic β–1,4–glycosidic linkages; cellulose's amorphous region
800	Ti—O—Ti
670	out-of-plane bending of C—OH
590	Ti—O—O

The chemical nature of surface functional groups in the functionalized film was investigated by FTIR spectroscopy. **Fig. 4.1** provides the chemical structure of the three components of the developed antimicrobial composite: cellulose nanofibrils (CNF) (**Fig. 4.1**(a)) and the conjugates (**Fig. 4.1**(b)), i.e., titanium dioxide (TiO_2) and meso-Tetra(4-carboxyphenyl)porphine (TCPP). The presence of each of the highlighted functional groups was confirmed in the resulting FTIR spectra in **Fig. 4.2**; where the functional group and molecular vibration type assigned to each wavenumber are listed in **Table 4.1**. The identified stretching vibrations of (free) O—H or hydrogen bonds were present in phenolic and aliphatic structures (Md Salim, Asik, and Sarjadi 2021). These broad bands correlated to scission by the equatorially positioned hydroxyl groups of cellulose that form inter/intra-molecular hydrogen bonds between its sequential glucose units and with water, either as the solvent or existing moisture in the air (Wohlert et al. 2022; Tang et al. 2018). The same peak could also be ascribed to the O–H stretching vibrations, confirming the presence of hydroxyl groups on the TiO_2 surface (Erdem et al. 2001). The (anti)symmetric stretching, scissoring, and wagging of C—H of methylene groups (CH_2), as well as the C—H stretching of methyl groups (CH_3) and C—O—C antisymmetric stretching, belonged to the pyranose ring of the cellulose's glucose units (Roberta Grazia Toro et al. 2020). Another band indicative of interstitial or adsorbed water was the bending of O—H and H–O–H bonds (Roberta Grazia Toro et al. 2020; An et al. 2016; Jiaoxing Xu et al. 2008). More typical absorption bands of cellulose were observed, contributing to β–1,4–glycosidic linkages and amorphous/crystalline regions (Maślana et al. 2021). These aforementioned bonds were present in all N-film and F-film samples, thus shown in their spectra. Furthermore, speaking of the conjugate incorporated into CNF, TiO_2 characteristic wide bands are located below 800 cm^{-1} wavelength and identified in the spectra, which attributed to the following bonds: Ti—O—Ti (Sui, Rizkalla, and Charpentier 2004; Choudhury and Choudhury 2012), Ti—O—O (Rajakumar et al. 2012), Ti—OH and Ti—O—C bonds (Kalaiarasi and Jose 2017; Maślana et al. 2021; Vasconcelos et al. 2011), and TiO_2 lattice vibration (Nyquist and Kagel 2012). This finding verified the successful loading of TiO_2 without destruction of chemical reactions between cellulose and TiO_2, as the building block of the developed metal-organic framework (MOF), onto the CNF substrate (An et al. 2016). Lastly, TCPP, which acts as the conjugate's bridging ligand, is a porphyrin type with four carboxyl groups on its exterior benzene rings, and the presence of such an aromatic ring skeleton (Reagen et al. 2022; L.-J. Feng et al. 2017; J. Wu, Wang, and Wang 2020) and carboxyl groups (Roberta Grazia Toro et al. 2020; J. Wu, Wang, and Wang 2020) were evidenced in the resulting spectra. Some other characteristic peaks of TCPP were too located in all the F-films spectra, which are assigned to the stretching and (in-plane) bending of the N—H bonds that belong to the pyrrole groups (C_4H_5N) of TCPP (L.-J. Feng et al. 2017; J. Wu, Wang, and Wang 2020).

The position and intensity of FTIR bands are related to changes in the chemical surface groups (Hamad et al. 2018; Wade 2003). As seen in similar reports (D. Huang et al. 2020; Ilyas et al. 2019), the resulting spectra of N-films are identical, which indicates no chemical composition change occurred, meaning no new bonds formed post-homogenization. Meanwhile, for F-films, though mostly identical, different intensities were observed for the peaks around the 3350 cm^{-1} region, which correspond to stretching vibrations of hydroxyl groups. Using unhomogenized CNF that contained

less-fibrillated cellulose fibrils, the TiO_2-TCPP conjugates were not dispersed evenly. On top of the conjugate's self-aggregation and self-quenching tendency (An et al. 2016), this phenomenon led to much fewer hydrogen bonds being formed, either between CNF fibrils or between CNF and conjugates, as evidenced in the F-0 spectra. In contrast, F-5, F-15, and F-25 films produced stronger peaks in the said region due to the promoted hydrogen bonding from using the homogenized CNFs with enhanced fibrillation as the matrix; more specifically, strong interaction between —OH groups of CNF & Ti—O bonds in TiO_2 (Shu and Li 2012). Similar findings of strong hydrogen bond interaction between CNF and the loaded conjugates were reported (An et al. 2016; Zeng et al. 2010; Roberta Grazia Toro et al. 2020), which confirmed the fruitful immobilization in the matrix and low detachment tendency of the conjugate nanoparticles (Mohamed et al. 2015). In terms of the developed films' application as a visible light-responsive antimicrobial packaging, such an increase of —OH surface groups promoted hydroxyl radicals (•OH) formation during the photocatalytic process (de Almeida et al. 2020; Roberta G. Toro et al. 2022). As already known, hydroxyl radical is among the prominent reactive oxygen species (ROS) that exert microbicidal/bactericidal activity against a broad range of pathogens (Vatansever et al. 2013; Kohanski et al. 2007). In addition, the film's functionalization could also be proved by observing the C—H stretching vibration (2900 cm^{-1}). Upon the incorporation of conjugates into CNF, the peak intensity decreased as a result of steric hindrance and blocking of C—H in-plane stretching (Roberta Grazia Toro et al. 2020). More in-depth analysis of these phenomena morphologically through the lens of microscopic images is discussed in the next section.

4.3.2. Morphology, surface roughness, and transparency

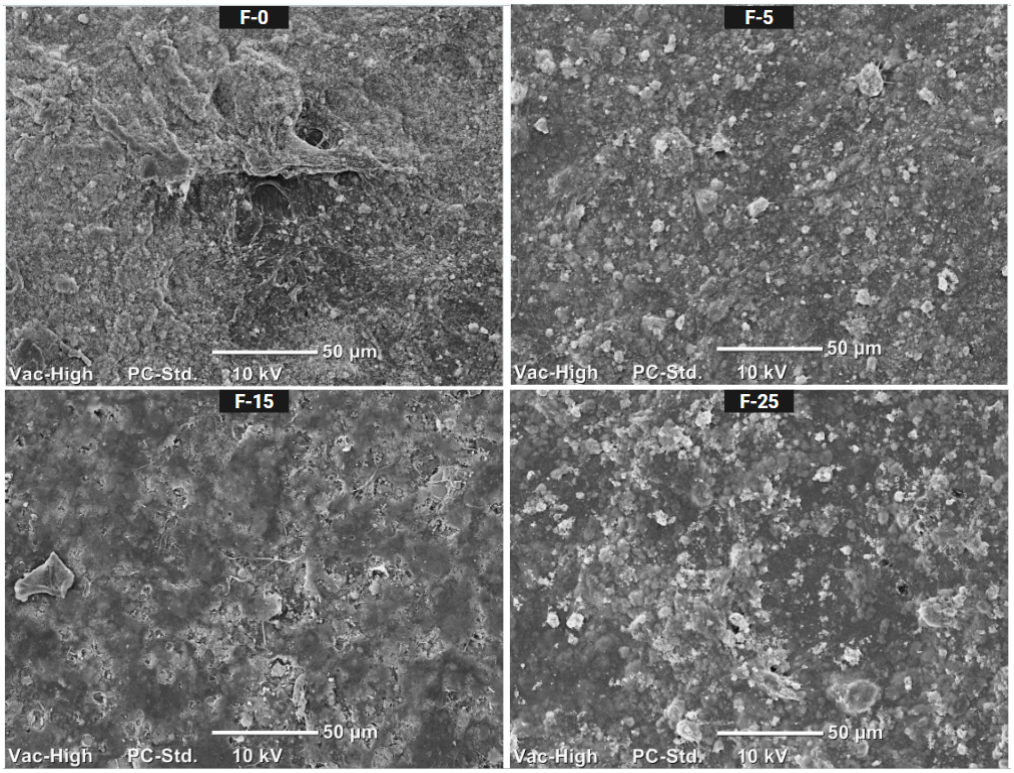

(a)

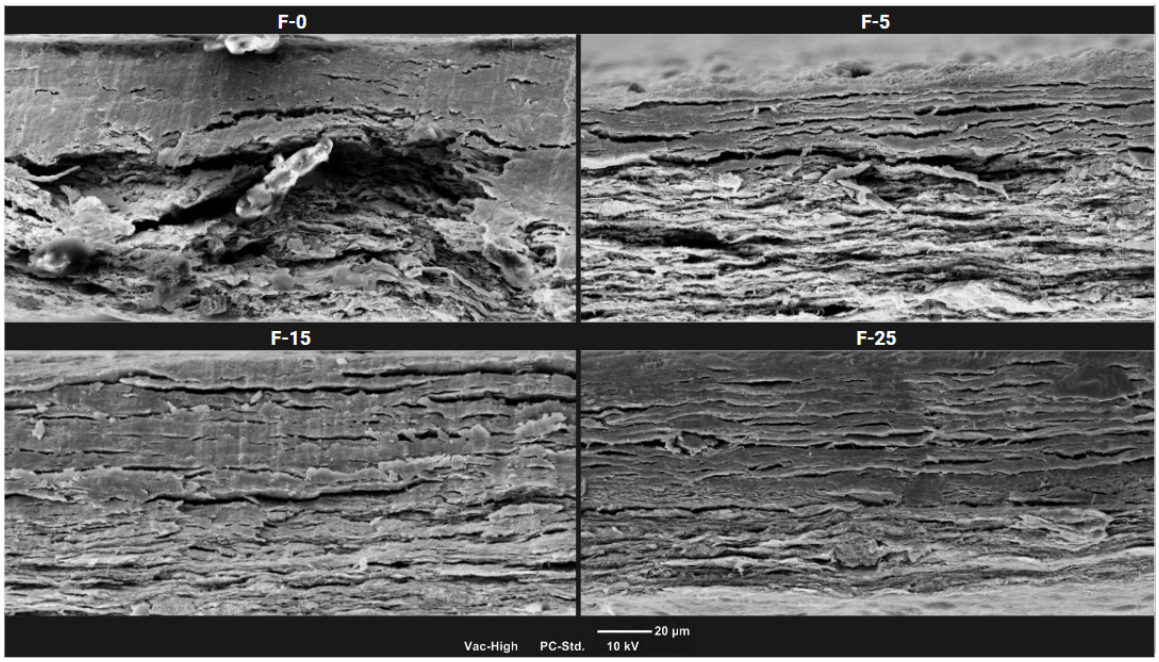

(**b**)

Fig. 4.3. SEM images of functionalized CNF films: (**a**) surface and (**b**) cross-section, at 500x and 1000x magnifications, respectively

The surface and cross-sectional SEM images of the functionalized CNF films post-homogenization are presented in **Fig. 4.3**(a) and **Fig. 4.3**(b), respectively. Prior homogenization (F-0), surface observation (**Fig. 4.3**(a)) showed massive agglomerates of cellulose fibers and TiO_2-TCPP conjugates, creating a rough and coarse appearance of fragments (repeating units of cellulose) (Gautam et al. 2010; Redlinger-Pohn, Petkovšek, et al. 2022). This is led by the untreated cellulose fibrils pre-fibrillation that were still so strongly entangled, forming thick irregularly-shaped bundles that prevent an even dispersion of the incorporated conjugate granules throughout the matrix system, and many eventually aggregated since both TiO_2 and TCPP, like the majority of MOFs, suffer from self-aggregation/quenching tendency issues, especially when nanosized (An et al. 2016). The naturally high surface energy of TiO_2 also caused conjugates to agglomerate into big clusters (G.-Q. Liu et al. 2021). The effect of the hindered conjugate distribution could be explained better by the cross-section image (**Fig. 4.3**(b)). Conjugates could not maneuver through the not-fibrillated and compacted thick mass of cellulose fibrils and sank to the bottom of the petri dish when the film was being dried, creating two separate 'layers' where the bottom one was significantly rougher due to the accumulated conjugate aggregates. The conducted multi-cycled homogenization provides pressure drop, high shear, and impact forces that trigger mechanical release or fibrillation of the aforementioned cellulose bundles. The produced fine fibrils possess high surface areas, which means more inter-/intramolecular hydrogen bonding (Nagarajan et al. 2021; H. Lee, Sundaram, and Mani 2017; Chun et al. 2011). This allowed the formation of pores/cavities for inorganic nanoparticles like the conjugates to be dispersed more evenly and homogeneously (Zeng et al. 2010), as evidenced in the post-homogenization surface images (**Fig. 4.3**(a)), even after only five passes (F-5). Aggregates still remained,

although significantly less in number and size. At F-15, as the degree of fibrillation increased, so did the intermolecular hydrogen bonding and the high amount of conjugates dispersed within the numerous cavities that were responsible for the sheet/layer-like nature (Gautam et al. 2010; Zeng et al. 2010), as seen in F-15's surface image (**Fig. 4.3**(a)). Individual ultra-long-and-fine cellulose fibrils and evenly dispersed conjugate granules could be seen peeking out underneath. Cross-sectionally (**Fig. 4.3**(b)), 'layers' existing in F-0 became significantly less apparent the more homogenized the CNF was, indicating the more uniform scatter of conjugates throughout the matrix. The less aggregated conjugates also meant a smoother cross-sectional appearance. However, the 'over-shearing' effect was evident after 25 passes of homogenization (F-25). As also investigated in similar reports (L. Wang et al. 2020; Redlinger-Pohn, Brouzet, et al. 2022; Y. Zhou et al. 2018; Dilamian and Noroozi 2019; Kose et al. 2011), excessive mechanical treatment ended up dismantling the ultra-long-and-fine cellulose fibrils into shorter, smaller fibrils. The reduced aspect ratio, on top of the self-aggregation/quenching tendency, led to the return of agglomeration of cellulose fibrils and conjugates despite the promoted fibrillation, as seen in both surface and cross-sectional images of F-25 (**Fig. 4.3**(a) and (b)).

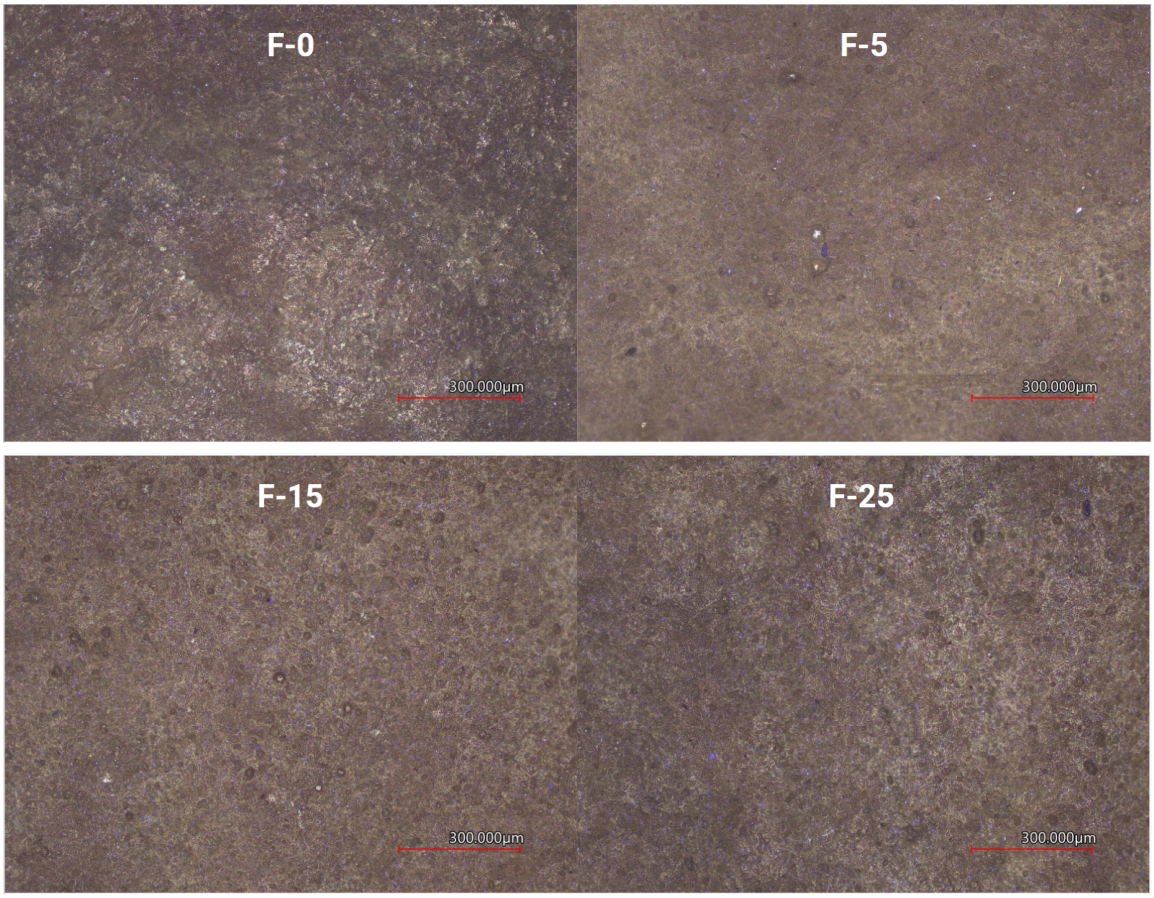

(**a**)

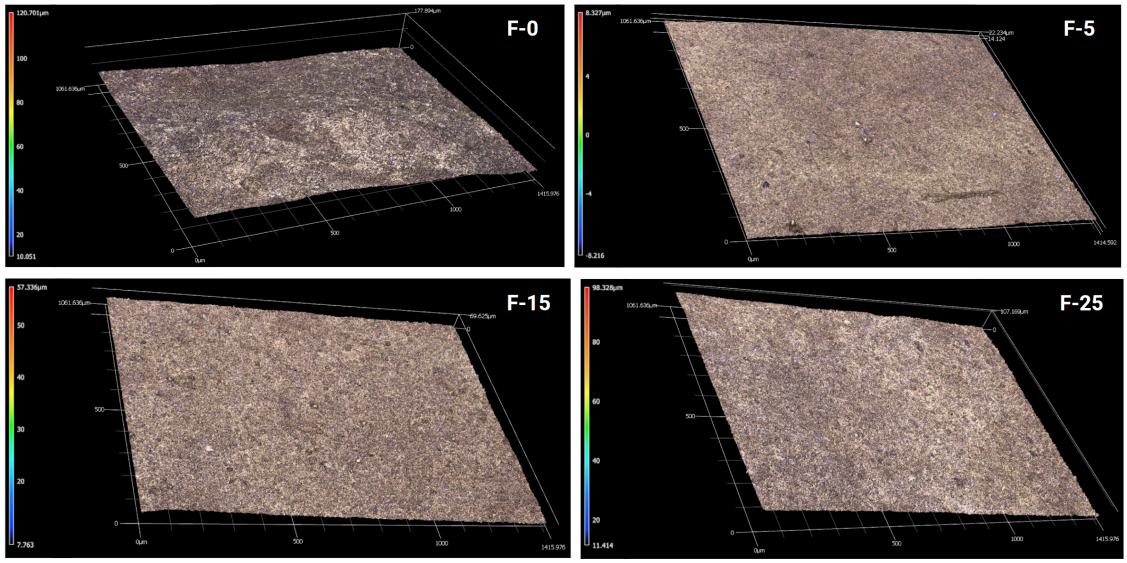

(**b**)

Fig. 4.4. Surface roughness of functionalized-CNF films: (**a**) z-stack and (**b**) 3D images

The images depicting the surface roughness property of the functionalized CNF films are presented in **Fig. 4.4**. On top of 3D microscopic images (**Fig. 4.4**(a)), Z/focus-stack images (**Fig. 4.4**(b)) were also taken to illustrate the roughness comparison through topography. It is by combining multiple images taken at different focal distances, producing a composite image with a greater depth of field (e.g., the plane of focus' thickness) than the individual source images (Ray 2002; D. Johnson 2008). Being a numerical and high-magnifying aperture whose major constraint is the decreasing depth-of-field, image processing through filtering (by referring the reference plane to the films' real surface to reduce height variability) could capture in-focus images (Larson and Banks 2022). The roughness values of the functionalized CNF films' top surface were expressed in Sa (**Fig. 4.5a**). This surface micro-geometry and irregularity characteristic is calculated by the arithmetic mean deviation (μm) of the height of a line (Woch et al. 2022). Post-homogenization, the resulting range of optimum values (2.458-2.639 μm) was 65% smoother than the control film (F-0) (7.029 μm). This finding is comparable to similar studies (Miettinen, Chinga-Carrasco, and Kataja 2014; Xue et al. 2021; Żołek-Tryznowska et al. 2023). This phenomenon, similar to morphology (**Fig. 4.3**), indicates the relationship between the two characteristics—morphology and roughness (Chinga-Carrasco et al., 2014), and can be explained as the impact of the promoted fibrillation. There is no significant difference between the roughness of F-5, F-15, and F-25. Despite the starting phenomenon of oversharing at F-25 that produced shorter/smaller fibrils, the smoothness remained due to the inevitable effect of homogenization-induced fibrillation that still produced sufficient porosity and an even enough dispersion of the conjugates. It is important to note that the reason only the films' top surfaces were analyzed for roughness properties was due to the fact that the bottom surface conforms to the petri dishes' surface; hence, it would not suffice as well as the top surface as the roughness indicator (Miettinen, Chinga-Carrasco, and Kataja 2014). Regarding applicability, functionalized CNFs with desirable smoothness have the potential to be used as a glossy finish for packaging and laminating purposes. Meanwhile,

ones with rougher surfaces can be advantageous to be used in antimicrobial and self-cleaning smart textile surface coating with dye removal and water-oil separation purposes (Görgülüer, Çakıroğlu, and Özacar 2021).

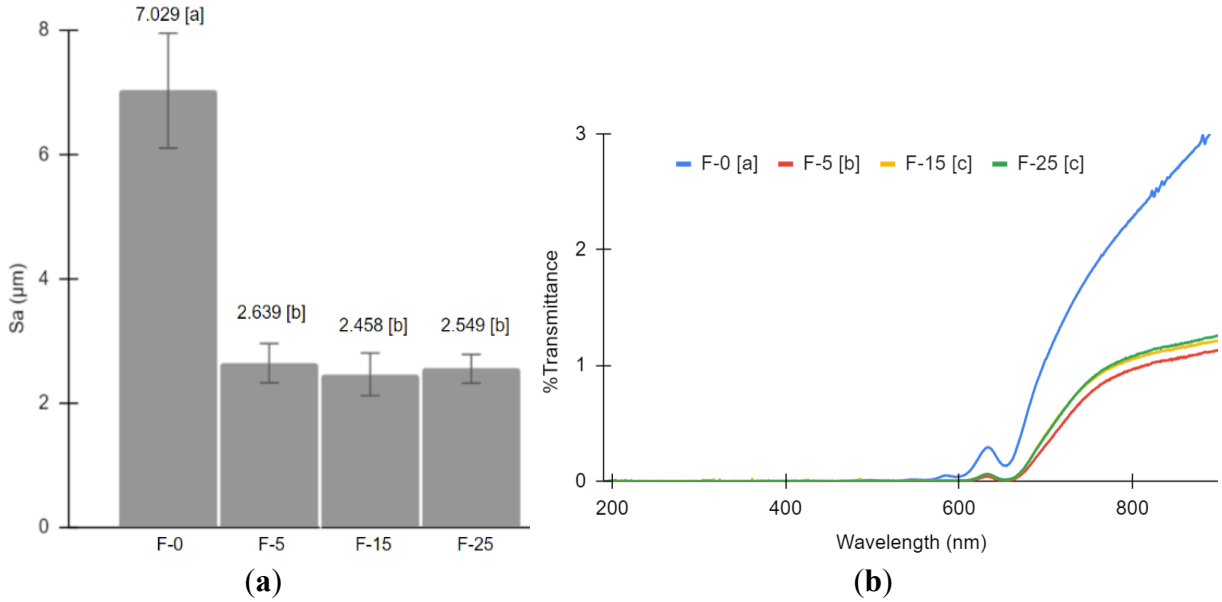

Fig. 4.5. (**a**) Surface roughness (arithmetical mean height (Sa)); and (**b**) UV-vis spectra or opacity of functionalized CNF films

Lastly, following the morphological and surface roughness characteristics, the opacity of the developed functionalized CNF films was analyzed. Especially for films comprised of a matrix with incorporated conjugates, this property is often affiliated with the degree of distribution/dispersity and homogeneity (Alves et al. 2023; Dinesh and Kandasubramanian 2022). It is apparent from both UV-vis spectra results (**Fig. 4.5**(b)) and visual observations (**Fig. S.3**) that the functionalized films made with homogenized CNFs were far more opaque. This is after the effect of promoted fibrillation and inter-/intra-molecular hydrogen bonding post-homogenization—as proven in morphological results above (**Fig. 4.3**)—that allowed a better dispersion of the incorporated conjugates throughout the CNF matrix. The developed MOF consisted of TiO_2 as the secondary building blocks linked and bound using dark-colored dye (TCPP); hence, the opaque appearance of the produced films. Generally, the functionalized film using F-5 was slightly more opaque than F-15 and F-20, which shows the effect of the number of homogenization cycles. The resulting spectra also suggested the complete UV-blocking-ability for all UV-A (320–400 nm), UV-B (280–320 nm), and UV-C (200–280 nm) (Parit et al. 2018; WHO 2016) by all functionalized films. Exposure to UV sunlight radiation increases the risk of biological damage, organic compound degradation, discoloration, weathering, and loss of mechanical properties (cracking) (Sadeghifar et al. 2017). The more transparent functionalized films would be suitable for packaging (X. Zhao et al. 2023), while other fields of applications, e.g., wastewater decontamination/disinfection (Maldonado-Carmona et al. 2020), would not be opposed to the opaque appearance.

4.3.3. Barrier property

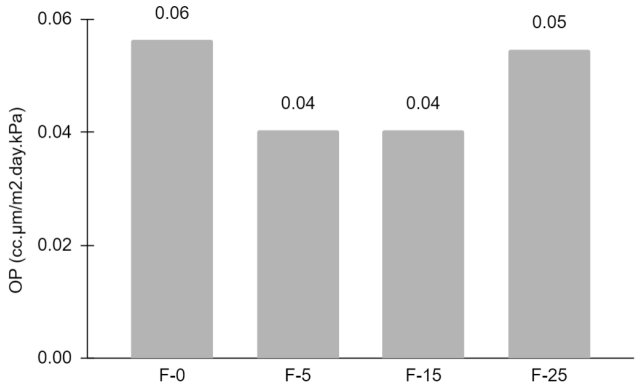

Fig. 4.6. Oxygen permeability (OP) of functionalized CNF films at 50%RH

Fig. 4.6. presents the oxygen permeability (OP) of the functionalized CNF films at 50%RH. There is no significant difference between films prepared at different numbers of homogenization cycles. However, the obtained values are comparable to numerous commercial high-barrier polymers often used in the packaging field, such as ethylene vinyl alcohol (EVOH), PVDC, PVA, MXD6, and PET (Michiels, Van Puyvelde, and Sels 2017; Artzi, Narkis, and Siegmann 2005; Kuraray 1972). These findings are also far superior to N-films (**Fig. 3.6**) owing to F-films' extremely dense composite structure after TiO_2-TCPP conjugate incorporation, which could be compared morphologically with that of neat-CNF (**Fig. 4.3** and **Fig. 3.3**).

4.3.4. Mechanical properties

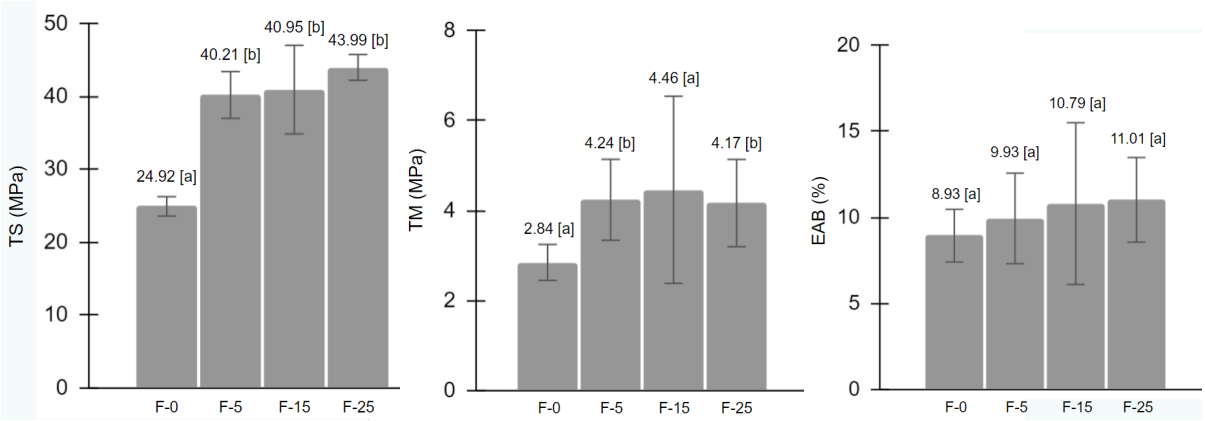

Fig. 4.7. Mechanical properties of functionalized CNF films: (**a**) tensile strength or TS, (**b**) tensile/Young's modulus or E, (**c**) elongation-at-break or EAB

Fig. 4.7 displays three different mechanical properties of functionalized CNF films. There are likewise not many significant differences between films prepared at different numbers of homogenization cycles, except in regards to tensile strength and tensile modulus, where the only noticeable improvement was between the use of CNF before

and after homogenization. The enhanced fibrillation and hydrogen bonding post-homogenization (as seen morphologically in **Fig. 4.3**) (Mokhena et al. 2021; Peresin et al. 2017) played a key role in the even dispersion and less tendency of self-quenching/aggregation of conjugates, which are among the most detrimental challenges of MOF-based materials to not only their antibacterial activity but also functional properties like mechanical strength.

4.3.5. Thermal properties

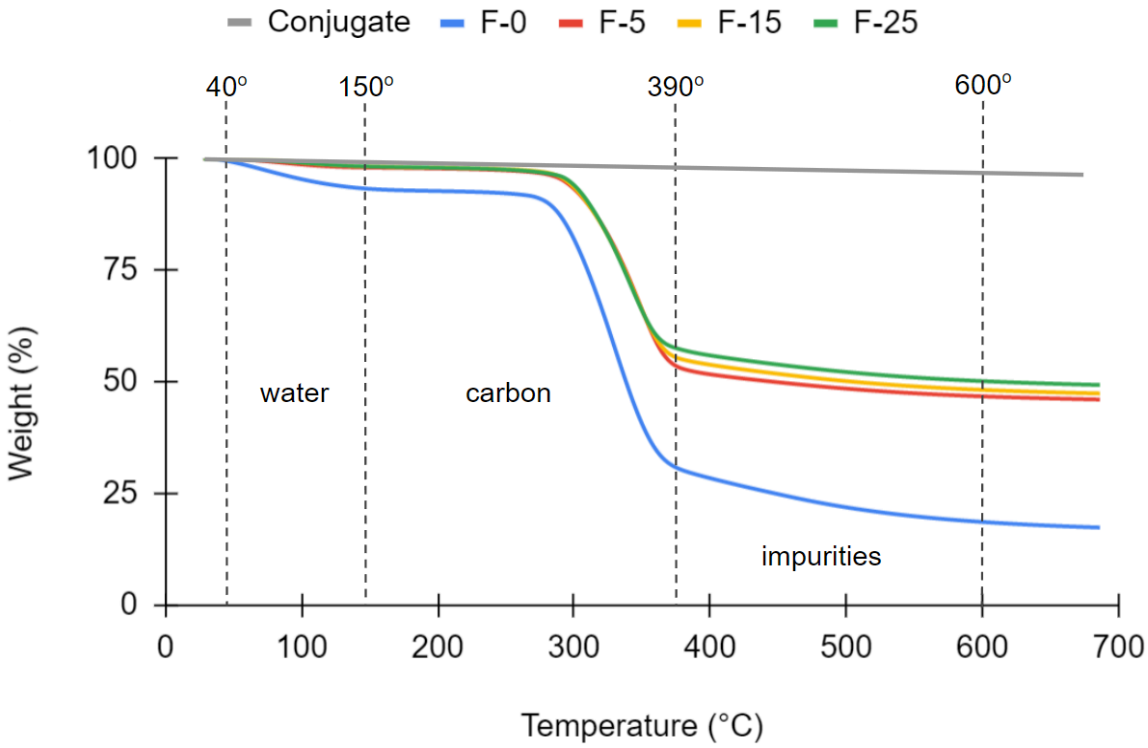

Fig. 4.8. Thermogravimetric spectra of conjugate and functionalized CNF films

Table 4.2. Degradation temperature and weight loss profile of conjugate and functionalized CNF films

Sample	$T_{d5\%}$ (°C)	%W at 700°C
Conjugate	-	96
F-0	100	17
F-5	291	46
F-15	293	48
F-25	295	49

Thermogravimetric analysis (TGA) provides insights into thermal stability by measuring weight/mass (loss or gain) as a function of temperature or time. The decomposition behavior output may be crucial when determining one's (bio)degradibility (Brunšek et al. 2023). **Fig. 4.8** presents TGA spectra of conjugate powder and all F-films, and **Table 4.2** lists each specimen's $T_{d,5\%}$ (the temperature at 5%-weight loss), and %weight at 700 °C, which is in the pyrolysis temperature range where usually material's

stagnant weight change is achieved (D. D. Jiang et al. 1999; M. A. Islam et al. 2016). As seen in the produced spectra, conjugate, being a metal-organic framework (MOF) that contains metal ions/nodes in the form of TiO_2 that act as the inorganic cluster/building blocks, displaying a distinctly different thermal behavior compared to any of the organic, cellulose-based F-films. Due to the lack of carbon/hydrogen atoms and strong covalent bonds (Malakhov and Samsonov 1966; Johns, McElhill, and Smith 1962), conjugate retains the residual masses of 96.23% at 700 °C, a slight increment from that of neat-TiO_2 (X. W. Li et al. 2013) due to the linkage with TCPP, which as a monomer would lose roughly half of its mass at 700 ºC (L.-J. Feng et al. 2017; Ji et al. 2024). In terms of F-films spectra, temperatures at 40-47 ºC and 100 ºC marked the first and least significant decompositions assigned to the absorbed moisture or loosely-bound water contained in the films, typically through evaporation or dehydration (B. Yang et al. 2019; Ilyas et al. 2018). F-0, due to the still-naturally high hydrophilicity (Abral et al. 2020), displayed the water's highest evaporation effect, meaning the earliest decomposition. Overall, cellulose only started to decompose extensively through pyrolysis at 260-360 °C (Abral et al. 2019; Araújo et al. 2018), where this time was shown by the identical spectrum of all three homogenized films (F-5, F-15, and F-25). Again, contrary to the homogenized films, F-0 displayed weight loss much earlier at around 200°, which was attributed to CNF's dehydration and decarboxylation that produced combustion gases (e.g., levoglucosan) (Cao et al. 2019). Finally, the most rapid thermal-oxidative decomposition of char/ash around 300-360 ºC was the last decomposition stage (Asrofi et al. 2018; Jiangqi Zhao et al. 2013), where a slight improvement in thermal resistance was discovered at the increasing passes of homogenization. After 400 °C, the thermal degradation rates decreased, marking the start of a slow thermal decomposition (G.-Q. Liu et al. 2021). F-25 suffered a 5%-weight loss at the highest temperature (295 ºC) and maintained the most weight (49%), followed by F-15 (293 ºC and 48%), and lastly, F-5 (291 ºC and 46%). Homogenized films meant fibrillated structure, higher surface area, and enhanced interlinking hydrogen bonding between the polymer chains that required higher decomposition energy (A. Islam, Yasin, and Rehman 2014; U.-J. Kim, Eom, and Wada 2010). These findings are comparable to those of other reports (Min et al. 2021). Post-homogenized, these resulting thermal stability indicators were far superior to the untreated film (F-0) (100 ºC and 17%); where due to the lacking amount of hydrogen bonding present, when the temperature reached around 500 ºC, CNF itself decomposed nearly completely, while the conjugate aggregates remained. The incorporated inorganic nanoparticles—TiO_2 as clusters or building blocks in the MOFs-based conjugates—into CNF possess catalytic and conductivity properties that negatively affect decomposition temperature (Zeng et al. 2010; Ma, Li, and Bai 2006), which can be proven by the decreasing $T_{d,5\%}$ of F-0 (100 ºC) compared to N-0 (257 ºC) The same phenomenon occurred in other reports on cellulose incorporated with ZnO (S.-W. Zhao et al. 2017; Onyszko et al. 2022), a similar metal ion/node commonly used in MOFs as UV-blocker and antimicrobial, where its lower thermal decomposition temperature was caused by the direct interaction between cellulose and ZnO particles that allowed an easier heat flow within the composite. The resulting thermostable films possess a high potential to be used as medical devices (L. Sun et al. 2023) and personal thermal management (Gu et al. 2020). Despite heightened concerns on TiO_2 use as food additives, which still deals with difficulties and uncertainties to date to reach a proper and retrospective safety assessment

(Winkler et al. 2018), there has yet any regulation on its use as packaging, especially when incorporated in composite structure like the developed CNF-MOF with negligible migration (W. Zhang and Rhim 2022). Moreover, when speaking of degradibility, TiO_2 addition in different packaging systems were also proven advantageous in promoting photo/bio-degradation rate (Tu-morn et al. 2019; Bang, Bang, and Lee 2007; Iacovone et al. 2023).

4.3.6. Contact angle or wettability

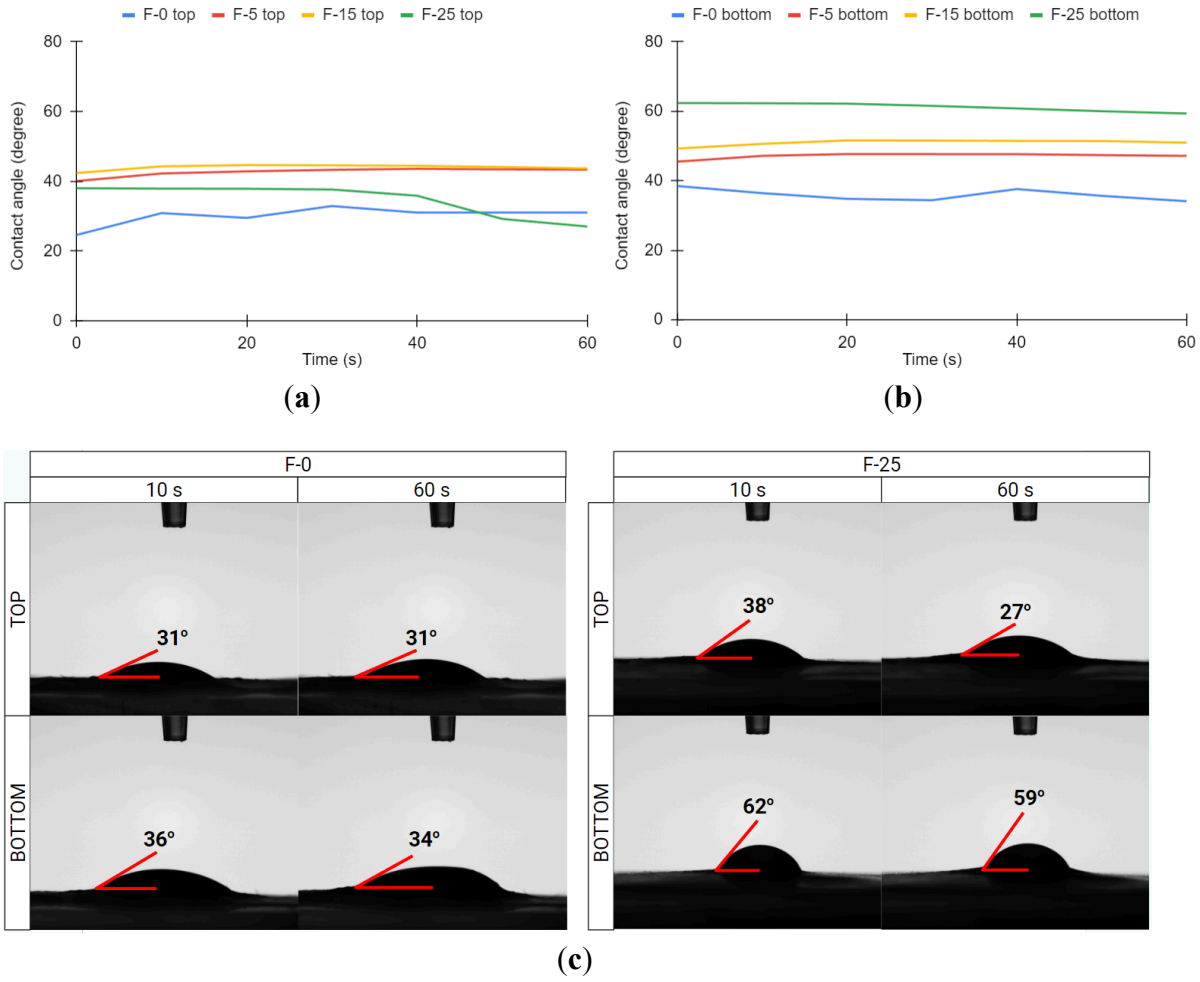

Fig. 4.9. Contact angle of functionalized CNF films: (**a**) top surface, (**b**) bottom surface, and (**c**) image comparison

Contact angle or wettability dictates if the material is either hydrophobic or hydrophilic, measured by the angle produced between the tangent to the droplet of liquid of choice, at the point of contact with the material's surface. The standard measuring liquid ought to be of low volatility to avoid evaporation as well as non-reactive to the tested surface. Some parameters can be customized, such as droplet size and liquid dispenser speed; meanwhile, many other factors may pertain to the resulting contact angle, including humidity, temperature, roughness (topography), morphology, and physical/chemical homogeneity (Jagodzińska et al. 2021; Wawro and Kazimierczak

2008; Jonoobi, Harun, Mathew, Hussein, et al. 2010). Wenzel and Cassie–Baxter equations are commonly used to explain hydrophobicity, where the liquid cannot penetrate the grooves on a rough surface, leaving air gaps (J. Song and Rojas 2013; Alimohammadzadeh, Sanhueza, and Córdova 2023). It is important to note the significant difference between wettability tested on top and bottom surfaces when analyzing films prepared using casting techniques, which vary in microstructure, porosity, and pore size. In the case of a single-layered, non-composite film that comprises one singular polymeric ingredient, the top surface tends to possess a higher contact angle value (Jagodzińska et al. 2021; McGaughey et al. 2020). However, the developed films consisted of continuous and dispersed phases (CNF and conjugates, respectively), where the composite's degree of distribution and homogeneity (as seen in morphological, cross-sectional images in **Fig. 4.3**(b)) influence the surface roughness (**Fig. 4.4** and **Fig. 4.5**(a)) and subsequent wettability profile. **Fig. 4.9** displayed the contact angle of the functionalized CNF films plotted over time, which shows the top side of the film's surface (**Fig. 4.9**(a)) was more hydrophobic compared to the bottom (**Fig. 4.9**(b)), regardless of the cycle of homogenization. As described in the surface roughness analysis, F-0 was discovered to have the roughest surface; despite that, it appeared to be the most hydrophilic regardless of the surface sides. This phenomenon was caused by the unhomogenized CNF as the matrix of F-0 still suffers from the intrinsic, naturally high hydrophilicity of cellulose, thanks to their plentiful polar groups (e.g., hydroxyl and carboxyl groups) that negatively affects hydrophobicity (Q. Wang et al. 2018; X. Sun et al. 2021; G. Zhou et al. 2015; Oh and Park 2022). Furthermore, specifically on the bottom surface's contact angle results, it was found that films prepared using CNF with more passes of homogenization were more hydrophobic. The even dispersion of the conjugates within the fibrillated CNF matrix produced films with better hydrophobicity. The most hydrophobic result was achieved by F-25's bottom surface, which produced 62^{o} after 10 seconds—a comparable finding to other reports on conjugates-incorporated composite (X. Zhao et al. 2023; El-Wakil et al. 2015). F-25's top surface is an exception due to the effect of over-shearing, where the lower aspect ratio on top of the conjugates' self-aggregation/quenching tendency (An et al. 2016) led to agglomeration and sinking of the produced agglomerates to the bottom of the film, resulting in a smoother top surface. The hydrophilicity of F-25 even surpassed that of F-0 after 50 seconds. Functionalized films with a hydrophilic profile would suffice as hydrogel/aerogel in drug delivery and tissue engineering applications (De France, Hoare, and Cranston 2017; Y. Sun et al. 2024); meanwhile, the acquired hydrophobicity would be beneficial for the development of active and intelligent/smart food packaging (X. Zhao et al. 2023; El-Wakil et al. 2015).

4.3.7. Antibacterial activity

The antibacterial efficacy of functionalized CNF films was evaluated against *Escherichia coli* (*E. coli*)—a common foodborne pathogen found not only in polluted water and soil but also in wildlife, livestock, and humans as their carriers (FDA 2019b). *E. coli* was selected because cellulose and TiO_2 performed better antibacterial efficacy against Gram-negative bacteria, e.g., *E. coli*, than against Gram-positive bacteria (Maślana et al. 2021). The difference between Gram-negative/-positive bacteria is in their cell wall structure difference; the former contains a thin peptidoglycan layer in the cell wall, whereas the latter is much thicker, which provides cell resistance against Ti ions. Gram-negative bacteria's structure with lipopolysaccharide in their outer membrane favors an affinity in the adherence of the Ti ion to the cell membrane (Arularasu, Harb, and Sundaram 2020; Slavin et al. 2017). To evaluate such bactericidal activity between CNF films before and after functionalization (N-films and F-films, respectively), the viable bacterial counts recovered under different light intensities and contact durations are shown in **Fig. 4.10**. Time-kill test/curve is a standardized method for determining bactericidal activity of antimicrobial agents (Clinical and Laboratory Standards Institute 1999) and 0-96 hours are the usual contact duration applied for *E. coli* studies (Elliker and Frazier 1938). Speaking of the light intensity factor, 1000-10,000 lux is the range of illuminance used to activate photoactive antimicrobial surfaces (K. Wu et al., 2020). Two light intensities (3000 and 6000 lux) were selected after the optimum conditions obtained by several previous studies on light-activated antimicrobial surfaces for *E. coli* bactericidal inhibition (Noimark, Allan, and Parkin 2014; Noimark et al. 2013; Sehmi et al. 2016).

Antibacterial efficacy under 6000 lux light was reported in **Fig. 4.10**(a). Under 24 hours, the functionalized film using five-passes homogenized-CNF (F-5) under light was the best-performing film with a 41% antibacterial rate. The next day, F-5 and F-15, under light, were the joint films with the highest antibacterial rate at 80%. After 72 hours, all homogenized CNF films functionalized with conjugates (F-5, F-15, F-25) under light succeeded in completely inhibiting *E.coli* growth (100% antibacterial rate). These findings were superior compared to similar studies (Min et al. 2021; X. Zhao et al. 2023; El-Wakil et al. 2015). A former report on porphyrin-based MOF (Min et al. 2021) further proved this exceptional antibacterial efficacy through SEM analysis of *E.coli* showing wrinkled/distorted morphology after light irradiation that led to bacteria death. This result certified the impact of TCPP as a photosensitizer for the high-efficiency generation of reactive oxygen species (ROS), especially singlet oxygen ($^1O_2$). By utilizing oxygen and light, the photosensitizer absorbs light energy to form an excited singlet state, then an excited triplet state, before the final product of ROS in the form of $^1O_2$ (DeRosa and Crutchley 2002). Speaking of the antibacterial activity of neat-CNF films prior to conjugates incorporation (N-films) in the dark, five-passes homogenized-CNF film (N-5) performed the highest antibacterial rate at 24%, which was obtained after 48-hour-long storage. This finding is aligned with the result about N-5 possessing the lowest oxygen permeability (**Fig. 4.6**) among all N-films that helped to reduce the growth rate of food spoilage bacteria, including facultative anaerobes like *E. coli* (Couvert et al. 2023). Interestingly, after 72 hours under light irradiation, N-25 showed an exceptional antibacterial rate at 74%, exceeding other N-films stored for the same duration.

Fig. 4.10(b) and **Table 4.3/Table 4.4** presents the films' antibacterial activity under 3000 lux light. After being stored for 24 hours under light, F-5 was once more the one exhibiting the highest antibacterial rate among all films, at 41%—identical to its performance under 6000 lux light. The next day, all homogenized CNF films functionalized with conjugates (F-5, F-15, F-25) under light became the joint top-performing films with an 80% antibacterial rate. After 72 and 92 hours, all F-films, including one prepared using unhomogenized CNF (F-0) under light, achieved the same antibacterial rate (80%). This best outcome under the 3000 lux light scenario was lower than that treated under 6000 lux, which performed a complete inhibition growth (100% antibacterial rate). This finding is in agreement with former reports (K. Wu et al. 2020; Macdonald et al. 2016) that determined 6000 lux as the minimum light intensity in order to reach the optimum E. coli growth inhibition rate. Regarding N-films, the best-performing specimen in the dark was N-5, with a 25% antibacterial rate after 48 hours. Meanwhile, under light, N-25 performed exceptionally well after 92 hours, exhibiting a 75% antibacterial rate. Both of these N-film results were identical to the ones under 6000 lux light, certifying the insignificant effect of higher light intensity on N-films' bactericidal efficacy, as similarly found in some photodynamic antimicrobial studies on *E. coli* (Ullah et al. 2018; Sehmi et al. 2016). The promising potential of the developed antimicrobial films ranges from food packaging (El-Wakil et al. 2015; Larrea et al. 2024; Min et al. 2021; X. Zhao et al. 2023), converter (Cherian and Wamser 2000; Gao et al. 2019), biomedical (Carpenter et al. 2012; J. Park et al. 2016), until micropollutants removal (G.-Q. Liu et al. 2021; Rathod et al. 2018; Roberta Grazia Toro et al. 2020).

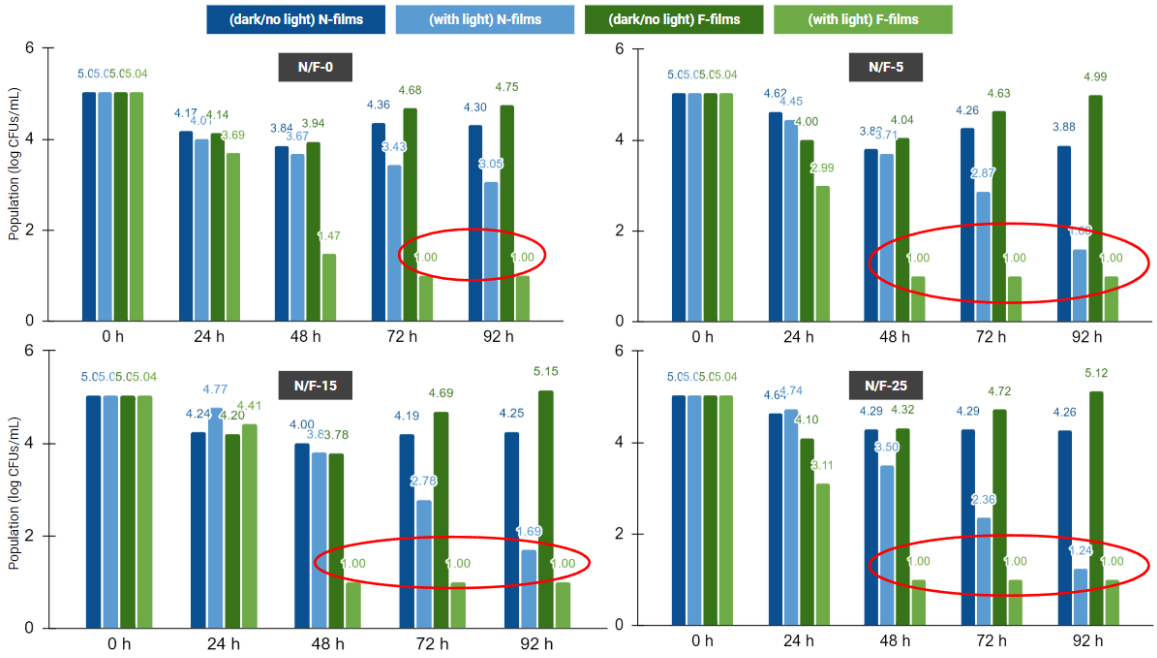

(a)

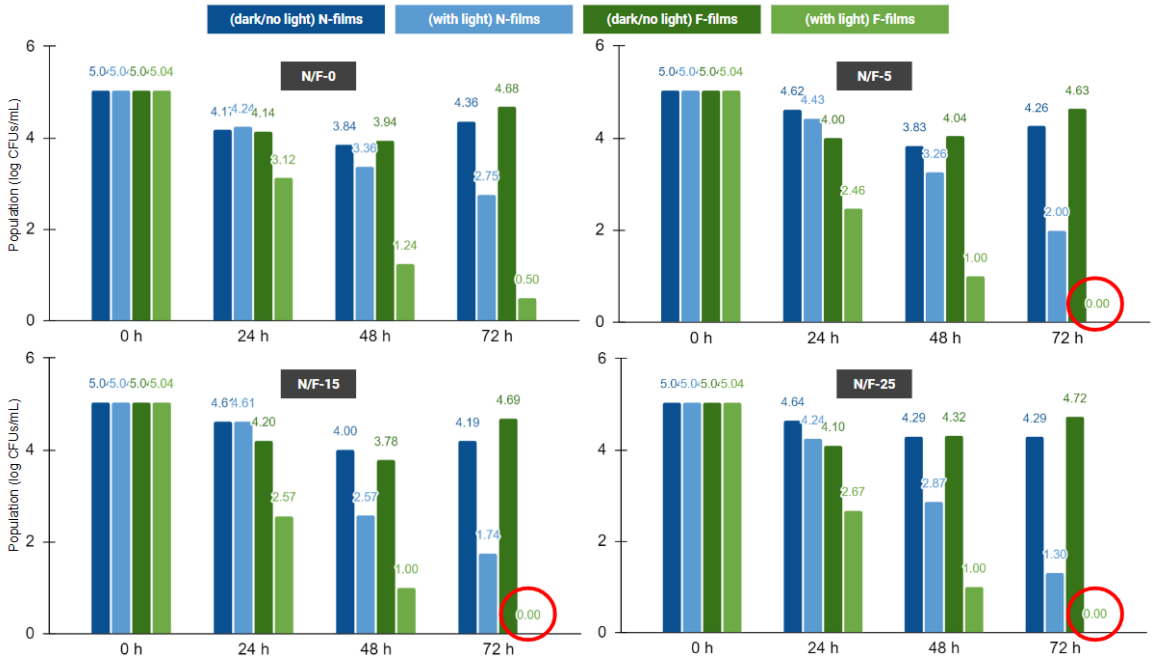

(b)

Fig. 4.10. Antibacterial activity of neat CNF and functionalized CNF films on *E. coli* under varying light intensities: (**a**) 3000 and (**b**) 6000 lux

Table 4.3. The best performing films under 3000 lux-light

Contact period (h)	The best-performing film and its antibacterial rate (%) or E. coli population (log CFUs/mL)
24	F-5, under light = **41%** (2.99 log CFUs/mL)
48	F-5/15/25, under light = **80%** (1.00 log CFUs/mL)
72	F-0/5/15/25, under light = **80%** (1.00 log CFUs/mL)

Table 4.4. The best performing films under 6000 lux-light

Contact period (h)	The best-performing film and its antibacterial rate (%) or E. coli population (log CFUs/mL)
24	F-5, under light = **51%** (2.46 log CFUs/mL)
48	F-5/15/25, under light = **80%** (1.00 log CFUs/mL)
72	F-0/5/15/25, under light = **100%** (0.00 log CFUs/mL)

4.4. Conclusions

Cellulose nanofibril (CNF) film functionalized with a metal-organic framework (MOF)-based photosensitive antibacterial agent involving reactive oxygen species (ROS) generation was successfully fabricated. CNF was initially prepared by different cycles of homogenization before being impregnated with TiO_2-TCPP conjugates. Chosen for its excellent UV-blocking ability, TiO_2 potential was proven by its complete absorption of all UV spectrums (A, B, and C). Meanwhile, TCPP was selected as a photosensitizer for its photodynamic activity even under the visible light spectrum and verified likewise by the observed complete inhibition of *Escherichia coli* growth (100% antibacterial rate) under 6000 lux-light irradiation after 72 hours. Improvement in conjugate's even dispersion, surface smoothness, mechanical properties, thermal stability, and hydrophobicity on functionalized films was also obtained, indicating the positive effect of enhanced fibrillation and the subsequent inter/intra-molecular hydrogen bonding post-homogenization. This work overall certified TiO_2-TCPP biocompatibility and collective prospect as a remarkable photosensitive antimicrobial agent, as well as the cellulose's fruitful performance taking the role of MOF conjugate's ex-situ carrier that solved the notoriously challenging self-aggregation and self-quenching tendency.

CHAPTER 5

Conclusions

To help the globally recurring food spoilage and food waste issue, nanocomposite films made of cellulose, titanium dioxide (TiO_2), and porphyrin with high-barrier, UV-blocking, and visible light-responsive antimicrobial features were developed. Metal-organic framework (MOF) consisting of TiO_2 and TCPP (a biocompatible porphyrin derivative) was chosen as the antibacterial modality due to its excellent photodynamic activity and generation of reactive oxygen species (ROS) that can kill bacteria under not only UV but also visible light spectrum. Other than being the Earth's most abundant and naturally biodegradable, cellulose was employed as an ex-situ carrier of the MOF conjugate to solve the common constraint of MOF-based conjugates on their self-quenching/aggregation tendency, and cellulose nanofibril (CNF)—a type of nanosized cellulose—was specially chosen for its high specific surface area and surface activity. To solve neat cellulose's challenge of natural hydrophilicity that limits its processability, a straightforward, cheap, and environmentally friendly approach of multicycle homogenization was conducted, where low pressure was applied to prevent the common over-shearing effect. Other than the functional properties, the antimicrobial efficiency of the functionalized films against *Escherichia coli* was analyzed with and without light of different intensities to confirm the photosensitivity effect. Complete UV-A/B/C blocking was observed, and so was the complete growth inhibition (100% antibacterial rate) under 6000 lux-light irradiation after 72 hours. Collectively, improvement in crystallinity, conjugate's even dispersion, surface smoothness, mechanical properties, thermal stability, hydrophobicity, and oxygen barrier (comparable to ethylene-vinyl alcohol (EVOH), a commercial high-barrier polymer) on the functionalized films was also obtained. These findings depicted the positive effect of enhanced fibrillation and the subsequent inter/intra-molecular hydrogen bonding post-homogenization, as well as the promising photosensitive antibacterial performance of TiO_2-TCPP. The applicability prospect of the developed films with notable features of high-barrier, UV-blocking, and/or visible light-responsive antibacterial ranges from food/drug packaging, biomedical (including photodynamic therapy), nanodevices, sensors, gas storage/separation, pollutant removal, and energy conversion.

REFERENCES

Abdelhameed, Reda M., Mohamed Rehan, and Hossam E. Emam. 2018. "Figuration of Zr-Based MOF@cotton Fabric Composite for Potential Kidney Application." *Carbohydrate Polymers* 195 (September): 460–67.

Abdelhamid, Hani Nasser, and Aji P. Mathew. 2022. "Cellulose–metal Organic Frameworks (CelloMOFs) Hybrid Materials and Their Multifaceted Applications: A Review." *Coordination Chemistry Reviews* 451 (January): 214263.

Abdul Khalil, H. P. S., Chaturbhuj K. Saurabh, M. I. Syakir, M. R. Nurul Fazita, Aamir Bhat, A. Banerjee, H. M. Fizree, Samsul Rizal, and Paridah Tahir. 2019. "13 - Barrier Properties of Biocomposites/hybrid Films." In *Mechanical and Physical Testing of Biocomposites, Fibre-Reinforced Composites and Hybrid Composites*, edited by Mohammad Jawaid, Mohamed Thariq, and Naheed Saba, 241–58. Woodhead Publishing.

Abral, Hairul, Jeri Ariksa, Melbi Mahardika, Dian Handayani, Ibtisamatul Aminah, Neny Sandrawati, Eni Sugiarti, Ahmad Novi Muslimin, and Santi Dewi Rosanti. 2020. "Effect of Heat Treatment on Thermal Resistance, Transparency and Antimicrobial Activity of Sonicated Ginger Cellulose Film." *Carbohydrate Polymers* 240 (July): 116287.

Abral, Hairul, Azmi Basri, Faris Muhammad, Yuzalmi Fernando, Fadli Hafizulhaq, Melbi Mahardika, Eni Sugiarti, S. M. Sapuan, R. A. Ilyas, and Ilfa Stephane. 2019. "A Simple Method for Improving the Properties of the Sago Starch Films Prepared by Using Ultrasonication Treatment." *Food Hydrocolloids* 93 (August): 276–83.

Adamčík, Lukáš, Ladislav Dzurenda, Adrián Banski, and Richard Kminiak. 2023. "Comparison of Surface Roughness of Beech Wood after Sanding with an Eccentric and Belt Sander." *Forests, Trees and Livelihoods* 15 (1): 45.

Adel, Abeer M., Mona T. Al-Shemy, Mohamed A. Diab, Mohamed El-Sakhawy, Roberta G. Toro, Roberta Montanari, Tilde de Caro, and Daniela Caschera. 2021. "Fabrication of Packaging Paper Sheets Decorated with Alginate/oxidized Nanocellulose-silver Nanoparticles Bio-Nanocomposite." *International Journal of Biological Macromolecules* 181 (June): 612–20.

Adel, Abeer M., Amira M. El-Shafei, Atef A. Ibrahim, and Mona T. Al-Shemy. 2019. "Chitosan/Nanocrystalline Cellulose Biocomposites Based on Date Palm (Phoenix Dactylifera L.) Sheath Fibers." *Journal of Renewable Materials* 7 (6): 567–82.

Adel, Abeer M., Atef A. Ibrahim, Amira M. El-Shafei, and Mona T. Al-Shemy. 2019. "Inclusion Complex of Clove Oil with Chitosan/β-Cyclodextrin Citrate/oxidized Nanocellulose Biocomposite for Active Food Packaging." *Food Packaging and Shelf Life* 20 (June): 100307.

Adler, Alan D., Frederick R. Longo, Frank Kampas, and Jean Kim. 1970. "On the Preparation of Metalloporphyrins." *Journal of Inorganic and Nuclear Chemistry* 32 (7): 2443–45.

Aguayo, Encarna, Martha Patricia Tarazona-Díaz, Ascensión Martínez-Sánchez, and Antonio García-González. 2017. "Influence of Moderate High-Pressure Homogenization on Quality of Bioactive Compounds of Functional Food Supplements." *Journal of Food Quality* 2017 (August). https://doi.org/10.1155/2017/2856125.

Ahmadi, Ebrahim, Ali Ramazani, Zahra Hamdi, Asemeh Mashhadi-Malekzadeh, and Zahra Mohamadnia. 2015. "5,10,15,20-tetrakis(4-Carboxyphenyl)porphyrin Covalently Bound to Nano-Silica Surface: Preparation, Characterization and Chemosensor Application to Detect TNT." *Silicon Chemistry* 7 (4): 323–32.

Ahmed, Md Wadud, Md Azizul Haque, Mohibbullah, Md Sirajul Islam Khan, Mohammed Ariful Islam, Md Hasan Tarek Mondal, and Raju Ahmmed. 2022. "A Review on Active Packaging for Quality and Safety of Foods: Current Trends, Applications, Prospects and Challenges." *Food Packaging and Shelf Life* 33 (September): 100913.

Alimohammadzadeh, Rana, Italo Sanhueza, and Armando Córdova. 2023. “Design and Fabrication of Superhydrophobic Cellulose Nanocrystal Films by Combination of Self-Assembly and Organocatalysis.” *Scientific Reports* 13 (1): 1–12.

Almeida, Jéssica C. de, Mateus T. Corrêa, Rafaella H. Koga, Douglas M. S. Del Duque, Osmando F. Lopes, Gelson T. S. T. da Silva, Caue Ribeiro, and Vagner R. de Mendonça. 2020. “Crystallization Time in ZnO: The Role of Surface OH Groups in Its Photoactivity.” *New Journal of Chemistry = Nouveau Journal de Chimie* 44 (42): 18216–24.

Almenar, Eva. 2023. “Minding the Gap: Consumer Awareness of Packaging & Food Waste Reduction.”

Alves, Luís, Ana Ramos, Eduardo Ferraz, Pedro Sanguino, Julio Santarén, Maria G. Rasteiro, and José A. F. Gamelas. 2023. “Effect of the Dispersion State of Minerals on the Properties of Cellulose Nanofiber-Based Composite Films.” *Applied Clay Science* 233 (March): 106823.

Antonov, Dmitrii V., Anastasya G. Islamova, and Pavel A. Strizhak. 2023. “Hydrophilic and Hydrophobic Surfaces: Features of Interaction with Liquid Drops.” *Materials* 16 (17). https://doi.org/10.3390/ma16175932.

An, Xingye, Yangbing Wen, Abdullah Almujil, Dong Cheng, Jianguo Li, Xu Jia, Jijun Zou, and Yonghao Ni. 2016. “Nano-Fibrillated Cellulose (NFC) as Versatile Carriers of TiO2 Nanoparticles (TNPs) for Photocatalytic Hydrogen Generation.” *RSC Advances* 6 (92): 89457–66.

Araki, Takeo, Mitsuhiro Shibayama, and Qui Tran-Cong. 1998. *Structure and Properties of Multiphase Polymeric Materials*. CRC Press.

Araújo, Inês M. S., Robson R. Silva, Guilherme Pacheco, Wilton R. Lustri, Agnieszka Tercjak, Junkal Gutierrez, José R. S. Júnior, et al. 2018. “Hydrothermal Synthesis of Bacterial Cellulose-Copper Oxide Nanocomposites and Evaluation of Their Antimicrobial Activity.” *Carbohydrate Polymers* 179 (January): 341–49.

Artzi, N., M. Narkis, and A. Siegmann. 2005. “Review of Melt‐processed Nanocomposites Based on EVOH/organoclay.” *Journal of Polymer Science. Part B, Polymer Physics* 43 (15): 1931–43.

Arularasu, M. V., M. Harb, and R. Sundaram. 2020. “Synthesis and Characterization of cellulose/TiO2 Nanocomposite: Evaluation of in Vitro Antibacterial and in Silico Molecular Docking Studies.” *Carbohydrate Polymers* 249 (December): 116868.

Arun, Ramachandran, Ramesh Shruthy, Radhakrishnan Preetha, and Valiathan Sreejit. 2022. “Biodegradable Nano Composite Reinforced with Cellulose Nano Fiber from Coconut Industry Waste for Replacing Synthetic Plastic Food Packaging.” *Chemosphere* 291 (Pt 1): 132786.

Asrofi, Mochamad, Hairul Abral, Anwar Kasim, Adjar Pratoto, Melbi Mahardika, and Fadli Hafizulhaq. 2018. “Mechanical Properties of a Water Hyacinth Nanofiber Cellulose Reinforced Thermoplastic Starch Bionanocomposite: Effect of Ultrasonic Vibration during Processing.” *Fibers and Polymers* 6 (2): 40.

Assi, Hala, Georges Mouchaham, Nathalie Steunou, Thomas Devic, and Christian Serre. 2017. “Titanium Coordination Compounds: From Discrete Metal Complexes to Metal-Organic Frameworks.” *Chemical Society Reviews* 46 (11): 3431–52.

ASTM. 2022. “ASTM D638-14: Standard Test Method for Tensile Properties of Plastics.” https://www.astm.org/d0638-14.html.

Atiqah, M. S. Nurul, Deepu A. Gopakumar, Owolabi F A T, Yasir Beeran Pottathara, Samsul Rizal, N. A. Sri Aprilia, D. Hermawan, M. T. T. Paridah, Sabu Thomas, and Abdul Khalil H P S. 2019. “Extraction of Cellulose Nanofibers via Eco-Friendly Supercritical Carbon Dioxide Treatment Followed by Mild Acid Hydrolysis and the Fabrication of Cellulose Nanopapers.” *Polymers* 11 (11). https://doi.org/10.3390/polym11111813.

Aulin, Christian, Mikael Gällstedt, and Tom Lindström. 2010. “Oxygen and Oil Barrier Properties of Microfibrillated Cellulose Films and Coatings.” *Cellulose* 17 (3): 559–74.

Ausili, Alessio, Marina Sánchez, and Juan C. Gómez-Fernández. 2015. “Attenuated Total Reflectance Infrared Spectroscopy: A Powerful Method for the Simultaneous Study of Structure and Spatial Orientation of Lipids and Membrane Proteins.” *Biomedical Spectroscopy and Imaging* 4 (2): 159–70.

Ayranci, Erol, and Sibel Tunc. 2003. “A Method for the Measurement of the Oxygen Permeability and the Development of Edible Films to Reduce the Rate of Oxidative Reactions in Fresh Foods.” *Food Chemistry* 80 (3): 423–31.

Aziz, Tariq, Fazal Haq, Arshad Farid, Mehwish Kiran, Shah Faisal, Asmat Ullah, Naveed Ullah, et al. 2023. “Challenges Associated with Cellulose Composite Material: Facet Engineering and Prospective.” *Environmental Research* 223 (April): 115429.

Babaee, Mehran, Mehdi Jonoobi, Yahya Hamzeh, and Alireza Ashori. 2015. “Biodegradability and Mechanical Properties of Reinforced Starch Nanocomposites Using Cellulose Nanofibers.” *Carbohydrate Polymers* 132 (November): 1–8.

Bahrami, Akbar, Rana Delshadi, Elham Assadpour, Seid Mahdi Jafari, and Leonard Williams. 2020. “Antimicrobial-Loaded Nanocarriers for Food Packaging Applications.” *Advances in Colloid and Interface Science* 278 (April): 102140.

Bang, Hee-Seon, Han-Sur Bang, and Yoon-Ki Lee. 2007. “The Functional TiO2-Biodegradable Plastic Composite Material Produced by HVOF Spraying Process.” *Journal of Nanoscience and Nanotechnology* 7 (11): 3830–33.

Barnes, Robert J., Rodrigo Molina, Jianbin Xu, Peter J. Dobson, and Ian P. Thompson. 2013. “Comparison of TiO2 and ZnO Nanoparticles for Photocatalytic Degradation of Methylene Blue and the Correlated Inactivation of Gram-Positive and Gram-Negative Bacteria.” *Journal of Nanoparticle Research: An Interdisciplinary Forum for Nanoscale Science and Technology* 15 (2): 1432.

Baş, Yağmur, Linn Berglund, Totte Niittylä, Elisa Zattarin, Daniel Aili, Zeljana Sotra, Ivana Rinklake, Johan Junker, Jonathan Rakar, and Kristiina Oksman. 2023. “Preparation and Characterization of Softwood and Hardwood Nanofibril Hydrogels: Toward Wound Dressing Applications.” *Biomacromolecules* 24 (12): 5605–19.

Batten, Stuart R., Neil R. Champness, Xiao-Ming Chen, Javier Garcia-Martinez, Susumu Kitagawa, Lars Öhrström, Michael O’Keeffe, Myunghyun Paik Suh, and Jan Reedijk. 2013. “Terminology of metal–organic frameworks and coordination polymers (IUPAC Recommendations 2013).” *Journal of Macromolecular Science, Part A:Pure and Applied Chemistry* 85 (8): 1715–24.

Bavykina, A., N. Kolobov, I. S. Khan, and J. A. Bau. 2020. “Metal–organic Frameworks in Heterogeneous Catalysis: Recent Progress, New Trends, and Future Perspectives.” *Journal of Molecular Catalysis A: Chemical*. https://pubs.acs.org/doi/abs/10.1021/acs.chemrev.9b00685?casa_token=YS6u38KL2RMAAAAA:rR0tkCahaQuB8dW9q17dRmq0NCov1m0fLt4GhS9pQP1bS_PeGRc9QFz_-Vh3uJN17D-A_071NrNAhZPL.

Bayer, Ilker S., Despina Fragouli, Agnese Attanasio, Barbara Sorce, Giovanni Bertoni, Rosaria Brescia, Riccardo Di Corato, et al. 2011. “Water-Repellent Cellulose Fiber Networks with Multifunctional Properties.” *ACS Applied Materials & Interfaces* 3 (10): 4024–31.

BEE International. 2015. “Patented Emulsifying Cell.” 2015. https://www.beei.com/technology/homogenizing-cell.

Benhamou, Karima, Hamid Kaddami, Albert Magnin, Alain Dufresne, and Azizan Ahmad. 2015. “Bio-Based Polyurethane Reinforced with Cellulose Nanofibers: A Comprehensive Investigation on the Effect of Interface.” *Carbohydrate Polymers* 122 (May): 202–11.

Bhirud, Ashwini P., Shivaram D. Sathaye, Rupali P. Waichal, Jalindar D. Ambekar, Chan-J Park, and Bharat B. Kale. 2015. “In-Situ Preparation of N-TiO2/graphene Nanocomposite and Its Enhanced Photocatalytic Hydrogen Production by H2S Splitting under Solar Light.” *Nanoscale* 7 (11): 5023–34.

Bhunia, Arun K. 2008. “Chapter 1 - Biosensors and Bio‐Based Methods for the Separation and Detection of Foodborne Pathogens.” In *Advances in Food and Nutrition Research*, edited by Steve L. Taylor, 54:1–44. Academic Press.

Bian, Huiyang, Xuan Shu, Wenhao Su, Dan Luo, Maolin Dong, Xiuyu Liu, Xingxiang Ji, and Hongqi Dai. 2022. “Biodegradable, Flexible and Ultraviolet Blocking Nanocellulose Composite Film Incorporated with Lignin Nanoparticles.” *International Journal of Molecular Sciences* 23 (23). https://doi.org/10.3390/ijms232314863.

Biradha, Kumar, Arunachalam Ramanan, and Jagadese J. Vittal. 2009. “Coordination Polymers Versus Metal−Organic Frameworks.” *Crystal Growth & Design* 9 (7): 2969–70.

Birkett, Gareth Christian, Steven Sicoli, Laszlo Horvath, Johan Foster, Young-Teck Kim, Scott Renneckar, and Barry Goodell. 2017. “Investigation of Nanofibrillated Cellulose for Hydrophobic Packaging Material: Examining Alternatives to Solvent Exchange and Lyophilization.” *BioResources* 12 (2): 4314–26.

Bogdan, Janusz, Joanna Zarzyńska, and Joanna Pławińska-Czarnak. 2015. “Comparison of Infectious Agents Susceptibility to Photocatalytic Effects of Nanosized Titanium and Zinc Oxides: A Practical Approach.” *Nanoscale Research Letters* 10 (1): 309.

Bondeson, Daniel, Peder Syre, and Kristiina Oksman Niska. 2007. “All Cellulose Nanocomposites Produced by Extrusion.” *Journal of Biobased Materials and Bioenergy* 1 (3): 367–71.

Bonilla, J., L. Atarés, M. Vargas, and A. Chiralt. 2012. “Edible Films and Coatings to Prevent the Detrimental Effect of Oxygen on Food Quality: Possibilities and Limitations.” *Journal of Food Engineering* 110 (2): 208–13.

Boulemkahel, S., E. Betoret, L. Benatallah, and C. M. Rosell. 2021. “Effect of Low Pressures Homogenization on the Physico-Chemical and Functional Properties of Rice Flour.” *Food Hydrocolloids* 112 (March): 106373.

Bragg, W. L. 1913. “The Diffraction of Short Electromagnetic Waves by a Crystal.” *Proc Camb Philos Soc* 17: 43–57.

Brittain, Harry G. 2011. “2 - Characterization of Pharmaceutical Compounds in the Solid State.” In *Separation Science and Technology*, edited by Satinder Ahuja and Stephen Scypinski, 10:11–58. Academic Press.

Brown, Natalie. 1992. *Plastics in Food Patkaging: Properties: Design and Fabrication*. CRC Press.

Brunšek, Ružica, Dragana Kopitar, Ivana Schwarz, and Paula Marasović. 2023. “Biodegradation Properties of Cellulose Fibers and PLA Biopolymer.” *Polymers* 15 (17). https://doi.org/10.3390/polym15173532.

Budynas, R., and J. Nisbett. 2006. *Shigley’s Mechanical Engineering Design, 8th Edition*. McGraw-Hill Science/Engineering/Math.

Burtch, Nicholas C., Himanshu Jasuja, and Krista S. Walton. 2014. “Water Stability and Adsorption in Metal–Organic Frameworks.” *Chemical Reviews* 114 (20): 10575–612.

Byun, Youngjae, Katia Rodriguez, Jung H. Han, and Young Teck Kim. 2015. “Improved Thermal Stability of Polylactic Acid (PLA) Composite Film via PLA-β-Cyclodextrin-Inclusion Complex Systems.” *International Journal of Biological Macromolecules* 81 (November): 591–98.

Callister, William, Jr, and David G. Rethwisch. 2019. *Fundamentals of Materials Science and Engineering: An Integrated Approach*. John Wiley & Sons, Incorporated.

Candan, Zeki, Douglas J. Gardner, and Stephen M. Shaler. 2016. “Dynamic Mechanical Thermal Analysis (DMTA) of Cellulose nanofibril/nanoclay/pMDI Nanocomposites.” *Composites Part B Engineering* 90 (April): 126–32.

Cao, Wenhan, Jun Li, Teresa Martí-Rosselló, and Xiaolei Zhang. 2019. “Experimental Study on the Ignition Characteristics of Cellulose, Hemicellulose, Lignin and Their Mixtures.” *Journal of the Energy Institute* 92 (5): 1303–12.

Carpenter, Bradley L., Elke Feese, Hasan Sadeghifar, Dimitris S. Argyropoulos, and Reza A. Ghiladi. 2012. “Porphyrin‐cellulose Nanocrystals: A Photobactericidal Material That Exhibits Broad Spectrum Antimicrobial Activity†.” *Photochemistry and Photobiology* 88 (4): 1034–1034.

Carrasco, Sergio. 2018. “Metal-Organic Frameworks for the Development of Biosensors: A Current Overview.” *Biosensors* 8 (4). https://doi.org/10.3390/bios8040092.

Castro, Kelly A. D. F., Nuno M. M. Moura, Flávio Figueira, Rosalina I. Ferreira, Mário M. Q. Simões, José A. S. Cavaleiro, M. Amparo F. Faustino, et al. 2019. “New Materials Based on Cationic Porphyrins Conjugated to Chitosan or Titanium Dioxide: Synthesis, Characterization and Antimicrobial Efficacy.” *International Journal of Molecular Sciences* 20 (10). https://doi.org/10.3390/ijms20102522.

Charles, Dominic, and Laurent Kimman. 2023. “Plastic Waste Makers Index 2023.” Minderoo Foundation. 2023. https://cdn.minderoo.org/content/uploads/2023/02/04205527/Plastic-Waste-Makers-Index-2023.pdf.

Charles, Florence, José Sanchez, and Nathalie Gontard. 2006. “Absorption Kinetics of Oxygen and Carbon Dioxide Scavengers as Part of Active Modified Atmosphere Packaging.” *Journal of Food Engineering* 72 (1): 1–7.

Cheng, Qingzheng, and Brian Via. 2017. “Characterization of Cellulose Fibril Aggregates Isolated by the Combination of Ultrasonication and Homogenizer.” *Wood Material Science & Engineering* 12 (4): 197–202.

Cheng, Shaoling, Yapei Zhang, Ruitao Cha, Jinliang Yang, and Xingyu Jiang. 2015. “Water-Soluble Nanocrystalline Cellulose Films with Highly Transparent and Oxygen Barrier Properties.” *Nanoscale* 8 (2): 973–78.

Chen, Guangjun, Ming Wei, Jinghua Chen, Jin Huang, Alain Dufresne, and Peter R. Chang. 2008. “Simultaneous Reinforcing and Toughening: New Nanocomposites of Waterborne Polyurethane Filled with Low Loading Level of Starch Nanocrystals.” *Polymer* 7 (49): 1860–70.

Cheng, Weiwei, Xiaozhi Tang, Yan Zhang, Di Wu, and Wenjian Yang. 2021. “Applications of Metal-Organic Framework (MOF)-Based Sensors for Food Safety: Enhancing Mechanisms and Recent Advances.” *Trends in Food Science & Technology* 112 (June): 268–82.

Cheng, Wenjian, Jianchu Chen, Donghong Liu, Xingqian Ye, and Fansheng Ke. 2010. “Impact of Ultrasonic Treatment on Properties of Starch Film-Forming Dispersion and the Resulting Films.” *Carbohydrate Polymers* 81 (3): 707–11.

Cheng, Zheng, Jialin Li, Miao Su, Naiyu Xiao, Le Zhong, Xueqin Zhang, Shaowu Chen, Qifeng Chen, Weiquan Liang, and Meixian Liu. 2024. “High-Barrier Oxidized Cellulose Nanofibril/Chitosan Coating for Functional Food Packaging Materials.” *ACS Applied Polymer Materials*, February. https://doi.org/10.1021/acsapm.3c03115.

Chen, Jiajie, Yufang Zhu, and Stefan Kaskel. 2021. “Porphyrin-Based Metal-Organic Frameworks for Biomedical Applications.” *Angewandte Chemie* 60 (10): 5010–35.

Chen, Mian, Zhou Long, Ruihua Dong, Le Wang, Jiangjiang Zhang, Sixiang Li, Xiaohui Zhao, Xiandeng Hou, Huawu Shao, and Xingyu Jiang. 2020. “Titanium Incorporation into Zr-Porphyrinic Metal-Organic Frameworks with Enhanced Antibacterial Activity against Multidrug-Resistant Pathogens.” *Small* 16 (7): e1906240.

Chen, Wenbo, Hui He, Hongxiang Zhu, Meixiao Cheng, Yunhua Li, and Shuangfei Wang. 2018. “Thermo-Responsive Cellulose-Based Material with Switchable Wettability for Controllable Oil/Water Separation.” *Polymers* 10 (6). https://doi.org/10.3390/polym10060592.

Cherian, Suman, and Carl C. Wamser. 2000. “Adsorption and Photoactivity of Tetra(4-Carboxyphenyl)porphyrin (TCPP) on Nanoparticulate TiO2.” *The Journal of Physical Chemistry. B* 104 (15): 3624–29.

Chinga-Carrasco, Gary, Natalia Averianova, Olga Kondalenko, Milyausha Garaeva, Vladimir

Petrov, Berit Leinsvang, and Trond Karlsen. 2014. “The Effect of Residual Fibres on the Micro-Topography of Cellulose Nanopaper.” *Micron* 56 (January): 80–84.
Choudhury, Biswajit, and Amarjyoti Choudhury. 2012. “Luminescence Characteristics of Cobalt Doped TiO2 Nanoparticles.” *Journal of Luminescence* 132 (1): 178–84.
Chun, Sang-Jin, Sun-Young Lee, Geum-Hyun Doh, Soo Lee, and Jung Hyeun Kim. 2011. “Preparation of Ultrastrength Nanopapers Using Cellulose Nanofibrils.” *Journal of Industrial and Engineering Chemistry* 17 (3): 521–26.
Clinical and Laboratory Standards Institute. 1999. “M26-A: Methods for Determining Bactericidal Activity of Antimicrobial Agents; Approved Guideline.”
CLSI. 2024. “CLSI M02™ Performance Standards for Antimicrobial Disk Susceptibility Tests (14th Edition).”
Cobb, Samuel J., Zoe J. Ayres, and Julie V. Macpherson. 2018. “Boron Doped Diamond: A Designer Electrode Material for the Twenty-First Century.” *Annual Review of Analytical Chemistry* 11 (1): 463–84.
Contreras, Cintia B., German Charles, Ricardo Toselli, and Miriam C. Strumia. 2017. *Antimicrobial Active Packaging*. Edited by CRC Press.
Couvert, Olivier, Loona Koullen, Anne Lochardet, Véronique Huchet, Jonathan Thevenot, and Yvan Le Marc. 2023. “Effects of Carbon Dioxide and Oxygen on the Growth Rate of Various Food Spoilage Bacteria.” *Food Microbiology* 114 (September): 104289.
Dabestani, Reza, Allen J. Bard, Alan Campion, Marye Anne Fox, Thomas E. Mallouk, Stephen E. Webber, and J. M. White. 1988. “Sensitization of Titanium Dioxide and Strontium Titanate Electrodes by ruthenium(II) tris(2,2’-Bipyridine-4,4'-Dicarboxylic Acid) and Zinc tetrakis(4-Carboxyphenyl)porphyrin: An Evaluation of Sensitization Efficiency for Component Photoelectrodes in a Multipanel Device.” *The Journal of Physical Chemistry* 92 (7): 1872–78.
Daéid, N. N. 2005. “FORENSIC SCIENCES | Systematic Drug Identification.” In *Encyclopedia of Analytical Science (Second Edition)*, edited by Paul Worsfold, Alan Townshend, and Colin Poole, 471–80. Oxford: Elsevier.
Daicho, Kazuho, Tsuguyuki Saito, Shuji Fujisawa, and Akira Isogai. 2018. “The Crystallinity of Nanocellulose: Dispersion-Induced Disordering of the Grain Boundary in Biologically Structured Cellulose.” *ACS Applied Nano Materials* 1 (10): 5774–85.
Dainelli, Dario, Nathalie Gontard, Dimitrios Spyropoulos, Esther Zondervan-van den Beuken, and Paul Tobback. 2008. “Active and Intelligent Food Packaging: Legal Aspects and Safety Concerns.” *Trends in Food Science & Technology* 19 (November): S103–12.
Dalrymple, Omatoyo K., Elias Stefanakos, Maya A. Trotz, and D. Yogi Goswami. 2010. “A Review of the Mechanisms and Modeling of Photocatalytic Disinfection.” *Applied Catalysis. B, Environmental* 98 (1): 27–38.
Dan-Hardi, Meenakshi, Christian Serre, Théo Frot, Laurence Rozes, Guillaume Maurin, Clément Sanchez, and Gérard Férey. 2009. “A New Photoactive Crystalline Highly Porous titanium(IV) Dicarboxylate.” *Journal of the American Chemical Society* 131 (31): 10857–59.
Daniels, Carole A. 1989. *Polymers: Structure and Properties*. Lancaster, PA, USA: Technomic Pub. Co.
Das, Kuntal, R. Tiwari, and D. Shrivastava. 2010. “Techniques for Evaluation of Medicinal Plant Products as Antimicrobial Agents: Current Methods and Future Trends.” *Journal of Medicinal Plants Research* 4 (January): 104–11.
Davoudpour, Yalda, Sohrab Hossain, H. P. S. Abdul Khalil, M. K. Mohamad Haafiz, Z. A. Mohd Ishak, Azman Hassan, and Zaidul Islam Sarker. 2015. “Optimization of High Pressure Homogenization Parameters for the Isolation of Cellulosic Nanofibers Using Response Surface Methodology.” *Industrial Crops and Products* 74 (November): 381–87.
Deepa, B., Cintil Jose Chirayil, Laly A. Pothan, and Sabu Thomas. 2019. “Chapter 4 -

Lignocellulose-Based Nanoparticles and Nanocomposites: Preparation, Properties, and Applications." In *Lignocellulose for Future Bioeconomy*, edited by Hidayah Ariffin, S. M. Sapuan, and Mohd Ali Hassan, 41–69. Elsevier.
De France, Kevin J., Todd Hoare, and Emily D. Cranston. 2017. "Review of Hydrogels and Aerogels Containing Nanocellulose." *Chemistry of Materials: A Publication of the American Chemical Society* 29 (11): 4609–31.
Delcour, Anne H. 2009. "Outer Membrane Permeability and Antibiotic Resistance." *Biochimica et Biophysica Acta* 1794 (5): 808–16.
DeRosa, Maria C., and Robert J. Crutchley. 2002. "Photosensitized Singlet Oxygen and Its Applications." *Coordination Chemistry Reviews* 233-234 (November): 351–71.
Deville, Jean-Paul, and Costel Sorin Cojocaru. 2006. "Chapter 12 - Spectroscopic Analyses of Surfaces and Thin Films." In *Materials Surface Processing by Directed Energy Techniques*, edited by Yves Pauleau, 411–41. Oxford: Elsevier.
Dias, Otavio Augusto Titton, Samir Konar, Alcides Lopes Leão, Weimin Yang, Jimi Tjong, and Mohini Sain. 2020. "Current State of Applications of Nanocellulose in Flexible Energy and Electronic Devices." *Frontiers in Chemistry* 8 (May): 420.
Dijken, A. van, A. H. Janssen, M. H. P. Smitsmans, D. Vanmaekelbergh, and A. Meijerink. 1998. "Size-Selective Photoetching of Nanocrystalline Semiconductor Particles." *Chemistry of Materials: A Publication of the American Chemical Society* 10 (11): 3513–22.
Dijk, Michiel van, Tom Morley, Marie Luise Rau, and Yashar Saghai. 2021. "A Meta-Analysis of Projected Global Food Demand and Population at Risk of Hunger for the Period 2010–2050." *Nature Food* 2 (7): 494–501.
Dilamian, Mandana, and Babak Noroozi. 2019. "A Combined Homogenization-High Intensity Ultrasonication Process for Individualizaion of Cellulose Micro-Nano Fibers from Rice Straw." *Cellulose* 26 (10): 5831–49.
Dinesh, Geethanjali, and Balasubramanian Kandasubramanian. 2022. "Fabrication of Transparent Paper Devices from Nanocellulose Fiber." *Materials Chemistry and Physics* 281 (April): 125707.
Djafari Petroudy, S. R. 2017. "3 - Physical and Mechanical Properties of Natural Fibers." In *Advanced High Strength Natural Fibre Composites in Construction*, edited by Mizi Fan and Feng Fu, 59–83. Woodhead Publishing.
Doebelin, Nicola, and Reinhard Kleeberg. 2015. "Profex: A Graphical User Interface for the Rietveld Refinement Program BGMN." *Journal of Applied Crystallography* 48 (Pt 5): 1573–80.
Dowling, Norman E. 2007. *Mechanical Behavior of Materials: Engineering Methods for Deformation, Fracture, and Fatigue*. Pearson Prentice Hall.
Duan, Chao, Xin Meng, Chaoran Liu, Wanli Lu, Jun Liu, Lei Dai, Wenliang Wang, Wei Zhao, Chuanyin Xiong, and Yonghao Ni. 2019. "Carbohydrates-Rich Corncobs Supported Metal-Organic Frameworks as Versatile Biosorbents for Dye Removal and Microbial Inactivation." *Carbohydrate Polymers* 222 (October): 115042.
Du, Chao, Hailong Li, Bingyun Li, Mengru Liu, and Huaiyu Zhan. 2016. "Characteristics and Properties of Cellulose Nanofibers Prepared by TEMPO Oxidation of Corn Husk." *BioResources* 11 (2): 5276–84.
Durot, Stéphanie, Julien Taesch, and Valérie Heitz. 2014. "Multiporphyrinic Cages: Architectures and Functions." *Chemical Reviews* 114 (17): 8542–78.
Duval, Clément. 1963. *Inorganic Thermogravimetric Analysis*. Elsevier Publishing Company.
Dwivedi, Charu, Ishan Pandey, Himanshu Pandey, Pramod W. Ramteke, Avinash C. Pandey, Shanti Bhushan Mishra, and Sandip Patil. 2017. "Chapter 9 - Electrospun Nanofibrous Scaffold as a Potential Carrier of Antimicrobial Therapeutics for Diabetic Wound Healing and Tissue Regeneration." In *Nano- and Microscale Drug Delivery Systems*, edited by Alexandru Mihai Grumezescu, 147–64. Elsevier.

Egerton, Ray F. 2005. “The Scanning Electron Microscope.” In *Physical Principles of Electron Microscopy: An Introduction to TEM, SEM, and AEM*, edited by Ray F. Egerton, 125–53. Boston, MA: Springer US.
Ehrmann, Klaus. 2024. “Chapter 7 - Soft Lens Measurement.” In *Contact Lens Practice (Fourth Edition)*, edited by Nathan Efron, 76–89.e2. New Delhi: Elsevier.
Elliker, P. R., and W. C. Frazier. 1938. “Influence of Time and Temperature of Incubation on Heat Resistance of Escherichia Coli.” *Journal of Bacteriology* 36 (1): 83–98.
El-Wakil, Nahla A., Enas A. Hassan, Ragab E. Abou-Zeid, and Alain Dufresne. 2015. “Development of Wheat Gluten/nanocellulose/titanium Dioxide Nanocomposites for Active Food Packaging.” *Carbohydrate Polymers* 124 (June): 337–46.
EPA. 2015a. “Reducing Wasted Food and Packaging: A Guide for Food Services and Restaurants.” 2015. https://www.epa.gov/nscep.
———. 2015b. “Reducing Wasted Food and Packaging: A Guide for Food Services and Restaurants.” 2015. https://www.epa.gov/nscep.
———. 2016a. “International Efforts on Wasted Food Recovery.” 2016. https://www.epa.gov/.
———. 2016b. “International Efforts on Wasted Food Recovery.” 2016. https://www.epa.gov/.
Epp, J. 2016. “4 - X-Ray Diffraction (XRD) Techniques for Materials Characterization.” In *Materials Characterization Using Nondestructive Evaluation (NDE) Methods*, edited by Gerhard Hübschen, Iris Altpeter, Ralf Tschuncky, and Hans-Georg Herrmann, 81–124. Woodhead Publishing.
Ercolini, D. 2014. “IDENTIFICATION METHODS | Introduction.” In *Encyclopedia of Food Microbiology (Second Edition)*, edited by Carl A. Batt and Mary Lou Tortorello, 241–47. Oxford: Academic Press.
Erdem, Bedri, Robert A. Hunsicker, Gary W. Simmons, E. David Sudol, Victoria L. Dimonie, and Mohamed S. El-Aasser. 2001. “XPS and FTIR Surface Characterization of TiO2 Particles Used in Polymer Encapsulation.” *Langmuir: The ACS Journal of Surfaces and Colloids* 17 (9): 2664–69.
Eslami, Zahra, Saïd Elkoun, Mathieu Robert, and Kokou Adjallé. 2023. “A Review of the Effect of Plasticizers on the Physical and Mechanical Properties of Alginate-Based Films.” *Molecules* 28 (18). https://doi.org/10.3390/molecules28186637.
EUCAST. 2021. “Antimicrobial Susceptibility Testing: EUCAST Disk Diffusion Method.” European Committee on Antimicrobial Susceptibility Testing.
European Commission. 2023. “Waste Framework Directive.” 2023. https://environment.ec.europa.eu/topics/waste-and-recycling/waste-framework-directive_en.
Evans, John S. O., and Ivana Radosavljevic Evans. 2004. “Beyond Classical Applications of Powder Diffraction.” *Chemical Society Reviews* 33 (8): 539–47.
Ewing, Galen Wood. 1997. *Analytical Instrumentation Handbook, Second Edition*. CRC Press.
Fang, Wei-Hui, Jian-Fang Wang, Lei Zhang, and Jian Zhang. 2017. “Titanium–Oxo Cluster Based Precise Assembly for Multidimensional Materials.” *Chemistry of Materials: A Publication of the American Chemical Society* 29 (7): 2681–84.
Fang, Wei-Hui, Lei Zhang, and Jian Zhang. 2016. “A 3.6 Nm Ti52-Oxo Nanocluster with Precise Atomic Structure.” *Journal of the American Chemical Society* 138 (24): 7480–83.
FAO. 2013a. “Food Wastage Footprint: Impacts on Natural Resources : Summary Report.” 2013. https://www.fao.org/3/i3347e/i3347e.pdf.
———. 2013b. “Food Wastage Footprint: Impacts on Natural Resources : Summary Report.” 2013. https://www.fao.org/3/i3347e/i3347e.pdf.
———. 2021a. “Food Waste FAQs.” Https://www.usda.gov/foodwaste/faqs. 2021.
———. 2021b. “Food Waste FAQs.” Https://www.usda.gov/foodwaste/faqs. 2021.
———. 2022a. “Voluntary Code of Conduct for Food Loss and Waste Reduction.” 2022. https://doi.org/10.4060/cb9433en.
———. 2022b. *Voluntary Code of Conduct for Food Loss and Waste Reduction*. Food &

Agriculture Org.
FDA. 2019a. “Escherichia Coli (E. Coli).” 2019. https://www.fda.gov/food/foodborne-pathogens/escherichia-coli-e-coli.
———. 2019b. “Escherichia Coli (E. Coli).” 2019.
———. 2022. “Outbreaks of Foodborne Illness.” 2022. https://www.fda.gov/food/recalls-outbreaks-emergencies/outbreaks-foodborne-illness.
Fein, Kendra, Douglas W. Bousfield, and William M. Gramlich. 2021. “Processing Effects on Structure, Strength, and Barrier Properties of Refiner-Produced Cellulose Nanofibril Layers.” *ACS Applied Polymer Materials* 3 (7): 3666–78.
Feng, Ligang, Xiujuan Sun, Shikui Yao, Changpeng Liu, Wei Xing, and Jiujun Zhang. 2014. “3 - Electrocatalysts and Catalyst Layers for Oxygen Reduction Reaction.” In *Rotating Electrode Methods and Oxygen Reduction Electrocatalysts*, edited by Wei Xing, Geping Yin, and Jiujun Zhang, 67–132. Amsterdam: Elsevier.
Feng, Li-Juan, Min Wang, Zhi-Yong Sun, Yun Hu, and Zhen-Tao Deng. 2017. “Hypercrosslinked Porous Polyporphyrin by Metal-Free Protocol: Characterization, Uptake Performance, and Heterogeneous Catalysis.” *Designed Monomers and Polymers* 20 (1): 344–50.
Firouz, Mahmoud Soltani, Khaled Mohi-Alden, and Mahmoud Omid. 2021. “A Critical Review on Intelligent and Active Packaging in the Food Industry: Research and Development.” *Food Research International* 141 (March): 110113.
Flores, Zoila, Diego San-Martin, Tatiana Beldarraín-Iznaga, Javier Leiva-Vega, and Ricardo Villalobos-Carvajal. 2021. “Effect of Homogenization Method and Carvacrol Content on Microstructural and Physical Properties of Chitosan-Based Films.” *Foods (Basel, Switzerland)* 10 (1). https://doi.org/10.3390/foods10010141.
Forte, V. C. 2014. “Understanding Ultraviolet LED Applications and Precautions.” 2014. https://marktechopto.com/understanding-ultraviolet-led-applications-and-precautions/.
Fourati-Ben Fguira, Lilia, Serge Fotso, Raoudha Ben Ameur-Mehdi, Lotfi Mellouli, and Hartmut Laatsch. 2005. “Purification and Structure Elucidation of Antifungal and Antibacterial Activities of Newly Isolated Streptomyces Sp. Strain US80.” *Research in Microbiology* 156 (3): 341–47.
Freund, Ralph, Ulrich Lächelt, Tobias Gruber, Bastian Rühle, and Stefan Wuttke. 2018. “Multifunctional Efficiency: Extending the Concept of Atom Economy to Functional Nanomaterials.” *ACS Nano* 12 (3): 2094–2105.
Fukuzumi, Hayaka, Shuji Fujisawa, Tsuguyuki Saito, and Akira Isogai. 2013. “Selective Permeation of Hydrogen Gas Using Cellulose Nanofibril Film.” *Biomacromolecules* 14 (5): 1705–9.
Fukuzumi, Hayaka, Tsuguyuki Saito, Tadahisa Iwata, Yoshiaki Kumamoto, and Akira Isogai. 2009. “Transparent and High Gas Barrier Films of Cellulose Nanofibers Prepared by TEMPO-Mediated Oxidation.” *Biomacromolecules* 10 (1): 162–65.
Fukuzumi, Hayaka, Tsuguyuki Saito, Yusuke Okita, and Akira Isogai. 2010. “Thermal Stabilization of TEMPO-Oxidized Cellulose.” *Polymer Degradation and Stability* 95 (9): 1502–8.
Fularz, Agata, Sawsan Almohammed, and James H. Rice. 2021. “SERS Enhancement of Porphyrin-Type Molecules on Metal-Free Cellulose-Based Substrates.” *ACS Sustainable Chemistry & Engineering* 9 (49): 16808–19.
Fularz, Agata, James H. Rice, and Pietro Ballone. 2021. “Morphology of Nanometric Overlayers Made of Porphyrin-Type Molecules Physisorbed on Cellulose Iβ Crystals and Nanocrystals.” *The Journal of Physical Chemistry. B* 125 (41): 11432–43.
Furukawa, Hiroyasu, Kyle E. Cordova, Michael O’Keeffe, and Omar M. Yaghi. 2013. “The Chemistry and Applications of Metal-Organic Frameworks.” *Science* 341 (6149): 1230444.
Fu, Zong-Qiang, Li-Jun Wang, Dong Li, Qing Wei, and Benu Adhikari. 2011. “Effects of High-Pressure Homogenization on the Properties of Starch-Plasticizer Dispersions and Their

Films." *Carbohydrate Polymers* 86 (1): 202–7.
Gadgil, R. B. 1981. "A Study of UV Spectral Transmission Through Different Transparent Media with Spectrophotometer." *Indian Journal of Dermatology, Venereology and Leprology* 47 (5): 255–58.
Gao, Hongyi, Junyong Wang, Mengyi Jia, Fucheng Yang, Radoelizo S. Andriamitantsoa, Xiubing Huang, Wenjun Dong, and Ge Wang. 2019. "Construction of TiO2 Nanosheets/tetra (4-Carboxyphenyl) Porphyrin Hybrids for Efficient Visible-Light Photoreduction of CO2." *Chemical Engineering Journal* 374 (October): 684–93.
Gautam, S. P., P. S. Bundela, A. K. Pandey, Jamaluddin Jamaluddin, M. K. Awasthi, and S. Sarsaiya. 2010. "A Review on Systematic Study of Cellulose." *Journal of Applied and Natural Science* 2 (2): 330–43.
Gendreau, R. M., and R. Burton. 1979. "The KBr Pellet: A Useful Technique for Obtaining Infrared Spectra of Inorganic Species." *Applied Spectroscopy* 33 (6): 581–84.
Gere, James M. 2003. *Mechanics of Materials: Sixth Edition*. Thomson-Engineering.
Germain, Y. 1997. "Conception de Films Polymère à Perméabilité Contrôlée Pour L'emballage Alimentaire." *Industries Alimentaires et Agricoles* 114 (3): 137–40.
Geyer, Roland, Jenna R. Jambeck, and Kara Lavender Law. 2017. "Production, Use, and Fate of All Plastics Ever Made." *Science Advances* 3 (7): e1700782.
Ghamarpoor, Reza, Akram Fallah, and Masoud Jamshidi. 2023. "Investigating the Use of Titanium Dioxide (TiO2) Nanoparticles on the Amount of Protection against UV Irradiation." *Scientific Reports* 13 (1): 9793.
Gnanasekaran, Karthikeyan, Roderick Snel, Gijsbertus de With, and Heiner Friedrich. 2016. "Quantitative Nanoscopy: Tackling Sampling Limitations in (S)TEM Imaging of Polymers and Composites." *Ultramicroscopy* 160 (January): 130–39.
Goldstein, I. S. 2004. "WOOD FORMATION AND PROPERTIES | Chemical Properties of Wood." In *Encyclopedia of Forest Sciences*, edited by Jeffery Burley, 1835–39. Oxford: Elsevier.
Goldstein, Joseph I., Dale E. Newbury, Patrick Echlin, David C. Joy, Charles E. Lyman, Eric Lifshin, Linda Sawyer, and Joseph R. Michael. 2003. "Specimen Preparation of Polymer Materials." In *Scanning Electron Microscopy and X-Ray Microanalysis: Third Edition*, edited by Joseph I. Goldstein, Dale E. Newbury, Patrick Echlin, David C. Joy, Charles E. Lyman, Eric Lifshin, Linda Sawyer, and Joseph R. Michael, 565–90. Boston, MA: Springer US.
Goldstein, Joseph I., Dale E. Newbury, Joseph R. Michael, Nicholas W. M. Ritchie, John Henry J. Scott, and David C. Joy. 2017. *Scanning Electron Microscopy and X-Ray Microanalysis*. Springer.
Gomaa, Eman Zakaria. 2022. "Microbial Mediated Synthesis of Zinc Oxide Nanoparticles, Characterization and Multifaceted Applications." *Journal of Inorganic and Organometallic Polymers and Materials* 32 (11): 4114–32.
Gomes, Maria C., Sandrina Silva, Maria A. F. Faustino, Maria G. P. M. S. Neves, Adelaide Almeida, José A. S. Cavaleiro, João P. C. Tomé, and Ângela Cunha. 2013. "Cationic Galactoporphyrin Photosensitisers against UV-B Resistant Bacteria: Oxidation of Lipids and Proteins by 1O2." *Photochemical & Photobiological Sciences: Official Journal of the European Photochemistry Association and the European Society for Photobiology* 12 (2): 262–71.
Gong, Guan, Jinkyung Pyo, Aji P. Mathew, and Kristiina Oksman. 2011. "Tensile Behavior, Morphology and Viscoelastic Analysis of Cellulose Nanofiber-Reinforced (CNF) Polyvinyl Acetate (PVAc)." *Composites. Part A, Applied Science and Manufacturing* 42 (9): 1275–82.
Good, Robert J. 1992. "Contact Angle, Wetting, and Adhesion: A Critical Review." *Journal of Adhesion Science and Technology* 6 (12): 1269–1302.
Görgülüer, Hakan, Bekir Çakıroğlu, and Mahmut Özacar. 2021. "Ag NPs Deposited TiO2

Coating Material for Superhydrophobic, Antimicrobial and Self-Cleaning Surface Fabrication on Fabric." *Journal of Coatings Technology and Research* 18 (2): 569–79.
Goriletsky, V. I., A. I. Mitichkin, L. E. Belenko, and T. P. Rebrova. 2001. "IR Spectroscopy of KBr Salt and Crystals." *Semiconductor Physics, Quantum Electronics & Optoelectronics* 4 (2): 139–41.
Gottfried, J. Michael. 2015. "Surface Chemistry of Porphyrins and Phthalocyanines." *Surface Science Reports* 70 (3): 259–379.
Grabowska, Beata, and Jacek Kasperski. 2018. "Modeling of Thermal Properties of Thermal Insulation Layered with Transparent, Opaque and Reflective Film." *Journal of Thermal Science* 27 (5): 463–69.
Gu, Bin, Xueyun Huang, Fengxian Qiu, Dongya Yang, and Tao Zhang. 2020. "Laminated Cellulose Hybrid Membranes with Triple Thermal Insulation Functions for Personal Thermal Management Application." *ACS Sustainable Chemistry & Engineering* 8 (42): 15936–45.
Guillard, Valérie, Sébastien Gaucel, Claudio Fornaciari, Hélène Angellier-Coussy, Patrice Buche, and Nathalie Gontard. 2018. "The Next Generation of Sustainable Food Packaging to Preserve Our Environment in a Circular Economy Context." *Frontiers in Nutrition* 5 (December): 121.
Guo, Zebin, Beibei Zhao, Liding Chen, and Baodong Zheng. 2019. "Physicochemical Properties and Digestion of Lotus Seed Starch under High-Pressure Homogenization." *Nutrients* 11 (2). https://doi.org/10.3390/nu11020371.
Guzman-Puyol, Susana, Jesús Hierrezuelo, José J. Benítez, Giacomo Tedeschi, José M. Porras-Vázquez, Antonio Heredia, Athanassia Athanassiou, Diego Romero, and José A. Heredia-Guerrero. 2022. "Transparent, UV-Blocking, and High Barrier Cellulose-Based Bioplastics with Naringin as Active Food Packaging Materials." *International Journal of Biological Macromolecules* 209 (June): 1985–94.
Hafez, Islam, Ezatollah Amini, and Mehdi Tajvidi. 2020. "The Synergy between Cellulose Nanofibrils and Calcium Carbonate in a Hybrid Composite System." *Cellulose* 27 (7): 3773–87.
Hafid, Halimatun Saadiah, Farah Nadia Omar, Ezyana Kamal Bahrin, and Minato Wakisaka. 2023. "Extraction and Surface Modification of Cellulose Fibers and Its Reinforcement in Starch-Based Film for Packaging Composites." *Bioresources and Bioprocessing* 10 (1): 1–17.
Hamad, Hesham, Esther Bailón-García, Sergio Morales-Torres, Francisco Carrasco-Marín, Agustín F. Pérez-Cadenas, and Francisco J. Maldonado-Hódar. 2018. "Physicochemical Properties of New Cellulose-TiO2 Composites for the Removal of Water Pollutants: Developing Specific Interactions and Performances by Cellulose Functionalization." *Journal of Environmental Chemical Engineering* 6 (4): 5032–41.
Hariharan, C. 2006. "Photocatalytic Degradation of Organic Contaminants in Water by ZnO Nanoparticles: Revisited." *Applied Catalysis, A: General* 304 (May): 55–61.
Hatano, Tomohiro, Satoshi Nakaba, Yoshiki Horikawa, and Ryo Funada. 2022. "A Combination of Scanning Electron Microscopy and Broad Argon Ion Beam Milling Provides Intact Structure of Secondary Tissues in Woody Plants." *Scientific Reports* 12 (1): 1–10.
Hayashi, Jisuke, Akinori Sufoka, Junji Ohkita, and Sadayoshi Watanabe. 1975. "The Confirmation of Existences of Cellulose III_I, III_{II}, IV_I, and IV_{II} by the X‐ray Method." *Journal of Polymer Science Polymer Letters Edition* 13 (1): 23–27.
Heatley, N. G. 1944. "A Method for the Assay of Penicillin." *Biochemical Journal* 38 (1): 61–65.
Henriksson, Marielle, Lars A. Berglund, Per Isaksson, Tom Lindström, and Takashi Nishino. 2008. "Cellulose Nanopaper Structures of High Toughness." *Biomacromolecules* 9 (6): 1579–85.
Herrera, Martha. 2015. "Preparation and Characterization of Nanocellulose Films and Coatings

from Industrial Bio-Residues." Luleå tekniska universitet. https://www.diva-portal.org/smash/record.jsf?pid=diva2:990113.
Herrera, Martha A., Aji P. Mathew, and Kristiina Oksman. 2012. "Comparison of Cellulose Nanowhiskers Extracted from Industrial Bio-Residue and Commercial Microcrystalline Cellulose." *Materials Letters* 71 (March): 28–31.
Herrick, F. W., R. L. Casebier, J. Hamilton, and K. R. Sandberg. 1983. "Microfibrillated Cellulose: Morphology and Accessibility." *Https://www.semanticscholar.org › Paper › Microfibrillat...https://www.semanticscholar.org › Paper › Microfibrillat...* https://www.semanticscholar.org/paper/acb8a50450158c2eb6962059d077f51817c8720e.
He, Siyu, Li Wu, Xue Li, Hongyu Sun, Ting Xiong, Jie Liu, Chengxi Huang, et al. 2021. "Metal-Organic Frameworks for Advanced Drug Delivery." *Acta Pharmaceutica Sinica. B* 11 (8): 2362–95.
Hibbeler, Russell C. 2016. *Mechanics of Materials: 10th Edition*. Pearson.
Hong, Seok-In, and John M. Krochta. 2006. "Oxygen Barrier Performance of Whey-Protein-Coated Plastic Films as Affected by Temperature, Relative Humidity, Base Film and Protein Type." *Journal of Food Engineering* 77 (3): 739–45.
Hong, Yuzhi, Jie Zeng, Xiuhong Wang, Karl Drlica, and Xilin Zhao. 2019. "Post-Stress Bacterial Cell Death Mediated by Reactive Oxygen Species." *Proceedings of the National Academy of Sciences of the United States of America* 116 (20): 10064–71.
Hoover, R., and W. S. Ratnayake. 2002. "Starch Characteristics of Black Bean, Chick Pea, Lentil, Navy Bean and Pinto Bean Cultivars Grown in Canada." *Food Chemistry* 78 (4): 489–98.
Hossain, Md Lokman, Lee Yong Lim, Katherine Hammer, Dhanushka Hettiarachchi, and Cornelia Locher. 2022. "A Review of Commonly Used Methodologies for Assessing the Antibacterial Activity of Honey and Honey Products." *Antibiotics (Basel, Switzerland)* 11 (7). https://doi.org/10.3390/antibiotics11070975.
Houck, Max M., and Jay A. Siegel. 2015. "Chapter 5 - Light and Matter." In *Fundamentals of Forensic Science (Third Edition)*, edited by Max M. Houck and Jay A. Siegel, 93–119. San Diego: Academic Press.
Huang, Dayong, Min Wu, Chao Wang, Shigenori Kuga, and Yong Huang. 2020. "Effect of Partial Dehydration on Freeze-Drying of Aqueous Nanocellulose Suspension." *ACS Sustainable Chemistry & Engineering* 8 (30): 11389–95.
Huang, Haoyuan, Wentao Song, James Rieffel, and Jonathan F. Lovell. 2015. "Emerging Applications of Porphyrins in Photomedicine." *Frontiers of Physics* 3 (April). https://doi.org/10.3389/fphy.2015.00023.
Huang, Shancong, Xiyun Wang, Yu Zhang, Yu Meng, Feiguo Hua, and Xinxing Xia. 2022. "Cellulose Nanofibers/polyvinyl Alcohol Blends as an Efficient Coating to Improve the Hydrophobic and Oleophobic Properties of Paper." *Scientific Reports* 12 (1): 1–10.
Huang, Wenyi. 2018. "Chapter 5 - Cellulose Nanopapers." In *Nanopapers*, edited by Wenyi Huang, 121–73. William Andrew Publishing.
Iacovone, Carolina, Federico Yulita, Daniel Cerini, Daniel Peña, Roberto Candal, Silvia Goyanes, Lía I. Pietrasanta, Lucas Guz, and Lucía Famá. 2023. "Effect of TiO2 Nanoparticles and Extrusion Process on the Physicochemical Properties of Biodegradable and Active Cassava Starch Nanocomposites." *Polymers* 15 (3). https://doi.org/10.3390/polym15030535.
Ibrahim, H., N. Sazali, I. N. Ibrahim, and M. S. Sharip. 2019. "Nano-Structured Cellulose as Green Adsorbents for Water Purification: A Mini Review." *Amstelodamum* 23 (2). https://doi.org/10.11113/amst.v23n2.154.
Ilyas, R. A., S. M. Sapuan, M. R. Ishak, and E. S. Zainudin. 2018. "Development and Characterization of Sugar Palm Nanocrystalline Cellulose Reinforced Sugar Palm Starch Bionanocomposites." *Carbohydrate Polymers* 202 (December): 186–202.
———. 2019. "Sugar Palm Nanofibrillated Cellulose (Arenga Pinnata (Wurmb.) Merr): Effect of Cycles on Their Yield, Physic-Chemical, Morphological and Thermal Behavior."

International Journal of Biological Macromolecules 123 (February): 379–88.
Inkson, B. J. 2016. "2 - Scanning Electron Microscopy (SEM) and Transmission Electron Microscopy (TEM) for Materials Characterization." In *Materials Characterization Using Nondestructive Evaluation (NDE) Methods*, edited by Gerhard Hübschen, Iris Altpeter, Ralf Tschuncky, and Hans-Georg Herrmann, 17–43. Woodhead Publishing.
Islam, Atif, Tariq Yasin, and Ihtesham ur Rehman. 2014. "Synthesis of Hybrid Polymer Networks of Irradiated Chitosan/poly(vinyl Alcohol) for Biomedical Applications." *Radiation Physics and Chemistry* 96 (March): 115–19.
Islam, Md Azharul, M. Auta, G. Kabir, and B. H. Hameed. 2016. "A Thermogravimetric Analysis of the Combustion Kinetics of Karanja (Pongamia Pinnata) Fruit Hulls Char." *Bioresource Technology* 200 (January): 335–41.
Isogai, Akira, Makoto Usuda, Takashi Kato, Toshiyuki Uryu, and Rajai H. Atalla. 1989. "Solid-State CP/MAS Carbon-13 NMR Study of Cellulose Polymorphs." *Macromolecules* 22 (7): 3168–72.
Iwamoto, S., A. N. Nakagaito, and H. Yano. 2007. "Nano-Fibrillation of Pulp Fibers for the Processing of Transparent Nanocomposites." *Applied Physics A: Materials Science & Processing* 89 (2): 461–66.
Jagodzińska, Sylwia, Research Network Łukasiewicz - Institute of Biopolymers and Chemical Fibres, Beata Pałys, Dariusz Wawro, and Institute of Security Technologies "MORATEX." 2021. "Effect of Chitosan Film Surface Structure on the Contact Angle." *Progress on Chemistry and Application of Chitin and Its Derivatives* 26 (September): 89–100.
Jain, Prashant K., Pulak M. Pandey, and P. V. M. Rao. 2009. "Selective Laser Sintering of Clay-Reinforced Polyamide." *Polymer Composites*, NA – NA.
Jakobsen, Marianne, Lone Jespersen, Dorte Juncher, Eleonora Miquel Becker, and Jens Risbo. 2005. "Oxygen- and Light-Barrier Properties of Thermoformed Packaging Materials Used for Modified Atmosphere Packaging. Evaluation of Performance under Realistic Storage Conditions." *Packaging Technology & Science* 18 (5): 265–72.
Janjarasskul, Theeranun, and Panuwat Suppakul. 2018. "Active and Intelligent Packaging: The Indication of Quality and Safety." *Critical Reviews in Food Science and Nutrition* 58 (5): 808–31.
Jasat, Ayub, and David Dolphin. 1997. "Expanded Porphyrins and Their Heterologs." *Chemical Reviews* 97 (6): 2267–2340.
Jawaid, Mohammad, Othman Y. Alothman, Naheed Saba, Paridah Md Tahir, and H. P. S. Abdul Khalil. 2015. "Effect of Fibers Treatment on Dynamic Mechanical and Thermal Properties of Epoxy Hybrid Composites." *Polymer Composites* 36 (9): 1669–74.
Jiang, David D., Q. Yao, Michael A. McKinney, and Charles A. Wilkie. 1999. "TGA/FTIR Studies on the Thermal Degradation of Some Polymeric Sulfonic and Phosphonic Acids and Their Sodium Salts." *Polymer Degradation and Stability* 63 (3): 423–34.
Jiang, Zhong Wei, Yang Chun Zou, Ting Ting Zhao, Shu Jun Zhen, Yuan Fang Li, and Cheng Zhi Huang. 2020. "Controllable Synthesis of Porphyrin-Based 2D Lanthanide Metal-Organic Frameworks with Thickness- and Metal-Node-Dependent Photocatalytic Performance." *Angewandte Chemie* 59 (8): 3300–3306.
Jia, Tao, Yifan Gu, and Fengting Li. 2022. "Progress and Potential of Metal-Organic Frameworks (MOFs) for Gas Storage and Separation: A Review." *Journal of Environmental Chemical Engineering* 10 (5): 108300.
Ji, Zhiqiang, Mengnan Yuan, Zhaoqin He, Hao Wei, Xuemin Wang, Jianxin Song, and Lisha Jiang. 2024. "Construction of Porphyrin-Based Bimetallic Nanomaterials with Photocatalytic Properties." *Molecules* 29 (3). https://doi.org/10.3390/molecules29030708.
Johns, I. B., E. A. McElhill, and J. O. Smith. 1962. "Thermal Stability of Organic Compounds." *I&EC Product Research and Development* 1 (1): 2–6.
Johnson, Dave. 2008. *How to Do Everything: Digital Camera*. 5th ed. USA: Mcgraw-hill.

Johnson, Jacob A., Xu Zhang, Tyler C. Reeson, Yu-Sheng Chen, and Jian Zhang. 2014. “Facile Control of the Charge Density and Photocatalytic Activity of an Anionic Indium Porphyrin Framework via in Situ Metalation.” *Journal of the American Chemical Society* 136 (45): 15881–84.

Jonoobi, Mehdi, Jalaluddin Harun, Aji P. Mathew, Mohd Zobir B. Hussein, and Kristiina Oksman. 2010. “Preparation of Cellulose Nanofibers with Hydrophobic Surface Characteristics.” *Cellulose* 17 (2): 299–307.

Jonoobi, Mehdi, Jalaluddin Harun, Aji P. Mathew, and Kristiina Oksman. 2010. “Mechanical Properties of Cellulose Nanofiber (CNF) Reinforced Polylactic Acid (PLA) Prepared by Twin Screw Extrusion.” *Composites Science and Technology* 70 (12): 1742–47.

Josset, Sébastien, Paola Orsolini, Gilberto Siqueira, Alvaro Tejado, Philippe Tingaut, and Tanja Zimmermann. 2014. “Energy Consumption of the Nanofibrillation of Bleached Pulp, Wheat Straw and Recycled Newspaper through a Grinding Process.” *Nordic Pulp & Paper Research Journal* 29 (1): 167–75.

Jun, Byung-Moon, Yasir A. J. Al-Hamadani, Ahjeong Son, Chang Min Park, Min Jang, Am Jang, Nam Chan Kim, and Yeomin Yoon. 2020. “Applications of Metal-Organic Framework Based Membranes in Water Purification: A Review.” *Separation & Purification Technology* 247 (September): 116947.

Jurowski, Krystian, and Stefania Grzeszczyk. 2015. “The Influence of Concrete Composition on Young’s Modulus.” *Procedia Engineering* 108 (January): 584–91.

Kafle, B. 2020. “Introduction to Nanomaterials and Application of UV–Visible Spectroscopy for Their Characterization.” *Characterization by Spectrophotometry*, 147–98.

Kalaiarasi, S., and M. Jose. 2017. “Streptomycin Loaded TiO2 Nanoparticles: Preparation, Characterization and Antibacterial Applications.” *Journal of Nanostructure in Chemistry* 7 (1): 47–53.

Kalia, Susheel, Sami Boufi, Annamaria Celli, and Sarita Kango. 2014. “Nanofibrillated Cellulose: Surface Modification and Potential Applications.” *Colloid and Polymer Science* 292 (1): 5–31.

Kalyanasundaram, K., N. Vlachopoulos, V. Krishnan, A. Monnier, and M. Graetzel. 1987. “Sensitization of Titanium Dioxide in the Visible Light Region Using Zinc Porphyrins.” *The Journal of Physical Chemistry* 91 (9): 2342–47.

Kaper, James B., James P. Nataro, and Harry L. Mobley. 2004. “Pathogenic Escherichia Coli.” *Nature Reviews. Microbiology* 2 (2): 123–40.

Kaper, J. B. 2005. “Pathogenic Escherichia Coli.” *International Journal of Medical Microbiology* 295 (6/7): 355–511.

Kasemwong, Kittiwut, Uracha Rungsardthong Ruktanonchai, Wanwisa Srinuanchai, Teerarat Itthisoponkul, and Klanarong Sriroth. 2011. “Effect of High-Pressure Microfluidization on the Structure of Cassava Starch Granule.” *Die Starke* 63 (3): 160–70.

Keattch, Cyril Jack, and David Dollimore. 1975. *An Introduction to Thermogravimetry*. Heyden.

Keshavarzi, Zahra, Sahar Barzegari Banadkoki, Mehrdad Faizi, Yalda Zolghadri, and Farshad H. Shirazi. 2020. “Comparison of Transmission FTIR and ATR Spectra for Discrimination between Beef and Chicken Meat and Quantification of Chicken in Beef Meat Mixture Using ATR-FTIR Combined with Chemometrics.” *Journal of Food Science and Technology* 57 (4): 1430–38.

Keyence. 2021. “Contact-Type Surface Roughness/profile Measuring Instruments.” 2021. https://www.keyence.com/ss/products/microscope/roughness/equipment/line_01.jsp.

Khalifeh, Sulaiman. 2020. “1 - INTRODUCTION TO POLYMERS FOR ELECTRONIC ENGINEERS.” In *Polymers in Organic Electronics*, edited by Sulaiman Khalifeh, 1–31. ChemTec Publishing.

Khan, Hayat, Aditya S. Yerramilli, Adrien D’Oliveira, Terry L. Alford, Daria C. Boffito, and Gregory S. Patience. 2020. “Experimental Methods in Chemical Engineering: X‐ray

Diffraction Spectroscopy— XRD." *The Canadian Journal of Chemical Engineering* 98 (6): 1255–66.
Khan, Muhammad Qamar, Davood Kharaghani, Nazish Nishat, Amir Shahzad, Tanveer Hussain, Zeeshan Khatri, Chunhong Zhu, and Ick Soo Kim. 2019. "Preparation and Characterizations of Multifunctional PVA/ZnO Nanofibers Composite Membranes for Surgical Gown Application." *Journal of Materials Research and Technology* 8 (1): 1328–34.
Khorasaninejad, Mohammadreza, Wei Ting Chen, Alexander Y. Zhu, Jaewon Oh, Robert C. Devlin, Charles Roques-Carmes, Ishan Mishra, and Federico Capasso. 2017. "Visible Wavelength Planar Metalenses Based on Titanium Dioxide." *IEEE Journal of Selected Topics in Quantum Electronics* 23 (3): 43–58.
Kim, Insoo, Karthika Viswanathan, Gopinath Kasi, Sarinthip Thanakkasaranee, Kambiz Sadeghi, and Jongchul Seo. 2022. "ZnO Nanostructures in Active Antibacterial Food Packaging: Preparation Methods, Antimicrobial Mechanisms, Safety Issues, Future Prospects, and Challenges." *Food Reviews International* 38 (4): 537–65.
Kim, Minju, Abdul Razzaq, Young Kwang Kim, Soonhyun Kim, and Su-Il In. 2014. "Synthesis and Characterization of Platinum Modified TiO2-Embedded Carbon Nanofibers for Solar Hydrogen Generation." *RSC Advances* 4 (93): 51286–93.
Kim, Ung-Jin, Seok Hyun Eom, and Masahisa Wada. 2010. "Thermal Decomposition of Native Cellulose: Influence on Crystallite Size." *Polymer Degradation and Stability* 95 (5): 778–81.
Kintek. 2024. "How FTIR Pellet Press Works In Sample Preparation For Spectroscopy Analysis." 2024. https://kindle-tech.com/articles/how-ftir-pellet-press-works-in-sample-preparation-for-spectroscopy-analysis.
Kleiner, Florian, Christian Matthes, and Christiane Rößler. 2021. "Argon Broad Ion Beam Sectioning and High Resolution Scanning Electron Microscopy Imaging of Hydrated Alite." *Cement and Concrete Research* 150 (December): 106583.
Klemm, Dieter, Bertram Philipp, Thomas Heinze, Ute Heinze, and W. Wagenknecht. 1998. *Comprehensive Cellulose Chemistry, Comprehensive Cellulose Chemistry: Fundamentals and Analytical Methods*. Wiley.
Kohanski, Michael A., Daniel J. Dwyer, Boris Hayete, Carolyn A. Lawrence, and James J. Collins. 2007. "A Common Mechanism of Cellular Death Induced by Bactericidal Antibiotics." *Cell* 130 (5): 797–810.
Konaté, Kiessoun, Jacques François Mavoungou, Alexis Nicaise Lepengué, Raïssa Rr Aworet-Samseny, Adama Hilou, Alain Souza, Mamoudou H. Dicko, and Bertrand M'batchi. 2012. "Antibacterial Activity against β- Lactamase Producing Methicillin and Ampicillin-Resistants Staphylococcus Aureus: Fractional Inhibitory Concentration Index (FICI) Determination." *Annals of Clinical Microbiology and Antimicrobials* 11 (June): 18.
Koo, J. H., R. Ortiz, B. Ong, and H. Wu. 2017. "8 - Polymer Nanocomposites for Laser Additive Manufacturing." In *Laser Additive Manufacturing*, edited by Milan Brandt, 205–35. Woodhead Publishing.
Koontz, John L. 2016. "Chapter 13 - Packaging Technologies to Control Lipid Oxidation." In *Oxidative Stability and Shelf Life of Foods Containing Oils and Fats*, edited by Min Hu and Charlotte Jacobsen, 479–517. AOCS Press.
Korhonen, Juuso T., Marjo Kettunen, Robin H. A. Ras, and Olli Ikkala. 2011. "Hydrophobic Nanocellulose Aerogels as Floating, Sustainable, Reusable, and Recyclable Oil Absorbents." *ACS Applied Materials & Interfaces* 3 (6): 1813–16.
Kose, Ryota, Ikue Mitani, Wakako Kasai, and Tetsuo Kondo. 2011. "'Nanocellulose' as a Single Nanofiber Prepared from Pellicle Secreted by Gluconacetobacter Xylinus Using Aqueous Counter Collision." *Biomacromolecules* 12 (3): 716–20.
Kourkoumelis, N. 2013. "PowDLL, a Reusable .NET Component for Interconverting Powder Diffraction Data: Recent Developments." *Powder Diffraction* 28: 137–48.

Koutsoumanis, K., A. Allende, A. Alvarez-Ordóñez, S. Bover-Cid, M. Chemaly, R. Davies, A. De Cesare, et al. 2020. “Pathogenicity Assessment of Shiga Toxin-Producing Escherichia Coli (STEC) and the Public Health Risk Posed by Contamination of Food with STEC. Efs2 18: e05967.”

Kulshreshtha, A. K. 1979. “2—A REVIEW OF THE LITERATURE ON THE FORMATION OF CELLULOSE IV, ITS STRUCTURE, AND ITS SIGNIFICANCE IN THE TECHNOLOGY OF RAYON MANUFACTURE.” *Journal of the Textile Institute* 70 (1): 13–18.

Kuraray. 1972. “Oxygen Barrier.” 1972. https://eval.kuraray.com/products-services/about-eval-evoh/properties/barrier-to-oxygen/.

Kusuma, Heri Septya, Puput Yugiani, Ayu Iftah Himana, Amri Aziz, and Deva Afriga Wardana Putra. 2023. “Reflections on Food Security and Smart Packaging.” *Polymer Bulletin* , February, 1–47.

Kuswandi, Bambang, and Jumina. 2020. “12 - Active and Intelligent Packaging, Safety, and Quality Controls.” In *Fresh-Cut Fruits and Vegetables*, edited by Mohammed Wasim Siddiqui, 243–94. Academic Press.

Kwan, Kermit S. 1998. “The Role of Penetrant Structure in the Transport and Mechanical Properties of a Thermoset Adhesive.” Edited by Thomas C. Ward. Ann Arbor, United States: Virginia Polytechnic Institute and State University. http://login.ezproxy.lib.vt.edu/login?url=https://www.proquest.com/dissertations-theses/role-penetrant-structure-transport-mechanical/docview/304460968/se-2.

Labthink. 2018. “Oxygen Transmission Rate (OTR) Tester.”

Laplace, Pierre Simon Marquis de. 1805. *Traité de mécanique céleste /par P.S. Laplace ... ; tome premier [-quatrieme]*. de l’Imprimerie de Crapelet.

Larrea, Giuliana A., Natalia S. Gsponer, Javier E. Durantini, Daniel A. Heredia, and Edgardo N. Durantini. 2024. “Development of New Photoinactivation Strategies for Microbial Decontamination in Fruits and Packaging.” *ACS Food Science & Technology* 4 (1): 207–17.

Larson, Brad, and Peter Banks. 2022. “Z-Stacking of Single Plane Digital Widefield Fluorescent Images.” Agilent Technologies, Inc.

Lee, Chang Yeon, Omar K. Farha, Bong Jin Hong, Amy A. Sarjeant, Sonbinh T. Nguyen, and Joseph T. Hupp. 2011. “Light-Harvesting Metal-Organic Frameworks (MOFs): Efficient Strut-to-Strut Energy Transfer in Bodipy and Porphyrin-Based MOFs.” *Journal of the American Chemical Society* 133 (40): 15858–61.

Lee, Dong Sun. 2016. “Carbon Dioxide Absorbers for Food Packaging Applications.” *Trends in Food Science & Technology* 57 (November): 146–55.

Lee, Hansol, Jaya Sundaram, and Sudhagar Mani. 2017. “Production of Cellulose Nanofibrils and Their Application to Food: A Review.” In *Nanotechnology: Food and Environmental Paradigm*, edited by Ram Prasad, Vivek Kumar, and Manoj Kumar, 1–33. Singapore: Springer Singapore.

Lee, Jae-Chul, Jin-Ah Lee, Dae-Young Lim, and Ki-Young Kim. 2018. “Fabrication of Cellulose Nanofiber Reinforced Thermoplastic Composites.” *Fibers and Polymers* 19 (8): 1753–59.

Lehmann, Daniel, and Dietrich R. T. Zahn. 2009. “The Electrical and Dielectrical Behavior of N-Conducting Perylene Tetracarboxylic Diimide Derivatives.” *Applied Physics A: Materials Science & Processing* 95 (1): 203–7.

Lei, Chao, Junkuo Gao, Wenjing Ren, Yuanbo Xie, Somia Yassin Hussain Abdalkarim, Shunli Wang, Qingqing Ni, and Juming Yao. 2019. “Fabrication of Metal-Organic Frameworks@cellulose Aerogels Composite Materials for Removal of Heavy Metal Ions in Water.” *Carbohydrate Polymers* 205 (February): 35–41.

Leppänen, Ilona, Ari Hokkanen, Monika Österberg, Mika Vähä-Nissi, Ali Harlin, and Hannes Orelma. 2022. “Hybrid Films from Cellulose Nanomaterials—properties and Defined Optical Patterns.” *Cellulose* 29 (16): 8551–67.

Li, Aurelia, Rocio Bueno-Perez, Seth Wiggin, and David Fairen-Jimenez. 2020. “Enabling

Efficient Exploration of Metal–organic Frameworks in the Cambridge Structural Database." *CrystEngComm / RSC* 22 (43): 7152–61.
Lindeburg, Michael R. 2013. *Mechanical Engineering Reference Manual for the PE Exam, 13th Edition*. PPI, A Kaplan Company.
Li, Rui, Tongtong Chen, and Xiangliang Pan. 2021. "Metal–Organic-Framework-Based Materials for Antimicrobial Applications." *ACS Nano* 15 (3): 3808–48.
Liu, Chao, Kunhui Liu, Chiming Wang, Heyuan Liu, Hailong Wang, Hongmei Su, Xiyou Li, Banglin Chen, and Jianzhuang Jiang. 2020. "Elucidating Heterogeneous Photocatalytic Superiority of Microporous Porphyrin Organic Cage." *Nature Communications* 11 (1): 1047.
Liu, Dagang, Jinlei Li, Fengxiang Sun, Ruimin Xiao, Yi Guo, and Jianwei Song. 2014. "Liquid Crystal Microphase Separation of Cellulose Nanocrystals in Wet-Spun PVA Composite Fibers." *RSC Advances* 4 (58): 30784–89.
Liu, Guo-Qing, Xiang-Jun Pan, Jing Li, Cheng Li, and Chen-Lu Ji. 2021. "Facile Preparation and Characterization of Anatase TiO2/nanocellulose Composite for Photocatalytic Degradation of Methyl Orange." *Journal of Saudi Chemical Society* 25 (12): 101383.
Liu, Jiewei, Yan-Zhong Fan, Xin Li, Zhangwen Wei, Yao-Wei Xu, Li Zhang, and Cheng-Yong Su. 2018. "A Porous rhodium(III)-Porphyrin Metal-Organic Framework as an Efficient and Selective Photocatalyst for CO2 Reduction." *Applied Catalysis. B, Environmental* 231 (September): 173–81.
Liu, Jin-Xiu, Mei-Yan Gao, Wei-Hui Fang, Lei Zhang, and Jian Zhang. 2016. "Bandgap Engineering of Titanium-Oxo Clusters: Labile Surface Sites Used for Ligand Substitution and Metal Incorporation." *Angewandte Chemie* 55 (17): 5160–65.
Liu, Xiao-Min, Lin-Hua Xie, and Yufeng Wu. 2020. "Recent Advances in the Shaping of Metal–organic Frameworks." *Inorganic Chemistry Frontiers* 7 (15): 2840–66.
Liu, Xiaowen, Hongnan Sun, Taihua Mu, Marie Laure Fauconnier, and Mei Li. 2023. "Preparation of Cellulose Nanofibers from Potato Residues by Ultrasonication Combined with High-Pressure Homogenization." *Food Chemistry* 413 (July): 135675.
Liu, Xiongli, Yun Xiao, Zhiyuan Zhang, Zifeng You, Jinli Li, Dingxuan Ma, and Baiyan Li. 2021. "Recent Progress in Metal‐organic Frameworks@cellulose Hybrids and Their Applications." *Chinese Journal of Chemistry* 39 (12): 3462–80.
Liu, Yue, Hongqiao Fu, Wei Zhang, and Haichao Liu. 2022. "Effect of Crystalline Structure on the Catalytic Hydrolysis of Cellulose in Subcritical Water." *ACS Sustainable Chemistry & Engineering* 10 (18): 5859–66.
Li, Vincent C. F., Arie Mulyadi, Conner K. Dunn, Yulin Deng, and H. Jerry Qi. 2018. "Direct Ink Write 3D Printed Cellulose Nanofiber Aerogel Structures with Highly Deformable, Shape Recoverable, and Functionalizable Properties." *ACS Sustainable Chemistry & Engineering* 6 (2): 2011–22.
Li, Xinran, Xinchun Yang, Huaiguo Xue, Huan Pang, and Qiang Xu. 2020. "Metal–organic Frameworks as a Platform for Clean Energy Applications." *EnergyChem* 2 (2): 100027.
Li, X. W., R. G. Song, Y. Jiang, C. Wang, and D. Jiang. 2013. "Surface Modification of TiO2 Nanoparticles and Its Effect on the Properties of fluoropolymer/TiO2 Nanocomposite Coatings." *Applied Surface Science* 276 (July): 761–68.
Lizundia, Erlantz, Debora Puglia, Thanh-Dinh Nguyen, and Ilaria Armentano. 2020. "Cellulose Nanocrystal Based Multifunctional Nanohybrids." *Progress in Materials Science* 112 (July): 100668.
Lizundia, E., A. Urruchi, J. L. Vilas, and L. M. León. 2016. "Increased Functional Properties and Thermal Stability of Flexible Cellulose nanocrystal/ZnO Films." *Carbohydrate Polymers* 136 (January): 250–58.
Longevial, Jean-François, Sébastien Clément, Jennifer A. Wytko, Romain Ruppert, Jean Weiss, and Sébastien Richeter. 2018. "Peripherally Metalated Porphyrins with Applications in Catalysis, Molecular Electronics and Biomedicine." *Chemistry* 24 (58): 15442–60.

Lou, Ding, Travis Grablander, Mingyang Mao, Haiping Hong, and G. P. Peterson. 2021. "Improved Thermal Conductivity of PEG-Based Fluids Using Hydrogen Bonding and Long Chain of Nanoparticle." *Journal of Nanoparticle Research: An Interdisciplinary Forum for Nanoscale Science and Technology* 23 (4): 98.

Lu, Kuangda, Chunbai He, and Wenbin Lin. 2014. "Nanoscale Metal–Organic Framework for Highly Effective Photodynamic Therapy of Resistant Head and Neck Cancer." *Journal of the American Chemical Society* 136 (48): 16712–15.

Lu, Lu, Cuicui Hu, Yanjie Zhu, Huanhuan Zhang, Rong Li, and Yanjun Xing. 2018. "Multi-Functional Finishing of Cotton Fabrics by Water-Based Layer-by-Layer Assembly of Metal–organic Framework." *Cellulose* 25 (7): 4223–38.

Macdonald, Thomas J., Ke Wu, Sandeep K. Sehmi, Sacha Noimark, William J. Peveler, Hendrik du Toit, Nicolas H. Voelcker, et al. 2016. "Thiol-Capped Gold Nanoparticles Swell-Encapsulated into Polyurethane as Powerful Antibacterial Surfaces Under Dark and Light Conditions." *Scientific Reports* 6 (1): 1–11.

Macpherson, Julie V. 2015. "A Practical Guide to Using Boron Doped Diamond in Electrochemical Research." *Physical Chemistry Chemical Physics: PCCP* 17 (5): 2935–49.

Magoulas, Argyris. 2016. "Protecting Your Family from Food Spoilage." 2016.

Majowicz, Shannon E., Elaine Scallan, Andria Jones-Bitton, Jan M. Sargeant, Jackie Stapleton, Frederick J. Angulo, Derrick H. Yeung, and Martyn D. Kirk. 2014. "Global Incidence of Human Shiga Toxin–Producing Escherichia Coli Infections and Deaths: A Systematic Review and Knowledge Synthesis." *Foodborne Pathogens and Disease* 11 (6): 447–55.

Malakhov, Ya S., and G. V. Samsonov. 1966. "Regularities Governing the Thermal Stability of Oxides of the Transition Metals." *Soviet Powder Metallurgy and Metal Ceramics* 5 (12): 981–86.

Maldonado-Carmona, Nidia, Guillaume Marchand, Nicolas Villandier, Tan-Sothea Ouk, Mariette M. Pereira, Mário J. F. Calvete, Claude Alain Calliste, et al. 2020. "Porphyrin-Loaded Lignin Nanoparticles Against Bacteria: A Photodynamic Antimicrobial Chemotherapy Application." *Frontiers in Microbiology* 11 (November): 606185.

Malucelli, L. C., M. Matos, C. Jordão, L. G. Lacerda, M. A. S. Carvalho Filho, and W. L. E. Magalhães. 2018. "Grinding Severity Influences the Viscosity of Cellulose Nanofiber (CNF) Suspensions and Mechanical Properties of Nanopaper." *Cellulose* 25 (11): 6581–89.

Manahan, Stanley E. 2011. *Green Chemistry and the Ten Commandments of Sustainability*. ChemChar Research.

Manimaran, P., S. P. Saravanan, M. R. Sanjay, Suchart Siengchin, Mohammad Jawaid, and Anish Khan. 2019. "Characterization of New Cellulosic Fiber: Dracaena Reflexa as a Reinforcement for Polymer Composite Structures." *Journal of Materials Research and Technology* 8 (2): 1952–63.

Mao, Congyang, Yiming Xiang, Xiangmei Liu, Yufeng Zheng, Kelvin Wai Kwok Yeung, Zhenduo Cui, Xianjin Yang, et al. 2019. "Local Photothermal/Photodynamic Synergistic Therapy by Disrupting Bacterial Membrane To Accelerate Reactive Oxygen Species Permeation and Protein Leakage." *ACS Applied Materials & Interfaces* 11 (19): 17902–14.

Maryani, E., N. S. Nurjanah, E. P. Hadisantoso, and R. B. Wijayanti. 2020. "The Effect of TiO2 Additives on the Antibacterial Properties (Escherichia Coli and Staphylococcus Aureus) of Glaze on Ceramic Tiles." *IOP Conference Series: Materials Science and Engineering* 980 (1): 012011.

Maślana, Klaudia, Anna Żywicka, Karolina Wenelska, and Ewa Mijowska. 2021. "Boosting of Antibacterial Performance of Cellulose Based Paper Sheet via TiO2 Nanoparticles." *International Journal of Molecular Sciences* 22 (3). https://doi.org/10.3390/ijms22031451.

Maxfield, F. R. 1994. "Introduction: Optical Microscopy in Physiological Investigations." *FASEB Journal: Official Publication of the Federation of American Societies for Experimental Biology* 8 (9): 571–72.

Ma, Zhenye, Fengsheng Li, and Huaping Bai. 2006. “Effect of Fe_2O_3 in Fe_2O_3/AP Composite Particles on Thermal Decomposition of AP and on Burning Rate of the Composite Propellant.” *Propellants, Explosives, Pyrotechnics* 31 (6): 447–51.
McGaughey, Allyson L., Prathamesh Karandikar, Malancha Gupta, and Amy E. Childress. 2020. “Hydrophobicity versus Pore Size: Polymer Coatings to Improve Membrane Wetting Resistance for Membrane Distillation.” *ACS Applied Polymer Materials* 2 (3): 1256–67.
Md Salim, Rafidah, Jahimin Asik, and Mohd Sani Sarjadi. 2021. “Chemical Functional Groups of Extractives, Cellulose and Lignin Extracted from Native Leucaena Leucocephala Bark.” *Wood Science and Technology* 55 (2): 295–313.
Meng, Jiashen, Xiong Liu, Chaojiang Niu, Quan Pang, Jiantao Li, Fang Liu, Ziang Liu, and Liqiang Mai. 2020. “Advances in Metal–organic Framework Coatings: Versatile Synthesis and Broad Applications.” *Chemical Society Reviews* 49 (10): 3142–86.
Meng, Shuang, Ying Ma, Da-Wen Sun, Lifeng Wang, and Tianyi Liu. 2014. “Properties of Starch-Palmitic Acid Complexes Prepared by High Pressure Homogenization.” *Journal of Cereal Science* 59 (1): 25–32.
Michiels, Youri, Peter Van Puyvelde, and Bert Sels. 2017. “Barriers and Chemistry in a Bottle: Mechanisms in Today’s Oxygen Barriers for Tomorrow’s Materials.” *NATO Advanced Science Institutes Series E: Applied Sciences* 7 (7): 665.
Miettinen, Arttu, Gary Chinga-Carrasco, and Markku Kataja. 2014. “Three-Dimensional Microstructural Properties of Nanofibrillated Cellulose Films.” *International Journal of Molecular Sciences* 15 (4): 6423–40.
Mike. 2022. “Sa Does Not Equal Ra!” Michigan Metrology. Michigan Metrology, LLC. October 18, 2022. https://michmet.com/sa-does-not-equal-ra/.
Miller, K. S., and J. M. Krochta. 1997. “Oxygen and Aroma Barrier Properties of Edible Films: A Review.” *Trends in Food Science & Technology* 8 (7): 228–37.
Min, Tiantian, Xiaoli Sun, Liping Zhou, Haiyu Du, Zhu Zhu, and Yongqiang Wen. 2021. “Electrospun pullulan/PVA Nanofibers Integrated with Thymol-Loaded Porphyrin Metal−organic Framework for Antibacterial Food Packaging.” *Carbohydrate Polymers* 270 (October): 118391.
Mirabal, Alex, Ilker Loza-Hernandez, Courtney Clark, Daniel E. Hooks, Michael McBride, and Jamie A. Stull. 2023. “Roughness Measurements across Topographically Varied Additively Manufactured Metal Surfaces.” *Additive Manufacturing* 69 (May): 103540.
Misko, George G. 2022. “The Regulation of Active and Intelligent Food Packaging in the U.S. and the EU.” *Food Safety Magazine*, 2022.
Missoum, Karim, Florian Martoïa, Mohamed Naceur Belgacem, and Julien Bras. 2013. “Effect of Chemically Modified Nanofibrillated Cellulose Addition on the Properties of Fiber-Based Materials.” *Industrial Crops and Products* 48 (July): 98–105.
Mohamed, Mohamad Azuwa, W. N. W. Salleh, Juhana Jaafar, A. F. Ismail, Muhazri Abd Mutalib, and Siti Munira Jamil. 2015. “Incorporation of N-Doped TiO2 Nanorods in Regenerated Cellulose Thin Films Fabricated from Recycled Newspaper as a Green Portable Photocatalyst.” *Carbohydrate Polymers* 133 (November): 429–37.
Mohan, Saeed, Robert H. Olley, Alun S. Vaughan, and Geoffrey R. Mitchell. 2016. “Evaluating Scales of Structures.” In *Controlling the Morphology of Polymers: Multiple Scales of Structure and Processing*, edited by Geoffrey R. Mitchell and Ana Tojeira, 29–67. Cham: Springer International Publishing.
Mokhena, Teboho Clement, Emmanuel Rotimi Sadiku, Mokgaotsa Jonas Mochane, Suprakas Sinha Ray, Maya Jacob John, and Asanda Mtibe. 2021. “Mechanical Properties of Cellulose Nanofibril Papers and Their Bionanocomposites: A Review.” *Carbohydrate Polymers* 273 (December): 118507.
Monção, Érica da Costa, Cristiani Viegas Brandão Grisi, Janaína de Moura Fernandes, Priscila Santos Souza, and Antônia Lucia de Souza. 2022. “Active Packaging for Lipid Foods and

Development Challenges for Marketing." *Food Bioscience* 45 (February): 101370.
Morán, Juan I., Vera A. Alvarez, Viviana P. Cyras, and Analia Vázquez. 2008. "Extraction of Cellulose and Preparation of Nanocellulose from Sisal Fibers." *Cellulose* 15 (1): 149–59.
Munekata, Paulo E. S., Mirian Pateiro, David Rodríguez-Lázaro, Rubén Domínguez, Jian Zhong, and Jose M. Lorenzo. 2020. "The Role of Essential Oils against Pathogenic Escherichia Coli in Food Products." *Microorganisms* 8 (6). https://doi.org/10.3390/microorganisms8060924.
Murray, Patrick R., Ken S. Rosenthal, and Michael A. Pfaller. 2009. *Medical Microbiology*. Philadelphia: Mosby/Elsevier.
Naderi, Ali, Tom Lindström, and Jonas Sundström. 2015. "Repeated Homogenization, a Route for Decreasing the Energy Consumption in the Manufacturing Process of Carboxymethylated Nanofibrillated Cellulose?" *Cellulose* 22 (2): 1147–57.
Nagarajan, K. J., N. R. Ramanujam, M. R. Sanjay, Suchart Siengchin, B. Surya Rajan, K. Sathick Basha, P. Madhu, and G. R. Raghav. 2021. "A Comprehensive Review on Cellulose Nanocrystals and Cellulose Nanofibers: Pretreatment, Preparation, and Characterization." *Polymer Composites* 42 (4): 1588–1630.
Nakagaito, A. N., and H. Yano. 2004. "The Effect of Morphological Changes from Pulp Fiber towards Nano-Scale Fibrillated Cellulose on the Mechanical Properties of High-Strength Plant Fiber Based Composites." *Applied Physics A: Materials Science & Processing* 78 (4): 547–52.
Nasir, Mohammed, Rokiah Hashim, Othman Sulaiman, and Mohd Asim. 2017. "11 - Nanocellulose: Preparation Methods and Applications." In *Cellulose-Reinforced Nanofibre Composites*, edited by Mohammad Jawaid, Sami Boufi, and Abdul Khalil H. P. S., 261–76. Woodhead Publishing.
Nechyporchuk, Oleksandr, Mohamed Naceur Belgacem, and Julien Bras. 2016. "Production of Cellulose Nanofibrils: A Review of Recent Advances." *Industrial Crops and Products* 93 (December): 2–25.
Neppolian, B., S. Sakthivel, Banumathi Arabindoo, M. Palanichamy, and V. Murugesan. 1999. "Degradation of Textile Dye by Solar Light Using TiO2and ZnO Photocatalysts." *Journal of Environmental Science and Health. Part A, Toxic/hazardous Substances & Environmental Engineering* 34 (9): 1829–38.
Neto, Jorge S. S., Henrique F. M. de Queiroz, Ricardo A. A. Aguiar, and Mariana D. Banea. 2021. "A Review on the Thermal Characterisation of Natural and Hybrid Fiber Composites." *Polymers* 13 (24). https://doi.org/10.3390/polym13244425.
Nie, Xiaolin, Shuanglin Wu, Alfred Mensah, Qingqing Wang, Fenglin Huang, Dawei Li, and Qufu Wei. 2020. "Insight into Light-Driven Antibacterial Cotton Fabrics Decorated by in Situ Growth Strategy." *Journal of Colloid and Interface Science* 579 (November): 233–42.
Nishiyama, Yoshiharu, Paul Langan, and Henri Chanzy. 2002. "Crystal Structure and Hydrogen-Bonding System in Cellulose Iβ from Synchrotron X-Ray and Neutron Fiber Diffraction." *Journal of the American Chemical Society* 124 (31): 9074–82.
Nishiyama, Yoshiharu, Junji Sugiyama, Henri Chanzy, and Paul Langan. 2003. "Crystal Structure and Hydrogen Bonding System in Cellulose Iα from Synchrotron X-Ray and Neutron Fiber Diffraction." *Journal of the American Chemical Society* 125 (47): 14300–306.
Nisizawa, K. 1973. "Mode of Action of Cellulases." *Journal of Fermentation and Bioengineering*.
Niu, Xun, Siqi Huan, Haiming Li, Hui Pan, and Orlando J. Rojas. 2021. "Transparent Films by Ionic Liquid Welding of Cellulose Nanofibers and Polylactide: Enhanced Biodegradability in Marine Environments." *Journal of Hazardous Materials* 402 (January): 124073.
Noimark, Sacha, Elaine Allan, and Ivan P. Parkin. 2014. "Light-Activated Antimicrobial Surfaces with Enhanced Efficacy Induced by a Dark-Activated Mechanism." *Chemical Science* 5 (6): 2216–23.
Noimark, Sacha, Melissa Bovis, Alexander J. MacRobert, Annapaula Correia, Elaine Allan,

Michael Wilson, and Ivan P. Parkin. 2013. “Photobactericidal Polymers; the Incorporation of Crystal Violet and Nanogold into Medical Grade Silicone.” *RSC Advances* 3 (40): 18383–94.
Noorian, Seyyed Abbas, Nahid Hemmatinejad, and Jorge A. R. Navarro. 2019. “BioMOF@cellulose Fabric Composites for Bioactive Molecule Delivery.” *Journal of Inorganic Biochemistry* 201 (December): 110818.
NRDC. 2020. “Composting 101.” 2020. https://www.nrdc.org/stories/composting-101#whatis.
Nunes, R. C. R. 2017. “13 - Rubber Nanocomposites with Nanocellulose.” In *Progress in Rubber Nanocomposites*, edited by Sabu Thomas and Hanna J. Maria, 463–94. Woodhead Publishing.
Nurhadi, Bambang, Angeline Angeline, Nandi Sukri, Nanang Masruchin, Heni Radiani Arifin, and Rudy Adi Saputra. 2022. “Characteristics of Microcrystalline Cellulose from Nata de Coco: Hydrochloric Acid versus Maleic Acid Hydrolysis.” *Journal of Applied Polymer Science* 139 (5): 51576.
Nyquist, Richard A., and Ronald O. Kagel. 2012. *Handbook of Infrared and Raman Spectra of Inorganic Compounds and Organic Salts: Infrared Spectra of Inorganic Compounds*. Academic Press.
Obrig, Tom G. 2010. “Escherichia Coli Shiga Toxin Mechanisms of Action in Renal Disease.” *Toxins* 2 (12): 2769–94.
Ogawa, Yu, Yoshiharu Nishiyama, and Karim Mazeau. 2020. “Drying-Induced Bending Deformation of Cellulose Nanocrystals Studied by Molecular Dynamics Simulations.” *Cellulose* 27 (17): 9779–86.
Oh, Jee Eun, and Nae-Man Park. 2022. “Hydrophilic, Transparent, and Stretchable Film Using Unmodified Cellulose Fibers.” *Materials Letters* 309 (February): 131385.
Ojeda, Jesús J., and Maria Dittrich. 2012. “Fourier Transform Infrared Spectroscopy for Molecular Analysis of Microbial Cells.” In *Microbial Systems Biology: Methods and Protocols*, edited by Ali Navid, 187–211. Totowa, NJ: Humana Press.
Olsvik, O., Y. Wasteson, A. Lund, and E. Hornes. 1991. “Pathogenic Escherichia Coli Found in Food.” *International Journal of Food Microbiology* 12 (1): 103–13.
Oms-Oliu, G., R. Soliva-Fortuny, and O. Martín-Belloso. 2008. “Edible Coatings with Antibrowning Agents to Maintain Sensory Quality and Antioxidant Properties of Fresh-Cut Pears.” *Postharvest Biology and Technology* 50 (1): 87–94.
Onyszko, M., A. Markowska-Szczupak, R. Rakoczy, O. Paszkiewicz, J. Janusz, A. Gorgon-Kuza, K. Wenelska, and E. Mijowska. 2022. “The Cellulose Fibers Functionalized with Star-like Zinc Oxide Nanoparticles with Boosted Antibacterial Performance for Hygienic Products.” *Scientific Reports* 12 (1): 1–13.
Owen, T. 1996. *Fundamentals of UV-Visible Spectroscopy: A Workbook. 1st Edition*. Berlin: Hewlett Packard.
Ozer, R. R., and J. P. Hinestroza. 2015. “One-Step Growth of Isoreticular Luminescent Metal–organic Frameworks on Cotton Fibers.” *RSC Advances* 5 (20): 15198–204.
Paixão, Louryval Coelho, Ilmar Alves Lopes, Allan Kardec Duailibe Barros Filho, and Audirene Amorim Santana. 2019. “Alginate Biofilms Plasticized with Hydrophilic and Hydrophobic Plasticizers for Application in Food Packaging.” *Journal of Applied Polymer Science* 136 (48): 48263.
Pan, Cheng, Feifan Wu, Guozhi Fan, Yifei Long, Haitao Yang, Guangying Yang, and Xiaofei Li. 2023. “A Multifunctional Flexible Composite Film with Excellent Insulation Flame Retardancy, Thermal Management and Solar-Thermal Conversion Properties Based on CNF-Modified Mica/electrospun Fibrous Networks Structure.” *Solar Energy Materials & Solar Cells* 261 (October): 112530.
Parit, Mahesh, Partha Saha, Virginia A. Davis, and Zhihua Jiang. 2018. “Transparent and Homogenous Cellulose Nanocrystal/Lignin UV-Protection Films.” *ACS Omega* 3 (9): 10679–91.

Park, Jihye, Qin Jiang, Dawei Feng, Lanqun Mao, and Hong-Cai Zhou. 2016. “Size-Controlled Synthesis of Porphyrinic Metal–Organic Framework and Functionalization for Targeted Photodynamic Therapy.” *Journal of the American Chemical Society* 138 (10): 3518–25.

Park, Sunkyu, John O. Baker, Michael E. Himmel, Philip A. Parilla, and David K. Johnson. 2010. “Cellulose Crystallinity Index: Measurement Techniques and Their Impact on Interpreting Cellulase Performance.” *Biotechnology for Biofuels* 3 (May): 10.

Patiño Vidal, Cristian, Carol López de Dicastillo, Francisco Rodríguez-Mercado, Abel Guarda, María José Galotto, and Cristina Muñoz-Shugulí. 2022. “Electrospinning and Cyclodextrin Inclusion Complexes: An Emerging Technological Combination for Developing Novel Active Food Packaging Materials.” *Critical Reviews in Food Science and Nutrition* 62 (20): 5495–5510.

Pavlík, Z., M. Pavlíková, and M. Záleská. 2019. “9 - Properties of Concrete with Plastic Polypropylene Aggregates.” In *Use of Recycled Plastics in Eco-Efficient Concrete*, edited by Fernando Pacheco-Torgal, Jamal Khatib, Francesco Colangelo, and Rabin Tuladhar, 189–213. Woodhead Publishing.

Peak, D. 2005. “FOURIER TRANSFORM INFRARED SPECTROSCOPY.” In *Encyclopedia of Soils in the Environment*, edited by Daniel Hillel, 80–85. Oxford: Elsevier.

Pednekar, Priti P., Shilpa C. Godiyal, Kisan R. Jadhav, and Vilasrao J. Kadam. 2017. “Chapter 23 - Mesoporous Silica Nanoparticles: A Promising Multifunctional Drug Delivery System.” In *Nanostructures for Cancer Therapy*, edited by Anton Ficai and Alexandru Mihai Grumezescu, 593–621. Elsevier.

Pelissari, Franciele Maria, Margarita María Andrade-Mahecha, Paulo José do Amaral Sobral, and Florencia Cecilia Menegalli. 2017. “Nanocomposites Based on Banana Starch Reinforced with Cellulose Nanofibers Isolated from Banana Peels.” *Journal of Colloid and Interface Science* 505 (November): 154–67.

Pelleg, Joshua. 2012. *Mechanical Properties of Materials*. Springer Netherlands.

Peresin, Maria Soledad, Kari Kammiovirta, Harri Heikkinen, Leena-Sisko Johansson, Jari Vartiainen, Harri Setälä, Monika Österberg, and Tekla Tammelin. 2017. “Understanding the Mechanisms of Oxygen Diffusion through Surface Functionalized Nanocellulose Films.” *Carbohydrate Polymers* 174 (October): 309–17.

Pérez, Serge, and Daniel Samain. 2010. “Structure and Engineering of Celluloses.” *Advances in Carbohydrate Chemistry and Biochemistry* 64: 25–116.

Pinto, Deesy, Luís Bernardo, Ana Amaro, and Sérgio Lopes. 2015. “Mechanical Properties of Epoxy Nanocomposites Using Titanium Dioxide as Reinforcement – A Review.” *Construction and Building Materials* 95 (October): 506–24.

Pinto, V. C., Tiago Ramos, Sofia Alves, J. Xavier, Paulo Tavares, P. M. G. P. Moreira, and Rui Miranda Guedes. 2015. “Comparative Failure Analysis of PLA, PLA/GNP and PLA/CNT-COOH Biodegradable Nanocomposites Thin Films.” *Procedia Engineering* 114 (January): 635–42.

Popelka, Anton, Sifani Zavahir, and Salma Habib. 2020. “Chapter 2 - Morphology Analysis.” In *Polymer Science and Innovative Applications*, edited by Mariam Al Ali AlMaadeed, Deepalekshmi Ponnamma, and Marcelo A. Carignano, 21–68. Elsevier.

Qamar, M., and M. Muneer. 2009. “A Comparative Photocatalytic Activity of Titanium Dioxide and Zinc Oxide by Investigating the Degradation of Vanillin.” *Desalination* 249 (2): 535–40.

Qian, Liwei, Dan Lei, Xiao Duan, Sufeng Zhang, Wenqi Song, Chen Hou, and Ruihua Tang. 2018. “Design and Preparation of Metal-Organic Framework Papers with Enhanced Mechanical Properties and Good Antibacterial Capacity.” *Carbohydrate Polymers* 192 (July): 44–51.

Quiévy, N., N. Jacquet, M. Sclavons, C. Deroanne, M. Paquot, and J. Devaux. 2010. “Influence of Homogenization and Drying on the Thermal Stability of Microfibrillated Cellulose.” *Polymer Degradation and Stability* 95 (3): 306–14.

Rahbar Shamskar, Kobra, Hannaneh Heidari, and Alimorad Rashidi. 2019. “Study on Nanocellulose Properties Processed Using Different Methods and Their Aerogels.” *Journal of Polymers and the Environment* 27 (7): 1418–28.
Rajakumar, G., A. Abdul Rahuman, S. Mohana Roopan, V. Gopiesh Khanna, G. Elango, C. Kamaraj, A. Abduz Zahir, and K. Velayutham. 2012. “Fungus-Mediated Biosynthesis and Characterization of TiO2 Nanoparticles and Their Activity against Pathogenic Bacteria.” *Spectrochimica Acta. Part A, Molecular and Biomolecular Spectroscopy* 91 (June): 23–29.
Rathod, Manali, Pareshkumar G. Moradeeya, Soumya Haldar, and Shaik Basha. 2018. “Nanocellulose/TiO2 Composites: Preparation, Characterization and Application in the Photocatalytic Degradation of a Potential Endocrine Disruptor, Mefenamic Acid, in Aqueous Media.” *Photochemical & Photobiological Sciences: Official Journal of the European Photochemistry Association and the European Society for Photobiology* 17 (10): 1301–9.
Ray, Sidney. 2002. *Applied Photographic Optics*. Routledge.
Reagen, Sarah, Yingfen Wu, Rahul Shahni, Wen Sun, Jin Zhang, Qianli R. Chu, Xiaodong Hou, Colin Combs, and Julia Xiaojun Zhao. 2022. “Development of Red-Emissive Porphyrin Graphene Quantum Dots (PGQDs) for Biological Cell-Labeling Applications.” *ACS Omega* 7 (43): 38902–11.
Redlinger-Pohn, Jakob D., Christophe Brouzet, Christian Aulin, Åsa Engström, Anastasia V. Riazanova, Claes Holmqvist, Fredrik Lundell, and L. Daniel Söderberg. 2022. “Mechanisms of Cellulose Fiber Comminution to Nanocellulose by Hyper Inertia Flows.” *ACS Sustainable Chemistry & Engineering* 10 (2): 703–19.
Redlinger-Pohn, Jakob D., Martin Petkovšek, Korneliya Gordeyeva, Mojca Zupanc, Alisa Gordeeva, Qilun Zhang, Matevž Dular, and L. Daniel Söderberg. 2022. “Cavitation Fibrillation of Cellulose Fiber.” *Biomacromolecules* 23 (3): 847–62.
ReFED. 2018. “2018 Retail Food Waste Action Guide.” 2018. https://refed.org/downloads/retail-food-waste-action-guide/.
Rehman, Abdur, Seid Mahdi Jafari, Rana Muhammad Aadil, Elham Assadpour, Muhammad Atif Randhawa, and Shahid Mahmood. 2020. “Development of Active Food Packaging via Incorporation of Biopolymeric Nanocarriers Containing Essential Oils.” *Trends in Food Science & Technology* 101 (July): 106–21.
Reimer, Bennett. 2006. “Introduction.” *Arts Education Policy Review* 107 (3): 3–4.
Reimer, Ludwig. 2000. “Scanning Electron Microscopy: Physics of Image Formation and Microanalysis.” *Measurement Science and Technology* 11 (12): 1826–1826.
Reusch, W. 1999. *Virtual Textbook of Organic Chemistry*. Michigan State University.
Rezaeifard, Abdolreza, and Maasoumeh Jafarpour. 2014. “The Catalytic Efficiency of Fe-Porphyrins Supported on Multi-Walled Carbon Nanotubes in the Heterogeneous Oxidation of Hydrocarbons and Sulfides in Water.” *Catalysis Science & Technology* 4 (7): 1960–69.
Río, O. I., and A. W. Neumann. 1997. “Axisymmetric Drop Shape Analysis: Computational Methods for the Measurement of Interfacial Properties from the Shape and Dimensions of Pendant and Sessile Drops.” *Journal of Colloid and Interface Science* 196 (2): 136–47.
Ritchie, Hannah, Lucas Rodés-Guirao, Edouard Mathieu, Marcel Gerber, Esteban Ortiz-Ospina, Joe Hasell, and Max Roser. 2023. “Population Growth.” 2023. https://ourworldindata.org/population-growth.
Robertson, Gordon L. 2012. *Food Packaging: Principles and Practice, Third Edition*. CRC Press.
Rocha, Fellipy S., Anderson J. Gomes, Claure N. Lunardi, Serge Kaliaguine, and Gregory S. Patience. 2018. “Experimental Methods in Chemical Engineering: Ultraviolet Visible Spectroscopy-UV-Vis.” *The Canadian Journal of Chemical Engineering* 96 (12): 2512–17.
Rodríguez, Haendel S., Juan P. Hinestroza, Cristian Ochoa-Puentes, Cesar A. Sierra, and Carlos Y. Soto. 2014. “Antibacterial Activity against *Escherichia Coli* of Cu‐BTC (MOF‐199) Metal‐organic Framework Immobilized onto Cellulosic Fibers.” *Journal of Applied Polymer*

Science 131 (19). https://doi.org/10.1002/app.40815.
Roilo, David, Cecilia Ada Maestri, Marina Scarpa, Paolo Bettotti, and Riccardo Checchetto. 2018. “Gas Barrier and Optical Properties of Cellulose Nanofiber Coatings with Dispersed TiO2 Nanoparticles.” *Surface and Coatings Technology* 343 (June): 131–37.
Rojas-Graü, M. A., M. S. Tapia, F. J. Rodríguez, A. J. Carmona, and O. Martin-Belloso. 2007. “Alginate and Gellan-Based Edible Coatings as Carriers of Antibrowning Agents Applied on Fresh-Cut Fuji Apples.” *Food Hydrocolloids* 21 (1): 118–27.
Roodbar Shojaei, Taha, Abdollah Hajalilou, Meisam Tabatabaei, Hossein Mobli, and Mortaza Aghbashlo. 2019. “Characterization and Evaluation of Nanofiber Materials.” In *Handbook of Nanofibers*, edited by Ahmed Barhoum, Mikhael Bechelany, and Abdel Salam Hamdy Makhlouf, 491–522. Cham: Springer International Publishing.
Rowell, Roger M., and Susan L. LeVan-Green. 2005. “Chapter 6: Thermal Properties.” In *Handbook of Wood Chemistry and Wood Composites*, edited by Roger M. Rowell, 121–38. CRC Press: CRC Press.
Rubin, Heather N., Bella H. Neufeld, and Melissa M. Reynolds. 2018. “Surface-Anchored Metal-Organic Framework-Cotton Material for Tunable Antibacterial Copper Delivery.” *ACS Applied Materials & Interfaces* 10 (17): 15189–99.
Russo, G. M., G. P. Simon, and L. Incarnato. 2006. “Correlation between Rheological, Mechanical, and Barrier Properties in New Copolyamide-Based Nanocomposite Films.” *Macromolecules* 39 (11): 3855–64.
Saba, N., Ahmad Safwan, M. L. Sanyang, F. Mohammad, M. Pervaiz, M. Jawaid, O. Y. Alothman, and M. Sain. 2017. “Thermal and Dynamic Mechanical Properties of Cellulose Nanofibers Reinforced Epoxy Composites.” *International Journal of Biological Macromolecules* 102 (September): 822–28.
Sadeghifar, Hasan, Richard Venditti, Jesse Jur, Russell E. Gorga, and Joel J. Pawlak. 2017. “Cellulose-Lignin Biodegradable and Flexible UV Protection Film.” *ACS Sustainable Chemistry & Engineering* 5 (1): 625–31.
Saïd Azizi Samir, My Ahmed, Fannie Alloin, Michel Paillet, and Alain Dufresne. 2004. “Tangling Effect in Fibrillated Cellulose Reinforced Nanocomposites.” *Macromolecules* 37 (11): 4313–16.
Sand, Claire Koelsch. 2020. “Active and Intelligent Packaging = Longer Shelf Life.” *Food Technology Magazine*, 2020.
Santiago Portillo, Andrea, Herme G. Baldoví, Maria Teresa García Fernandez, Sergio Navalón, Pedro Atienzar, Belen Ferrer, Mercedes Alvaro, Hermenegildo Garcia, and Zhaohui Li. 2017. “Ti as Mediator in the Photoinduced Electron Transfer of Mixed-Metal NH2–UiO-66(Zr/Ti): Transient Absorption Spectroscopy Study and Application in Photovoltaic Cell.” *Journal of Physical Chemistry C* 121 (12): 7015–24.
Sanyang, M. L., S. M. Sapuan, M. Jawaid, M. R. Ishak, and J. Sahari. 2016. “Development and Characterization of Sugar Palm Starch and Poly(lactic Acid) Bilayer Films.” *Carbohydrate Polymers* 146 (August): 36–45.
Sauer, Dominik Georg, Michael Melcher, Magdalena Mosor, Nicole Walch, Matthias Berkemeyer, Theresa Scharl-Hirsch, Friedrich Leisch, Alois Jungbauer, and Astrid Dürauer. 2019. “Real-Time Monitoring and Model-Based Prediction of Purity and Quantity during a Chromatographic Capture of Fibroblast Growth Factor 2.” *Biotechnology and Bioengineering* 116 (8): 1999–2009.
Schneider, Jenny, Masaya Matsuoka, Masato Takeuchi, Jinlong Zhang, Yu Horiuchi, Masakazu Anpo, and Detlef W. Bahnemann. 2014. “Understanding TiO2 Photocatalysis: Mechanisms and Materials.” *Chemical Reviews* 114 (19): 9919–86.
Sears, Margaret E. 2013. “Chelation: Harnessing and Enhancing Heavy Metal Detoxification--a Review.” *TheScientificWorldJournal* 2013 (April): 219840.
Segal, L., J. J. Creely, A. E. Martin, and C. M. Conrad. 1959. “An Empirical Method for

Estimating the Degree of Crystallinity of Native Cellulose Using the X-Ray Diffractometer." *Textile Research Journal* 29 (10): 786–94.
Sehmi, Sandeep K., Sacha Noimark, Sebastian D. Pike, Joseph C. Bear, William J. Peveler, Charlotte K. Williams, Milo S. P. Shaffer, Elaine Allan, Ivan P. Parkin, and Alexander J. MacRobert. 2016. "Enhancing the Antibacterial Activity of Light-Activated Surfaces Containing Crystal Violet and ZnO Nanoparticles: Investigation of Nanoparticle Size, Capping Ligand, and Dopants." *ACS Omega* 1 (3): 334–43.
Selva, Thiago Matheus Guimarães, Jéssica Soares Guimarães Selva, and Raphael Bacil Prata. 2023. "Sensing Materials: Diamond-Based Materials." In *Encyclopedia of Sensors and Biosensors (First Edition)*, edited by Roger Narayan, 45–72. Oxford: Elsevier.
Sharma, Ravi, D. P. Bisen, Usha Shukla, and B. G. Sharma. 2012. "X-Ray Diffraction: A Powerful Method of Characterizing Nanomaterials." *Recent Res Sci Technol* 4 (8): 77–79.
Shu, Shun Xin, and Chao Rong Li. 2012. "Fabrication and Characterization of Regenerated cellulose/TiO2 Nanocomposite Hybrid Fibers." *Advanced Materials Research* 418: 237–41.
Silva Pinto, Marcia da, Cesar Augusto Sierra-Avila, and Juan P. Hinestroza. 2012. "In Situ Synthesis of a Cu-BTC Metal–organic Framework (MOF 199) onto Cellulosic Fibrous Substrates: Cotton." *Cellulose* 19 (5): 1771–79.
Sinko, Robert, and Sinan Keten. 2014. "Effect of Moisture on the Traction-Separation Behavior of Cellulose Nanocrystal Interfaces." *Applied Physics Letters* 105 (24): 243702.
Siracusa, Valentina. 2012. "Food Packaging Permeability Behaviour: A Report." *International Journal of Polymer Science* 2012 (May). https://doi.org/10.1155/2012/302029.
Siti Syazwani, N., M. N. Ervina Efzan, C. K. Kok, and M. J. Nurhidayatullaili. 2022. "Analysis on Extracted Jute Cellulose Nanofibers by Fourier Transform Infrared and X-Ray Diffraction." *Journal of Building Engineering* 48 (May): 103744.
Sjostrom, Eero. 2013. *Wood Chemistry: Fundamentals and Applications*. San Diego, California: Elsevier.
Slavin, Yael N., Jason Asnis, Urs O. Häfeli, and Horacio Bach. 2017. "Metal Nanoparticles: Understanding the Mechanisms behind Antibacterial Activity." *Journal of Nanobiotechnology* 15 (1): 65.
Sofla, M. Rahimi Kord, R. J. Brown, T. Tsuzuki, and T. J. Rainey. 2016. "A Comparison of Cellulose Nanocrystals and Cellulose Nanofibres Extracted from Bagasse Using Acid and Ball Milling Methods." *Advances in Natural Sciences Nanoscience and Nanotechnology* 7 (3): 035004.
Song, Guanghui, Yaojin Wang, and Daniel Q. Tan. 2022. "A Review of Surface Roughness Impact on Dielectric Film Properties." *IET Nanodielectrics* 5 (1): 1–23.
Song, Junlong, and Orlando J. Rojas. 2013. "PAPER CHEMISTRY: Approaching Super-Hydrophobicity from Cellulosic Materials: A Review." *Nordic Pulp & Paper Research Journal* 28 (2): 216–38.
Soni, Bhawna, El Barbary Hassan, and Barakat Mahmoud. 2015. "Chemical Isolation and Characterization of Different Cellulose Nanofibers from Cotton Stalks." *Carbohydrate Polymers* 134 (December): 581–89.
Sothornvit, Rungsinee, and John M. Krochta. 2005. "23 - Plasticizers in Edible Films and Coatings." In *Innovations in Food Packaging*, edited by Jung H. Han, 403–33. London: Academic Press.
Spence, John C. H. 2013. *High-Resolution Electron Microscopy*. OUP Oxford.
Spence, Kelley L., Richard A. Venditti, Youssef Habibi, Orlando J. Rojas, and Joel J. Pawlak. 2010. "The Effect of Chemical Composition on Microfibrillar Cellulose Films from Wood Pulps: Mechanical Processing and Physical Properties." *Bioresource Technology* 101 (15): 5961–68.
Spiess, Lothar, Gerd Teichert, Robert Schwarzer, Herfried Behnken, and Christoph Genzel. 2009. *Moderne Röntgenbeugung: Röntgendiffraktometrie für Materialwissenschaftler, Physiker*

und Chemiker. Vieweg+Teubner Verlag.
SriBala, G., Ramanaiah Chennuru, Sudarshan Mahapatra, and R. Vinu. 2016. "Effect of Alkaline Ultrasonic Pretreatment on Crystalline Morphology and Enzymatic Hydrolysis of Cellulose." *Cellulose* 23 (3): 1725–40.
Stanssens, Dirk, Henk Van den Abbeele, Leo Vonck, Gustaaf Schoukens, Marlies Deconinck, and Pieter Samyn. 2011. "Creating Water-Repellent and Super-Hydrophobic Cellulose Substrates by Deposition of Organic Nanoparticles." *Materials Letters* 65 (12): 1781–84.
Steer, Ronald P. 2018. "Prospects for Efficient Solar Energy Upconversion Using Metalloporphyrins as Dual Absorber-Upconverters." *Dalton Transactions* 47 (26): 8517–25.
Stelte, Wolfgang, and Anand R. Sanadi. 2009. "Preparation and Characterization of Cellulose Nanofibers from Two Commercial Hardwood and Softwood Pulps." *Industrial & Engineering Chemistry Research* 48 (24): 11211–19.
Sui, Ruohong, Amin S. Rizkalla, and Paul A. Charpentier. 2004. "Synthesis and Formation of Silica Aerogel Particles By a Novel Sol−Gel Route in Supercritical Carbon Dioxide." *The Journal of Physical Chemistry. B* 108 (32): 11886–92.
Sultana, Afreen, Ajay Kathuria, and Kirtiraj K. Gaikwad. 2022. "Metal–organic Frameworks for Active Food Packaging. A Review." *Environmental Chemistry Letters* 20 (2): 1479–95.
Sun, Dengrong, and Zhaohui Li. 2017. "Robust Ti‐ and Zr‐based Metal‐organic Frameworks for Photocatalysis." *Chinese Journal of Chemistry* 35 (2): 135–47.
Sun, Limin, Dong Zhang, Stephen Z. D. Cheng, and Frank W. Harris. 2023. "Thermally Stable Transparent Polymer Films for Flexible Electronics: Properties and Applications." *Giant* 14 (June): 100156.
Sun, Xiuxuan, Qinglin Wu, David H. Picha, Mary Helen Ferguson, Ikenna E. Ndukwe, and Parastoo Azadi. 2021. "Comparative Performance of Bio-Based Coatings Formulated with Cellulose, Chitin, and Chitosan Nanomaterials Suitable for Fruit Preservation." *Carbohydrate Polymers* 259 (May): 117764.
Sun, Xiuxuan, Qinglin Wu, Xiuqiang Zhang, Suxia Ren, Tingzhou Lei, Wencai Li, Guangyin Xu, and Quanguo Zhang. 2018. "Nanocellulose Films with Combined Cellulose Nanofibers and Nanocrystals: Tailored Thermal, Optical and Mechanical Properties." *Cellulose* 25 (2): 1103–15.
Sun, Ying, Jiayi Wang, Duanxin Li, and Feng Cheng. 2024. "The Recent Progress of the Cellulose-Based Antibacterial Hydrogel." *Gels (Basel, Switzerland)* 10 (2). https://doi.org/10.3390/gels10020109.
Supian, Muhammad Arif Fahmi, Khairatun Najwa Mohd Amin, Saidatul Shima Jamari, and Shahril Mohamad. 2020. "Production of Cellulose Nanofiber (CNF) from Empty Fruit Bunch (EFB) via Mechanical Method." *Journal of Environmental Chemical Engineering* 8 (1): 103024.
Tan, Chen, Michelle C. Lee, Mohammad Arshadi, Morteza Azizi, and Alireza Abbaspourrad. 2020. "A Spiderweb-like Metal-Organic Framework Multifunctional Foam." *Angewandte Chemie* 59 (24): 9506–13.
Tang, Fujie, Tatsuhiko Ohto, Taisuke Hasegawa, Wen Jun Xie, Limei Xu, Mischa Bonn, and Yuki Nagata. 2018. "Definition of Free O–H Groups of Water at the Air–Water Interface." *Journal of Chemical Theory and Computation* 14 (1): 357–64.
Tao, Bailong, Weikang Zhao, Chuanchuan Lin, Zhang Yuan, Ye He, Lu Lu, Maowen Chen, et al. 2020. "Surface Modification of Titanium Implants by ZIF-8@Levo/LBL Coating for Inhibition of Bacterial-Associated Infection and Enhancement of in Vivo Osseointegration." *Chemical Engineering Journal* 390 (June): 124621.
Tian, Jia, Baoxuan Huang, Mian Hasnain Nawaz, and Weian Zhang. 2020. "Recent Advances of Multi-Dimensional Porphyrin-Based Functional Materials in Photodynamic Therapy." *Coordination Chemistry Reviews* 420 (October): 213410.
Tiernan, Hannah, Bernadette Byrne, and Sergei G. Kazarian. 2020. "ATR-FTIR Spectroscopy and

Spectroscopic Imaging for the Analysis of Biopharmaceuticals." *Spectrochimica Acta. Part A, Molecular and Biomolecular Spectroscopy* 241 (November): 118636.
Toivonen, Matti S., Olimpia D. Onelli, Gianni Jacucci, Ville Lovikka, Orlando J. Rojas, Olli Ikkala, and Silvia Vignolini. 2018. "Anomalous-Diffusion-Assisted Brightness in White Cellulose Nanofibril Membranes." *Advanced Materials* 30 (16): e1704050.
Toro, Roberta G., Abeer M. Adel, Tilde de Caro, Bruno Brunetti, Mona T. Al-Shemy, and Daniela Caschera. 2022. "A Facile One-Pot Approach to the Fabrication of Nanocellulose-Titanium Dioxide Nanocomposites with Promising Photocatalytic and Antimicrobial Activity." *Materials* 15 (16). https://doi.org/10.3390/ma15165789.
Toro, Roberta Grazia, Mohamed Diab, Tilde de Caro, Mona Al-Shemy, Abeer Adel, and Daniela Caschera. 2020. "Study of the Effect of Titanium Dioxide Hydrosol on the Photocatalytic and Mechanical Properties of Paper Sheets." *Materials* 13 (6). https://doi.org/10.3390/ma13061326.
Tranter, G. E. 2017. "FTIR Spectroscopy of Aqueous Solutions." In *Encyclopedia of Spectroscopy and Spectrometry (Third Edition)*, edited by John C. Lindon, George E. Tranter, and David W. Koppenaal, 762–69. Oxford: Academic Press.
Tripathy, Manamohan, Sandip Padhiari, and Garudadhwaj Hota. 2023. "Chapter 3 - Surface Functionalization Techniques and Characterization Methods of Electrospun Nanofibers." In *Functionalized Nanofibers*, edited by Kalim Deshmukh, S. K. Khadheer Pasha, Ahmed Barhoum, and Chaudhery Mustansar Hussain, 49–73. Elsevier.
Tu, Jiping, Xiaoliang Zeng, Fujian Xu, Xi Wu, Yunfei Tian, Xiandeng Hou, and Zhou Long. 2017. "Microwave-Induced Fast Incorporation of Titanium into UiO-66 Metal–organic Frameworks for Enhanced Photocatalytic Properties." *Chemical Communications* 53 (23): 3361–64.
Tu-morn, Maleewan, Naruenart Pairoh, Wimonlak Sutapun, and Tatiya Trongsatitkul. 2019. "Effects of Titanium Dioxide Nanoparticle on Enhancing Degradation of Polylactic Acid/low Density Polyethylene Blend Films." *Materials Today: Proceedings* 17 (January): 2048–61.
Turbak, A. F., F. W. Snyder, and K. R. Sandberg. 1983. "Microfibrillated Cellulose, a New Cellulose Product: Properties, Uses, and Commercial Potential." CONF-8205234-Vol.2. Vol. 37. ITT Rayonier Inc., Shelton, WA. https://www.osti.gov/biblio/5062478.
Tweedy, B. G. 1964. "Plant Extracts with Metal Ions as Potential Antimicrobial Agents." *Phytopathology* 55: 910–14.
Ueda, Tsubasa, Akira Ishigami, Supaphorn Thumsorn, Takashi Kurose, Yutaka Kobayashi, and Hiroshi Ito. 2022. "Structural, Rheological, and Mechanical Properties of Polyvinyl Alcohol Composites Reinforced with Cellulose Nanofiber Treated by Ultrahigh-Pressure Homogenizer." *Materials Today Communications* 33 (December): 104316.
Ulbrich, Marco, and Eckhard Flöter. 2014. "Impact of High Pressure Homogenization Modification of a Cellulose Based Fiber Product on Water Binding Properties." *Food Hydrocolloids* 41 (December): 281–89.
Ullah, Azeem, Yuxiang Zhang, Zafar Iqbal, Yaxin Zhang, Dong Wang, Jincan Chen, Ping Hu, Zhuo Chen, and Mingdong Huang. 2018. "Household Light Source for Potent Photo-Dynamic Antimicrobial Effect and Wound Healing in an Infective Animal Model." *Biomedical Optics Express* 9 (3): 1006–19.
UNEP. 2022. "United Nations Environment Programme Finance Initiative: Beat Plastic Pollution." 2022. https://www.unep.org/interactives/beat-plastic-pollution/.
Usenko, Sascha, Bikram Subedi, Lissette Aguilar, and Eleanor Robinson. 2013. "Chapter 6 - High-Throughput Analysis of PPCPs, PCDD/Fs, and PCBs in Biological Matrices Using GC–MS/MS." In *Comprehensive Analytical Chemistry*, edited by Imma Ferrer and E. Michael Thurman, 61:143–58. Elsevier.
Uzun, İlhan. 2023. "Methods of Determining the Degree of Crystallinity of Polymers with X-Ray

Diffraction: A Review." *Journal of Polymer Research* 30 (10): 394.
Vaidya, Ankur, and Kamla Pathak. 2019. "17 - Mechanical Stability of Dental Materials." In *Applications of Nanocomposite Materials in Dentistry*, edited by Abdullah M. Asiri, Inamuddin, and Ali Mohammad, 285–305. Woodhead Publishing.
Vaishampayan, Ankita, and Elisabeth Grohmann. 2021. "Antimicrobials Functioning through ROS-Mediated Mechanisms: Current Insights." *Microorganisms* 10 (1). https://doi.org/10.3390/microorganisms10010061.
Valencia, Luis, Emma M. Nomena, Susanna Monti, Walter Rosas-Arbelaez, Aji P. Mathew, Sugam Kumar, and Krassimir P. Velikov. 2020. "Multivalent Ion-Induced Re-Entrant Transition of Carboxylated Cellulose Nanofibrils and Its Influence on Nanomaterials' Properties." *Nanoscale* 12 (29): 15652–62.
Varghese, Sandhya Alice, Danaya Phothisarattana, Atcharawan Srisa, Yeyen Laorenza, Lerpong Jarupan, Nattinee Bumbudsanpharoke, Vanee Chonhenchob, and Nathdanai Harnkarnsujarit. 2023. "Novel Eco-Friendly Antimicrobial UV-Blocking PBAT/PBS/TiO2 Nanocomposite Films for Improved Shelf-Life of Bananas." *Food Bioscience* 55 (October): 102993.
Vasconcelos, Daniela Cordeiro Leite, Vilma Conceição Costa, Eduardo Henrique Martins Nunes, Antônio Claret Soares Sabioni, Massimo Gasparon, and Wander Luiz Vasconcelos. 2011. "Infrared Spectroscopy of Titania Sol-Gel Coatings on 316L Stainless Steel." *Materials Sciences and Applications* 02 (10): 1375–82.
Vatansever, Fatma, Wanessa C. M. A. de Melo, Pinar Avci, Daniela Vecchio, Magesh Sadasivam, Asheesh Gupta, Rakkiyappan Chandran, et al. 2013. "Antimicrobial Strategies Centered around Reactive Oxygen Species--Bactericidal Antibiotics, Photodynamic Therapy, and beyond." *FEMS Microbiology Reviews* 37 (6): 955–89.
Verghese, Karli, Helen Lewis, Simon Lockrey, and Helén Williams. 2015. "Packaging's Role in Minimizing Food Loss and Waste across the Supply Chain." *Packaging Technology & Science* 28 (7): 603–20.
Vidal, Cristian Patiño, Cristina Muñoz-Shugulí, Marcelo Patiño Vidal, María José Galotto, and Carol López de Dicastillo. 2022. "Active Electrospun Mats: A Promising Material for Active Food Packaging." In *Electrospinning - Material Technology of the Future*, edited by Tomasz Tański and Paweł Jarka.
Vinet, Luc, and Alexei Zhedanov. 2011. "A 'missing' Family of Classical Orthogonal Polynomials." *Journal of Physics A: Mathematical and Theoretical* 44 (8): 085201.
Vlachopoulos, N., P. Liska, A. J. McEvoy, and M. Grätzel. 1987. "Efficient Spectral Sensitisation of Polycrystalline Titanium Dioxide Photoelectrodes." *Surface Science* 189-190 (October): 823–31.
Wade, L. G. 2003. *Organic Chemistry*. Prentice Hall.
Wang, Bao, Dong Li, Li-Jun Wang, Yu Lung Chiu, Xiao Dong Chen, and Zhi-Huai Mao. 2008. "Effect of High-Pressure Homogenization on the Structure and Thermal Properties of Maize Starch." *Journal of Food Engineering* 87 (3): 436–44.
Wang, Lu, Cong Chen, Jinwu Wang, Douglas J. Gardner, and Mehdi Tajvidi. 2020. "Cellulose Nanofibrils versus Cellulose Nanocrystals: Comparison of Performance in Flexible Multilayer Films for Packaging Applications." *Food Packaging and Shelf Life* 23 (March): 100464.
Wang, Lu, Kai Li, Katie Copenhaver, Susan Mackay, Meghan E. Lamm, Xianhui Zhao, Brandon Dixon, et al. 2021. "Review on Nonconventional Fibrillation Methods of Producing Cellulose Nanofibrils and Their Applications." *Biomacromolecules* 22 (10): 4037–59.
Wang, Qingbo, Haishun Du, Fang Zhang, Yuedong Zhang, Meiyan Wu, Guang Yu, Chao Liu, Bin Li, and Hui Peng. 2018. "Flexible Cellulose Nanopaper with High Wet Tensile Strength, High Toughness and Tunable Ultraviolet Blocking Ability Fabricated from Tobacco Stalk via a Sustainable Method." *Journal of Materials Chemistry. A, Materials for Energy and Sustainability* 6 (27): 13021–30.

Wang, Shengnan, Hekai Zhao, Guoqiang Shao, Lina Yang, Lijie Zhu, Jun Li, Dayu Zhou, et al. 2020. “Microstructural Analysis of ZIF-8 Particles Using Soy Hull Polysaccharide Gel as a Coating Induced by Different Metal Cations.” *Microporous and Mesoporous Materials: The Official Journal of the International Zeolite Association* 306 (October): 110408.
Wang, Tao, and Lawrence T. Drzal. 2012. “Cellulose-Nanofiber-Reinforced Poly(lactic Acid) Composites Prepared by a Water-Based Approach.” *ACS Applied Materials & Interfaces* 4 (10): 5079–85.
Wang, Yanzi, Jing Sun, Haohai Zhang, Zhiping Zhao, and Wenfang Liu. 2018. “Tetra(4-Carboxyphenyl)porphyrin for Efficient Cofactor Regeneration under Visible Light and Its Immobilization.” *Catalysis Science & Technology* 8 (10): 2578–87.
Wan, Junmin, Meng Wei, Zhiwen Hu, Zhiqin Peng, Bing Wang, Daoyan Feng, and Yuewei Shen. 2016. “Ternary Composites of TiO2 Nanotubes with Reduced Graphene Oxide (rGO) and Meso-Tetra (4-Carboxyphenyl) Porphyrin for Enhanced Visible Light Photocatalysis.” *International Journal of Hydrogen Energy* 41 (33): 14692–703.
Wawro, D., and J. Kazimierczak. 2008. “Forming Conditions and Mechanical Properties of Potato Starch Films.” *Fibres & Textiles in Eastern Europe*. https://www.semanticscholar.org/paper/da3d8a6ec45bc05896f4f69b72b1bf20e9f0b755.
Wazzan, A. A., H. A. Al-Turaif, and A. F. Abdelkader. 2006. “Influence of Submicron TiO2 Particles on the Mechanical Properties and Fracture Characteristics of Cured Epoxy Resin.” *Polymer-Plastics Technology and Engineering* 45 (10): 1155–61.
Werpy, T., and G. Petersen. 2004. “Top Value Added Chemicals from Biomass: Volume I -- Results of Screening for Potential Candidates from Sugars and Synthesis Gas.” US Department of Energy (US). https://doi.org/10.2172/15008859.
West, G. T., and P. J. Kelly. 2011. “Influence of Inert Gas Species on the Growth of Silver and Molybdenum Films via a Magnetron Discharge.” *Surface and Coatings Technology* 206 (7): 1648–52.
WHO. 2016. “Radiation: Ultraviolet (UV) Radiation.” WHO. 2016. https://www.who.int/news-room/questions-and-answers/item/radiation-ultraviolet-(uv).
———. 2022. “Food Safety.” 2022. https://www.who.int/news-room/fact-sheets/detail/food-safety.
Winkler, Hans Christian, Tina Notter, Urs Meyer, and Hanspeter Naegeli. 2018. “Critical Review of the Safety Assessment of Titanium Dioxide Additives in Food.” *Journal of Nanobiotechnology* 16 (1): 51.
Woch, Julia, Edyta Małachowska, Kamil Korasiak, Aneta Lipkiewicz, Marcin Dubowik, Justyna Chrobak, Jolanta Iłowska, and Piotr Przybysz. 2022. “Barrier Dispersion-Based Coatings Containing Natural and Paraffin Waxes.” *Molecules* 27 (3). https://doi.org/10.3390/molecules27030930.
Wohlert, Malin, Tobias Benselfelt, Lars Wågberg, István Furó, Lars A. Berglund, and Jakob Wohlert. 2022. “Cellulose and the Role of Hydrogen Bonds: Not in Charge of Everything.” *Cellulose* 29 (1): 1–23.
World Packaging Organisation. 2008. “Position Paper-Market Trends and Developments.” 2008.
Wu, Jing, Wenjing Wang, and Zonghua Wang. 2020. “Porphin-Based Carbon Dots for ‘Turn Off-On’ Phosphate Sensing and Cell Imaging.” *Nanomaterials (Basel, Switzerland)* 10 (2). https://doi.org/10.3390/nano10020326.
Wu, Ke, Gaowei Wu, Alexander J. MacRobert, Elaine Allan, Asterios Gavriilidis, and Ivan P. Parkin. 2020. “Ultra High Molecular Weight Polyethylene with Incorporated Crystal Violet and Gold Nanoclusters Is Antimicrobial in Low Intensity Light and in the Dark.” *Materials Advances* 1 (9): 3339–48.
Wu, Yuhang, Yuanbo Xie, Fangyuan Zhong, Junkuo Gao, and Juming Yao. 2020. “Fabrication of Bimetallic Hofmann-Type Metal-Organic Frameworks@Cellulose Aerogels for Efficient Iodine Capture.” *Microporous and Mesoporous Materials: The Official Journal of the*

International Zeolite Association 306 (October): 110386.
Wu, Zhenhua, Jun Xu, Jie Gong, Jun Li, and Lihuan Mo. 2018. "Preparation, Characterization and Acetylation of Cellulose Nanocrystal Allomorphs." *Cellulose* 25 (9): 4905–18.
Wyrwa, Joanna, and Anetta Barska. 2017. "Innovations in the Food Packaging Market: Active Packaging." *European Food Research and Technology = Zeitschrift Fur Lebensmittel-Untersuchung Und -Forschung. A* 243 (10): 1681–92.
Xia, Jianyu, Zhe Zhang, Wei Liu, Vincent C. F. Li, Yunfeng Cao, Wei Zhang, and Yulin Deng. 2018. "Highly Transparent 100% Cellulose Nanofibril Films with Extremely High Oxygen Barriers in High Relative Humidity." *Cellulose* 25 (7): 4057–66.
Xie, Ming-Hua, Xiu-Li Yang, Chao Zou, and Chuan-De Wu. 2011. "A Sn(IV)-Porphyrin-Based Metal-Organic Framework for the Selective Photo-Oxygenation of Phenol and Sulfides." *Inorganic Chemistry* 50 (12): 5318–20.
Xue, Yu, Letian Qi, Zhaoyun Lin, Guihua Yang, Ming He, and Jiachuan Chen. 2021. "High-Strength Regenerated Cellulose Fiber Reinforced with Cellulose Nanofibril and Nanosilica." *Nanomaterials (Basel, Switzerland)* 11 (10). https://doi.org/10.3390/nano11102664.
Xu, Jiaoxing, Liping Li, Youjun Yan, Hui Wang, Xuxu Wang, Xianzhi Fu, and Guangshe Li. 2008. "Synthesis and Photoluminescence of Well-Dispersible Anatase TiO2 Nanoparticles." *Journal of Colloid and Interface Science* 318 (1): 29–34.
Xu, Jinchuan, Domenico Sagnelli, Marwa Faisal, Alixander Perzon, Vincenzo Taresco, Marco Mais, Concetta Valeria L. Giosafatto, et al. 2021. "Amylose/cellulose Nanofiber Composites for All-Natural, Fully Biodegradable and Flexible Bioplastics." *Carbohydrate Polymers* 253 (February): 117277.
Xu, Shanhong, Natalie Girouard, Gregory Schueneman, Meisha L. Shofner, and J. Carson Meredith. 2013. "Mechanical and Thermal Properties of Waterborne Epoxy Composites Containing Cellulose Nanocrystals." *Polymer* 54 (24): 6589–98.
Yaghi, Omar M., Michael O'Keeffe, Nathan W. Ockwig, Hee K. Chae, Mohamed Eddaoudi, and Jaheon Kim. 2003. "Reticular Synthesis and the Design of New Materials." *Nature* 423 (6941): 705–14.
Yaghi, O. M., Guangming Li, and Hailian Li. 1995. "Selective Binding and Removal of Guests in a Microporous Metal–organic Framework." *Nature* 378 (6558): 703–6.
Yang, Bin, Meiyun Zhang, Zhaoqing Lu, Jiaojun Tan, Jingjing Luo, Shunxi Song, Xueyao Ding, Lin Wang, Peng Lu, and Qiuyu Zhang. 2019. "Comparative Study of Aramid Nanofiber (ANF) and Cellulose Nanofiber (CNF)." *Carbohydrate Polymers* 208 (March): 372–81.
Yang, Ning, Zhan-Xiang Sun, Liang-Shan Feng, Mu-Zi Zheng, Dao-Cai Chi, Wei-Zhong Meng, Zhi-Yan Hou, Wei Bai, and Kai-Yu Li. 2015. "Plastic Film Mulching for Water-Efficient Agricultural Applications and Degradable Films Materials Development Research." *Materials and Manufacturing Processes* 30 (2): 143–54.
Yang, Shih-Chun, Chih-Hung Lin, Ibrahim A. Aljuffali, and Jia-You Fang. 2017. "Current Pathogenic Escherichia Coli Foodborne Outbreak Cases and Therapy Development." *Archives of Microbiology* 199 (6): 811–25.
Yang, Yingying, Zengpei Guo, Wei Huang, Shiyu Zhang, Jingjing Huang, Hongjun Yang, Yingshan Zhou, Weilin Xu, and Shaojin Gu. 2020. "Fabrication of Multifunctional Textiles with Durable Antibacterial Property and Efficient Oil-Water Separation via in Situ Growth of Zeolitic Imidazolate Framework-8 (ZIF-8) on Cotton Fabric." *Applied Surface Science* 503 (February): 144079.
Yano, Hiroyuki, Haruo Omura, Yoko Honma, Hiroaki Okumura, Hironari Sano, and Fumiaki Nakatsubo. 2018. "Designing Cellulose Nanofiber Surface for High Density Polyethylene Reinforcement." *Cellulose* 25 (6): 3351–62.
Yen, Chih-Ching, Chih-Jie Shen, Wu-Huei Hsu, Yi-Hsin Chang, Hsin-Tang Lin, Hsiao-Ling Chen, and Chuan-Mu Chen. 2011. "Lactoferrin: An Iron-Binding Antimicrobial Protein

against Escherichia Coli Infection." *Biometals: An International Journal on the Role of Metal Ions in Biology, Biochemistry, and Medicine* 24 (4): 585–94.
Yildirim, Selçuk, Bettina Röcker, Marit Kvalvåg Pettersen, Julie Nilsen-Nygaard, Zehra Ayhan, Ramune Rutkaite, Tanja Radusin, Patrycja Suminska, Begonya Marcos, and Véronique Coma. 2018. "Active Packaging Applications for Food." *Comprehensive Reviews in Food Science and Food Safety* 17 (1): 165–99.
Young, Thomas. 1805. "III. An Essay on the Cohesion of Fluids." *Philosophical Transactions of the Royal Society of London* 95 (January): 65–87.
Yu, Wantong, Jiefen Cui, Shaojie Zhao, Liping Feng, Yanqi Wang, Junmei Liu, and Jinkai Zheng. 2021. "Effects of High-Pressure Homogenization on Pectin Structure and Cloud Stability of Not-From-Concentrate Orange Juice." *Frontiers in Nutrition* 8 (May): 647748.
Zacher, Denise, Osama Shekhah, Christof Wöll, and Roland A. Fischer. 2009. "Thin Films of Metal–organic Frameworks." *Chemical Society Reviews* 38 (5): 1418–29.
Zeng, Jian, Shilin Liu, Jie Cai, and Lina Zhang. 2010. "TiO2 Immobilized in Cellulose Matrix for Photocatalytic Degradation of Phenol under Weak UV Light Irradiation." *Journal of Physical Chemistry C* 114 (17): 7806–11.
Zhang, Chi, Sinan Keten, Dominique Derome, and Jan Carmeliet. 2021. "Hydrogen Bonds Dominated Frictional Stick-Slip of Cellulose Nanocrystals." *Carbohydrate Polymers* 258 (April): 117682.
Zhang, Jian, Bo Xu, Pengyan Zhang, Maolin Cai, and Bo Li. 2023. "Effects of Surface Roughness on Wettability and Surface Energy of Coal." *Frontiers of Earth Science* 10 (January). https://doi.org/10.3389/feart.2022.1054896.
Zhang, Wanli, and Jong-Whan Rhim. 2022. "Titanium Dioxide (TiO2) for the Manufacture of Multifunctional Active Food Packaging Films." *Food Packaging and Shelf Life* 31 (March): 100806.
Zhang, Xiong-Fei, Zhongguo Wang, Meili Ding, Yi Feng, and Jianfeng Yao. 2021. "Advances in Cellulose-Metal Organic Framework Composites: Preparation and Applications." *Journal of Materials Chemistry. A, Materials for Energy and Sustainability* 9 (41): 23353–63.
Zhang, Xuan, Megan C. Wasson, Mohsen Shayan, Ellan K. Berdichevsky, Joseph Ricardo-Noordberg, Zujhar Singh, Edgar K. Papazyan, et al. 2021. "A Historical Perspective on Porphyrin-Based Metal-Organic Frameworks and Their Applications." *Coordination Chemistry Reviews* 429 (February). https://doi.org/10.1016/j.ccr.2020.213615.
Zhao, Chenmin, Bing Wang, Shuncong Zhong, Akhtaruzzaman, Wei Liang, and Hui Chen. 2023. "Chapter 12 - NDT Studies of Nanoscale Polymeric Coatings." In *Polymer-Based Nanoscale Materials for Surface Coatings*, edited by Sabu Thomas and Jesiya Susan George, 235–57. Elsevier.
Zhao, Guomin, Jun Du, Weimin Chen, Mingzhu Pan, and Dengyu Chen. 2019. "Preparation and Thermostability of Cellulose Nanocrystals and Nanofibrils from Two Sources of Biomass: Rice Straw and Poplar Wood." *Cellulose* 26 (16): 8625–43.
Zhao, Jiangqi, Wei Zhang, Xiaodan Zhang, Xinxing Zhang, Canhui Lu, and Yulin Deng. 2013. "Extraction of Cellulose Nanofibrils from Dry Softwood Pulp Using High Shear Homogenization." *Carbohydrate Polymers* 97 (2): 695–702.
Zhao, Jian, Chang-Sheng Liu, Yuan Yuan, Xin-Yi Tao, Xiao-Qian Shan, Yan Sheng, and Fan Wu. 2007. "Preparation of Hemoglobin-Loaded Nano-Sized Particles with Porous Structure as Oxygen Carriers." *Biomaterials* 28 (7): 1414–22.
Zhao, Si-Wei, Ming Zheng, Xiao-Hang Zou, Yuanru Guo, and Qing-Jiang Pan. 2017. "Self-Assembly of Hierarchically Structured cellulose@ZnO Composite in Solid–liquid Homogeneous Phase: Synthesis, DFT Calculations, and Enhanced Antibacterial Activities." *ACS Sustainable Chemistry & Engineering* 5 (8): 6585–96.
Zhao, Xu, Ting-Jiao Shi, Yao-Yao Liu, and Li-Jian Chen. 2023. "Porphyrinic Metal–Organic Framework-Loaded Polycaprolactone Composite Films with a High Photodynamic

Antibacterial Activity for the Preservation of Fresh-Cut Apples." *ACS Applied Polymer Materials* 5 (1): 560–66.
Zheng, Xiaohua, Lei Wang, Ming Liu, Pengpeng Lei, Feng Liu, and Zhigang Xie. 2018. "Nanoscale Mixed-Component Metal–organic Frameworks with Photosensitizer Spatial-Arrangement-Dependent Photochemistry for Multimodal-Imaging-Guided Photothermal Therapy." *Chemistry of Materials: A Publication of the American Chemical Society* 30 (19): 6867–76.
Zhou, Gang, Cuicui Xu, Weimin Cheng, Qi Zhang, and Wen Nie. 2015. "Effects of Oxygen Element and Oxygen-Containing Functional Groups on Surface Wettability of Coal Dust with Various Metamorphic Degrees Based on XPS Experiment." *Journal of Analytical Methods in Chemistry* 2015 (July): 467242.
Zhou, Yaxin, Tsuguyuki Saito, Lennart Bergström, and Akira Isogai. 2018. "Acid-Free Preparation of Cellulose Nanocrystals by TEMPO Oxidation and Subsequent Cavitation." *Biomacromolecules* 19 (2): 633–39.
Zhou, Zuocheng, Qin Li, and X. S. Zhao. 2006. "Evolution of Interparticle Capillary Forces during Drying of Colloidal Crystals." *Langmuir: The ACS Journal of Surfaces and Colloids* 22 (8): 3692–97.
Zhu, Chuantao, Susanna Monti, and Aji P. Mathew. 2020. "Evaluation of Nanocellulose Interaction with Water Pollutants Using Nanocellulose Colloidal Probes and Molecular Dynamic Simulations." *Carbohydrate Polymers* 229 (February): 115510.
Zhu, Hongli, Sepideh Parvinian, Colin Preston, Oeyvind Vaaland, Zhichao Ruan, and Liangbing Hu. 2013. "Transparent Nanopaper with Tailored Optical Properties." *Nanoscale* 5 (9): 3787–92.
Zhu, Jianjun, Pei-Zhou Li, Wenhan Guo, Yanli Zhao, and Ruqiang Zou. 2018. "Titanium-Based Metal–organic Frameworks for Photocatalytic Applications." *Coordination Chemistry Reviews* 359 (March): 80–101.
Zhu, Luting, Lu Zong, Xiaochen Wu, Mingjie Li, Haisong Wang, Jun You, and Chaoxu Li. 2018. "Shapeable Fibrous Aerogels of Metal-Organic-Frameworks Templated with Nanocellulose for Rapid and Large-Capacity Adsorption." *ACS Nano* 12 (5): 4462–68.
Zielińska, Daria, Katarzyna Siwińska-Ciesielczyk, Karol Bula, Teofil Jesionowski, and Sławomir Borysiak. 2022. "TiO2/nanocellulose Hybrids as Functional Additives for Advanced Polypropylene Nanocomposites." *Industrial Crops and Products* 176 (February): 114314.
Żołek-Tryznowska, Zuzanna, Ewa Bednarczyk, Mariusz Tryznowski, and Tomasz Kobiela. 2023. "A Comparative Investigation of the Surface Properties of Corn-Starch-Microfibrillated Cellulose Composite Films." *Materials* 16 (9). https://doi.org/10.3390/ma16093320.